

DISS. ETH NO. 17422

**A THERMODYNAMIC APPROACH TO CEMENT
HYDRATION: THE ROLE OF RETARDING
ADMIXTURES AND FE-MINERALS DURING THE
HYDRATION OF CEMENTS**

Görl Möschner

Zurich, 2007

DISS. ETH NO. 17422

**A THERMODYNAMIC APPROACH TO CEMENT HYDRATION:
THE ROLE OF RETARDING ADMIXTURES AND FE-MINERALS
DURING THE HYDRATION OF CEMENTS**

A dissertation submitted to

ETH ZURICH

for the degree of
Doctor of Sciences

presented by

GÖRIL MÖSCHNER

Dipl.-Geoökol., University of Karlsruhe (TH)

born January, 26th, 1979

citizen of Germany

accepted on the recommendation of

Prof. Dr. Ruben Kretzschmar, examiner

Prof. Dr. Jürgen Neubauer, co-examiner

Dr. Barbara Lothenbach, co-examiner

2007

“Lisa, in this house we obey the laws of thermodynamics!”

H. J. Simpson, *1956

Table of contents

| | |
|---|-----|
| Summary | VII |
| Zusammenfassung | XI |
| 1 Introduction | 1 |
| 1.1 Ordinary Portland cement and its hydration..... | 1 |
| 1.2 Fe-minerals / Fe-hydrates | 4 |
| 1.3 Admixtures | 7 |
| 1.4 Thermodynamic modeling..... | 10 |
| 1.4.1 The geochemical modeling code GEMS-PSI..... | 11 |
| 1.4.2 Time depending dissolution of the clinker phases..... | 12 |
| 1.4.3 Release and uptake of alkalis | 13 |
| 1.5 Research objectives | 14 |
| 1.6 References | 16 |
| 2 Solubility of Fe-ettringite ($\text{Ca}_6[\text{Fe}(\text{OH})_6]_2(\text{SO}_4)_3 \cdot 26\text{H}_2\text{O}$) | 23 |
| 2.1 Abstract | 23 |
| 2.2 Introduction | 24 |
| 2.3 Methods | 25 |
| 2.3.1 Time-series study of Fe-ettringite formation..... | 25 |
| 2.3.2 Precipitation and dissolution experiments..... | 25 |
| 2.3.3 Characterization of the solid phase..... | 26 |
| 2.3.4 Characterization of the liquid phase | 27 |
| 2.4 Experimental results | 28 |
| 2.4.1 Time-series study | 28 |
| 2.4.2 Precipitation and dissolution experiments..... | 33 |
| 2.5 Thermodynamic modeling..... | 45 |
| 2.5.1 Solubilities at 20 °C..... | 45 |
| 2.5.2 Solubilities at standard conditions..... | 49 |
| 2.6 Conclusion..... | 53 |
| 2.7 References | 54 |
| 3 Solid solution between Al-ettringite and Fe-ettringite ($\text{Ca}_6[\text{Al}_{1-x}\text{Fe}_x(\text{OH})_6](\text{SO}_4)_3 \cdot 26\text{H}_2\text{O}$) | 61 |
| 3.1 Abstract | 61 |
| 3.2 Introduction | 61 |

| | | |
|------------------|---|------------|
| 3.3 | Methods | 63 |
| 3.3.1 | Synthesis of the solid solution series | 63 |
| 3.3.2 | Characterization of the solid phases | 64 |
| 3.3.3 | Characterization of the liquid phase | 64 |
| 3.3.4 | Thermodynamic modeling | 65 |
| 3.4. | Experimental results..... | 66 |
| 3.4.1 | Solid phases of the solid solution series | 66 |
| 3.4.2 | Liquid phase of the solid solution series | 75 |
| 3.5 | Thermodynamic modeling | 76 |
| 3.6 | Conclusion | 84 |
| 3.7 | References..... | 85 |
| 4 | Thermodynamic modeling of the influence of citric acid on the hydration of Portland cement | 91 |
| 4.1 | Abstract..... | 91 |
| 4.2 | Introduction..... | 91 |
| 4.3 | Materials and methods | 93 |
| 4.3.1 | Experiments | 93 |
| 4.3.2 | Thermodynamic calculations | 95 |
| 4.4 | Results and discussion | 97 |
| 4.4.1 | Calorimetry | 97 |
| 4.4.2 | Solid phases | 98 |
| 4.4.3 | Pore solution | 104 |
| 4.4.4 | Citrate..... | 109 |
| 4.5 | Conclusion | 112 |
| 4.6 | References..... | 113 |
| 5 | Conclusions | 117 |
| 6 | Outlook | 121 |
| Appendix 1: | Solubility of Fe-ettringite..... | 123 |
| Appendix 2: | Solid solution Al-/Fe-ettringite | 129 |
| Appendix 3: | Influence of citric acid on the hydration of OPC | 137 |
| Appendix 4 | Chromate reducing agent in OPC | 145 |
| Acknowledgements | | 151 |
| Curriculum Vitae | | 153 |

Summary

Most important material properties of cementitious materials such as workability, setting behavior, strength development but also durability are related to the cement hydration process. Thus, specific material design must be based on a profound understanding of the process, especially of the early hydration.

Thermodynamic modeling of the interactions between solid and liquid phases in cements using geochemical speciation codes allows following the observed macroscopic evolution of the solid and liquid phase during cement hydration on a molecular scale and can therefore be the basis for the understanding of many of the observed experimental results. In addition, adequate thermodynamic models allow easy and fast parameter variations, make it possible to predict the composition of hydrate assemblages under different conditions, to extrapolate the composition to longer time scale as well as to calculate whether and to what extent the presence of concrete admixtures influences the equilibrium between liquid and solid phase by ion association and chelation reactions of the aqueous ions. Experimental data concerning the solubility of Fe-containing hydrates as formed under cementitious conditions have been missing and no attempt has been made to apply thermodynamic modeling to understand the interactions between concrete admixtures, dissolved ions and cement minerals.

The main objectives of this study were i) to determine experimentally the solubility of different typical Fe-containing endmember hydrates (such as Fe-ettringite and Fe-monosulfate), ii) to investigate the possibility of a solid solution series between Al- and Fe-ettringite and to determine their solubility, and iii) to compare experimentally obtained data during the hydration of ordinary Portland cement (OPC) in the presence of a retarding admixture with thermodynamically modeled results.

Ordinary Portland cement consists of several phases. The main constituents are the cement clinker phases (idealized compositions: Ca_3SiO_5 , Ca_2SiO_4 , $\text{Ca}_3\text{Al}_2\text{O}_6$, and $\text{Ca}_2\text{AlFeO}_5$) together with minor constituents such as Na_2SO_4 , K_2SO_4 , MgO , CaCO_3 , and CaSO_4 . The

aluminates ($\text{Ca}_3\text{Al}_2\text{O}_6$) and the alumino-ferrites ($\text{Ca}_2\text{AlFeO}_5$, where this phase represents one member of the solid solution series between $\text{Ca}_2\text{Fe}_2\text{O}$ and $\text{Ca}_6\text{Al}_4\text{Fe}_2\text{O}_{15}$) amount each $\sim 3 - 15\%$ and are therefore an essential part of the OPC clinkers. During cement hydration aluminate reacts with water, and with different ions present in the pore solution, to Al-containing hydrates such as ettringite ($\text{Ca}_6[\text{Al}(\text{OH})_6]_2(\text{SO}_4)_3 \cdot 26\text{H}_2\text{O}$), monosulfate ($\text{Ca}_4[\text{Al}(\text{OH})_6]_2(\text{SO}_4) \cdot 6\text{H}_2\text{O}$), and monocarbonate ($\text{Ca}_4[\text{Al}(\text{OH})_6]_2(\text{CO}_3) \cdot 6\text{H}_2\text{O}$). The fate of iron during the hydration of Portland cement, however, is unclear. It has been proposed i) that the hydration yields similar hydration products and that iron substitutes for aluminum in these hydrates (e.g. $\text{Ca}_6[\text{Al}_{1-x}\text{Fe}_x(\text{OH})_6]_2(\text{SO}_4)_3 \cdot 26\text{H}_2\text{O}$), and ii) that during hydration iron precipitates as an amorphous Fe(-Ca)-rich gel and is not or only partly incorporated in Al-containing hydrates. To investigate the thermodynamic possibility of the formation of Fe-ettringite ($\text{Ca}_6[\text{Fe}(\text{OH})_6]_2(\text{SO}_4)_3 \cdot 26\text{H}_2\text{O}$) during cement hydration the solubility of Fe-ettringite was determined. Therefore, Fe-ettringite was synthesized within a pH-range from 11 to 14. After equilibrium was reached the aqueous and the solid phases were analyzed. Fe-ettringite was stable up to a pH ~ 13 . At higher pH-values Fe-monosulfate and Fe-monocarbonate were formed. The calculated solubility products were $\log K_{\text{S0,Fe-ettringite}} = -44.0 \pm 0.7$, $\log K_{\text{S0,Fe-monosulfate}} = -33.2 \pm 0.5$, and $\log K_{\text{S0,Fe-monocarbonate}} = -35.5 \pm 0.3$. The solubility of Fe-ettringite is close to the solubility of Al-ettringite which has a solubility product of $\log K_{\text{S0}} = -44.9$. The solubility products of Fe-monosulfate and Fe-monocarbonate are ~ 4 log units lower than their Al-containing analogues ($\log K_{\text{S0,Al-monosulfate}} = -29.3$, $K_{\text{S0, Al-monocarbonate}} = -31.5$). Since generally in cementitious systems the dissolved concentrations of aluminum are at least 1000 times higher than the concentrations of iron it is probable that iron is hardly incorporated into the ettringite structure but rather incorporated into monosulfate and/or monocarbonate.

The solid solution series of Al-/Fe-ettringite was synthesized at constant pH (pH = 12.5) with different amounts of aluminum and iron added: $\text{Ca}_6[\text{Al}_{1-x}\text{Fe}_x(\text{OH})_6]_2(\text{SO}_4)_3 \cdot 26\text{H}_2\text{O}$, where $x = 0.0 - 1.0$ increased in 0.1 steps. X-ray diffraction analysis of the solid phases showed a peak broadening between 25 and 65 % aluminum in the system indicating a miscibility gap in this range. The composition of the aqueous solution, however, would have been in agreement with both, the existence of a miscibility gap or a continuous solid solution. The calculated total solubility products of the Al-/Fe-ettringite solid solution series varied between $\log \Sigma \Pi = -46.4$ and $\log \Sigma \Pi = -43.6$ at 20 °C.

Concrete admixtures are added in many cases to improve workability of the fresh concrete and properties of the hardened concrete. Retarding admixtures delay the setting of concrete by influencing the rate of cement hydration. Common retarding admixtures include a number of organic materials such as sugar, sucrose, citrate or calcium lignin sulfonate and inorganic salts (e.g. Pb-nitrate, Ca-sulfates, Ca-phosphates). In case of organic retarders it is believed that hydration is retarded because i) they adsorb onto the surface of the clinker grains and/or precipitate on the clinker surface and form a protective layer, and ii) they complex dissolved cations and, hence, retard the precipitation of hydration products. In this study retardation of cement hydration was investigated in the presence of citric acid ($C_6H_8O_7$) which was added to the mixing water. The hydration was stopped after different hydration times and the pore solution as well as the solid phases were analyzed. Measured concentrations of the dissolved organic carbon in pore solution as well as thermodynamic modeling revealed that the citrate was taken up within the first hours by the solid phases and that no significant complexation of dissolved ions occurred. This indicates that citrate does not retard hydration through complexation of dissolved ions but that retardation is caused rather by the formation of a protective layer. X-ray diffraction analysis of the solid phases showed that citrate retarded the dissolution of Ca_3SiO_5 and $Ca_3Al_2O_6$ which argued for the precipitation of citrate around or adsorption onto the surface of these clinkers.

In conclusion, the thermodynamic database for solids that are expected to form under cementitious conditions could be expanded by adding thermodynamic constants for Fe-ettringite, Fe-monosulfate, and Fe-monocarbonate. It could be confirmed that iron can substitute for aluminum in the ettringite structure in the range of 0 – 25 and 65 – 100 % Al. Between 25 and 65 % Al there is a miscibility gap. Furthermore it could be shown that the retardation of cement hydration in the presence of citric acid depends on adsorption of citrate or precipitation of citrate containing phases on the surface of the clinker grains.

Zusammenfassung

Die Eigenschaften von zementhaltigen Materialien, z.B. ihre Verarbeitbarkeit, das Erhärten, Festigkeitsentwicklung und Dauerhaftigkeit, werden durch den Verlauf der Zementhydratation beeinflusst. Um gezielt bestimmte Materialeigenschaften herstellen zu können, ist es besonders wichtig, den Prozess der frühen Zementhydratation umfassend zu verstehen.

Die Wechselwirkungen zwischen den verschiedenen Feststoffen im Zement und der Porenlösung während der Zementhydratation können mit Hilfe von thermodynamischen Modellen berechnet werden. Die experimentell beobachtete Veränderung der Zusammensetzung der Feststoffe und der Lösung kann somit auf einer chemischen Ebene nachvollzogen werden und erlaubt ein besseres Verständnis der experimentellen Ergebnisse. Mit Hilfe eines thermodynamischen Modells kann außerdem die Zusammensetzung der Hydratationsprodukte unter verschiedenen Bedingungen vorher gesagt werden, da die entsprechenden Parameter schnell und einfach im Modell geändert werden können. Es erlaubt z.B. die Phasenzusammensetzungen auf einen längeren Zeitraum hin zu extrapolieren oder auch die Auswirkung eines Betonzusatzmittels auf die Phasenzusammensetzung zu berechnen. Experimentelle Daten bezüglich der Löslichkeiten eisenhaltiger Hydratphasen, die während der Zementhydratation gebildet werden, fehlen bisher, und auch thermodynamisches Modellieren wurde noch nicht angewendet, um die Wechselwirkungen zwischen Betonzusatzmittel, gelösten Ionen und Zementmineralien zu verstehen.

Die wichtigsten Aufgabenstellungen dieser Arbeit waren: i) die Löslichkeit von verschiedenen eisenhaltigen Hydratationsphasen (z. B. Fe-Ettringit und Fe-Monosulfat) experimentell zu bestimmen, ii) die Möglichkeit einer Mischkristallreihe zwischen Al- und Fe-Ettringite zu untersuchen und deren Löslichkeit zu bestimmen und iii) experimentelle Daten der, mit Hilfe eines Zusatzmittels, verzögerten Zementhydratation von Portlandzement (OPC) mit thermodynamisch berechneten Daten zu vergleichen.

Portlandzement ist aus verschiedenen Phasen zusammengesetzt. Die Hauptbestandteile sind die Zementklinker (idealisierte Zusammensetzung: Ca_3SiO_5 , Ca_2SiO_4 , $\text{Ca}_3\text{Al}_2\text{O}_6$, and $\text{Ca}_2\text{AlFeO}_5$) und die Nebenbestandteile sind z.B. Na_2SO_4 , K_2SO_4 , MgO , CaCO_3 und CaSO_4 . Der Anteil von Aluminat ($\text{Ca}_3\text{Al}_2\text{O}_6$) und Aluminoferrat ($\text{Ca}_2\text{AlFeO}_5$, repräsentiert ein Mischkristall aus der Mischkristallreihe zwischen $\text{Ca}_2\text{Fe}_2\text{O}$ und $\text{Ca}_6\text{Al}_4\text{Fe}_2\text{O}_{15}$) im Portlandzement beträgt $\sim 3 - 15 \%$ und ist damit relative hoch. Während der Zementhydratation reagiert Aluminat mit Wasser und verschiedenen Ionen in der Porenlösung zu aluminiumhaltigen Hydratphasen, z.B. zu Ettringit ($\text{Ca}_6[\text{Al}(\text{OH})_6]_2(\text{SO}_4)_3 \cdot 26\text{H}_2\text{O}$), Monosulfat ($\text{Ca}_4[\text{Al}(\text{OH})_6]_2(\text{SO}_4) \cdot 6\text{H}_2\text{O}$) und Monocarbonat ($\text{Ca}_4[\text{Al}(\text{OH})_6]_2(\text{CO}_3) \cdot 6\text{H}_2\text{O}$). Wie das gelöste Eisen sich während der Zementhydratation verhält ist bisher unklar. Es wird angenommen, dass i) die Hydratation von Aluminoferrat zu ähnlichen Hydratationsprodukten führt wie von Aluminat und dass Eisen Aluminium zu einem gewissen Teil in diesen Phasen ersetzt (z.B. $\text{Ca}_6[\text{Al}_{1-x}\text{Fe}_x(\text{OH})_6]_2(\text{SO}_4)_3 \cdot 26\text{H}_2\text{O}$), und dass ii) Eisen während der Hydratation als amorphes Fe-(Ca-)reiches Gel ausfällt und es nicht oder nur teilweise in die aluminiumhaltigen Hydratphasen eingebaut wird. Um festzustellen, ob thermodynamisch die Möglichkeit vorhanden ist, dass Fe-Ettringit ($\text{Ca}_6[\text{Fe}(\text{OH})_6]_2(\text{SO}_4)_3 \cdot 26\text{H}_2\text{O}$) während der Zementhydratation gebildet wird, wurde die Löslichkeit von Fe-Ettringit bestimmt. Dafür wurde Fe-Ettringit in einem pH-Bereich von 11 bis 14 synthetisiert. Nach der Gleichgewichtseinstellung wurden der Niederschlag und auch die Gleichgewichtslösung analysiert. Fe-Ettringit war bis zu einem pH von ~ 13 stabil. Bei höheren pH-Werten waren sowohl Fe-Monosulfat als auch Fe-Monocarbonat ausgefallen. Die berechneten Löslichkeitsprodukte waren: $\log K_{\text{SO,Fe-Ettringit}} = -44.0 \pm 0.7$, $\log K_{\text{SO,Fe-Monosulfat}} = -33.2 \pm 0.5$ und $\log K_{\text{SO,Fe-Monocarbonat}} = -35.5 \pm 0.3$. Die Löslichkeit von Fe-Ettringit liegt damit nahe bei der Löslichkeit von Al-Ettringit, das ein Löslichkeitsprodukt von $\log K_{\text{SO}} = -44.9$ aufweist. Dagegen waren die Löslichkeitsprodukte von Fe-Monosulfat und Fe-Monocarbonat ungefähr 4 log Einheiten tiefer als die Löslichkeitsprodukte der entsprechenden Aluminiumphase ($\log K_{\text{SO,Al-Monosulfat}} = -29.3$, $K_{\text{SO,Al-Monocarbonat}} = -31.5$). In zementhaltigen Systemen ist die Konzentration des gelösten Aluminiums jedoch ungefähr 1000mal höher als die Konzentration des gelösten Eisens. Daher ist es wahrscheinlicher, dass Eisen bevorzugt in Monosulfat und/oder Monocarbonat eingebaut wird als in Ettringit.

Die Mischkristallreihe zwischen Al- und Fe-Ettringit wurde bei einem konstanten pH-Wert (12.5) hergestellt. Die Menge des verwendeten Aluminiums und Eisens wurde so variiert, dass in der Reihe $\text{Ca}_6[\text{Al}_{1-x}\text{Fe}_x(\text{OH})_6]_2(\text{SO}_4)_3 \cdot 26\text{H}_2\text{O}$, x von 0.0 bis 1.0 in 0.1 Schritten zunahm. Die Analyse der verschiedenen Niederschläge mittels Röntgendiffraktometrie zeigte, dass zwischen 25 und 65 % Aluminiumgehalt eine Mischungslücke auftrat, da in diesem Bereich deutliche Peakverbreiterungen detektiert wurden. Die Zusammensetzung der Gleichgewichtslösung allerdings hätte mit beiden Annahmen übereingestimmt, mit der Annahme dieser Mischungslücke, aber auch mit der Annahme einer durchgehenden Mischkristallreihe. Die berechneten totalen Löslichkeitsprodukte der Al-/Fe-Ettringit Mischkristallreihe schwankten zwischen $\log \Sigma II = -46.4$ und $\log \Sigma II = -43.6$ bei 20 °C.

Betonzusatzmittel werden oft eingesetzt, um die Verarbeitbarkeit des frischen Betons und auch die Eigenschaftent des erhärteten Betons zu verbessern. Verzögernde Zusatzmittel (Verzögerer) verlangsamen das Erhärten von Betonen und Zementen indem sie das Voranschreiten der Zementhydratation verzögern. Handelsübliche Verzögerer sind zum einen organische Substanzen wie Zucker, Sucrose, Citrat oder Calciumligninsulfonat, aber auch anorganische Salze (z.B. Pb-Nitrat, Ca-Sulfat, Ca-Phosphat). Im Falle der organischen Verzögerer wird vermutet, dass sie die Hydratation verlangsamen, indem sie i) an der Oberfläche der Klinkerphasen adsorbieren oder ausfallen und eine Schutzschicht um die Körner ausbilden und indem sie ii) gelöste Ionen komplexieren und somit die Ausfällung von Hydratationsprodukten verhindern. In dieser Arbeit wurde die verzögernde Wirkung von Zitronensäure ($\text{C}_6\text{H}_8\text{O}_7$) auf die Zementhydratation untersucht. Dafür wurde Zitronensäure dem Mischwasser zugegeben. Die Hydratation wurde nach unterschiedlich langen Hydratationszeiten gestoppt und sowohl die Porenlösung als auch die Feststoffe wurden dann analysiert. Die gemessenen Konzentrationen des gelösten organischen Kohlenstoffs (DOC) und auch thermodynamisches Modellieren zeigten, dass Citrat schon während den ersten Stunden von den Feststoffen aufgenommen wurde, d.h. dass keine signifikante Komplexierung von gelösten Ionen stattgefunden hat. Das deutet darauf hin, dass Citrat die Zementhydratation nicht durch Komplexierung von Ionen, sondern durch die Bildung einer Schutzschicht um die Zementkörner verzögert. Die Analyse des hydratitisierten Zements mittels Röntgendiffraktometrie ergab, das Citrat die Auflösung von Ca_3SiO_5 und $\text{Ca}_3\text{Al}_2\text{O}_6$ verzögerte und bekräftigte damit die Annahme, dass die

verzögernde Wirkung auf die Adsorption oder Ausfällung von Citrat an der Klinkeroberfläche zurückzuführen ist.

Im Rahmen dieser Arbeit konnte die thermodynamische Datenbank der Hydratationsprodukte der Zementhydratation mit den thermodynamischen Konstanten des Fe-Ettringits, Fe-Monosulfats und des Fe-Monocarbonats erweitert werden. Es konnte gezeigt werden, dass Eisen Aluminium im Ettringit im Bereich von 0 – 25 und 65 – 100 % Al ersetzen kann. Zwischen 25 und 65 % Al existiert eine Mischungslücke. Ausserdem konnte ermittelt werden, dass die Zementhydratation mit Zitronensäure aufgrund der Adsorption des Citrats oder aufgrund der Ausfällung citrathaltiger Phasen an der Klinkeroberfläche verzögert wird.

1 Introduction

1.1 Ordinary Portland cement and its hydration

Ordinary Portland cement (OPC) is the most commonly used cement. This hydraulic cement was named after the island “Portland” in Great Britain and was developed by Joseph Aspdin in 1824. Joseph Aspdin chose that name because the color of the produced cement was the same as the color of the Portland stone (oolitic limestone) which was commonly used for buildings in this area. For production Aspdin used a hard limestone crushed and calcined it, and mixed the lime with clay, grinding it to a slurry with water. This mixture was then broken and calcined in a kiln till CO_2 was expelled. Afterwards the material (so-called “clinker”) was ground to a fine powder: cement (Blezard, 1998).

For modern Portland cement a clay limestone is, after grinding, burnt in a rotary kiln at an ultimately temperature of about $1450\text{ }^\circ\text{C}$ and cooled rapidly. This process results in the formation of four different clinker phases (see Table 1.1). In addition to the main constituents, a number of other elements (Na_2SO_4 , K_2SO_4 , MgO , and CaCO_3) are present in these clinker phases (Taylor, 1997).

Table 1.1: The main clinker phases (Stark and Wicht, 2000)

| Name of the pure mineral | Idealized chemical composition | Shorthand notation ^a | Name of the mineral existent in the clinker | Average content in OPC [%] |
|---------------------------|--|---------------------------------|---|----------------------------|
| Tricalcium silicate | Ca_3SiO_5 | C_3S | Alite | 40 – 80 |
| Dicalcium silicate | Ca_2SiO_4 | C_2S | Belite | 2 – 30 |
| Tricalcium aluminate | $\text{Ca}_3\text{Al}_2\text{O}_6$ | C_3A | Aluminate | 3 – 15 |
| Calcium aluminate ferrite | $\text{Ca}_2\text{AlFeO}_5^{\text{b}}$ | C_4AF | Aluminate ferrite | 4 - 15 |

(a) Key to cement shorthand notation: A = Al_2O_3 , C = CaO , F = Fe_2O_3 , H = H_2O , S = SiO_2

(b) Present as member of the solid solution series between $\text{Ca}_2\text{Fe}_2\text{O}$ and $\text{Ca}_6\text{Al}_4\text{Fe}_2\text{O}_{15}$

The chemical composition of OPC can vary considerably because it depends on the chemical and mineralogical composition of the used raw materials and combustibles. The average chemical composition of OPC (see Table 1.2) shows that OPC consists mainly of CaO and SiO₂, and somewhat less Al₂O₃ and Fe₂O₃.

Table 1.2: Average chemical composition of OPC (Stark and Wicht, 2000).

| | |
|--------------------------------------|-------------|
| CaO | 60 – 69 % |
| SiO ₂ | 20 – 25 % |
| Al ₂ O ₃ | 4 – 7 % |
| Fe ₂ O ₃ | 0.2 – 7 % |
| MgO | 0.5 – 5 % |
| Na ₂ O + K ₂ O | 0.5 – 1.5 % |
| SO ₃ | 0.1 – 1.3 % |

In order to warrant the workability of the cement paste, calcium sulfate is interground to the clinker phases. Calcium sulfate is a set regulator and prolongs the workability of the cement paste. Without additional sulfate, calcium aluminate hydrate (Ca₄[Al(OH)₆]₂(OH)₂·6H₂O) would be formed instantly after adding the mixing water to the cement which would cause a rapid setting of the cement paste and would abolish workability. In the presence of additional sulfate, ettringite (Ca₆[Al(OH)₆]₂(SO₄)₃·26H₂O) is formed on the surface of Ca₃Al₂O₆ during hydration which causes a delay of the otherwise rapid dissolution of Ca₃Al₂O₆ (Stark and Wicht, 2000).

In cement chemistry the reaction of a non-hydrated cement with water is called *hydration* which leads to chemical and physico-mechanical changes: i) setting of the cement paste which is characterized by a sudden loss of plasticity, and ii) hardening of the cement paste where a certain hardness and strength is developed. The progress of hydration of Portland cement and its kinetics are influenced by different factors: e.g. i) the phase composition of the cement and the presence of foreign ions (mostly alkalis) within the latter of the clinker phases, ii) the fineness of the cement (particle size distribution, specific surface), iii) water/cement-ratio, iv) curing temperature, and v) presence of chemical admixtures (Odler, 1998). During the first ~ 8 – 16 hours of cement hydration the composition of the pore

solution is dominated by K, Na, and S which is due to the fast dissolution of the alkali-sulfates. The concentrations of Ca, hydroxide, and S are controlled by the presence of Ca(OH)_2 and CaSO_4 and the pore solution is highly oversaturated with respect to portlandite (Ca(OH)_2), gypsum ($\text{CaSO}_4 \cdot 2\text{H}_2\text{O}$), and ettringite ($\text{Ca}_6[\text{Al(OH)}_6]_2(\text{SO}_4)_3 \cdot 26\text{H}_2\text{O}$) at early hydration times (Gartner et al., 1985; Reardon, 1992; Schwarz, 1995; Rothstein et al., 2002; Lothenbach and Winnefeld, 2006). For Al, Fe, and Si generally low concentrations are measured in pore solution. During the first hours the concentrations of these ions are presumably limited by the precipitation of (relatively metastable) initial hydrates around the clinker grains (Lothenbach and Winnefeld, 2006). At later hydration times the ions in pore solution are limited by the following precipitating hydrates.

The hydration process of the siliceous clinker phases can be described as follows:

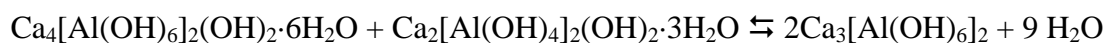


Because the formed amorphous calcium silicate hydrates show variable stoichiometry they are summarized as so-called C-S-H phases or C-S-H gel. In Portland cements the CaO/SiO_2 molar ratio of the formed C-S-H phases is generally approximately 1.7 and therefore lower than in the starting clinker phases. Thus, always Ca(OH)_2 precipitates in cementitious systems as portlandite (Odler, 1998; Stark and Wicht, 2000). The formation of small amounts of C-S-H phases and portlandite is detectable within the first hours of hydration. With proceeding hydration the amounts increase strongly and after approximately one day the C-S-H phases are the main hydration products. In the beginning of hydration the dissolution of the clinker phases (and therefore the formation of C-S-H and portlandite) is inhibited due to protective layers (initial metastable hydrates) forming around the clinker grains. It has also been shown that the dissolution of Ca_2SiO_4 is slower than the dissolution of Ca_3SiO_5 (Parrot and Killoh, 1984; Taylor, 1997).

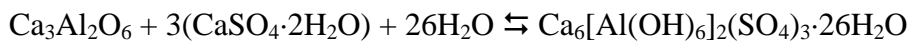
The hydration of aluminate can lead to different products depending on the ions available in the pore solution. If only water is incorporated into the forming Al-hydrates the hydration reactions can be described as:



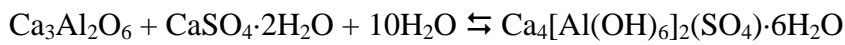
which react to



In the presence of sulfate, aluminate reacts to ettringite



or to monosulfate



The sulfate in the pore solution stems from the added gypsum and/or anhydrite (see above). The precipitation of ettringite and/or monosulfate leads to a continuous removal of the sulfate from pore solution. Therefore, the calcium sulfates dissolve slowly and are consumed within ~ 8 – 16 hours.

In the presence of CaCO_3 also hemicarbonates ($\text{Ca}_4[\text{Al}(\text{OH})_6]_2(\text{OH})(\text{CO}_3)_{0.5} \cdot 5.5\text{H}_2\text{O}$) and monocarbonates ($\text{Ca}_4[\text{Al}(\text{OH})_6]_2(\text{CO}_3) \cdot 6\text{H}_2\text{O}$) are formed (Odler, 1998; Stark and Wicht, 2000). After manufacture of the clinker phases different substances (e.g. CaCO_3 , fly ash, blast furnace slag) can be added and then further processed together with the burnt clinker phases. The addition of minor components (as CaCO_3) should improve the particle size distribution which results in an improved workability and improved water retention.

It is proposed that the hydration of calcium aluminate ferrite yields similar hydration products as those formed from aluminate: either iron is partly incorporated into the hydrates and/or precipitates as a Fe-(Ca-)rich gel. The distinction between iron free and the iron containing analogues in the hydrated cement samples is very difficult by the methods commonly used in cement chemistry (i.e. X-ray diffraction, thermogravimetric analysis, environmental scanning electron microscopy, Raman spectroscopy) because structural modification of the crystal is small and, therefore, difficult to detect. Since OPC can consist of up to ~ 15 % calcium aluminate ferrite several investigations were carried out dealing with $\text{Ca}_2\text{AlFeO}_5$ and its hydration behavior and hydration products. This is described more in detail in the next section (1.2).

1.2 Fe-minerals / Fe-hydrates

It is generally assumed that during the hydration of calcium aluminate ferrite the dissolved iron is incorporated into the hydrates forming, such as ettringite, monosulfate, and monocarbonate. This is manifested in the nomenclature of these phases: the short hand

notation *AFt-phases* ($\text{Al}_2\text{O}_3 - \text{Fe}_2\text{O}_3 - \text{tri}$) summarizes hydration products with a general composition of $\text{Ca}_6(\text{Al,Fe})_2(\text{OH})_{12}(\text{X})_3 \cdot y\text{H}_2\text{O}$, where X is one formula unit of a doubly charged anion (e.g. ettringite), while the term *AFm-phases* ($\text{Al}_2\text{O}_3 - \text{Fe}_2\text{O}_3 - \text{mono}$) is used to summarize hydration products with a general composition of $\text{Ca}_4(\text{Al,Fe})_2(\text{OH})_{12}(\text{X}) \cdot y\text{H}_2\text{O}$, where X denotes two formula units of a singly charged anion or one formula of a doubly charged anion (e.g. monosulfate, and monocarbonate). While ettringite is one of the first hydration products during hydration of cements in presence with gypsum, monosulfate as well as monocarbonate are generally formed at later hydration times depending on the concentrations of sulfate and carbonate present in the pore solution.

Investigations of the behavior of calcium aluminate ferrite during hydration showed that it exposes generally a slow hydration kinetic compared to the pure tricalcium aluminate (Schwiete and Ludwig, 1968; Parrot and Killoh, 1984; Swaddiwudhipong et al., 2002). For the reaction of $\text{Ca}_2\text{AlFeO}_5$ with water Tamas and Vertes (1973) found by Mössbauer spectroscopy that Fe-hydrogarnet ($\text{Ca}_3[\text{Fe}(\text{OH})_6]_2$), Al-hydrogarnet ($\text{Ca}_3[\text{Al}(\text{OH})_6]_2$), and $\text{Al}(\text{OH})_3$ have been formed, while Fortune and Coey (1983) stated that additionally to a non-crystalline ferrihydrite an iron-bearing Al-hydrogarnet ($\text{Ca}_3[\text{Al}_{0.89}\text{Fe}_{0.11}(\text{OH})_6]_2$) has been formed. In contrast to these findings Meller and Hall (2004) claimed, based on ESEM and chemical analysis of solution, that only minimal iron enters the solution and therefore, the hydration products are iron-free. In the presence of gypsum the hydration of calcium aluminate ferrite is retarded (Collepari et al., 1979). Fukuhara et al. (1981) estimated by conduction calorimetry for the reaction of $\text{Ca}_2\text{AlFeO}_5$, gypsum, and water that at least 25 % of the aluminum in ettringite is substituted by iron ($\text{Ca}_6[\text{Al}_{0.75}\text{Fe}_{0.25}(\text{OH})_6]_2(\text{SO}_4)_3 \cdot 26\text{H}_2\text{O}$) and that $\text{Fe}(\text{OH})_3$ precipitates additionally. Similar results were found by Liang and Nanru (1994) using XRD, EDX, and IR, who furthermore stated that iron is incorporated into AFm-phases up to a molar ratio of Fe of 0.12. On the contrary Brown (1987), Emanuelson and Hansen (1997), and Meller and Hall (2004) observed using different methods (ESEM, XRD, chemical analysis) that the hydration products (AFt-phases) of calcium aluminate ferrite in the presence of gypsum are iron-free, and that iron is bound in an amorphous Ca-Fe-rich gel. Only in the presence of gypsum, $\text{Ca}(\text{OH})_2$ and Ca_3SiO_5 Emanuelson and Hansen (1997) found that both iron and aluminum have entered the AFt-phase ($\text{Ca}_6[\text{Al}_{0.5}\text{Fe}_{0.5}(\text{OH})_6]_2(\text{SO}_4)_3 \cdot 26\text{H}_2\text{O}$).

As the obtained results of the investigations during the hydration of calcium aluminate ferrite are ambiguous, studies were carried out synthesizing pure iron containing hydrates, mainly Fe-ettringite, Fe-monosulfate, Fe-monocarbonate, Fe-containing hydroxy-AFm-phase ($\text{Ca}_4[\text{Fe}(\text{OH})_6]_2(\text{OH})_2 \cdot 6\text{H}_2\text{O}$), and Fe-hydrogarnet. For the synthesis of the different phases mostly $\text{Fe}(\text{OH})_3$, and CaO or $\text{Ca}(\text{OH})_2$ were mixed with the appropriate reaction partner, if necessary. In a few cases the hydration of $\text{Ca}_2\text{Fe}_2\text{O}_5$ (with or without gypsum) is described leading to the respective hydration products (Zur Strassen and Schmitt, 1960; Kuzel, 1968a; Kuzel, 1968b; Schwiete and Ludwig, 1968; Buhlert and Kuzel, 1971; Ecker and Pöllmann, 1994; Ecker, 1998). For Fe-hydrogarnet ($\text{Ca}_3[\text{Fe}(\text{OH})_6]_2$) it was found that it is not stable in the system $\text{CaO}-\text{Fe}_2\text{O}_3-\text{H}_2\text{O}$ unless it contains some Al or Si (Jones, 1945; Zur Strassen and Schmitt, 1960; Kuzel, 1968b; Schwiete and Ludwig, 1968). The hydroxyl-AFm-phase $\text{Ca}_4[\text{Fe}(\text{OH})_6]_2(\text{OH})_2 \cdot 6\text{H}_2\text{O}$ is unstable (Zur Strassen and Schmitt, 1960), even its observation has been reported (Rogers and Aldridge, 1977; Gallias, 1998). But as in both studies CO_2 was not excluded, it is more probable that CO_2 entered the solid phase and Fe-monocarbonate was formed which is more stable (Ecker, 1998). Fe-monocarbonate, Fe-monosulfate, and Fe-ettringite could be synthesized, but rather long equilibration times were needed (approximately 6 months) (Kuzel, 1968a; Buhlert and Kuzel, 1971; Galimova et al., 1988; Ecker and Pöllmann, 1994).

For monosulfate and ettringite also the possibility of a solid solution series between $\text{Ca}_4[\text{Al}_{1-x}\text{Fe}_x(\text{OH})_6]_2(\text{SO}_4) \cdot 6\text{H}_2\text{O}$, $\text{Ca}_6[\text{Al}_{1-x}\text{Fe}_x(\text{OH})_6]_2(\text{SO}_4)_3 \cdot 26\text{H}_2\text{O}$ respectively were investigated. While Kuzel (1968a) observed for $\text{Ca}_4[\text{Al}_{1-x}\text{Fe}_x(\text{OH})_6]_2(\text{SO}_4) \cdot 6\text{H}_2\text{O}$ a miscibility gap between $x = 0.1$ and $x = 0.7$, Ecker (1998) reported a continuous solid solution series for Al-/Fe-monosulfate. Ecker assumed that the samples investigated by Kuzel had not been in equilibrium, since the equilibration time was quite short (85 days). For the solid solution series of Al-/Fe-ettringite ($\text{Ca}_6[\text{Al}_{1-x}\text{Fe}_x(\text{OH})_6]_2(\text{SO}_4)_3 \cdot 26\text{H}_2\text{O}$) Buhlert and Kuzel (1971) found a miscibility gap between $x = 0.7$ and $x = 0.8$.

Although it has been shown that Fe-(Al)-containing hydrates, which are expected to form during cement hydration, can be (in the majority of cases) synthesized successfully, it is still ambiguous whether iron substitutes partially for aluminum in the forming hydrates during cement hydration.

1.3 Admixtures

Admixtures are liquid or powdery materials which can be added to the concrete during the mixing. They are added in small percentages (max. ~5%) relating to the used amount of cement. Admixtures influence the characteristics of concrete due to chemical or physical effects. Depending on the type of admixtures they can either affect the characteristics of fresh concrete or of the set concrete. In the first case the used admixture should e.g. change the setting behavior and improve the workability of the freshly mixed concrete. In the second case the characteristics of the hardened concrete should be changed/improved (e.g. compressive strength and durability). The main categories are:

Air-entraining admixtures

Air entraining agents incorporate air in the paste mainly to enhance freeze-thaw resistance. The used chemicals possess a hydrocarbon chain or a backbone terminating in a hydrophilic polar group (e.g. carboxylic or sulfonic acid group) which acts at the air – water interface in cement paste and thereby, stabilizing air entrapped during the mixing process. This leads to an aggregate-air-cement-air-aggregate type of bridge which improves the cohesion of the mixed materials and further stabilizes the air void system. Those stabilized air bubbles allow relatively free motion of shear which gets important when during placing and compaction of the concrete vigorous vibration is employed as air shows a tendency to escape during vibration. Examples for air entraining admixtures are: abietic acid, sodium dodecyl benzene sulfonate, and sodium oleate (Edmeades and Hewlett, 1998).

Water reducing admixtures / plasticizers

Water reducing admixtures (often referred to as plasticizers) are hydrophilic surfactants. Dissolved in water they deflocculate and disperse cement particles and prevent the formation of conglomerates of cement particles. The high molecular weight anions of the plasticizer are adsorbed on the surface of the clinker grains which leads to a mutual repulsion of particles and a reduction in interparticle friction. Therefore, less water is

needed to obtain an acceptable level of workability of the concrete. Generally the water/cement ratio is kept low to minimize segregation of the cement particles, sand and aggregates as well as the displacement of water (“bleeding”). A low water content has further positive side effects: higher strength, lower permeability and reduced shrinkage of the concrete is obtained. Plasticizers often cause simultaneously a retardation of the setting due to the exclusion of water from the clinker surfaces or due to the influence on nucleation and growth of the precipitating C-S-H phases. Examples for plasticizers are: salts of lignosulfonic acid and hydroxycarboxylic acids (Edmeades and Hewlett, 1998).

Superplasticizing admixtures

Superplasticizers are high-range water-reducing admixtures which can be used at considerably higher dosages than plasticizers without disadvantageous side effects such as strong retardation of set. These admixtures can be used to produce ‘flowing concrete’ without adding excessive water to the mix. Most of the superplasticizers are synthetic chemicals consisting of high molecular weight and water-soluble polymers. Hydroxyl, sulfonate or carboxylate groups ensure the solubility and the adsorption on the clinker grains of these substances. Superplasticizers are strongly adsorbed onto the surface of the clinker grains. It is suggested that these admixtures build up multi-layer but evidence is still lacking. However, in the case of hydroxyl and sulfonate groups the negative charge build-up results in dispersion of the particles and aggregates, while in the case of e.g. polycarboxylate ether the dispersion occurs due to steric hindrance. Because the water content is reduced e.g. strength and durability is improved. On other properties such as drying shrinkage and creep superplasticizers have only a marginally effect. For improving freeze-thaw durability of flowing concrete air has to be entrained which is made more difficult by the use of superplasticizers as the mechanisms (cohesion vs. dispersion) are competitive. Examples for superplasticizers are: condensates of sulfated melamine-formaldehyde and sulfonated naphthalene-formaldehyde, and polycarboxylate (Edmeades and Hewlett, 1998).

Retarding admixtures

Retarding admixtures (retarders) lengthen the setting time of concrete or cement and therefore prolong workability. As retarders inorganic salts as well as organic polyacids are used. Generally there are three mechanisms proposed in literature: i) inorganic salts precipitate on the surface of the cement particles and form a protective layer ii) organic polyacids adsorb onto the surfaces of the cement particle and form a protective layer and thus, dissolution of the clinker phases slows down and gets diffusion controlled (Ramachandran and Lowery, 1992; Neubauer et al., 1998), or they adsorb on the hydration products inhibiting nucleation and growth, iii) formation of complexes between the used organic polyacid and dissolved ions, mostly calcium that is liberated on hydration, and therefore, the precipitation of hydration products is retarded (Thomas and Birchall, 1983; Neubauer et al., 1998). Examples for retarding admixtures are: Ca-phosphate, Ca-borate, sugar, tartaric acid, and citric acid (Edmeades and Hewlett, 1998).

Accelerating admixtures

Accelerating admixtures (accelerators) are used to shorten the setting. This is necessary for shotcrete and advantageous at cold weather, when setting would be prolonged due to low temperatures. Accelerators can also provide an additional safety against freeze. For shotcrete rapid accelerators are used which affect mainly the tricalcium aluminate which results in a considerable evolution of heat and precipitation of insoluble calcium salts, partly of the used accelerators itself. Examples for rapid accelerators are: highly alkaline chemicals such as sodium carbonate or sodium-aluminum carbonate. The other types of accelerating admixtures are accelerators for setting and hardening. These accelerators affect mainly the alite phase which results in an increase of C-S-H gel at early age and in an increase in heat evolution. Examples for accelerators for setting and hardening are: Ca-chloride, Ca-formate, and Ca-nitrate (Edmeades and Hewlett, 1998).

1.4 Thermodynamic modeling

Thermodynamic modeling of the interactions between solid and liquid phase in cements using geochemical speciation codes can be the basis for the interpretation of many of the observed experimental results. In addition, adequate thermodynamic models allow easy and fast parameter variations and make it possible to predict the composition of hydrate assemblages under different conditions and to extrapolate it to longer time scales.

During the last few years, several thermodynamic cement models have been developed and applied to cementitious systems in order to predict the long-term behavior as envisaged in many countries for the disposal of low and intermediate level radioactive waste (Berner, 1990; Bennett et al., 1992; Reardon, 1992; Neall, 1994; Lee et al., 1995; Ayora et al., 1998; Sinitsyn et al., 1998). Attempts have been made to apply thermodynamic calculations to fresh cement system. Rothstein et al. (2002) compared the measured composition of pore solutions with the calculated saturation indices of different solids (portlandite, gypsum, ettringite, monosulfate and C-S-H phases), while Lothenbach and Winnefeld (2006) developed a thermodynamic model, which calculates the composition of pore solution and the dissolution and precipitation of the respective solids as function of time during the early cement hydration. This thermodynamic model (which was also applied in this study) was developed using the geochemical code GEMS-PSI (Kulik, 2007; see section 1.4.1). In order to model the composition of solid and liquid phases during cement hydration, the default database of GEMS-PSI code (Hummel et al., 2002) has to be expanded with data for solids that are expected to form under cementitious conditions (Lothenbach and Winnefeld, 2006) and the time depending dissolution of the clinker phases has been taken into account (Parrot and Killoh, 1984; see section 1.4.2).

The correctness and the reliability of this thermodynamic model for calculating the composition of the pore solution and the solid phases during cement hydration depends strongly on an accurate and comprehensive database. Although many thermodynamic data are already available for phases in cementitious systems (Lothenbach and Winnefeld, 2006), for some phases only estimated solubilities and/or Gibbs free energies exists and experimental data are still missing. Especially, for the Fe-containing hydrates information

about their stabilities and possible solid solutions to other hydration products are still missing or poorly investigated (Buhlert and Kuzel, 1971; Babushkin et al., 1985; Kolomatskii and Ryapolov, 1990; Kolomatskii and Ryapolov, 1991).

1.4.1 The geochemical modeling code GEMS-PSI

GEMS-PSI is a broad purpose geochemical modeling code which uses an advanced convex programming method of Gibbs energy minimization and computes equilibrium phase assemblage and speciation in a complex chemical system from its total bulk elemental composition.

The Gibbs free energy is a thermodynamical potential and provides information of the stability of substances. The standard Gibbs free energy of formation $\Delta_f G^0$ can be used to calculate the formation of 1 mol of substances from the elements in their standard states:

$$\Delta_f G^0 = \Delta_f H^0 - T\Delta_f S^0 \quad (1.1)$$

where $\Delta_f H^0$ is the enthalpy and $\Delta_f S^0$ is the entropy at standard conditions. T is the temperature in Kelvin (Anderson and Crerar, 1993; Nordstrom and Munoz, 1994).

GEMS-PSI includes a geochemical database (Thoenen and Kulik, 2003). Initially, this thermodynamic database was designed in “log K format” for application to codes such as PHREEQC. These codes use law of mass action algorithms at standard conditions (1 bar and 25 °C). In order to use Gibbs energy minimization the log K values of the solubility products were converted into standard Gibbs free energies:

$$\Delta_r G^0 = -RT \ln K_{s0} \quad (1.2)$$

where $\Delta_r G^0$ is the Gibbs free energy of reaction at standard conditions, R is the gas constant (8.3145 J/(K·mol)), and T is the temperature in Kelvin. $\Delta_r G^0$ is linked with the Gibbs free energy of formation $\Delta_f G^0$ as follows:

$$\Delta_r G^0 = \sum_i v_i \Delta_f G_i^0 \quad (1.3)$$

where i denotes the involved species and the v_i values are the stoichiometric coefficients (Anderson and Crerar, 1993; Nordstrom and Munoz, 1994).

In order to permit thermodynamic calculations at non-standard conditions, the converted log K values were merged with slop98.dat database (originally developed for the SUPCRT92 code (Johnson et al., 1992)). For aqueous species this dataset is based on the Helgeson-Kirkham-Flowers (HKF) equation of state which is used to calculate temperature and pressure corrections up to 1000 °C and 5 kbar (Shock et al., 1997; Sverjensky et al., 1997).

With the revised HKF model the Gibbs free energy of individual ions can be varied with temperature and pressure. The composition can be represented by

$$d\bar{G}_j = -\bar{S}_j dT + \bar{V}_j dP + \mu_j dn_j \quad (1.4)$$

where j is an ion in an aqueous solution, \bar{G}_j is the partial molar free energy of the j th ion, \bar{S}_j is the partial molar entropy, \bar{V}_j is the partial molar volume, T is the temperature in Kelvin, P is the pressure in bar, μ_j is the chemical potential and n_j is the mole fraction of the j th ion. By integrating this equation changes in \bar{G}_j due to changes in T , P or n_j can be found:

$$\int_{T_r, P_r, n_0}^{T, P, n} \bar{G}_j = -\int_{T_r}^T \bar{S}_{j, P_r, n_0} dT + \int_{P_r}^P \bar{V}_{j, T, n_0} dP + \int_{n_0}^n \mu_{j, T, P} dn_j \quad (1.5)$$

where T_r is the reference temperature (usually 298.15 K), P_r is the reference pressure (usually 1 bar). T and P are temperature and pressure of interest (Anderson and Crerar, 1993).

1.4.2 Time depending dissolution of the clinker phases

The time depending dissolution of the clinker phases is considered during thermodynamic modeling by using the approach of Parrot and Killoh (1984).

The approach of Parrot and Killoh describes the rate R of hydration of the single clinker phases by a set of equations where the lowest value of R at the time t is considered as the rate controlling step:

nucleation and growth

$$R_t = \frac{K_1}{N_1} (1 - \alpha_t) (-\ln(1 - \alpha_t))^{(1-N_1)} \quad (1.6)$$

or diffusion

$$R_t = \frac{K_2 \times (1 - \alpha_t)^{\frac{2}{3}}}{1 - (1 - \alpha_t)^{\frac{1}{3}}} \quad (1.7)$$

or hydration shell

$$R_t = K_3 \times (1 - \alpha_t)^{N_3} \quad (1.8)$$

where a is the degree of hydration at time t (in days) and is expressed as $\alpha_t = \alpha_{t-1} + \Delta t \cdot R_{t-1}$. The values K_1 , N_1 , K_2 , K_3 and N_3 for the cement system have been acquired empirically by Parrot and Killoh (1984). The influence of the water/cement ratio can be considered according to

$$f(w/c) = (1 + 4.444 \times (w/c) - 3.333 \times \alpha_t)^4 \quad (1.9)$$

for $\alpha_t > 1.333 \times (w/c)$

as well as the surface area using the data given in Parrot and Killoh (1984).

1.4.3 Release and uptake of alkalis

The released alkalis have also to be taken into account when modeling cement hydration, as they partially co-precipitate with the forming C-S-H gel. One part of the released alkalis stems from the dissolution of the alkali sulfates, the other part are slowly released from the clinker phases in which they are incorporated. The distribution of K, Na, Mg, and S in the cement clinkers can be calculated after Bogue.

The modified Bogue calculation is a solution of four linear simultaneous equations for four unknowns. As an example typical compositions of phases in Portland cement clinkers are given in Taylor (1997) and presented in Table 1.3.

In order to calculate, as an example, the distribution of K in the cement clinkers the equation is

$$0.1x_1 + 0.9x_2 + 0.7x_3 + 0.2x_4 = M_{K_2O} \quad (1.10)$$

where $x_1 - x_4$ are the mass percentages of alite, belite, aluminate and ferrite in the material. M_{K_2O} is the measured total mass percentage K_2O present in the four major phases (Taylor, 1997).

Table 1.3: Typical compositions of phases in Portland cement clinker (mass percent) (Taylor, 1997).

| Clinker phase | K ₂ O | Na ₂ O | MgO | SO ₃ |
|---------------|------------------|-------------------|-----|-----------------|
| Alite | 0.1 | 0.1 | 1.1 | 0.1 |
| Belite | 0.9 | 0.1 | 0.5 | 0.2 |
| Aluminate | 0.7 | 1.0 | 1.4 | 0.0 |
| Ferrite | 0.2 | 0.1 | 3.0 | 0.0 |

The alkali uptake by the precipitating C-S-H gel in fresh cement pastes is considered in this model by using the approach of Hong and Glasser (1999).

Hong and Glasser investigated the Na and K partitioning in C-S-H gels and obtained distribution ratios R_d which describe the partitioning of alkalis between C-S-H and solution as a function of the alkali concentration in the solution according to

$$R_d = \frac{c_s w}{c_d s} \left[\frac{mL}{g} \right] \quad (1.11)$$

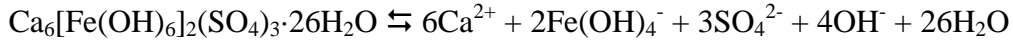
where c_s corresponds to the alkali concentration [mol/L] in the solid phase, c_d is the alkali concentration [mol/L] in the solution, and w/s is the water/solid ratio in mL/g.

1.5 Research objectives

As the fate of iron during the process of cement hydration is still unclear, the first main objective of the presented thesis was the determination of the solubilities of Fe-hydrates (Fe-ettringite, Fe-monosulfate and Fe-monocarbonate). These hydrates are the Fe-containing analogues to Al-hydrates which are known to be precipitating during cement hydration and thus, very well investigated. The solubilities of these hydrates provide information about their thermodynamical stability. The solubility products can be used for expanding a thermodynamic database which already enfolds data of other cement minerals. Then the probability of the formation of Fe-containing hydrates within a cementitious system can be calculated. The solubilities of these Fe-hydrates were determined from over-

and undersaturation. After equilibration the solid phase (XRD, TGA) and the liquid phase (ICP-OES, ICP-MS) were analyzed.

Fe-ettringite is in equilibrium with the following species:



The solubility product can be then calculated by multiplying the activities of these species:

$$K_{\text{SO,Fe-ettringite}} = \{\text{Ca}^{2+}\}^6 \cdot \{\text{Fe}(\text{OH})_4^-\}^2 \cdot \{\text{SO}_4^{2-}\}^3 \cdot \{\text{OH}^-\}^4 \cdot \{\text{H}_2\text{O}\}^{26}$$

The solubility products of Fe-monosulfate and Fe-monocarbonate are

$$K_{\text{SO,Fe-monosulphate}} = \{\text{Ca}^{2+}\}^4 \cdot \{\text{Fe}(\text{OH})_4^-\}^2 \cdot \{\text{SO}_4^{2-}\} \cdot \{\text{OH}^-\}^4 \cdot \{\text{H}_2\text{O}\}^6$$

$$K_{\text{SO,Fe-monocarbonate}} = \{\text{Ca}^{2+}\}^4 \cdot \{\text{Fe}(\text{OH})_4^-\}^2 \cdot \{\text{CO}_3^{2-}\} \cdot \{\text{OH}^-\}^4 \cdot \{\text{H}_2\text{O}\}^6$$

The second main objective of this thesis was to investigate the possibility of the formation of a solid solution series between the endmembers Al- and Fe-ettringite. The information of a continuous solid solution or a miscibility gap respectively between these two endmembers can also be considered during thermodynamic calculations and therefore, would refine the thermodynamic modeling of cement hydration. The solid solution series $\text{Ca}_6[\text{Al}_{1-x}\text{Fe}_x(\text{OH})_6]_2(\text{SO}_4)_3 \cdot 26\text{H}_2\text{O}$ was synthesized, x ranged from 0 to 1. The precipitated solids (XRD, TGA) and the aqueous solution (ICP-OES, ICP-MS) were analyzed after equilibrium had been reached. With X-ray diffraction (XRD) it is possible to detect changes of the ettringite structure due to the incorporation of iron. In the case of a continuous solid solution a slight shift of the peaks towards smaller Bragg angles with increasing amounts of Fe would occur due to the bigger ion radius of iron. In the case of a miscibility gap the peaks of both corresponding mixed endmembers would be detected.

The third main objective was to apply a thermodynamic model to the hydration of an ordinary Portland cement in the presence of a retarding admixture. Citric acid ($\text{C}_6\text{H}_8\text{O}_7$) was chosen as retarding admixture, because (besides its well defined chemical structure) sufficient thermodynamic data regarding complexation of alkalis, earth alkalis, Al(III), and Fe(III) were available. For the experiments cement pastes were prepared adding citric acid to the mixing water which was then mixed with ordinary Portland cement. Hydration was stopped after different hydration times (1 hour – 28 days) by separating the solid and the liquid phases which were then analyzed. On the basis of experimental data combined with thermodynamic modeling, it should be possible to explain which mechanism (complexation or adsorption) is responsible for the retardation of cement hydration.

1.6 References

- Anderson, G. M. and Crerar, D. A., 1993. *Thermodynamics in Geochemistry. The Equilibrium Model*. Oxford University Press, New York, Oxford.
- Ayora, C., Chinchón, S., Aguado, A., and Guirado, F., 1998. Weathering of iron sulfides and concrete alteration: Thermodynamic model and observation in dams from Central Pyrenees, Spain. *Cement and Concrete Research* **28**, 1223-1235.
- Babushkin, V. I., Matveyev, G. M., and Mchedlov-Petrossyan, O. P., 1985. *Thermodynamics of Silicates*. Springer-Verlag, Berlin.
- Bennett, D. G., Read, D., Atkins, M., and Glasser, F. P., 1992. A thermodynamic model for blended cements. II: Cement hydrate phases; thermodynamic values and modelling studies. *Journal of Nuclear Materials* **190**, 315-325.
- Berner, U., 1990. A thermodynamic description of the evolution of pore water chemistry and uranium speciation during degradation of cement. *Report 90-12, PSI, Villigen, Switzerland* **68**.
- Blezard, R. G., 1998. The history of calcareous cements. In: Hewlett, P. C. (Ed.), *Lea's Chemistry of Cement and Concrete*. Arnold, London.
- Brown, P. W., 1987. Early hydration of tetracalcium aluminoferrite in gypsum and lime-gypsum solutions. *Journal of the American Ceramic Society* **70**, 493-496.
- Buhlert, R. and Kuzel, H.-J., 1971. Ueber den Einbau von Cr^{3+} und Fe^{3+} in Ettringit. *Zement-Kalk-Gips* **2**, 83-85.
- Colleparidi, M., Monosi, S., and Moriconi, G., 1979. Tetracalcium aluminoferrite hydration in the presence of lime and gypsum. *Cement and Concrete Research* **9**, 431-437.
- Ecker, M., 1998. Diadochiebeziehungen in Calciumaluminatferraten und deren Hydratationsprodukten; Hallesches Jahrbuch für Geowissenschaften, Reihe B, Martin-Luther-Universität Halle-Wittenberg.

- Ecker, M. and Pöllmann, H., 1994. Investigations on lamellar calciumaluminate-ferratehydrates at different atmospheres and temperatures by in situ X-ray powder diffraction. *Materials Science Forum* **166-169**, 565-570.
- Edmeades, R. M. and Hewlett, P. C., 1998. Cement admixtures. In: Hewlett, P. C. (Ed.), *Lea's Chemistry of Cement and Concrete*. Arnold, London.
- Emanuelson, A. and Hansen, S., 1997. Distribution of iron among ferrite hydrates. *Cement and Concrete Research* **27**, 1167-1177.
- Fortune, J. M. and Coey, J. M. D., 1983. Hydration products of calcium aluminoferrite. *Cement and Concrete Research* **13**, 696-702.
- Fukuhara, M., Goto, S., Asage, K., Daimon, M., and Kondo, R., 1981. Mechanisms and kinetics of C₄AF hydration with gypsum. *Cement and Concrete Research* **11**, 407-414.
- Galimova, L. A., Danilov, V. P., Lepeshkov, I. N., Yudovich, B. E., and Shebanov, N. A., 1988. A study of the formation and decomposition of the calcium iron(III) double hydroxide sulphate Ca₆Fe₂(OH)₁₂(SO₄)₃ · 26H₂O in the 3Ca(OH)₂ + Fe₂(SO₄)₃ --> 3CaSO₄ + 2Fe(OH)₃-H₂O system at 20 °C. *Russian Journal of Inorganic Chemistry* **33**, 445-448.
- Gallias, J. L., 1998. Microstructure of the interfacial transition zone around corroded reinforcement. In: Katz, A. (Ed.), *Second International Conference on the Interfacial Transition Zone in Cementitious Composites. RILEM proceedings*. London : E & FN Spon, Haifa, Israel.
- Gartner, E. M., Tang, F. J., and Weiss, S. T., 1985. Saturation factors for calcium hydroxide and calcium sulfates in fresh Portland cement pastes. *Journal of the American Ceramic Society* **68**, 667-673.
- Hong, S.-Y. and Glasser, F. P., 1999. Alkali binding in cement pastes: Part I. The C-S-H phase. *Cement and Concrete Research* **29**, 1893-1903.

- Hummel, W., Berner, U., Curti, E., Pearson, F. J., and Thoenen, T., 2002. *Nagra/PSI Chemical Thermodynamic Data Base 01/01*. Universal Publishers/uPublish.com, Parkland, Florida.
- Johnson, J. W., Oelkers, E., and Helgeson, H. C., 1992. SUPCRT92: A software package for calculating the standard molal thermodynamic properties of minerals, gases, aqueous species, and reactions from 1 to 5000 bar and 0 to 1000 °C. *Computers & Geosciences* **18**, 899-947.
- Jones, F. E., 1945. The formation of the sulfoaluminates and sulfoferrites of calcium in the portland cement-water system. *Journal of Physical Chemistry* **49**, 344-357.
- Kolomatskii, A. S. and Ryapolov, V. D., 1990. Thermodynamic analysis of phase equilibria in the system CaO-Fe₂O₃-SO₃-H₂O. *Journal of Applied Chemistry of the USSR* **63**, 1125-1130.
- Kolomatskii, A. S. and Ryapolov, V. D., 1991. Solid solution formation in the CaO-Fe₂O₃-SO₃-H₂O system. *Journal of Applied Chemistry of the USSR* **64**, 1414-1417.
- Kulik, D. A., 2007. GEMS-PSI 2.13, PSI Villigen, Switzerland.
- Kuzel, H.-J., 1968a. Ersatz von Al³⁺ durch Cr³⁺ und Fe³⁺ in 3CaO·Al₂O₃·CaCl₂·nH₂O und 3CaO·Al₂O₃·CaSO₄·nH₂O. *Zement-Kalk-Gips* **21**, 493-499.
- Kuzel, H.-J., 1968b. Ueber die Diadochie von Al³⁺, Cr³⁺ und Fe³⁺ in 3 CaO · Al₂O₃ · 6 H₂O oberhalb 50°C. *Neues Jahrbuch der Mineralogie - Monatshefte*, 87-96.
- Lee, J. H., Roy, D. M., Mann, B., and D., S., 1995. Integrated approach to modeling long-term durability of concrete engineered barriers in LLRW disposal facility. *Material Research Society Symposium Proceedings* **353**, 881-889.
- Liang, T. and Nanru, Y., 1994. Hydration products of calcium aluminoferrite in the presence of gypsum. *Cement and Concrete Research* **24**, 150-158.
- Lothenbach, B. and Winnefeld, F., 2006. Thermodynamic modelling of the hydration of Portland cement. *Cement and Concrete Research* **36**, 209-226.

- Meller, N. and Hall, C., 2004. ESEM evidence for through-solution transport during brownmillerite hydration. *Journal of Materials Science* **39**, 6611-6614.
- Neall, F. B., 1994. Modelling of the near-field chemistry of the SMA repository at the Wellenberg Site. *Report 94-18, PSI, Villigen, Switzerland* **45**.
- Neubauer, C. M., Yang, M., and Jennings, H. M., 1998. Interparticle potential and sedimentation behavior of cement suspension: Effects of admixtures. *Advanced Cement Based Materials* **8**, 17-27.
- Nordstrom, D. K. and Munoz, J. L., 1994. *Geochemical Thermodynamics*. Blackwell Scientific Publications, Boston.
- Odler, I., 1998. Hydration, setting and hardening of Portland cement. In: Hewlett, P. C. (Ed.), *Lea's Chemistry of Cement and Concrete*. Arnold, London.
- Parrot, L. J. and Killoh, D. C., 1984. Prediction of cement hydration. *British Ceramic Proceedings* **35**, 41-53.
- Ramachandran, V. S. and Lowery, M. S., 1992. Conduction calorimetric investigation of the effect of retarders on the hydration of Portland cement. *Thermochimica Acta* **195**, 373-387.
- Reardon, E. J., 1992. Problems and approaches to the prediction of the chemical composition in cement/water systems. *Waste Management* **12**, 221-239.
- Rogers, D. E. and Aldridge, L. P., 1977. Hydrates of calcium ferrites and calcium aluminoferrites. *Cement and Concrete Research* **7**, 399-410.
- Rothstein, D., Thomas, J. J., Christensen, B. J., and Jennings, H. M., 2002. Solubility behavior of Ca-, S-, Al-, and Si-bearing solid phases in Portland cement pore solutions as a function of hydration time. *Cement and Concrete Research* **32**.
- Schwarz, W., 1995. Novel cement matrices by accelerated hydration of the ferrite phase in Portland cement via chemical activation: Kinetics and cementitious properties. *Advanced cement based materials* **2**, 189-200.

- Schwiete, H.-E. and Ludwig, U., 1968. Crystal structures and properties of cement hydration products (hydrated calcium aluminates and ferrites) *Proceedings of the Fifth International Symposium on the Chemistry of Cement*, Tokyo.
- Shock, E. L., Sassani, D. C., Willis, M., and Sverjensky, D. A., 1997. Inorganic species in geologic fluids: Correlations among standard molal thermodynamic properties of aqueous ions and hydroxide complexes. *Geochimica et Cosmochimica Acta* **61**, 907-950.
- Sinitsyn, V. A., Kulik, D. A., Khororivsky, M. S., and Karpov, I. K., 1998. Prediction of solid-aqueous equilibria in cementitious systems using Gibbs energy minimization: I. Multiphase aqueous ideal solution models. *Material Research Society Symposium Proceedings* **506**.
- Stark, J. and Wicht, B., 2000. *Zement und Kalk*. F. A. Finger Institut für Baustoffkunde der Bauhaus-Universität Weimar, Weimar.
- Sverjensky, D. A., Shock, E. L., and Helgeson, H. C., 1997. Prediction of the thermodynamic properties of aqueous metal complexes to 1000°C and 5 kb. *Geochimica et Cosmochimica Acta* **61**, 1359-1412.
- Swaddiwudhipong, S., Chen, D., and Zhang, M. H., 2002. Simulation of the exothermic hydration process of Portland cement. *Advances in Cement Research* **14**, 61-69.
- Tamas, F. D. and Vertes, A., 1973. A Mössbauer study on the hydration of brownmillerite ($4\text{CaO}\cdot\text{Al}_2\text{O}_3\cdot\text{Fe}_2\text{O}_3$). *Cement and Concrete Research* **3**, 575-581.
- Taylor, H. F. W., 1997. *Cement Chemistry*. Thomas Telford Publishing, London.
- Toenen, T. and Kulik, D., 2003. Nagra/PSI Chemical Thermodynamic Data Base 01/01 for the GEM-Selektor (V.2-PSI) Geochemical Modeling Code: Release 28-02-03.
- Thomas, N. L. and Birchall, J. D., 1983. The retarding action of sugars on cement hydration. *Cement and Concrete Research* **13**, 830-842.

zur Strassen, H. and Schmitt, C. H., 1960. On the stability of C_3FH_6 and C_4FH_{14} .
Proceedings of the fourth international symposium on chemistry of cement,
Washington.

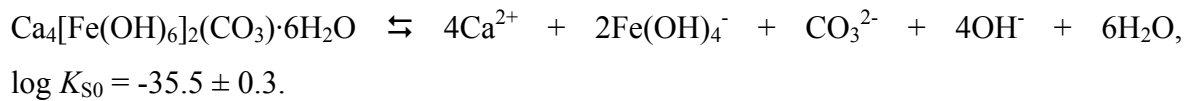
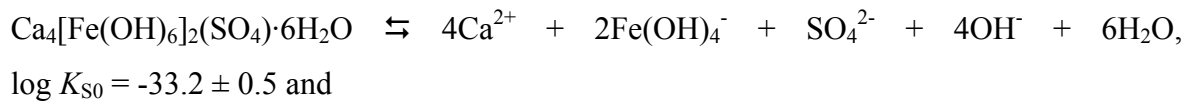
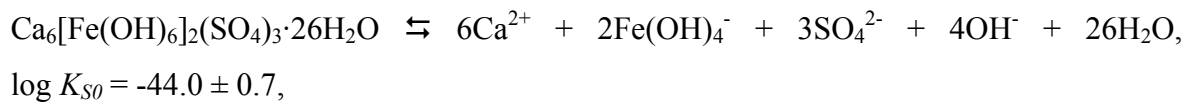
2 Solubility of Fe-ettringite ($\text{Ca}_6[\text{Fe}(\text{OH})_6]_2(\text{SO}_4)_3 \cdot 26\text{H}_2\text{O}$)

G. Möschner, B. Lothenbach, J. Rose, A. Ulrich, R. Figi, R. Kretzschmar

Accepted for publication in Geochimica et Cosmochimica Acta

2.1 Abstract

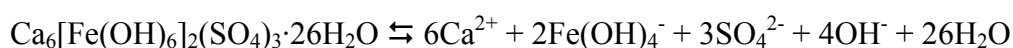
The solubility of Fe-ettringite ($\text{Ca}_6[\text{Fe}(\text{OH})_6]_2(\text{SO}_4)_3 \cdot 26\text{H}_2\text{O}$) was measured in a series of precipitation and dissolution experiments at 20 °C and at pH-values between 11.0 and 14.0 using synthesised material. A time-series study showed that equilibrium was reached within 180 days of ageing. After equilibrating, the solid phases were analysed by XRD and TGA while the aqueous solutions were analysed by ICP-OES (calcium, sulphur) and ICP-MS (iron). Fe-ettringite was found to be stable up to pH 13.0. At higher pH-values Fe-monosulphate ($\text{Ca}_4[\text{Fe}(\text{OH})_6]_2(\text{SO}_4) \cdot 6\text{H}_2\text{O}$) and Fe-monocarbonate ($\text{Ca}_4[\text{Fe}(\text{OH})_6]_2(\text{CO}_3) \cdot 6\text{H}_2\text{O}$) are formed. The solubilities of these hydrates at 25 °C are:



2.2 Introduction

Aluminium containing ettringite ($\text{Ca}_6[\text{Al}(\text{OH})_6]_2(\text{SO}_4)_3 \cdot 26\text{H}_2\text{O}$) occurs in natural alkaline environments like calcium-rich igneous rocks or sediments which were contact metamorphosed by igneous intrusions (e.g. Hurlbut and Baum, 1960; Murdoch and Chalmers, 1960; Bentor et al., 1963). It is also an important mineral formed during the hydration of Portland cement and super-sulphated blast furnace slag cements (Taylor, 1997). Because of that and its possibility to bind contaminants in exchange for its sulphate group or for Al(III), ettringite is a well investigated mineral (Hampson and Bailey, 1982; Atkins et al., 1992; Warren and Reardon, 1994; Barnett, 1998; Perkins and Palmer, 1999). The exchange of different anions (SeO_4^{2-} , CrO_4^{2-} and CO_3^{2-} for SO_4^{2-}) within ettringite has been shown (Poellmann et al., 1990; Perkins and Palmer, 2000; Baur and Johnson, 2003). Also the exchange of Al(III) by e.g. Cr(III) and Fe(III) has been observed (Jones, 1960; Buhlert and Kuzel, 1971; Andreeva and Sanzhaasurén, 1977; Brown, 1987; Galimova et al., 1988). Iron is a ubiquitous element in natural environments, and Portland cement clinker contains ~5 – 15 % ferrite ($\text{Ca}_2(\text{Al}_x\text{Fe}_{1-x})_2\text{O}_5$). It has been observed in Portland cement systems that Fe(III) partly exchanges for Al(III) in the lattice of ettringite and AFm-phases (Fukuhara et al., 1981; Emanuelson and Hansen, 1997; Csizmadia et al., 2001; Meller et al., 2004). AFm is the cement short hand notation for $\text{Ca}_4(\text{Al,Fe})_2(\text{OH})_{12}(\text{X})_y\text{H}_2\text{O}$ where X denotes two formula units of a singly charged anion or one formula unit of a doubly charged anion.

However, up to now measured solubility data for iron containing ettringite or AFm-phases are not available. Babushkin et al. (1985) and Lothenbach and Winnefeld (2006) estimated based on the solubility of Al-ettringite a solubility product of $\log K_{S0} = -49.8$, and $\log K_{S0} = -49.4$ respectively, for the dissolution reaction



The purpose of this study is to determine the solubility product of Fe-ettringite, Fe-monosulphate ($\text{Ca}_4[\text{Fe}(\text{OH})_6]_2(\text{SO}_4) \cdot 6\text{H}_2\text{O}$), and Fe-monocarbonate ($\text{Ca}_4[\text{Fe}(\text{OH})_6]_2(\text{CO}_3) \cdot 6\text{H}_2\text{O}$). The solubility products provide information about the stability of the iron containing hydrates compared to their aluminium containing analogues

and about the possibility of the formation of solid solutions $\text{Ca}_6[\text{Al}_{1-x}\text{Fe}_x(\text{OH})_6]_2(\text{SO}_4)_3 \cdot 26\text{H}_2\text{O}$. The obtained thermodynamic data are useful to investigate rock – water interactions, the behaviour of pollutants in alkaline environments and the immobilisation of contaminants in cement, and also to model thermodynamically the hydration of Portland cement.

2.3 Methods

2.3.1 Time-series study of Fe-ettringite formation

Fe-ettringite was synthesised by addition of 0.039 mol/L $\text{Fe}_2(\text{SO}_4)_3 \cdot 5.3\text{H}_2\text{O}$ and 0.229 mol/L freshly prepared CaO to 0.016 M KOH at a liquid/solid ratio of 20. The reactants were mixed in a N_2 -filled glove box (the atmosphere was continuously bubbled through KOH-solution) to exclude CO_2 contamination. The time-dependent formation of Fe-ettringite was investigated using five samples which were stored in sealed PE-bottles, shaken at 20 °C and stopped after 7, 24, 45, 90, and 180 days by separating the solid and liquid phases by vacuum filtration through 0.45 μm nylon filters under N_2 -gas atmosphere. The filtration equipment consisted of glass and was acid washed prior to its use. The solid phases were then analysed by XRD, TGA and XAS to determine the composition of the precipitates at the different equilibration times. The liquid phases were analysed by ICP-OES and ICP-MS to determine the concentration of the dissolved ions. In addition, the pH-values were measured. (For the exact procedure see sections 2.3.3 and 2.3.4.).

2.3.2 Precipitation and dissolution experiments

The precipitation and dissolution experiments were conducted using the method of Warren and Reardon (1994) with some modifications. Freshly prepared CaO (0.229 mol/L) and $\text{Fe}_2(\text{SO}_4)_3 \cdot 5.3\text{H}_2\text{O}$ (0.039 mol/L) were mixed with differently concentrated KOH-solutions

(0.001 – 1.0 M) for the precipitation experiments. Based on that, it was calculated that up to 2.5 g Fe-ettringite could precipitate. A liquid/solid ratio of 20 was chosen for the experiments. The target pH-value of the experiments varied in 0.2 unit steps from 11.0 to 14.0. After 180 days, solid and liquid phases were separated by filtration and the samples were analysed as described in section 2.3.1.

For the dissolution experiments 0.229 mol/L CaO and 0.039 mol/L $\text{Fe}_2(\text{SO}_4)_3 \cdot 5.3\text{H}_2\text{O}$ were mixed with KOH-solutions. The liquid/solid ratio and the concentrations of the used KOH-solutions were exactly the same as for the precipitation experiments. After 180 days equilibration the liquid/solid ratio was increased to 40 by adding the adequate KOH-solution. The mixtures were again equilibrated for further 180 days before the samples were separated by filtration and analysed (see section 2.3.1).

2.3.3 Characterization of the solid phase

The solid precipitates were dried in N_2 -filled desiccators in presence with saturated CaCl_2 -solution to equilibrate them with a relative humidity of approximately 30%. The dried solid phases were grinded by hand in the N_2 -filled glove box to $< 40 \mu\text{m}$ and analysed by X-ray powder diffraction (XRD) and thermogravimetric analyses (TGA). Filling of the sample holders and the measurements were done immediately prior to measurements under atmospheric conditions. The XRD analyses were performed on a PANalytical X'Pert PRO using $\text{CuK}\alpha$ radiation. For TGA (Mettler Toledo TGA/SDTA851^o) about 8 – 12 mg per sample were heated under N_2 over a temperature range of 30 to 980 °C at a rate of 20 °C/min.

The water loss measured by TGA was used to estimate the amount of Fe-ettringite ($\text{Ca}_6[\text{Fe}(\text{OH})_6]_2(\text{SO}_4)_3 \cdot 26\text{H}_2\text{O} - 32\text{H}_2\text{O} \rightleftharpoons 3\text{CaO} \cdot \text{Fe}_2\text{O}_3 \cdot 3\text{CaSO}_4$), portlandite ($\text{Ca}(\text{OH})_2 - \text{H}_2\text{O} \rightleftharpoons \text{CaO}$) and AFm-phases (Fe-monosulphate and Fe-monocarboante - ($\text{Ca}_4[\text{Fe}(\text{OH})_6]_2(\text{SO}_4) \cdot 6\text{H}_2\text{O} - 12\text{H}_2\text{O} \rightleftharpoons 3\text{CaO} \cdot \text{Fe}_2\text{O}_3 \cdot \text{CaSO}_4$ and $\text{Ca}_4[\text{Fe}(\text{OH})_6]_2(\text{CO}_3) \cdot 6\text{H}_2\text{O} - 12\text{H}_2\text{O} - \text{CO}_2 \rightleftharpoons 4\text{CaO} \cdot \text{Fe}_2\text{O}_3$)). Since the separation of Fe-monosulphate and Fe-monocarboante by TGA was not possible these two phases are summarised as AFm-phases. For estimation of the masses the corresponding range of temperature were taken into account (see section 2.4.2).

Two samples were also investigated by synchrotron X-ray absorption spectroscopy (XAS). XAS is a perfect tool to verify the presence of amorphous iron phases for the time-series study with respect to Fe-ettringite. XAS spectra were recorded at the ELETTRA synchrotron radiation facility (Trieste, Italy). Spectra were acquired in transmission mode at beamline 11.1 using a Si(111) monochromator from 100 eV below to 800 eV above the Fe K-edge (7.112 keV). EXAFS spectra were analysed using a standard procedure based on a series of programs developed by Michalowicz (Michalowicz, 1991; Michalowicz, 1997). EXAFS oscillations were theoretically recalculated using amplitude and phase functions obtained with the FEFF-8 code (Ankudinov et al., 1998). FEFF functions for the Fe-O, Fe-Fe, and Fe-Ca atomic pairs were tested by modelling the spectra of pure reference compounds (Andradite Fe-garnet, lepidocrocite (γ -FeOOH)). For each atomic shell of the samples, the interatomic distance R, the coordination number N, and the Debye-Waller factor σ were adjusted. During the fit the number of adjusted parameters was always lower than the maximum number of parameters statistically allowed to be adjusted (independent parameters $N_{ind} = \frac{2\Delta k \Delta R}{\pi - 1}$).

2.3.4 Characterization of the liquid phase

One part of the liquid phases of every sample was instantly diluted (1:10) with HNO₃ (supra-pure, 6.5%) to prevent the adsorption of the dissolved ions to the PE-vials used. The other part was left untreated to measure the pH-value. This was done without any delay to minimise CO₂-contamination. Prior to the measurements the pH meter (Knick pH-Meter 766 with a Knick SE 100 pH/Pt 1000 electrode) was calibrated with fresh KOH-solutions (0.001 to 1.0 mol/L) to minimise the alkali error. The obtained voltage was correlated to the calculated target pH-value of the respective KOH-solution considering ionic strength as well as the measured temperature of the solution. The concentrations of calcium, sulphur, and potassium were measured by ICP-OES (Varian, VISTA Pro), and the concentrations of iron were measured by ICP-MS (Finnigan MAT, ELEMENT2). In order to minimise contamination preparation of the samples for ICP-MS analysis was done in a clean laboratory. Rhodium was chosen as internal standard. As high concentrations of K and Ca

were present in the liquid phases, the Fe standard solutions were adjusted by adding appropriate concentrations of these elements.

2.4 Experimental results

2.4.1 Time-series study

Solid phase of the time-series study

The XRD analyses of the synthesised materials (Fig. 2.1) showed that in each sample Fe-ettringite was formed regardless of equilibration time. In the mixtures equilibrated for 7, 24, 45, and 90 days, gypsum could be detected in addition to Fe-ettringite. Fig. 2.1 shows that with increasing equilibration time the intensities of the gypsum peak decreased until after 180 days no gypsum could be detected. The Full Width Half Maximum (FWHM) of the Fe-ettringite peak at $2\Theta = 9.13^\circ$ (CuK α radiation; McMurdie et al., 1987) for the 180 days sample is larger than for shorter equilibration time suggesting a lower crystallinity.

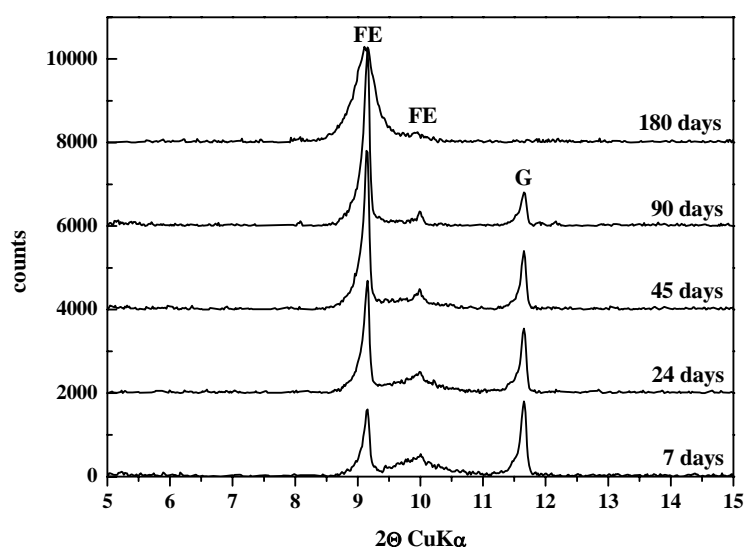


Fig. 2.1. X-ray diffraction spectra for Fe-ettringite synthesised at different equilibration times (7, 24, 45, 90 and 180 days). FE: Fe-ettringite (main peak at $2\Theta = 9.13^\circ$ (McMurdie et al, 1987); G: gypsum (main peak at $2\Theta = 11.59^\circ$).

Thermogravimetric analyses yielded the same results. In Fig. 2.2 the derivative curves of the weight loss of the mixtures revealed two peaks for the samples aged 7, 24, 45, and 90 days and only one peak for the sample equilibrated for 180 days. Fe-ettringite lost its water between 30 and 140 °C, while gypsum lost its water between 140 °C and 200 °C. Again a decrease of the gypsum peak with time was observed.

These results indicated that the formation of Fe-ettringite is kinetically inhibited and gypsum precipitated initially. This is contrary to the formation of Al-ettringite where steady state conditions have been reached within four to six days (Perkins and Palmer, 1999).

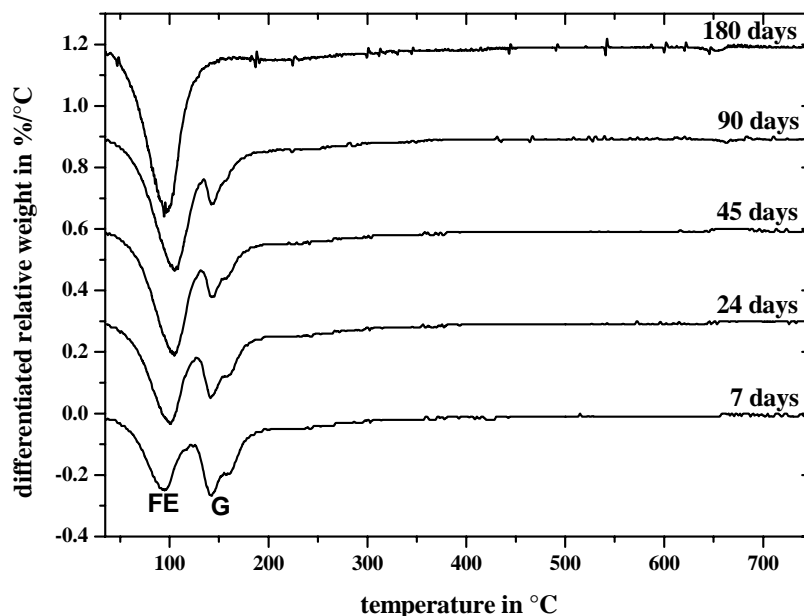


Fig. 2.2. Derivative curves of thermogravimetric analyses for Fe-ettringite synthesised at different equilibration times (7, 24, 45, 90 and 180 days). FE: Fe-ettringite; G: gypsum.

As stoichiometric amounts of Fe, Ca, and sulphate were mixed, the formation of gypsum in addition to Fe-ettringite indicated that some iron was bound in another phase. The red colour of the solids suggested the presence of a Fe-hydroxide phase. Freshly precipitated Fe-hydroxide is XRD amorphous and thus difficult to detect. Hence, EXAFS analyses were carried out on two samples (aged 40 and 180 days). The EXAFS spectra of both samples were different showing that the bonding environment of Fe has changed during ageing (Fig. 2.3A). The Fourier transforms of the EXAFS spectra (Fig. 2.3B) revealed the

presence of a second atomic shell at around 3 Å for the 40 days old sample. The modelling of both EXAFS spectra confirmed the differences of the second coordination sphere of iron (Table 2.1). For the sample aged for 180 days iron octahedra are linked to six calcium atoms at 3.47 Å which confirmed the presence of Fe-ettringite. Indeed, in the case of Al-ettringite, each aluminium atom is surrounded by six oxygen atoms at approximately 1.9 Å and six calcium atoms at 4 Å (Goetz-Neunhoeffer and Neubauer, 2006). If it is assumed that Fe substitutes Al, it can be expected that the measured interatomic distances of Fe-ettringite are somewhat larger than the mean distances observed by XRD for Al-ettringite. These larger distances agree with the larger size of Fe³⁺ (0.64 Å) compared to Al³⁺ (0.51 Å) (Holleman and Wiberg, 1985)

Table 2.1. Detailed modelling of the EXAFS spectra

| Atomic pair | Distance (Å) | Deby-waller (Å) | Number | Residual |
|----------------------------|--------------|-----------------|-----------|----------|
| 180 days old sample | | | | |
| Fe-O | 2.03 ± 0.02 | 0.075 | 6 ± 20% | 0.062 |
| Fe-Ca | 3.47 ± 0.02 | 0.106 | 6 ± 20% | |
| 40 days old sample | | | | |
| Fe-O | 1.98 ± 0.02 | 0.110 | 6 ± 20% | 0.024 |
| Fe-Fe | 3.00 ± 0.02 | 0.110 | 2.1 ± 20% | |
| Fe-Ca | 3.47 ± 0.02 | 0.088 | 1.9 ± 20% | |

In the sample hydrated for 40 days a Fe-Fe contribution existed at 3.01 Å. Such a contribution is a signature of an amorphous FeOOH (Rose et al., 2006). The number of Ca was far from 6 ($N_{Ca} = 2 \pm 20\%$, Table 2.1). If the crystallinity of Fe-ettringite did not change from 40 to 180 days, i.e. each iron was surrounded by six calcium atoms in the ettringite ($N_{Ca \text{ ettringite}}$), therefore, after 40 days at least one third ($\pm 20\%$) of the iron was present as Fe-ettringite ($\% \text{ ettringite} = N_{Ca \text{ from EXAFS}}/N_{Ca \text{ ettringite}} = 2/6$), while the rest precipitated as amorphous Fe-hydroxide. Therefore, two hypotheses can be formulated concerning the time-dependent formation of Fe-ettringite formation:

- i) FeOOH spontaneously precipitated, leading to an excess of Ca in the solution and the formation of gypsum.
- ii) The fast formation of gypsum lead to Fe excess in the solution and FeOOH can be formed.

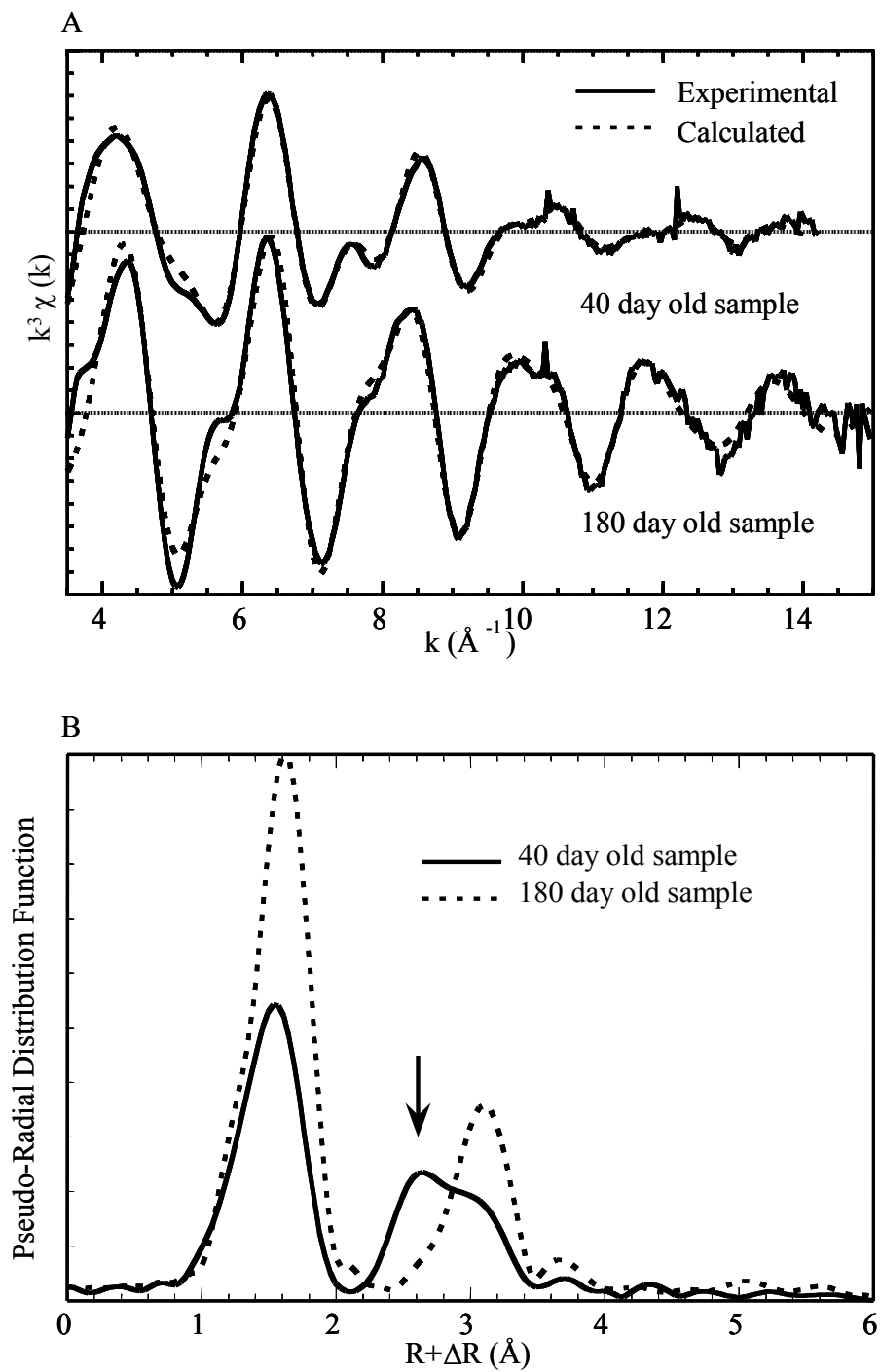


Fig. 2.3. Fe EXAFS spectra for the 40 and 180 days old samples (A) $k^3\chi(k)$ experimental functions (solid lines) compared to the calculated curves (dotted lines) and (B) their corresponding radial distribution functions (RDFs) uncorrected for phase shifts. Arrow indicates the Fe-Fe contribution.

Due to the very low solubility and very fast precipitation of ferric solution under many conditions, the first hypothesis can be favoured. It is also confirmed by the very low concentration of dissolved Fe even for very short equilibration times (Table 2.2).

Liquid phase of the time-series study

The results of the analyses of the ion concentrations in the liquid phase after different ageing times are presented in Table 2.2. The calcium concentration increased after 90 days up to 21 mmol/L but then decreased again to 15 mmol/L at 180 days when gypsum was not present any longer. The sulphur concentration increased slightly but steadily during 180 days ageing up to 17 mmol/L. The measured iron concentrations ranged from 0.08 to 0.1 $\mu\text{mol/L}$ but without a visible trend. Until 90 days of duration the pH is about 12.5, but at 180 days it decreased to 12.0. The calculated charge balance errors showed large negative errors for the first three samples (7, 24, and 45 days), indicating excess anions, respectively deficiency of cations (Table 2.2). Those samples were not considered for thermodynamic calculations.

On the basis of the solid characterization it became evident that after 180 days equilibrium was reached and that after 180 days the concentration of the ions in solution were determined by the solubility of Fe-ettringite. The very low concentration of iron confirmed the fast formation of amorphous FeOOH.

Table 2.2. Measured hydroxide (OH⁻), calcium (Ca), iron (Fe), sulphur (S) and potassium (K) concentrations in the aqueous solution after different times.

| Equilibration time in days | Measured pH | OH ⁻ [mmol/L] | Ca [mmol/L] | Fe [μmol/L] | S [mmol/L] | K [mmol/L] | Charge balance error ^a [%] |
|----------------------------|-------------|--------------------------|--------------|---------------|--------------|--------------|---------------------------------------|
| 7 | 12.4 | 28 | 7.03 ± 0.03 | 0.097 ± 0.001 | 13.30 ± 0.08 | 17.11 ± 0.07 | -27 |
| 24 | 12.5 | 35 | 6.94 ± 0.03 | 0.088 ± 0.002 | 13.96 ± 0.07 | 17.53 ± 0.11 | -33 |
| 45 | 12.5 | 32 | 8.22 ± 0.02 | 0.095 ± 0.001 | 15.46 ± 0.02 | 17.52 ± 0.04 | -30 |
| 90 | 12.5 | 29 | 21.37 ± 0.11 | 0.084 ± 0.001 | 15.65 ± 0.05 | 17.05 ± 0.07 | -0.6 |
| 180 | 12.0 | 10 | 14.62 ± 0.13 | 0.089 ± 0.001 | 17.07 ± 0.14 | 17.71 ± 0.16 | 3.1 |

Detection limits: Ca: 0.02 mmol/L; Fe: 0.001 μmol/L; S: 0.2 mmol/L; K: 0.03 mmol/L.

Blank (0.04 MKOH-solution): Ca: < 0.02 mmol/L; Fe: < 0.001 μmol/L; S: < 0.2 mmol/L.

Standard deviation was calculated from repeated analytical measurements of single samples.

$$(a) \text{ Charge balance error} = \frac{\sum_{\text{cations}} z_i c_i - \sum_{\text{anions}} z_j c_j}{\sum_{\text{cations}} z_i c_i + \sum_{\text{anions}} z_j c_j} \times 100$$

2.4.2 Precipitation and dissolution experiments

Solid phase of the precipitation and dissolution experiments

XRD analyses of the solid phases of the precipitation experiment indicated that Fe-ettringite was formed at pH-values from 11.6 up to 13.2 (cf. Fig. 2.4A). Above a pH of approximately 13.1 Fe-ettringite became instable with respect to Fe-monosulphate. At pH-values above 13.1, where Fe-monosulphate was present, portlandite precipitated as under these conditions an excess of calcium was present. At pH-values above 13.4 the formation of Fe-monocarbonate was observed.

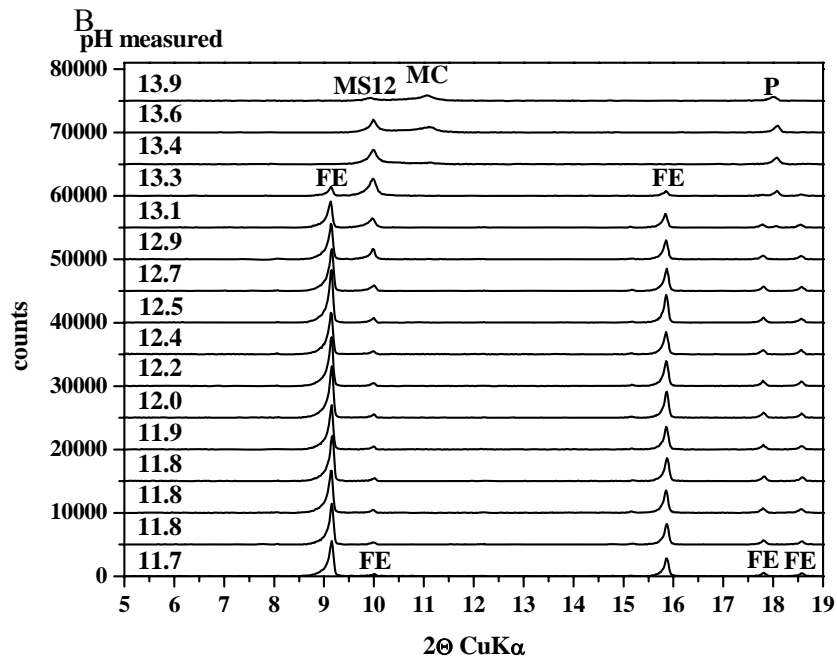
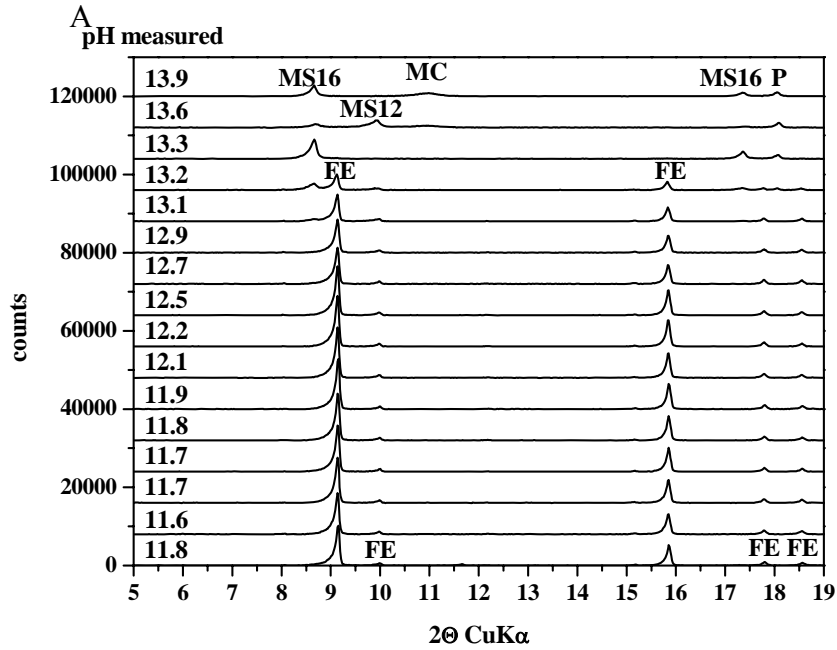


Fig. 2.4. X-ray diffraction spectra for precipitation (A) and dissolution (B) experiments. FE: Fe-ettringite (main peak at $2\theta = 9.13^\circ$ (McMurdie et al., 1987)); MS16: $\text{Ca}_4[\text{Fe}(\text{OH})_6]_2(\text{SO}_4) \cdot 10\text{H}_2\text{O}$ (main peak $2\theta = 8.65^\circ$ (Ecker and Pöllmann, 1994)); MS12: $\text{Ca}_4[\text{Fe}(\text{OH})_6]_2(\text{SO}_4) \cdot 6\text{H}_2\text{O}$ (main peak $2\theta = 9.94^\circ$ (Ecker and Pöllmann, 1994)); MC: $(\text{Ca}_4[\text{Fe}(\text{OH})_6]_2(\text{CO}_3) \cdot 6\text{H}_2\text{O})$, main peak $2\theta = 11.14^\circ$ (Ecker, 1998); P: portlandite (main peak $2\theta = 18.07^\circ$).

Based on the available data it was difficult to decide whether $\text{Ca}_4[\text{Fe}(\text{OH})_6]_2(\text{OH})_2 \cdot 6\text{H}_2\text{O}$ or Fe-monocarbonate was formed at $\text{pH} \geq 13.6$. The XRD peaks of both phases are in a similar range (cf. Fig. 2.5, Ecker, 1998 and Gallias, 1998). But it is possible that the XRD peaks for $\text{Ca}_4[\text{Fe}(\text{OH})_6]_2(\text{OH})_2 \cdot 6\text{H}_2\text{O}$ as given by Gallias (1998) correspond also to Fe-monocarbonate since in the experiments of Gallias CO_2 was not excluded.

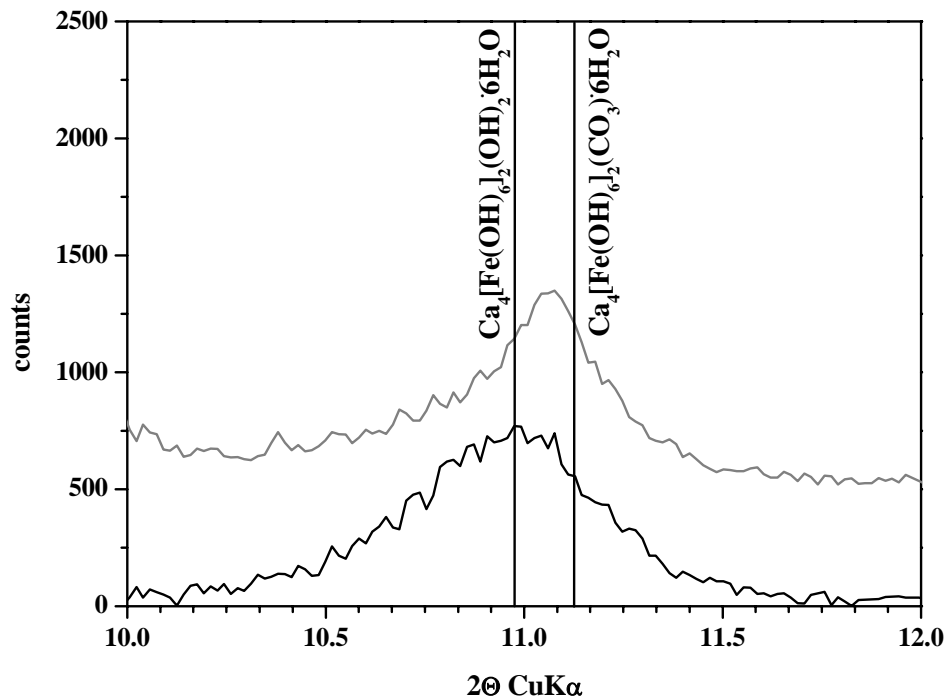


Fig. 2.5. X-ray diffraction spectra for the precipitation sample (black) and for the dissolution sample (grey) at $\text{pH} = 13.9$. The main peaks of $\text{Ca}_4[\text{Fe}(\text{OH})_6]_2(\text{OH})_2 \cdot 6\text{H}_2\text{O}$ $2\theta = 10.97^\circ$ (Gallias, 1998) and $\text{Ca}_4[\text{Fe}(\text{OH})_6]_2(\text{CO}_3) \cdot 6\text{H}_2\text{O}$ $2\theta = 11.14^\circ$ (Ecker, 1998) are plotted.

The presence of small amounts of calcite (at $\text{pH} \geq 12.9$) and Fe-monocarbonate (at $\text{pH} \geq 13.6$) in our experiments (Fig. 2.6) indicated the ingress of CO_2 during the experiments which is a prerequisite for the formation of Fe-monocarbonate. It is assumed but not confirmed that CO_2 entered the solid phase during the long equilibration times of 180, respectively 360 days, even special attention was paid to exclude the ingress of CO_2 .

In pure Al-systems the formation of Al-monocarbonate is observed in the presence of CaCO_3 and of Al-hemicarbonate at lower CO_2 -partial pressure while

$\text{Ca}_4[\text{Al}(\text{OH})_6]_2(\text{OH})_2 \cdot 6\text{H}_2\text{O}$ is only stable in the absence of CO_2 (cf. Kuzel and Pöllmann, 1991; Damidot et al., 1994). In analogue to the Al-system it seems therefore rather likely that the solid observed at $\text{pH} \geq 13.6$ was Fe-monocarbonate.

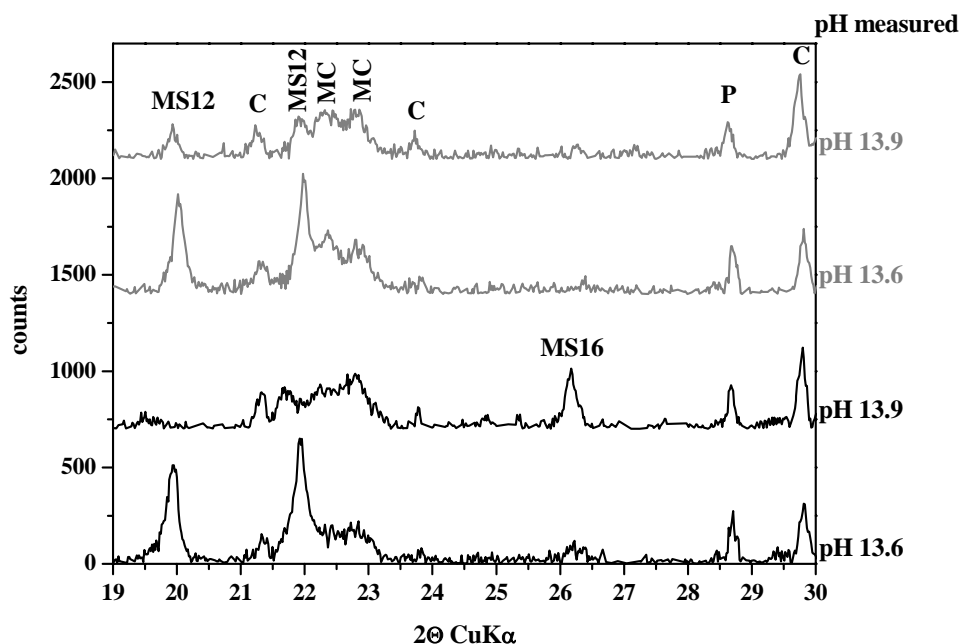


Fig. 2.6. X-ray diffraction spectra for the samples of the precipitation (black) and dissolution (grey) experiment at $\text{pH} = 13.6$ and 13.9 . MS12: $\text{Ca}_4[\text{Fe}(\text{OH})_6]_2(\text{SO}_4) \cdot 6\text{H}_2\text{O}$; C: calcite; MC: $\text{Ca}_4[\text{Fe}(\text{OH})_6]_2(\text{CO}_3) \cdot 6\text{H}_2\text{O}$; MS16: $\text{Ca}_4[\text{Fe}(\text{OH})_6]_2(\text{SO}_4) \cdot 10\text{H}_2\text{O}$; P: portlandite.

In pure Al-system the existence of CO_3 -ettringite (tricarboaluminate) has been reported (Poellmann et al., 1990). Its solubility is reported to be higher than the solubility of SO_4 -containing ettringite (Damidot et al., 1994). The formation of the iron containing analogue ($\text{Ca}_6[\text{Fe}(\text{OH})_6]_2(\text{CO}_3)_3 \cdot 26\text{H}_2\text{O}$) of tricarboaluminate is not likely as in the experiments presented here, carbonate activities were at least 1000 times lower than sulphate activities (cf. Table 2.3). In addition, inclusion of significant CO_3^{2-} would lead to a clear XRD peak shift towards higher 2θ values (Poellmann et al., 1990) which was not observed. In contrast to ettringite, no solid solution between monosulphate ($\text{Ca}_4[\text{Al}(\text{OH})_6]_2(\text{SO}_4) \cdot 6\text{H}_2\text{O}$) and monocarbonate ($\text{Ca}_4[\text{Al}(\text{OH})_6]_2(\text{CO}_3) \cdot 6\text{H}_2\text{O}$) exists in pure Al-systems (Poellmann, 1984; Matschei et al., 2007). For both, Fe-monosulphate and Fe-monocarbonate no significant peak shifts with regard to literature data were observed (cf. Table 2.4)

indicating that, analogue to Al-containing solids, no significant uptake of CO_3^{2-} in Fe-monosulphate or of SO_4^{2-} in Fe-monocarbonate occurred.

In the precipitation experiments two forms of Fe-monosulphate with different water content could be detected: $\text{Ca}_4[\text{Fe}(\text{OH})_6]_2(\text{SO}_4)\cdot 6\text{H}_2\text{O}$ (MS12) and $\text{Ca}_4[\text{Fe}(\text{OH})_6]_2(\text{SO}_4)\cdot 10\text{H}_2\text{O}$ (MS16). The presence of a monosulphate phase containing more water indicated that drying time (two weeks) was not long enough and some of the samples were not sufficiently dried.

Thermogravimetric analyses showed that Fe-ettringite lost its water between 30 and 140 °C (cf. Fig. 2.7A). The moles of crystalline water in the synthesised Fe-ettringite ranged between 29 and 33. The water of Fe-monosulphate evaporated between 160 and 200 °C. At pH 13.6 and 13.9 it was possible to see a peak between 140 and 160 °C indicating also the presence of Fe-monocarbonate. In addition, portlandite (water loss between 400 and 450 °C) could be detected at $\text{pH} \geq 13.2$ as well as the loss of CO_2 between 650 and 710 °C which is an evidence for both, Fe-monocarbonate and calcite. Evaluation of the crystalline water in Fe-monosulphate and Fe-monocarbonate was not possible due to coexistence of three to four phases and overlapping peaks. However, the amount of water as derived from XRD studies have been used (Ecker and Pöllmann 1994; Ecker 1998).

The XRD analyses indicated for Fe-ettringite in the presence of saturated CaCl_2 -solutions a total water content of around 32 H_2O (confirmed by water loss measured by TGA). Studies of McMurdie et al. (1987) indicate that Fe-ettringite contained approximately 32 H_2O molecules. This number corresponds to the number of water molecules found in Al-ettringite and is used throughout this paper.

For Fe-monosulphate 12 H_2O , respectively 16 H_2O molecules were observed. This agrees well with the findings of their Al-analogues where under identical drying conditions the same number of H_2O molecules is present (cf. Taylor, 1997). Fe-monocarbonate contains 12 H_2O molecules per formula unit as found by Ecker (1998) by TGA and XRD analyses.

Table 2.3. Calculated ion activities and solubility products of Fe-ettringite (FE), Fe-monosulphate (MS) and Fe-monocarbonate (MC) at 20 °C.

| Measured pH | log {Ca ²⁺ } | log {Fe(OH) ₄ ⁻ } | log {SO ₄ ²⁻ } | log {OH ⁻ } ^a | log {CO ₃ ²⁻ } | log {H ₂ O} | log K _{SO} FE | log K _{SO} MS | log _a K _{SO} MC |
|----------------------------------|-------------------------|---|--------------------------------------|-------------------------------------|--------------------------------------|------------------------|-----------------------------|---------------------------|-------------------------------------|
| Precipitation experiments | | | | | | | | | |
| 11.8 | -2.26 | -7.12 | -2.36 | -2.22 | - | -0.001 | -43.7 | | |
| 11.6 | -2.29 | -7.07 | -2.36 | -2.33 | - | -0.001 | -44.3 | | |
| 11.7 | -2.32 | -7.13 | -2.38 | -2.28 | - | -0.001 | -44.4 | | |
| 11.7 | -2.30 | -7.13 | -2.34 | -2.26 | - | -0.001 | -44.1 | | |
| 11.8 | -2.36 | -6.99 | -2.37 | -2.23 | - | -0.001 | -44.2 | | |
| 11.9 | -2.48 | -7.15 | -2.40 | -2.17 | - | -0.001 | -45.1 | | |
| 12.1 | -2.56 | -7.14 | -2.41 | -1.98 | - | -0.001 | -44.8 | | |
| 12.2 | -2.84 | -7.11 | -2.44 | -1.84 | - | -0.001 | -45.9 | | |
| 12.5 | -2.88 | -7.14 | -2.51 | -1.55 | - | -0.002 | -45.3 | | |
| 12.7 | -2.94 | -7.18 | -2.45 | -1.36 | - | -0.002 | -44.8 | | |
| 12.9 | -2.87 | -7.08 | -2.45 | -1.13 | -5.44 | -0.003 | -43.3 | | |
| 13.1 | -3.07 | -7.22 | -2.27 | -0.98 | -5.29 | -0.004 | -43.7 | -32.9 | |
| 13.2 | -3.28 | -7.12 | -2.04 | -0.86 | -5.03 | -0.005 | | -32.8 | |
| 13.3 | -3.54 | -7.15 | -1.92 | -0.71 | -4.78 | -0.008 | | -33.2 | |
| 13.6 | -4.03 | -6.91 | -1.99 | -0.45 | -4.30 | -0.011 | | -33.7 | -36.0 |
| 13.9 | -4.51 | -6.57 | -2.09 | -0.22 | -3.83 | -0.017 | | -34.2 | -35.9 |
| | | | | | | | Mean average | | |
| | | | | | | | -44.5 | -33.4 | -36.0 |
| | | | | | | | ± 0.7 | ± 0.6 | |
| Dissolution experiments | | | | | | | | | |
| 11.7 | -2.34 | -6.86 | -2.46 | -2.29 | - | -0.001 | -44.3 | | |
| 11.8 | -2.36 | -7.04 | -2.48 | -2.24 | - | -0.001 | -44.6 | | |
| 11.8 | -2.39 | -7.03 | -2.50 | -2.22 | - | -0.001 | -44.8 | | |
| 11.8 | -2.40 | -7.08 | -2.46 | -2.23 | - | -0.001 | -44.9 | | |
| 11.9 | -2.47 | n.d. | -2.51 | -2.14 | - | -0.001 | n.p. | | |
| 12.0 | -2.54 | -7.02 | -2.50 | -2.05 | - | -0.001 | -44.9 | | |
| 12.2 | -2.69 | -6.99 | -2.59 | -1.89 | - | -0.001 | -45.4 | | |
| 12.4 | -2.85 | -6.91 | -2.64 | -1.70 | - | -0.001 | -45.7 | | |
| 12.5 | -3.05 | -6.78 | -2.61 | -1.52 | - | -0.002 | -45.8 | | |
| 12.7 | -3.06 | -6.97 | -2.60 | -1.33 | - | -0.002 | -45.4 | -34.1 | |
| 12.9 | -3.07 | -7.03 | -2.57 | -1.10 | - | -0.003 | -44.6 | -33.3 | |
| 13.1 | -3.12 | -7.10 | -2.43 | -0.93 | - | -0.004 | -44.0 | -32.8 | |
| 13.3 | -3.43 | -7.06 | -2.24 | -0.80 | -4.99 | -0.005 | | -33.3 | |
| 13.4 | -3.78 | -7.00 | -2.19 | -0.60 | -4.55 | -0.008 | | -33.7 | -36.0 |
| 13.6 | -4.19 | -6.72 | -2.29 | -0.39 | -4.13 | -0.011 | | -34.1 | -35.9 |
| 13.9 | -4.63 | -6.21 | -2.38 | -0.18 | -3.71 | -0.017 | | -34.1 | -35.4 |
| | | | | | | | Mean average | | |
| | | | | | | | -44.9 | -33.6 | -35.8 ± |
| | | | | | | | ± 0.6 | ± 0.5 | 0.3 |
| | | | | | | | Overall mean average | | |
| | | | | | | | -44.7 | -33.5 | -35.9 ± |
| | | | | | | | ± 0.7 | ± 0.5 | 0.3 |

n.d.: not determined.

n.p.: Calculation was not possible due to the missing Fe concentration.

(a) {OH⁻} were adjusted to adjust charge balance. The calculated values agreed within ± 10% with the measured data (cf. Table 2.5).

Table 2.4. Comparison of powder XRD peaks from literature with selected solid phases of the dissolution experiments.

| Fe-ettringite | | | | | | | | | | | | | | | |
|------------------|---------------|--------------------------|---------------|-------------|---------------|-------------|---------------|-------------|---------------|--------------|---------------|--------------|---------------|--------------|--|
| | | McMurdie et al. (1987) | | pH 11.8 | | pH 12.2 | | pH 12.5 | | pH 12.9 | | pH 13.4 | | pH 13.9 | |
| h,k,l | $d(\text{Å})$ | I/I_{max} ^a | $d(\text{Å})$ | I/I_{max} | $d(\text{Å})$ | I/I_{max} | $d(\text{Å})$ | I/I_{max} | $d(\text{Å})$ | I/I_{max} | $d(\text{Å})$ | I/I_{max} | $d(\text{Å})$ | I/I_{max} | |
| 1 0 0 | 9.680 | 100 | 9.641 | 100 | 9.659 | 100 | 9.659 | 100 | 9.677 | 100 | - | - | - | - | |
| 1 0 1 | 8.860 | 8 | 8.855 | 5 | 8.855 | 6 | 8.855 | 8 | 8.880 | ^d | - | - | - | - | |
| 1 0 3 | 5.848 | 5 | 5.852 | < 1 | 5.852 | 2 | 5.852 | 2 | 5.846 | 2 | - | - | - | - | |
| 1 1 0 | 5.586 | 62 | 5.584 | 51 | 5.590 | 51 | 5.590 | 53 | 5.590 | 54 | - | - | - | - | |
| 1 1 2 | 4.981 | 14 | 4.981 | 10 | 4.985 | 11 | 4.981 | 10 | 4.981 | 10 | - | - | - | - | |
| 1 0 4 | 4.782 | 13 | 4.781 | 7 | 4.781 | 10 | 4.781 | 8 | 4.781 | 10 | - | - | - | - | |
| 2 0 3 | 4.039 | 7 | 4.039 | 5 | 4.039 | 5 | 4.039 | 5 | 4.042 | 7 | - | - | - | - | |
| 1 1 4 | 3.921 | 58 | 3.919 | 37 | 3.919 | 41 | 3.922 | 36 | 3.919 | 45 | - | - | - | - | |
| 2 0 4 | 3.633 | 14 | 3.635 | 10 | 3.635 | 10 | 3.635 | 9 | 3.635 | 12 | - | - | - | - | |
| 2 1 2 | 3.470 | 17 | 3.471 | 12 | 3.474 | 12 | 3.474 | 13 | 3.474 | 13 | - | - | - | - | |
| 2 1 3 | 3.273 | 4 | 3.275 | 3 | 3.275 | 2 | 3.275 | 3 | 3.275 | 3 | - | - | - | - | |
| 3 0 0 | 3.227 | 12 | 3.228 | 11 | 3.230 | 10 | 3.230 | 10 | 3.230 | 11 | - | - | - | - | |
| 1 1 6 | 3.066 | 4 | 3.067 | 2 | 3.067 | 3 | 3.067 | 3 | 3.067 | 3 | - | - | - | - | |
| 2 1 4 | 3.046 | 4 | 3.046 | 2 | 3.046 | 2 | 3.046 | 2 | 3.048 | 3 | - | - | - | - | |
| 3 0 4 | 2.783 | 33 | 2.784 | 22 | 2.785 | 23 | 2.785 | 21 | 2.785 | 25 | - | - | - | - | |
| 0 0 8 | 2.753 | 4 | 2.754 | 2 | 2.754 | 2 | 2.751 | 4 | 2.752 | 3 | - | - | - | - | |
| 2 2 2 | 2.710 | 2 | 2.711 | 1 | 2.711 | 1 | 2.710 | < 1 | 2.713 | 1 | - | - | - | - | |
| 3 1 2 | 2.610 | 13 | 2.610 | 7 | 2.611 | 7 | 2.611 | 6 | 2.611 | 8 | - | - | - | - | |
| 2 1 6 | 2.590 | 34 | 2.590 | 21 | 2.592 | 21 | 2.591 | 19 | 2.592 | 25 | - | - | - | - | |
| 3 1 6 | 2.166 | 14 | 2.167 | 8 | 2.168 | 8 | 2.168 | 8 | 2.169 | 8 | - | - | - | - | |
| Fe-monosulphate | | | | | | | | | | | | | | | |
| | | PDF 42-1472 ^b | | pH 11.8 | | pH 12.2 | | pH 12.5 | | pH 12.9 | | pH 13.4 | | pH 13.9 | |
| h,k,l | $d(\text{Å})$ | I/I_{max} | $d(\text{Å})$ | I/I_{max} | $d(\text{Å})$ | I/I_{max} | $d(\text{Å})$ | I/I_{max} | $d(\text{Å})$ | I/I_{max} | $d(\text{Å})$ | I/I_{max} | $d(\text{Å})$ | I/I_{max} | |
| 0 0 3 | 8.891 | 100 | - | - | - | - | - | - | 8.855 | 100 | 8.855 | 100 | 8.885 | 100 | |
| 0 1 2 | 4.761 | 5 | - | - | - | - | - | - | 4.760 | 6 | 4.751 | 3 | 4.769 | 2 | |
| 0 0 6 | 4.445 | 63 | - | - | - | - | - | - | 4.439 | 22 | 4.432 | 24 | 4.439 | 28 | |
| 1 0 4 | 4.051 | 45 | - | - | - | - | - | - | 4.048 | 26 | 4.048 | 26 | 4.057 | 49 | |
| 1 0 7 | 3.050 | 7 | - | - | - | - | - | - | 3.052 | 8 | 3.050 | 2 | 3.048 | 3 | |
| 1 1 0 | 2.944 | 28 | - | - | - | - | - | - | 2.946 | 12 | 2.943 | 32 | 2.945 | ^e | |
| 1 1 3 | 2.794 | 12 | - | - | - | - | - | - | 2.797 | 19 | 2.797 | 10 | 2.795 | 24 | |
| 2 0 2 | 2.505 | 7 | - | - | - | - | - | - | 2.505 | 5 | 2.504 | 6 | 2.505 | ^e | |
| 1 1 6 | 2.454 | 20 | - | - | - | - | - | - | 2.457 | 8 | 2.456 | 10 | 2.455 | 11 | |
| 0 2 4 | 2.382 | 9 | - | - | - | - | - | - | 2.383 | 6 | 2.383 | 8 | 2.379 | ^e | |
| 1 0 10 | 2.363 | 11 | - | - | - | - | - | - | 2.364 | 4 | 2.366 | 7 | 2.366 | ^e | |
| 0 1 11 | 2.188 | 3 | - | - | - | - | - | - | 2.188 | 3 | 2.190 | 2 | 2.187 | 10 | |
| 0 2 7 | 2.119 | 4 | - | - | - | - | - | - | 2.119 | 6 | 2.119 | 2 | 2.119 | 8 | |
| 1 1 9 | 2.089 | 17 | - | - | - | - | - | - | 2.090 | 6 | 2.089 | 8 | 2.085 | ^f | |
| 2 0 8 | 2.026 | 2 | - | - | - | - | - | - | 2.027 | 3 | 2.028 | < 1 | 2.027 | 6 | |
| 1 0 13 | 1.903 | 6 | - | - | - | - | - | - | 1.904 | 2 | 1.906 | 3 | 1.905 | 8 | |
| 2 1 4 | 1.852 | 4 | - | - | - | - | - | - | 1.850 | 1 | 1.853 | 3 | 1.852 | 12 | |
| 0 2 10 | 1.843 | 9 | - | - | - | - | - | - | 1.843 | 3 | 1.842 | 6 | 1.843 | 22 | |
| 1 1 12 | 1.774 | 3 | - | - | - | - | - | - | 1.774 | 3 | 1.776 | 4 | 1.774 | 9 | |
| 2 1 7 | 1.720 | 2 | - | - | - | - | - | - | 1.719 | 4 | 1.721 | 1 | 1.720 | 10 | |
| 3 0 0 | 1.700 | 10 | - | - | - | - | - | - | 1.701 | 9 | 1.701 | 10 | 1.701 | 30 | |
| Fe-monocarbonate | | | | | | | | | | | | | | | |
| | | PDF 43-480 ^c | | pH 11.8 | | pH 12.2 | | pH 12.5 | | pH 12.9 | | pH 13.4 | | pH 13.9 | |
| h,k,l | $d(\text{Å})$ | I | $d(\text{Å})$ | I/I_{max} | $d(\text{Å})$ | I/I_{max} | $d(\text{Å})$ | I/I_{max} | $d(\text{Å})$ | I/I_{max} | $d(\text{Å})$ | I/I_{max} | $d(\text{Å})$ | I/I_{max} | |
| 0 0 6 | 7.936 | 100 | - | - | - | - | - | - | - | - | 7.939 | 100 | 7.988 | 100 | |
| 0 0 12 | 3.973 | 65 | - | - | - | - | - | - | - | - | 3.972 | 46- | 3.984 | 30 | |
| 0 1 8 | 3.885 | 20 | - | - | - | - | - | - | - | - | 3.885 | 22 | 3.891 | 30 | |
| 1 1 0 | 2.959 | 23 | - | - | - | - | - | - | - | - | 2.961 | 64 | 2.959 | 53 | |
| 0 1 14 | 2.838 | 2 | - | - | - | - | - | - | - | - | 2.838 | ^f | 2.839 | 3 | |
| 1 1 6 | 2.773 | 15 | - | - | - | - | - | - | - | - | 2.774 | 33 | 2.770 | 19 | |
| 0 0 18 | 2.650 | 2 | - | - | - | - | - | - | - | - | 2.649 | ^g | 2.650 | ^g | |
| 1 1 9 | 2.582 | 15 | - | - | - | - | - | - | - | - | 2.582 | 16 | 2.582 | 14 | |
| 0 2 4 | 2.504 | 8 | - | - | - | - | - | - | - | - | 2.504 | ^d | 2.503 | 20 | |
| 1 1 12 | 2.373 | 23 | - | - | - | - | - | - | - | - | 2.372 | 60 | 2.374 | 27 | |
| 2 0 8 | 2.353 | 8 | - | - | - | - | - | - | - | - | 2.352 | 13 | 2.354 | 12 | |
| 0 1 20 | 2.162 | 22 | - | - | - | - | - | - | - | - | 2.159 | 11 | 2.166 | 11 | |

| | | | | | | | | | | | | | | | |
|--------|-------|----|---|---|---|---|---|---|---|---|---|-------|----|-------|----|
| 2 0 14 | 2.047 | 7 | - | - | - | - | - | - | - | - | - | 2.049 | 1 | 2.048 | 8 |
| 1 0 22 | 1.997 | 3 | - | - | - | - | - | - | - | - | - | 1.998 | 7 | 1.998 | 4 |
| 1 1 18 | 1.973 | 16 | - | - | - | - | - | - | - | - | - | 1.972 | 12 | 1.975 | 7 |
| 1 2 5 | 1.897 | 3 | - | - | - | - | - | - | - | - | - | 1.899 | f | 1.898 | 4 |
| 2 0 20 | 1.746 | 10 | - | - | - | - | - | - | - | - | - | 1.746 | 6 | 1.748 | 7 |
| 0 1 26 | 1.726 | 5 | - | - | - | - | - | - | - | - | - | 1.725 | 9 | 1.728 | 5 |
| 3 0 0 | 1.708 | 20 | - | - | - | - | - | - | - | - | - | 1.710 | 16 | 1.710 | 19 |
| 1 2 14 | 1.684 | 3 | - | - | - | - | - | - | - | - | - | 1.686 | g | 1.685 | g |
| 3 0 6 | 1.670 | 15 | - | - | - | - | - | - | - | - | - | 1.670 | g | 1.672 | 20 |
| 1 1 24 | 1.649 | 3 | - | - | - | - | - | - | - | - | - | 1.649 | 6 | 1.647 | 2 |
| 3 0 12 | 1.570 | 6 | - | - | - | - | - | - | - | - | - | 1.570 | 4 | 1.571 | 5 |

(a) I/I_{\max} : relative peak intensity (peak intensity/maximum peak intensity).

(b) PDF 42-1472: powder diffraction file for Fe-monosulphate ($\text{Ca}_4[\text{Fe}(\text{OH})_6]_2(\text{SO}_4)\cdot 6\text{H}_2\text{O}$) (Ecker and Pollmann, 1991)..

(c) PDF 43-480: powder diffraction file for Fe-monocarbonate ($\text{Ca}_4[\text{Fe}(\text{OH})_6]_2(\text{CO}_3)\cdot 6\text{H}_2\text{O}$) (Pollmann and Ecker, 1992).

(d) Peaks overlapped with peaks of Fe-monosulphate.

(e) Peaks overlapped with peaks of Fe-monocarbonate.

(f) Peaks overlapped with peaks of calcite.

(g) Peaks overlapped with peaks of portlandite.

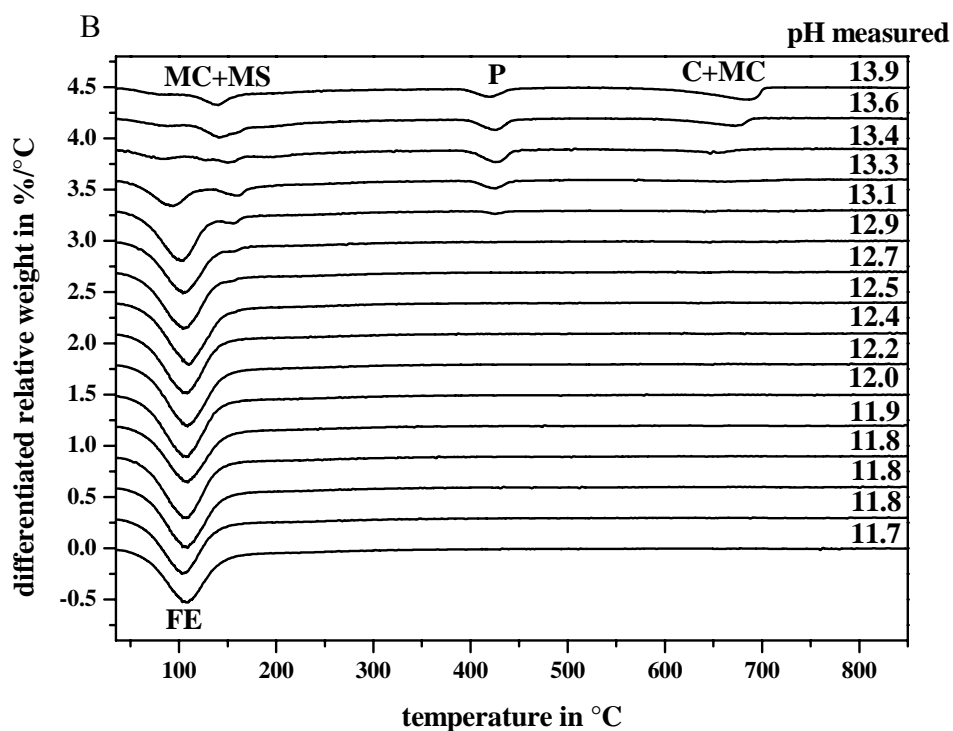
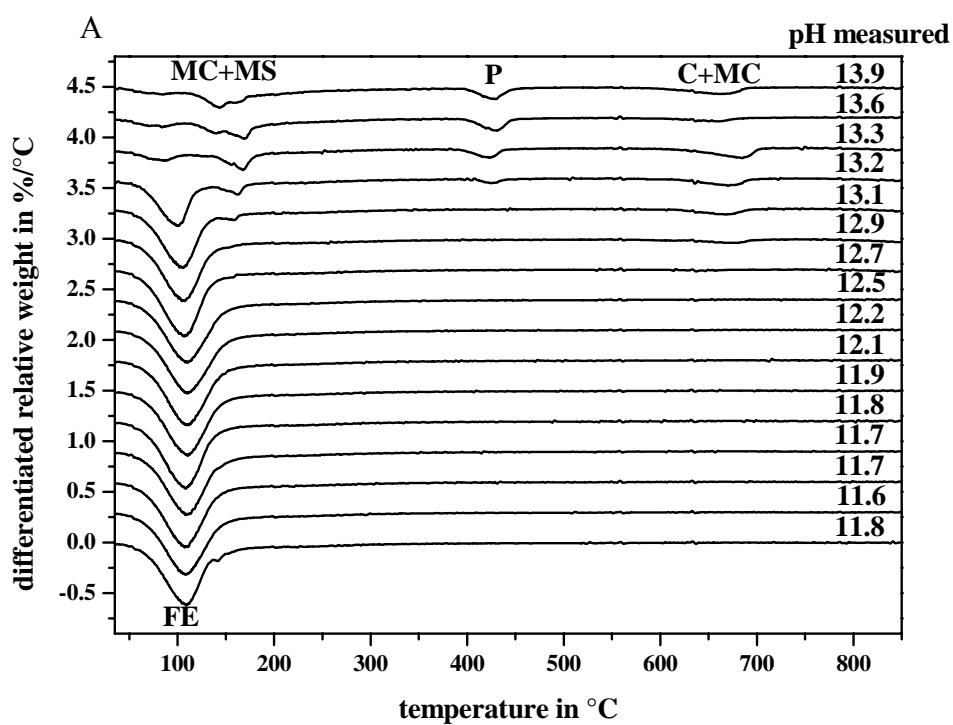


Fig. 2.7. Derivative curves of thermogravimetric analyses for precipitation (A) and dissolution (B) experiments. FE: Fe-ettringite; MS: Fe-monosulphate; MC: Fe-monocarbonate; P: portlandite; C: calcite.

From the loss of water of the solid phases the masses of the different phases were estimated. The results are presented in Fig. 2.8A. For the samples with pH-values between 12.7 and 13.2 a higher weight of the solid phases was measured than the maximum of 2.5 g which was calculated (cf. section 2.3.2) to precipitate. This indicated that the solids were not dried completely. The calculated weight for the samples at $\text{pH} \geq 13.3$ was lower than the measured weight, because differentiation between Fe-monosulphate and Fe-monocarbonate peaks and between calcite and Fe-monocarbonate peaks, respectively, was not possible.

XRD analyses of the solid phases of the dissolution experiment indicated that Fe-ettringite was formed at pH-values from 11.7 up to 13.3 (Fig. 2.4B). At pH-values between 12.7 and 13.3 Fe-ettringite coexisted with Fe-monosulphate, and Fe-monosulphate coexisted with Fe-monocarbonate at pH-values ≥ 13.4 . Portlandite could be determined for the samples at pH-values ≥ 13.1 . For the dissolution experiment selected XRD results are presented in Table 2.4 with relative intensities and ideally, crystallographic planes designated.

Thermogravimetric analyses confirmed the results of XRD analyses. The amount of Fe-monosulphate and Fe-monocarbonate, as well as Fe-monocarbonate and calcite, could not be determined separately by TGA as the peaks overlapped strongly (Fig. 2.7B). The determined moles of crystalline water in the synthesised Fe-ettringite ranged between 26 and 29. The masses of the different phases formed during dissolution experiment were estimated from the loss of water during TGA measurements (Fig. 2.8B). Below pH 12 the masses of Fe-ettringite (Fig. 2.8) were lower than at higher pH-values. Therefore, it can be concluded that the optimum for the synthesis of Fe-ettringite is between pH-values of 12.0 and 13.0.

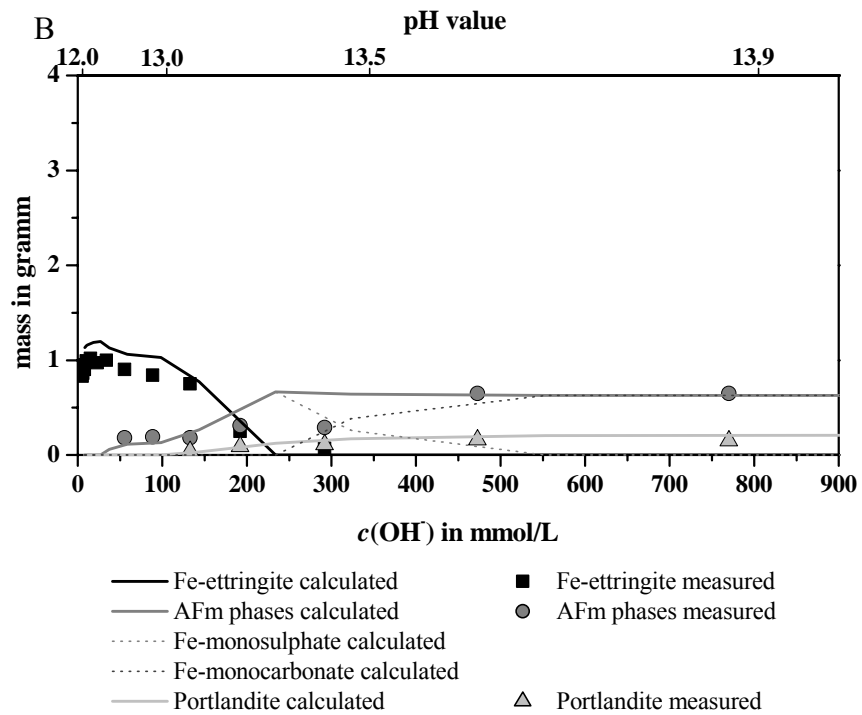
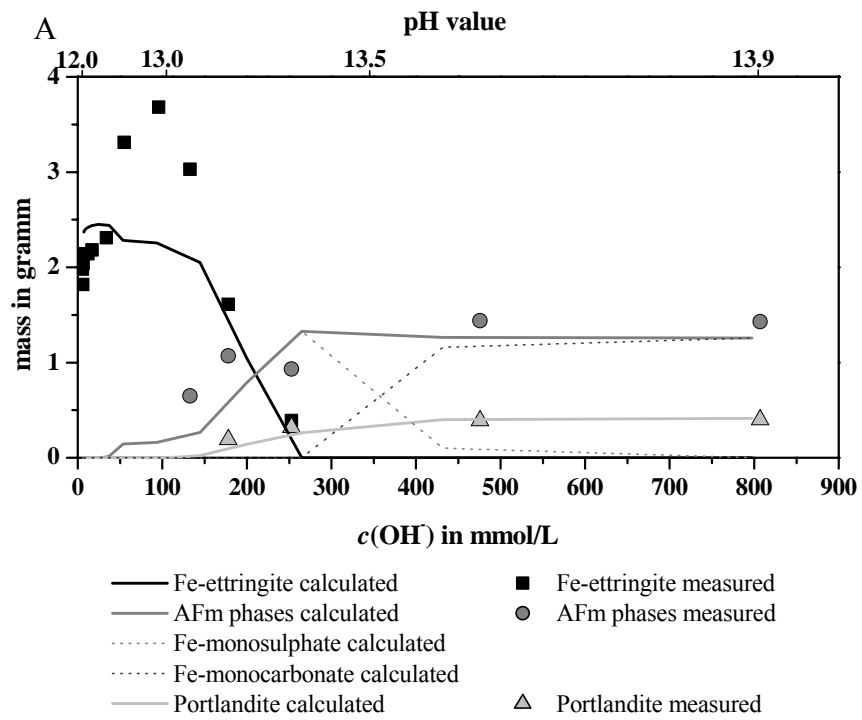


Fig. 2.8. Measured and calculated distribution and mass of the solid phases of precipitation (A) and dissolution (B) experiments.

Liquid phase of the precipitation and dissolution experiments

Analyses of the liquid phases of the precipitation and dissolution experiments gave information about the composition of the aqueous solution in equilibrium with the different solid phases. The results are presented in Table 2.5.

Table 2.5. Measured hydroxide (OH⁻), calcium (Ca), iron (Fe), sulphur (S), and potassium (K) concentrations in the aqueous solution.

| Measured pH | OH ⁻ [mmol/L] | Ca [mmol/L] | Fe [μmol/L] | S [mmol/L] | K [mmol/L] | Charge balance error [%] |
|----------------------------------|-----------------------------|----------------|-----------------------|---------------|---------------|-----------------------------|
| Precipitation experiments | | | | | | |
| 11.8 | 5.9 | 16.71 ± 0.03 | 0.091 ± 0.001 | 13.54 ± 0.07 | 1.23 ± 0.04 | 2.5 |
| 11.6 | 3.7 | 15.40 ± 0.05 | 0.102 ± 0.001 | 13.38 ± 0.09 | 1.69 ± 0.01 | 3.2 |
| 11.7 | 4.9 | 14.08 ± 0.01 | 0.091 ± 0.002 | 12.20 ± 0.18 | 2.64 ± 0.03 | 2.6 |
| 11.7 | 5.5 | 15.57 ± 0.03 | 0.090 ± 0.002 | 14.14 ± 0.14 | 4.01 ± 0.01 | 2.0 |
| 11.8 | 6.3 | 12.94 ± 0.04 | 0.124 ± 0.001 | 12.49 ± 0.02 | 6.30 ± 0.01 | 1.4 |
| 11.9 | 7.1 | 9.48 ± 0.02 | 0.084 ± 0.001 | 10.70 ± 0.05 | 10.52 ± 0.02 | 1.6 |
| 12.1 | 12 | 8.22 ± 0.01 | 0.086 ± 0.001 | 10.40 ± 0.04 | 16.86 ± 0.02 | 1.1 |
| 12.2 | 17 | 4.38 ± 0.01 | 0.094 ± 0.001 | 9.11 ± 0.07 | 26.45 ± 0.05 | 0.2 |
| 12.5 | 34 | 4.44 ± 0.02 | 0.088 ± 0.002 | 8.49 ± 0.06 | 42.07 ± 0.17 | -0.1 |
| 12.7 | 55 | 4.54 ± 0.01 | 0.084 ± 0.001 | 10.83 ± 0.05 | 64.96 ± 0.26 | -1.8 |
| 12.9 | 96 | 6.56 ± 0.09 | 0.109 ± 0.001 | 13.08 ± 0.17 | 104.7 ± 1.5 | -1.9 |
| 13.1 | 134 | 5.28 ± 0.01 | 0.082 ± 0.001 | 23.05 ± 0.12 | 165.1 ± 0.5 | -1.1 |
| 13.2 | 178 | 4.34 ± 0.01 | 0.107 ± 0.001 | 47.93 ± 0.10 | 263.4 ± 0.5 | -0.3 |
| 13.3 | 253 | 3.08 ± 0.02 | 0.104 ± 0.001 | 77.27 ± 0.15 | 395.7 ± 0.4 | -0.6 |
| 13.6 | 476 | 1.34 ± 0.01 | 0.187 ± 0.002 | 83.47 ± 0.25 | 630.7 ± 6.3 | -0.8 |
| 13.9 | 808 | 0.69 ± 0.01 | 0.417 ± 0.005 | 84.28 ± 1.69 | 974.7 ± 11.7 | 0.0 |
| Dissolution experiments | | | | | | |
| 11.7 | 5.1 | 12.46 ± 0.02 | 0.166 ± 0.003 | 9.90 ± 0.05 | 1.13 ± 0.04 | 2.2 |
| 11.8 | 6.0 | 11.75 ± 0.04 | 0.107 ± 0.001 | 9.13 ± 0.06 | 1.77 ± 0.01 | 2.1 |
| 11.8 | 6.4 | 10.74 ± 0.01 | 0.111 ± 0.001 | 8.47 ± 0.13 | 2.72 ± 0.03 | 1.8 |
| 11.8 | 6.2 | 10.75 ± 0.02 | 0.097 ± 0.001 | 9.37 ± 0.09 | 4.35 ± 0.01 | 1.8 |
| 11.9 | 7.8 | 8.85 ± 0.03 | <i>not determined</i> | 7.92 ± 0.02 | 6.85 ± 0.01 | 2.0 |
| 12.0 | 10 | 7.84 ± 0.02 | 0.114 ± 0.001 | 8.05 ± 0.04 | 11.13 ± 0.02 | 1.0 |
| 12.2 | 15 | 5.45 ± 0.01 | 0.121 ± 0.001 | 6.17 ± 0.02 | 16.73 ± 0.02 | 0.7 |
| 12.4 | 23 | 3.95 ± 0.01 | 0.148 ± 0.001 | 5.54 ± 0.04 | 26.52 ± 0.05 | 0.6 |
| 12.5 | 34 | 2.84 ± 0.01 | 0.202 ± 0.002 | 6.37 ± 0.04 | 42.92 ± 0.17 | 1.7 |
| 12.7 | 55 | 3.29 ± 0.01 | 0.136 ± 0.003 | 7.47 ± 0.04 | 65.14 ± 0.26 | 1.1 |
| 12.9 | 89 | 4.08 ± 0.06 | 0.121 ± 0.001 | 9.72 ± 0.13 | 109.3 ± 1.5 | 4.0 |
| 13.1 | 133 | 4.67 ± 0.01 | 0.107 ± 0.003 | 16.22 ± 0.08 | 169.0 ± 0.5 | 3.7 |
| 13.3 | 192 | 2.94 ± 0.01 | 0.121 ± 0.002 | 29.34 ± 0.06 | 252.8 ± 0.5 | 1.7 |
| 13.4 | 292 | 1.79 ± 0.01 | 0.146 ± 0.002 | 41.41 ± 0.08 | 404.3 ± 0.4 | 4.2 |
| 13.6 | 473 | 0.93 ± 0.01 | 0.289 ± 0.003 | 41.22 ± 0.12 | 618.2 ± 6.2 | 5.5 |
| 13.9 | 770 | 0.56 ± 0.01 | 0.975 ± 0.019 | 43.69 ± 0.87 | 966.0 ± 11.6 | 6.0 |

Detection limits: Ca: 0.02 mmol/L; Fe: 0.001 μmol/L; S: 0.2 mmol/L; K: 0.03 mmol/L.

Blank (0.04 MKOH-solution): Ca: < 0.02 mmol/L; Fe: < 0.001 μmol/L; S: < 0.2 mmol/L.

Standard deviation was calculated from repeated analytical measurements of single samples.

At pH-values from 11.6 to 11.9 the highest calcium concentrations for both, precipitation and dissolution experiment were obtained. The lowest calcium concentration occurred above pH 13 when additional to Fe-monosulphate and portlandite, Fe-monocarbonate was formed and Fe-ettringite was instable. The sulphur concentration in the solution increased

when Fe-monosulphate was formed and reached its maximum when in addition to Fe-monosulphate, Fe-monocarbonate was stable. The concentration of the iron ions in the aqueous solutions of the dissolution experiments was slightly higher than in the precipitation experiments. In both experiments the two samples with the highest pH-value also showed the highest iron concentrations. Fe(III) is present as $\text{Fe}(\text{OH})_4^-$ in alkaline solutions.

2.5 Thermodynamic modeling

2.5.1 Solubilities at 20 °C

The solubility of Fe-ettringite, Fe-monosulphate, and the apparent solubility of Fe-monocarbonate at 20 °C was calculated using GEMS (Kulik, 2006). GEMS is a broad-purpose geochemical modelling code which uses an advanced convex programming method of Gibbs energy minimisation and computes equilibrium phase assemblage and speciation in a complex chemical system from its total bulk elemental composition. Chemical interactions involving solids, solid solutions, gas mixture, and aqueous electrolyte are considered simultaneously in the chemical elemental stoichiometry of the system. The default database of GEMS code was used which is based on the PSI chemical thermodynamic database (Hummel et al., 2002). Initially, this database was designed in “log K format” for application to codes such as PHREEQC. These codes use law of mass action algorithms at standard conditions (1 bar and 25 °C). The log K values were converted into standard molar Gibbs energies and merged with slop98.dat database (originally developed for the SUPCRT92 code (Johnson et al. 1992)) to include it in GEMS (Thoenen and Kulik, 2003). For aqueous species this dataset is based on the Helgeson-Kirkham-Flowers (HKF) equation of state which is used to calculate temperature and pressure corrections up to 1000 °C and 5 kbar (Shock et al., 1997; Sverjensky et al. 1997). The thermodynamic data used are compiled in Table 2.6.

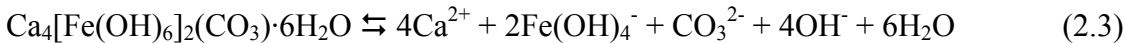
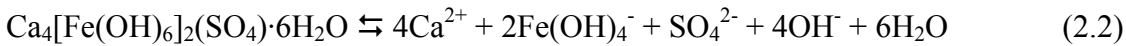
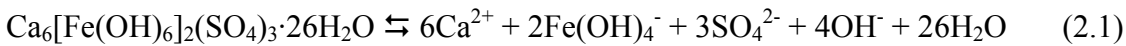
Table 2.6. Thermodynamic data of the used species to calculate ion and phase distribution of precipitation and dissolution experiments (at 25 °C).

| Aqueous species | | log K or log β | Reference |
|--|--|-------------------------------|-----------|
| $\text{Ca}^{2+} + \text{H}_2\text{O} \rightleftharpoons \text{CaOH}^+ + \text{H}^+$ | | -12.78 | a |
| $\text{Ca}^{2+} + \text{SO}_4^{2-} \rightleftharpoons \text{CaSO}_4^0$ | | 2.30 | a |
| $\text{Ca}^{2+} + \text{HCO}_3^- \rightleftharpoons \text{CaHCO}_3^+$ | | 1.106 | a |
| $\text{Ca}^{2+} + \text{HCO}_3^- \rightleftharpoons \text{CaCO}_3^0 + \text{H}^+$ | | -7.105 | a |
| $\text{K}^+ + \text{H}_2\text{O} \rightleftharpoons \text{KOH}^0 + \text{H}^+$ | | -14.46 | a |
| $\text{K}^+ + \text{SO}_4^{2-} \rightleftharpoons \text{KSO}_4^-$ | | 0.85 | a |
| $\text{H}_2\text{O} \rightleftharpoons \text{OH}^- + \text{H}^+$ | | -14.00 | a |
| $\text{Fe}^{3+} + \text{H}_2\text{O} \rightleftharpoons \text{Fe}(\text{OH})^{2+} + \text{H}^+$ | | -2.19 | a |
| $2\text{Fe}^{3+} + 2\text{H}_2\text{O} \rightleftharpoons \text{Fe}_2(\text{OH})_2^{4+} + 2\text{H}^+$ | | -2.95 | a |
| $3\text{Fe}^{3+} + 4\text{H}_2\text{O} \rightleftharpoons \text{Fe}_3(\text{OH})_4^{5+} + 4\text{H}^+$ | | -6.30 | a |
| $\text{Fe}^{3+} + 2\text{H}_2\text{O} \rightleftharpoons \text{Fe}(\text{OH})_2^+ + 2\text{H}^+$ | | -5.67 | a |
| $\text{Fe}^{3+} + 3\text{H}_2\text{O} \rightleftharpoons \text{Fe}(\text{OH})_3^0 + 3\text{H}^+$ | | -12.56 | a |
| $\text{Fe}^{3+} + 4\text{H}_2\text{O} \rightleftharpoons \text{Fe}(\text{OH})_4^- + 4\text{H}^+$ | | -21.60 | a |
| $\text{Fe}^{3+} + \text{H}^+ + \text{SO}_4^{2-} \rightleftharpoons \text{FeHSO}_4^{2+}$ | | 4.47 | a |
| $\text{Fe}^{3+} + \text{SO}_4^{2-} \rightleftharpoons \text{FeSO}_4^+$ | | 4.04 | a |
| $\text{Fe}^{3+} + 2\text{SO}_4^{2-} \rightleftharpoons \text{Fe}(\text{SO}_4)_2^-$ | | 5.38 | a |
| Minerals | Reactions | log K_{S0} | Reference |
| Gypsum | $\text{CaSO}_4 \cdot 2\text{H}_2\text{O}(\text{s}) \rightleftharpoons \text{Ca}^{2+} + \text{SO}_4^{2-} + 2\text{H}_2\text{O}$ | -4.58 | a |
| Portlandite | $\text{Ca}(\text{OH})_2(\text{s}) + 2\text{H}^+ \rightleftharpoons \text{Ca}^{2+} + 2\text{H}_2\text{O}$ | 22.80 | a |
| Calcite | $\text{CaCO}_3(\text{s}) + \text{H}^+ \rightleftharpoons \text{CaHCO}_3^+$ | 1.849 | a |
| Fe-ettringite | $\text{Ca}_6[\text{Fe}(\text{OH})_6]_2(\text{SO}_4)_3 \cdot 26\text{H}_2\text{O} \rightleftharpoons 6\text{Ca}^{2+} + 2\text{Fe}(\text{OH})_4^- + 3\text{SO}_4^{2-} + 4\text{OH}^- + 26\text{H}_2\text{O}$ | -44.0 ± 0.7 | b |
| Fe-monocarbonate | $\text{Ca}_4[\text{Fe}(\text{OH})_6]_2(\text{CO}_3) \cdot 5\text{H}_2\text{O} \rightleftharpoons 4\text{Ca}^{2+} + 2\text{Fe}(\text{OH})_4^- + \text{CO}_3^{2-} + 4\text{OH}^- + 6\text{H}_2\text{O}$ | -35.5 ± 0.3 (apparent) | b |
| Fe-monosulphate | $\text{Ca}_4[\text{Fe}(\text{OH})_6]_2(\text{SO}_4) \cdot 6\text{H}_2\text{O} \rightleftharpoons 4\text{Ca}^{2+} + 2\text{Fe}(\text{OH})_4^- + \text{SO}_4^{2-} + 4\text{OH}^- + 6\text{H}_2\text{O}$ | -33.2 ± 0.5 | b |
| Fe(OH) ₃ (am.) | $\text{Fe}(\text{OH})_3(\text{am}) + 3\text{H}^+ \rightleftharpoons \text{Fe}^{3+} + 3\text{H}_2\text{O}$ | 5.00 | a |
| Fe(OH) ₃ (microcr.) | $\text{Fe}(\text{OH})_3(\text{mic}) + 3\text{H}^+ \rightleftharpoons \text{Fe}^{3+} + 3\text{H}_2\text{O}$ | 3.00 | a |

(a) Hummel et al, 2002

(b) this study

The dissolution reactions of Fe-ettringite, Fe-monosulphate, and for Fe-monocarbonate are given by



According to these dissolution reactions the solubility products can be calculated from

$$K_{S0, \text{Fe-ettringite}} = \{\text{Ca}^{2+}\}^6 \cdot \{\text{Fe}(\text{OH})_4^-\}^2 \cdot \{\text{SO}_4^{2-}\}^3 \cdot \{\text{OH}^-\}^4 \cdot \{\text{H}_2\text{O}\}^{26} \quad (2.4)$$

$$K_{S0, \text{Fe-monosulphate}} = \{\text{Ca}^{2+}\}^4 \cdot \{\text{Fe}(\text{OH})_4^-\}^2 \cdot \{\text{SO}_4^{2-}\} \cdot \{\text{OH}^-\}^4 \cdot \{\text{H}_2\text{O}\}^6 \quad (2.5)$$

$$K_{S0, \text{Fe-monocarbonate}} = \{\text{Ca}^{2+}\}^4 \cdot \{\text{Fe}(\text{OH})_4^-\}^2 \cdot \{\text{CO}_3^{2-}\} \cdot \{\text{OH}^-\}^4 \cdot \{\text{H}_2\text{O}\}^6 \quad (2.6)$$

where $\{\}$ denotes the activity.

Activity coefficients of aqueous species γ_i were computed with the built-in expanded extended Debye-Hückel equation in Truesdell-Jones form with individual parameters a_i and common third parameter b_γ :

$$\log \gamma_i = \frac{-A_\gamma z_i^2 \sqrt{I}}{1 + B_\gamma a_i \sqrt{I}} + b_\gamma I \quad (2.7)$$

where z_i denotes the charge of species i , I the effective molal ionic strength, $b_\gamma = 0.064$, and A_γ and B_γ are P, T -dependent coefficients. This activity correction is thought to be applicable up to 1 – 2 molal ionic strength (Pearson and Berner, 1991; Kulik 2006).

GEMS minimises the Gibbs free energy of the system. The Gibbs free energy of reaction which is linked with the Gibbs free energy of formation $\Delta_r G^0$ is related to the solubility product K_{S0} by

$$\Delta_r G^0 = -RT \ln K_{S0} \quad (2.8)$$

where R is the gas constant (8.3145 J/(mol·K)) and T is the temperature in Kelvin.

On the basis of the measured ion concentrations and the analysed composition of the solid phases K_{S0} could be calculated with GEMS using the ion activities for every sample. The calculated solubility products as well as the calculated ion activities at 20 °C are presented in Table 2.3. No trends were observed for the calculated solubility products with increasing pH and ionic strength indicating that the used activity correction is applicable within the range of ionic strength studied. But the solubility products showed some variation and e.g. displayed a dip in the pH 12.2 – 12.5 region for Fe-ettringite. This dip might be the result of random measurement errors. However, it occurred in both the dissolution and precipitation samples. The reason for this is unknown. It could be due to missing thermodynamic data for key complexes that may effect ion activities. For the determination of the apparent solubility product (${}_aK_{S0}$) of Fe-monocarbonate it was assumed that the aqueous solutions were in equilibrium with the small amounts of calcite found at pH-values above 12.9. The equilibrium activities of CO_3^{2-} in equilibrium with calcite were used to calculate ${}_aK_{S0}$ of Fe-monocarbonate (Table 2.3). Because of the limited occurrence of Fe-monocarbonate and the estimated concentrations of CO_3^{2-} the

solubility of Fe-monocarbonates is called *apparent* solubility to stress the tenuous nature of the resulting solubility for this phase.

Using these solubility products reported in Table 2.3 and Eqn (2.8) the Gibbs free energies of reaction could be calculated for each phase at 20 °C:

$$\Delta_r G_{Fe-ettringite}^o = 250.87 \frac{kJ}{mol},$$

$$\Delta_r G_{Fe-monosulphate}^o = 188.01 \frac{kJ}{mol} \text{ and}$$

$$\Delta_r G_{Fe-monocarbonate}^o = 201.48 \frac{kJ}{mol}.$$

At 20 °C for Fe-ettringite $\Delta_r G^o$ is linked with the apparent Gibbs free energy of formation $\Delta_a G^o$ as follows

$$\Delta_r G^o = 6\Delta_a G^o (Ca^{2+}) + 2\Delta_a G^o (Fe(OH)_4^-) + 3\Delta_a G^o (SO_4^{2-}) + 4\Delta_a G^o (OH^-) + 26\Delta_a G^o (H_2O) - \Delta_a G_{Fe-ettringite}^o \quad (2.9)$$

Hence, $\Delta_a G_{Fe-ettringite}^o = -14272.73 \frac{kJ}{mol}$ was obtained using the apparent Gibbs free energies of formation of the individual species at 20 °C presented in Table 2.7. The apparent Gibbs free energy of formation refers to the Gibbs free energy of the elements at 25 °C; at 25 °C $\Delta_a G^o = \Delta_f G^o$. Further details concerning the apparent Gibbs free energy of formation (mostly used for elevated temperatures) is given in e.g. Anderson and Crerar (1993). The apparent Gibbs free energies of formation for Fe-monosulphate and Fe-monocarbonate were also calculated using Eqn. 2.9 and the apparent Gibbs free energies of formation of the individual species at 20 °C (see Table 2.7).

The measured and modelled ion concentrations (except potassium) as well as the measured and modelled solid phase composition (except iron hydroxide which is about 20 mg at pH = 12.0 decreased with increasing pH and vanished at pH-values ≥ 12.25) for the precipitation and dissolution experiments are presented in Fig. 2.8 and 2.9. The measured and the calculated data agree well.

Table 2.7. Thermodynamic data at 20 and 25 °C used to calculate the Gibbs free energy of formation of Fe-ettringite, Fe-monosulphate and Fe-monocarbonate.

| Species | $\Delta_a G^\circ$ [kJ/mol] at 20 °C | $\Delta_f G^\circ$ [kJ/mol] at 25 °C | Reference |
|------------------------------------|---|---|-----------|
| H ₂ O _{liquid} | -236.835 | -237.183 | a |
| OH ⁻ | -157.318 | -157.270 | a |
| Ca ²⁺ | -553.071 | -552.790 | a |
| CO ₃ ²⁻ | -528.220 | 527.982 | a |
| Fe(OH) ₄ ⁻ | -841.696 | -842.624 | a |
| SO ₄ ²⁻ | -744.353 | -744.459 | a |
| Fe-ettringite | -14272.73 | -14282.36 | b |
| Fe-monosulphate | -6878.32 | -6882.55 | b |
| Fe-monocarbonate | -6675.66 | -6679.20 | b |

(a) Thoenen and Kulik, 2003. In GEMS, the log K data of the PSI Database (Hummel et al, 2002) which are applicable at standard pressure and temperature only are merged with a subset of the SUPCRT database which is documented in detail in Thoenen and Kulik (2003)

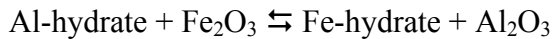
(b) this study

2.5.2 Solubilities at standard conditions

The Gibbs free energy of formation $\Delta_f G^\circ$ at 25 °C and respectively the solubility products of the different solids can be calculated from $\Delta_a G^\circ$, the entropy S° , and the heat capacity C_p° at 20 °C.

S° and C_p° were estimated from their Al-containing analogues at 20 °C (cf. Table 2.8) assuming $\Delta_r S^\circ = 0$ and $\Delta_r C_p^\circ = 0$ for isocolumbic reactions involving only solids (cf. Anderson and Crerar, 1993 or Gu et al., 1994).

The entropy and the heat capacity were calculated from their Al-containing analogues using the reaction:



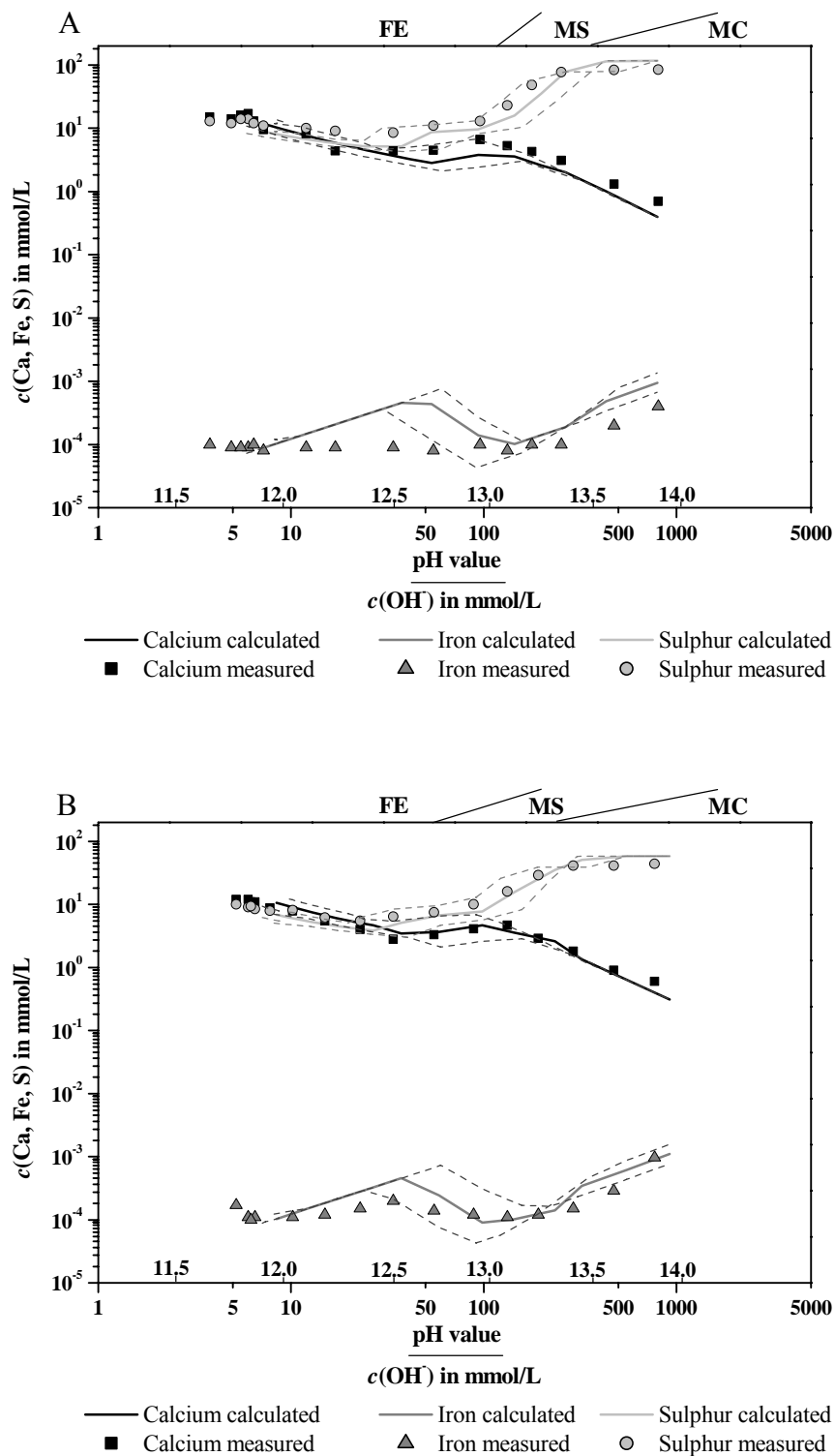


Fig. 2.9. Measured and calculated concentrations of calcium (Ca), sulphur (S), iron (Fe) and hydroxide (OH⁻) in the aqueous solution of precipitation (A) and dissolution (B) experiments. The dashed lines represent the standard deviation obtained for the solubility products. At the top of the figure are presented the stability fields of the solid phases found. FE: Fe-ettingite; MS: Fe-monosulphate; MC: Fe-monocarbonate.

Table 2.8. Thermodynamic data used to calculate the entropy and heat capacity of Fe-ettringite, Fe-monosulphate and Fe-monocarbonate.

| | H^0 at 25 °C in kJ/mol | S^0 at 25 °C in J/(mol·K) | a_0 | a_1 | a_2 | a_3 | C_p^0 at 25 °C in J/(mol·K) | S^0 at 20 °C in J/(mol·K) | Reference |
|--------------------------------|-----------------------------------|--------------------------------------|----------|-------|----------|-------|--|--------------------------------------|-----------|
| Al ₂ O ₃ | -1662 | 50.961 | 115.018 | 0.018 | -3506190 | 0 | 79.093 | 49.635 | a |
| Fe ₂ O ₃ | -8214 | 87.613 | 98.282 | 0.078 | -1485320 | 0 | 104.776 | 85.849 | a |
| Gypsum | -2023 | 193.800 | 91.379 | 0.318 | 0 | 0 | 186.191 | 190.665 | a |
| Anhydrite | -1435 | 106.692 | 70.208 | 0.099 | 0 | 0 | 99.648 | 105.011 | a |
| Al-ettringite | -17535 | 1900 | 1939.120 | 0.789 | 0 | 0 | 2174.360 | 1863 | b |
| Al-monosulphate | -8750 | 821 | 594.180 | 1.168 | 0 | 0 | 936.579 | 805 | b |
| Al-monocarbonate | -8250 | 657 | 617.903 | 0.982 | -2594080 | 0 | 881.371 | 642 | b |
| Fe-ettringite | -16600 | 1937 | 1922.384 | 0.855 | 2020870 | 0 | 2200 | 1899 | c |
| Fe-monosulphate | -7843 | 858 | 577.444 | 1.234 | 2020870 | 0 | 968 | 841 | c |
| Fe-monocarbonate | -7637 | 737 | 611.753 | 1.157 | -573210 | 0 | 950 | 721 | c |

(a) Thoenen and Kulik, 2003

(b) Lothenbach et al, 2007

(c) this study

For Fe-ettringite

$$S_{Fe-ettringite}^o = S_{ettringite}^o - S_{Al_2O_3}^o + S_{Fe_2O_3}^o = 1899 \frac{J}{mol \cdot K} \quad (2.10)$$

for Fe-monosulphate

$$S_{Fe-monosulphate}^o = S_{monosulphate}^o - S_{Al_2O_3}^o + S_{Fe_2O_3}^o = 841 \frac{J}{mol \cdot K} \quad (2.11)$$

and for Fe-monocarbonate

$$S_{Fe-monocarbonate}^o = S_{monocarbonate}^o - S_{Al_2O_3}^o + S_{Fe_2O_3}^o + \left(\frac{S_{gypsum}^o - S_{anhydrite}^o}{2} \right) = 721 \frac{J}{mol \cdot K} \quad (2.12)$$

were calculated at 20°C. In contrast to Al-monocarbonate, which contains 11 H₂O molecules, Fe-monocarbonate contains 12 H₂O molecules. Therefore, the missing H₂O

molecule was added in form of $\frac{S_{gypsum}^o - S_{anhydrite}^o}{2}$ assuming that the water molecule in

gypsum has the same S^o as in Fe-monocarbonate.

The heat capacity C_p^o can be calculated with

$$C_p^o = a_0 + a_1T + a_2T^{-2} + a_3T^{-0.5} \quad (2.13)$$

where a_0 , a_1 , a_2 and a_3 are empirical coefficients and T is the temperature in Kelvin. The coefficients were also estimated from the aluminium containing phases (cf. Table 2.8) in the same way as it was done for S^o .

The Gibbs free energy of formation $\Delta_f G^o$ at 25 °C can then be calculated:

$$\begin{aligned} \Delta_f G_{T_0}^o &= \Delta_a G_T^o - S_T^o(T_0 - T) - \int_T^{T_0} \int_T^{T_0} \frac{C_p^o}{T} dTdT \\ &= \Delta_a G_T^o - S_T^o(T_0 - T) - a_0 \left(T_0 \ln \frac{T_0}{T} - T_0 + T \right) - 0.5a_1(T_0 - T)^2 - a_2 \frac{(T_0 - T)^2}{2T_0 \cdot T^2} - a_3 \frac{2(\sqrt{T_0} - \sqrt{T})^2}{\sqrt{T}} \end{aligned} \quad (2.14)$$

where $T_0 = 298.15$ K, $T = 293.15$ K and a_0 , a_1 , a_2 , and a_3 are the empirical coefficients of the heat capacity equation (Eqn. 2.13). Temperature correction of Gibbs free energies is described in more detail in Anderson and Crerar (1993), Kulik (2002), and Kulik (2006).

After insertion of the results of Eqn. 14 in Eqn. 8 and 9 the solubility products at 25 °C obtained are: for Fe-ettringite $\log K_{S0} = -44.0 \pm 0.7$, for Fe-monosulphate $\log K_{S0} = -33.2 \pm 0.5$ and for Fe-monocarbonate $\log {}_aK_{S0} = -35.5 \pm 0.3$ Using these results the Gibbs free energies of formation for Fe-ettringite, Fe-monosulphate, and Fe-monocarbonate at 25 °C are:

$$\Delta_f G_{T_0, Fe-ettringite}^o = -14282.36 \pm 4.00 \frac{kJ}{mol}$$

$$\Delta_f G_{T_0, Fe-monosulphate}^o = -6882.55 \pm 2.85 \frac{kJ}{mol}$$

$$\Delta_f G_{T_0, Fe-monocarbonate}^o = -6679.20 \pm 1.71 \frac{kJ}{mol}$$

2.6 Conclusion

The formation of Fe-ettringite is much slower than the formation of the aluminium containing analogue where equilibrium is reached within four to six days (Perkins and Palmer, 1999). For Fe-ettringite equilibrium was reached only after half a year as the time-series study showed. In addition to Fe-ettringite, gypsum and iron oxy-hydroxide were initially formed. After 180 days of ageing no gypsum could be detected, neither by XRD nor by TGA. EXAFS analysis indicated that iron oxy-hydroxide was no longer present in this sample. It was found that after an equilibration time of 180 days Fe-ettringite was stable up to a pH-value of 13.2 in the precipitation experiments. In the dissolution experiments Fe-ettringite was stable up to a pH-value of 13.3. Fe-monosulphate was formed in the precipitation experiments at pH-values ≥ 13.1 . In the dissolution experiments it was already formed at pH-values ≥ 12.7 . Also Fe-monocarbonate precipitated at lower pH in the dissolution experiments (pH ≥ 13.4 instead of pH ≥ 13.6). These differences between the precipitation and dissolution experiments were due to the different solid liquid ratio in the two systems and could be well reproduced in the modelling (Fig. 8).

For Fe-ettringite a solubility product of $\log K_{S0} = -44.0 \pm 0.7$ was obtained from both, the precipitation and dissolution experiments. The hitherto estimated solubility products of -49.8 to -49.4 (cf. Babushkin et al., 1985; Lothenbach and Winnefeld, 2006) are much lower. Thus, the measurements showed Fe-ettringite to be much less stable than assumed.

The solubility product of Fe-ettringite obtained in this study is close to the solubility product of Al-ettringite ($K_{S0} = -44.9$, cf. Lothenbach et al., 2007) which indicates that a solid solution between these two end-members could be thermodynamically possible, in cement systems as well as in natural alkaline environments.

The solubility products of Fe-monosulphate ($\log K_{S0} = -33.2 \pm 0.5$) and the apparent solubility product of Fe-monocarbonate ($\log {}_aK_{S0} = -35.5 \pm 0.3$) are approximately 4 log units lower than the solubility products of their Al-containing analogues: Al-monosulphate $\log K_{S0} = -29.3$ (Matschei et al., 2007) and Al-monocarbonate $\log K_{S0} = -31.5$ (Lothenbach et al., 2007). These findings confirm the predictions of Babushkin who estimated for Fe-hydrates solubility products which were 4.3 log units lower than their Al-analogues

(Babushkin et al., 1985). The conditions used in these experiments were restricted. Therefore, the assignment of these thermodynamic data to other alkaline systems is not always possible. Especially the kinetic hindrance of Fe-ettringite formation has to be considered. For example, in freshly mixed cement pastes the high sulphate concentrations could change the kinetic hindrance of Fe-ettringite formation or also could lead to a shift of the stability limits of Fe-ettringite. Furthermore, the formation of a solid solution between Al and Fe-ettringite could have an effect to kinetics and stability of Fe-ettringite.

Acknowledgments

The authors would like to thank Frank Winnefeld and Luigi Brunetti (Empa Dübendorf) for their support and Friedlinde Goetz-Neunhoeffler and Jürgen Neubauer (University of Erlangen-Nürnberg) for the fruitful discussions, as well as Lucas Olivi in charge of the XAS Beamline at the Elettra synchrotron for his help during the experiments.

The financial support (Grant 20021-103546) of the Swiss National Foundation and of the European Community during EXAFS experiments in Italy (EU contract RII3-CT-2004-506008 (IA-SFS)) is gratefully acknowledged.

2.7 References

Anderson, G. M. and Crerar, D. A., 1993. *Thermodynamics in Geochemistry. The Equilibrium Model*. Oxford University Press, New York, Oxford.

Andreeva, E. P. and Sanzhaasurén, R., 1977. Investigation of the processes of chemical interaction in aqueous suspensions of tetracalcium aluminoferrite in the presence of gypsum dihydrate. *Colloid Journal of the USSR* **39**, 197-207.

- Ankudinov, A. L., Ravel, B., Rehr, J. J., and Conradson, S. D., 1998. Real space multiple scattering calculation and interpretation of X-ray absorption near-edge structure. *Physical Review B* **58**, 7565-7576.
- Atkins, M., Glasser, F. P., and Kindness, A., 1992. Cement hydrate phases: Solubility at 25°C. *Cement and Concrete Research* **22**, 241-246.
- Babushkin, V. I., Matveyev, G. M., and Mchedlov-Petrosyan, O. P., 1985. *Thermodynamics of Silicates*. Springer-Verlag, Berlin.
- Barnett, S. J., 1998. X-ray Powder Diffraction Studies of Ettringite and Related Systems, Ph. D. thesis, Staffordshire University, Stoke-on-Trent.
- Baur, I. and Johnson, C. A., 2003. The solubility of selenate-AFt ($3\text{CaO}\cdot\text{Al}_2\text{O}_3\cdot 3\text{CaSO}_4\cdot 37.5\text{H}_2\text{O}$) and selenate-AFm ($3\text{CaO}\cdot\text{Al}_2\text{O}_3\cdot\text{CaSeO}_4\cdot x\text{H}_2\text{O}$). *Cement and Concrete Research* **33**, 1741-1748.
- Bentor, Y. K., Gross, S., and Heller, L., 1963. High-temperature minerals in non-metamorphosed sediments in Israel. *Nature* **199**, 478-479.
- Brown, P. W., 1987. Early hydration of tetracalcium aluminoferrite in gypsum and lime-gypsum solutions. *Journal of the American Ceramic Society* **70**, 493-496.
- Buhlert, R. and Kuzel, H.-J., 1971. Über den Einbau von Cr^{3+} und Fe^{3+} in Ettringit. *Zement-Kalk-Gips* **2**, 83-85.
- Csizmadia, J., Balazs, G., and Tamas, F. D., 2001. Chloride ion binding capacity of aluminoferrites. *Cement and Concrete Research* **31**, 577-588.
- Damidot, D., Stronach, S., Kindness, A., Atkins, M., and Glasser, F. P., 1994. Thermodynamic investigation of the $\text{CaO}\text{-Al}_2\text{O}_3\text{-CaCO}_3\text{-H}_2\text{O}$ closed system at 25°C and the influence of Na_2O . *Cement and Concrete Research* **24**, 563-572.
- Ecker, M., 1998. Diadochiebeziehungen in Calciumaluminatferraten und deren Hydratationsprodukten. Ph. D. thesis, Hallesches Jahrbuch für Geowissenschaften, Reihe B, Martin-Luther-Universität Halle-Wittenberg.

- Ecker, M. and Pollmann, H., 1991. PDF 42-1472, ICDD, Grant-in-Aid.
- Ecker, M. and Pöllmann, H., 1994. Investigations on lamellar calciumaluminate-ferratehydrates at different atmospheres and temperatures by in situ X-ray powder diffraction. *Materials Science Forum* **166-169**, 565-570.
- Emanuelson, A. and Hansen, S., 1997. Distribution of iron among ferrite hydrates. *Cement and Concrete Research* **27**, 1167-1177.
- Fukuhara, M., Goto, S., Asage, K., Daimon, M., and Kondo, R., 1981. Mechanisms and kinetics of C₄AF hydration with gypsum. *Cement and Concrete Research* **11**, 407-414.
- Galimova, L. A., Danilov, V. P., Lepeshkov, I. N., Yudovich, B. E., and Shebanov, N. A., 1988. A study of the formation and decomposition of the calcium iron(III) double hydroxide sulphate Ca₆Fe₂(OH)₁₂(SO₄)₃ · 26H₂O in the 3Ca(OH)₂ + Fe₂(SO₄)₃ → 3CaSO₄ + 2Fe(OH)₃·H₂O system at 20 °C. *Russian Journal of Inorganic Chemistry* **33**, 445-448.
- Gallias, J. L., 1998. Microstructure of the interfacial transition zone around corroded reinforcement. In: Katz, A. (Ed.), *Second International Conference on the Interfacial Transition Zone in Cementitious Composites. RILEM proceedings*. London : E & FN Spon, Haifa, Israel.
- Goetz-Neunhoeffler, F. and Neubauer, J., 2006. Refined ettringite (Ca₆Al₂(SO₄)₃(OH)₁₂·26H₂O) structure for quantitative X-ray diffraction analysis. *Powder Diffraction* **21**, 4-11.
- Gu, Y., Gammons, C. H., and Bloom, M. S., 1994. A one-term extrapolation method for estimating equilibrium constants of aqueous reactions at elevated temperatures. *Geochimica et Cosmochimica Acta* **58**, 3545-3560.
- Hampson, C. J. and Bailey, J. E., 1982. On the structure of some precipitated calcium alumino-sulphate hydrates. *Journal of Material Science* **17**, 3341-3346.

- Holleman, A. F. and Wiberg, E., 1985. *Lehrbuch der anorganischen Chemie*. de Gruyter, Berlin.
- Hummel, W., Berner, U., Curti, E., Pearson, F. J., and Thoenen, T., 2002. *Nagra/PSI Chemical Thermodynamic Data Base 01/01*. Universal Publishers/uPublish.com, Parkland, Florida.
- Hurlbut, C. S. and Baum, J. L., 1960. Ettringite from Franklin, New Jersey. *The American Mineralogist* **45**, 1137-1143.
- Johnson, J. W., Oelkers, E. H., Helgeson, H. C., 1992. SUPCRT92: A software package for calculating the standard molal thermodynamic properties of minerals, gases, aqueous species, and reactions from 1 to 5000 bar and 0 to 1000 °C. *Computers & Geoscience* **18**, 899-947. (slop98.dat database available from <http://affinity.berkeley.edu>)
- Jones, F. E., 1960. Hydration of calcium aluminates and ferrites. In: *Proceedings of the Fourth International Symposium on the Chemistry of Cement*. National Bureau of Standards Monograph 43, National Bureau of Standards, Washington 25, D.C.
- Kulik, D. A., 2002. Minimising uncertainty induced by temperature extrapolations of thermodynamic data: A pragmatic view on the integration of thermodynamic databases into geochemical computer codes. *The use of thermodynamic databases in performance assessment*. OECD, Paris, Barcelona, Spain.
- Kulik, D. A., 2006. GEMS-PSI 2.1, PSI Villigen, Switzerland; available at <http://les.web.psi.ch/Software/GEMS-PSI/index.html>
- Kuzel, H.-J. and Pöllmann, H., 1991. Hydration of C₃A in the presence of Ca(OH)₂, CaSO₄·2H₂O and CaCO₃. *Cement and Concrete Research* **21**, 885-895.
- Lothenbach, B., Matschei, T., Möschner, G., and Glasser, F. P., 2007. Thermodynamic modelling of the effect of temperature on the hydration and porosity of Portland cement. *Cement and Concrete Research* **submitted**.

- Lothenbach, B. and Winnefeld, F., 2006. Thermodynamic modelling of the hydration of Portland cement. *Cement and Concrete Research* **36**, 209-226.
- Matschei, T., Lothenbach, B., and Glasser, F. P., 2007. The AFm-phase in Portland cement. *Cement and Concrete Research* **37**, 118-130.
- McMurdie, H. F., Morris, M. C., Evans, E. H., Paretzkin, B., Wong-Ng, W., and Zhang, Y., 1987. Standard X-ray diffraction powder patterns from the JCPDS research associateship. *Powder Diffraction* **2**, 41-52.
- Meller, N., Hall, C., Jupe, A. C., Colston, S. L., Jacques, S. D. M., Barnes, P., and Phipps, J., 2004. The paste hydration of brownmillerite with and without gypsum: a time resolved synchrotron diffraction study at 30, 70, 100 and 150 °C. *Journal of Materials Chemistry* **14**, 428-435.
- Michalowicz, A., 1991. EXAFS pour le MAC, *Logiciels pour la Chimie*. Société Française de Chimie, Paris.
- Michalowicz, A., 1997. EXAFS pour le MAC: A new version of an EXAFS data analysis code for the Macintosh. *Journal de Physique* **IV**, 235-236.
- Murdoch, J. and Chalmers, R. A., 1960. Ettringite ("Woodfordite") from Crestmore, California. *Am. Mineral.* **45**, 1275-1278.
- Pearson, F. J. and Berner, U., 1991. Nagra thermochemical data base. I. Core data. *Nagra – Technical Report 91-17*. Nagra, Wettingen (Switzerland).
- Perkins, R. B. and Palmer, C. D., 1999. Solubility of ettringite ($\text{Ca}_6[\text{Al}(\text{OH})_6]_2(\text{SO}_4)_3 \cdot 26\text{H}_2\text{O}$) at 5-75°C. *Geochimica et Cosmochimica Acta* **63**, 1969-1980.
- Perkins, R. B. and Palmer, C. D., 2000. Solubility of $\text{Ca}_6[\text{Al}(\text{OH})_6]_2(\text{CrO}_4)_3 \cdot 26\text{H}_2\text{O}$, the chromate analogue of ettringite; 5-75°C. *Applied Geochemistry* **15**, 1203-1218.

- Poellmann, H., 1984. Die Kristallchemie der Neubildungen bei Einwirkung von Schadstoffen auf hydraulische Bindemittel. Ph. D. Thesis. University of Erlangen-Nürnberg.
- Poellmann, H., Kuzel, H.-J., and Wenda, R., 1990. Solid solution of ettringites. Part I: Incorporation of OH⁻ and CO₃²⁻ in 3CaO·Al₂O₃·3CaSO₄·32H₂O. *Cement and Concrete Research* **20**, 941-947.
- Pollmann, H. and Ecker, M., 1992. PDF 43-480, ICDD, Grant-in-Aid.
- Rose, J., Benard, A., El Mrabet, S., Masion, A., Moulin, I., Briois, V., Olivi, L., and Bottero, J. Y., 2006. Evolution of iron speciation during hydration of C₄AF. *Waste Management* **26**, 720-724.
- Shock, E. L., Sassani, D. C., Willis M., Sverjensky, D., 1997. Inorganic species in geologic fluids: correlations among standard molal thermodynamic properties of aqueous ions and hydroxide complexes. *Geochimica et Cosmochimica Acta* **61**, 907-950.
- Sverjensky, D., Shock, E. L., Helgeson, H. C., 1997. Prediction of the thermodynamic properties of aqueous metal complexes to 1000 °C and 5 kbar. *Geochimica et Cosmochimica Acta* **61**, 1359-1412.
- Taylor, H. F. W., 1997. *Cement Chemistry*. Thomas Telford Publishing, London.
- Thoenen, T. and Kulik, D.A., 2003. Nagra/PSI Chemical Thermodynamic Data Base 01/01 for the GEM-Selektor (V.2-PSI) Geochemical Modeling Code: Release 28-02-03. Internal report TM-44-03-04, available at <http://les.web.psi.ch/software/GEMS-PSI/thermodata/index.html>.
- Warren, C. J. and Reardon, E. J., 1994. The solubility of ettringite at 25°C. *Cement and Concrete Research* **24**, 1515-1524.

3 Solid solution between Al-ettringite and Fe-ettringite ($\text{Ca}_6[\text{Al}_{1-x}\text{Fe}_x(\text{OH})_6]_2(\text{SO}_4)_3 \cdot 26\text{H}_2\text{O}$)

G. Möschner, B. Lothenbach, F. Winnefeld, A. Ulrich, R. Figi, R. Kretschmar
Submitted for publication in Cement and Concrete Research

3.1 Abstract

The solid solution between Al- and Fe-ettringite $\text{Ca}_6[\text{Al}_{1-x}\text{Fe}_x(\text{OH})_6]_2(\text{SO}_4)_3 \cdot 26\text{H}_2\text{O}$ was investigated. Ettringite phases were synthesized at different Al/(Al+Fe)-ratios ($= X_{\text{Al,total}}$), so that X_{Al} increased from 0.0 to 1.0 in 0.1 unit steps. After 8 months of equilibration, the solid phases were analyzed by X-ray diffraction (XRD) and thermogravimetric analysis (TGA), while the aqueous solutions were analyzed by inductively coupled plasma optical emission spectroscopy (ICP-OES) and inductively coupled plasma mass spectrometry (ICP-MS). XRD analyses of the solid phases indicated the existence of a miscibility gap between

$X_{\text{Al,total}} = 0.25 \pm 0.05 - 0.65 \pm 0.05$. Some of the XRD peaks showed broadening or even two peaks could be detected at these molar ratios. The composition of the aqueous solutions, however, would have been in agreement with both, the existence of a miscibility gap or a continuous solid solution between Al- and Fe-ettringite, based on thermodynamic modeling, simulating the experimental conditions.

3.2 Introduction

Ettringite occurs in natural alkaline environments (like Ca-rich igneous rocks, contact metamorphosed Ca-rich sediments or bioclastic sediments cemented by gypsum) with

different chemical compositions, e.g. $\text{Ca}_6(\text{Al})_2(\text{SO}_4)_3(\text{OH})_{12}\cdot 25\text{H}_2\text{O}$ (Bannister, 1936), $\text{Ca}_6(\text{Si},\text{Al},\text{B})_3(\text{SO}_4)_2(\text{O},\text{OH})_{12}(\text{OH})_4\cdot 26\text{H}_2\text{O}$ (Hurlbut and Baum, 1960) and $\text{Ca}_6(\text{Al},\text{Si})_2(\text{SO}_4)_2(\text{B}(\text{OH})_4)(\text{OH})_{12}\cdot 26\text{H}_2\text{O}$ (Dunn et al., 1983). Iron containing analogues $\text{Ca}_6(\text{Fe}(\text{III})_{1.5}\text{Al}_{0.3}\text{Mn}(\text{II})_{0.2})_2(\text{SO}_4)_{2.3}(\text{B}(\text{OH})_4)_{1.2}(\text{OH})_{12}\cdot 25\text{H}_2\text{O}$ (Peacor et al., 1983) and $\text{Ca}_6(\text{Si},\text{Al},\text{Fe})_2(\text{SO}_4)_3(\text{Cl},\text{OH})_x\cdot x\text{H}_2\text{O}$ (Rodgers and Courtney, 1988) have been reported. The structure of these minerals is well investigated (e.g. McConnell and Murdoch, 1962; Berry 1963; Moore and Taylor, 1968, Antao et al., 2002; Pushcharovsky et al., 2004). Ettringite and its analogues form hexagonal, prismatic crystals. For pure aluminum containing ettringite columns of $[\text{Al}(\text{OH})_6]^{3-}$ octahedra are linked together by calcium ions. The (OH) groups are shared between Al-octahedra and Ca-polyhedra and each of the latter contains four water molecules, which are located on the outer surface of the columns. Al(III) can be substituted by Fe(III) as well as by e.g. Cd(II) and Cr(III) (Buhlert and Kuzel, 1971; Galimova et al., 1988; Albino et al., 1996; Wieczorek-Ciurowa et al., 2001). The sulfate tetrahedra can be partially or entirely replaced by e.g. SeO_4^{2-} and CrO_4^{2-} (Perkins and Palmer, 2000; Baur and Johnson, 2003; Chrysochoou and Dermatas, 2006). Ettringite does not only occur in natural environments, but is also formed during hydration of Portland cement and super-sulfated blast furnace slag cements (Taylor, 1997). It forms from the cement clinker aluminate (idealized $\text{Ca}_3\text{Al}_2\text{O}_5$) and ferrite (idealized $\text{Ca}_2(\text{Al}_x\text{Fe}_{1-x})_2\text{O}_5$), gypsum/anhydrite and water. The Fe(III) present in ferrite can either partly replace Al(III) in ettringite or in other hydrates formed during cement hydration such as monosulfate ($\text{Ca}_4[\text{Al}_{1-x}\text{Fe}_x(\text{OH})_6]_2(\text{SO}_4)\cdot 6\text{H}_2\text{O}$) or hydrogarnet ($\text{Ca}_6[\text{Al}_{1-x}\text{Fe}_x(\text{OH})_4]_2(\text{OH})_4$) or it can precipitate as $\text{Fe}(\text{OH})_3$ or as Ca-Al-Fe-gel (Collepari et al., 1979; Fukuhara et al., 1981; Brown, 1993; Liang and Nanru, 1994; Emanuelson and Hansen, 1997; Csizmadia et al., 2001; Meller et al., 2004; Black et al., 2006). The distinction between iron free and iron containing phases in the hydrated cement samples is very difficult by the methods commonly used in cement chemistry (i.e. X-ray diffraction (XRD), thermogravimetric analysis (TGA), environmental scanning electron microscopy (ESEM), Raman spectroscopy), since the structural modification of the crystals is small and therefore difficult to detect. Pure iron containing ettringites ($\text{Ca}_6[\text{Fe}(\text{OH})_6]_2(\text{SO}_4)_3\cdot 26\text{H}_2\text{O}$) have been synthesized and their solubility has been determined (Schwiete and Ludwig, 1968; McMurdie et al., 1987; Galimova et al., 1988; work presented in Chapter 2). Buhlert and Kuzel (1971) investigated the solid solution series between Al- and Fe-ettringite. They

postulated a possible miscibility gap between 20 and 30 mol-% Al ($X_{\text{Al}} = 0.2 - 0.3$), but the results were ambiguous, since the detected peak broadening was weak.

The goal of this study was to examine the formation of solid solution of the system $\text{Ca}_6[\text{Al}_{1-x}\text{Fe}_x(\text{OH})_6]_2(\text{SO}_4)_3 \cdot 26\text{H}_2\text{O}$ and to determine the solubilities of the solid phases. The different solids were synthesized and a thermodynamic model was established and compared to the experimental results of the solid and the liquid phases.

3.3 Methods

3.3.1 Synthesis of the solid solution series

The solids of the solid solution series $\text{Ca}_6[\text{Al}_{1-x}\text{Fe}_x(\text{OH})_6]_2(\text{SO}_4)_3 \cdot 26\text{H}_2\text{O}$ were synthesized by adding freshly prepared CaO, $\text{Fe}_2(\text{SO}_4)_3 \cdot 5.3\text{H}_2\text{O}$ and/ or $\text{Al}_2(\text{SO}_4)_3 \cdot 16.2\text{H}_2\text{O}$ to 0.032 M KOH-solution. The amounts of the reactants were varied in that way that $X_{\text{Al},\text{total}}$ increased from $X_{\text{Al},\text{total}} = 0.0$ to $x = 1.0$ in 0.1 unit steps; the liquid/solid ratio was constant ($l/s = 10$) in all experiments.

The mixtures were stored in sealed PE bottles and shaken at 20 °C. In contrast to Al-ettringite, where equilibrium is reached after a couple of days (Perkins and Palmer, 1999), for Fe-ettringite equilibrium is reached only after approximately 6 months (work presented in Chapter 2). Therefore the different mixtures of the solid solution series were equilibrated for 8 months.

After equilibration, the solid and the liquid phases were separated by vacuum filtration through 0.45 μm nylon filters. Both the mixing and the filtration were done in a N_2 -filled glove box (N_2 was continuously bubbled through KOH-solution) to minimize CO_2 contamination. Afterwards the solid and the liquid phases were analyzed to characterize the precipitates and the dissolved concentrations of the different elements.

3.3.2 Characterization of the solid phases

After separating the liquid and solid phases, the solid precipitates were dried for three weeks in N₂-filled desiccators over saturated CaCl₂ solution; relative humidity was approximately 30%. The dry solid phases were ground by hand in the N₂-filled glove box to < 63 μm and analyzed by X-ray diffraction (XRD) and thermogravimetric analysis (TGA). For environmental scanning electron microscopy (ESEM) studies, a part of the dry solid phases was not ground but freshly fractured.

The XRD analyses were performed on a PANalytical X'Pert PRO system using CuKα radiation (generator: 40 kV and 40 mA). The samples were transferred by backloading into specimen holders of 16 mm diameter. The measurement was carried out between 5 and 80° 2θ with a step size of 0.0167° and a counting time of 19.685 s. For evaluation of the data the software X'Pert HighScore Plus V. 2.0a was used. To determine the lattice parameters of the different synthesized phases the following evaluation steps were carried out: first the background was set manually, and then a peak search was performed followed by a profile fitting. The indexing of the reflections was done using the Treor method. At last the cell parameters were refined by least square algorithm.

For TGA (Mettler Toledo TGA/SDTA851°) about 8 – 12 mg per sample were heated under N₂ over a temperature range of 30 to 980°C at a rate of 20 °C/min.

The water loss measured by TGA was used to calculate the amount of ettringite (Ca₆[Al_{1-x}Fe_x(OH)₆]₂(SO₄)₃·26H₂O – 32H₂O ⇌ 3CaO·[Al_{1-x}Fe_xO_{1.5}]₂·3CaSO₄) formed.

ESEM studies were performed on Philips ESEM FEG XL 30 using low vacuum mode (at approximately 1 Torr H₂O).

3.3.3 Characterization of the liquid phase

One part of the liquid phases of each sample was instantly diluted (1:10 for inductively coupled plasma optical emission spectroscopy (ICP-OES) and 1:100 for inductively coupled plasma mass spectrometry (ICP-MS)) with nitric acid (diluted 1:10 from Merck 64

HNO₃ suprapur quality, 65%, with high-purity water, prepared by a MilliQ-Gradient A10 System (Millipore) to stabilize metals in solution and prevent the adsorption of the dissolved ions to the PE vials used. Another part of each sample was left untreated to measure the pH-value. This was done without any delay to minimize CO₂-contamination. Prior to the measurements the pH-meter (Knick pH-Meter 766 with a Knick SE 100 pH/Pt 1000 electrode) was calibrated with 0.001 to 1.0 M KOH-solutions.

The concentrations of calcium, sulfur and potassium were measured by ICP-OES (Varian, VISTA Pro) and the concentration of aluminum and iron by ICP-MS (Finnigan MAT, ELEMENT2). For minimizing contamination preparation of the samples for ICP-MS analysis were done in a clean laboratory. Plasma spectrometric methods are valuable tools for sensitive chemical analysis. ICP-MS is characterized as a fast multi-element method with large dynamic range and high detection power, which enables element analysis down to sub ng/kg range (Ulrich and Wichser, 2003).

3.3.4 Thermodynamic modeling

Thermodynamic modeling was carried out using the geochemical code GEMS (Kulik, 2006). GEMS is a broad-purpose geochemical modeling code, which computes equilibrium phase assemblage and speciation in a complex chemical system from its total bulk elemental composition. Chemical interactions involving solids, solid solutions, gas mixture and aqueous electrolyte are considered simultaneously. The default database of GEMS code was used, which is based on the PSI chemical thermodynamic database (Hummel et al., 2002).

The Gibbs free energy of formation at 25 °C of the ettringite phases was adjusted to 20 °C using following equation:

$$\begin{aligned} \Delta_d G_T^0 &= \Delta_f G_{T_0}^0 - S_{T_0}^0 (T - T_0) - \int_{T_0}^T \int_{T_0}^T \frac{C_p^0}{T} dT dT \\ &= \Delta_f G_{T_0}^0 - S_{T_0}^0 (T - T_0) - a_0 \left(T \ln \frac{T}{T_0} - T + T_0 \right) - 0.5 a_1 (T - T_0)^2 - a_2 \frac{(T - T_0)^2}{2T \cdot T_0^2} - a_3 \frac{2(\sqrt{T} - \sqrt{T_0})^2}{\sqrt{T_0}} \end{aligned} \quad (3.1)$$

where $\Delta_a G^0$ is the apparent Gibbs free energy of formation at any given temperature, which refers to the Gibbs free energy of the elements at 25 °C, T = the given temperature (293.15 K in this study), $T_0 = 298.15$ K, S^0 is the entropy, C_p^0 is the heat capacity and a_0 , a_1 , a_2 and a_3 are empirical coefficients (see Eq. 3.2).

$$C_p^0 = a_0 + a_1 T + a_2 T^{-2} + a_3 T^{-0.5} \quad (3.2)$$

A more detailed description of the temperature correction used in GEMS is given in (Anderson and Crerar, 1993; Kulik, 2002; Kulik, 2006).

Activity coefficients of aqueous species γ_i were computed with the built-in expanded extended Debye-Hückel equation in Truesdell-Jones form with individual parameters a_i and common third parameter b_γ (Hummel et al., 2002):

$$\log \gamma_i = \frac{-A_\gamma z_i^2 \sqrt{I}}{1 + B_\gamma a_i \sqrt{I}} + b_\gamma I \quad (3.3)$$

where z_i denotes the charge of species i , I the effective molal ionic strength, $b_\gamma = 0.064$, and A_γ and B_γ are P, T -dependent coefficients. This activity correction is thought to be applicable up to 1 – 2 molal ionic strength (Pearson and Berner, 1991; Kulik, 2006).

3.4 Experimental results

3.4.1 Solid phases of the solid solution series

X-ray diffraction patterns of the solid phases are presented in Fig. 3.1. For the solid solution series $\text{Ca}_6[\text{Al}_{1-x}\text{Fe}_x(\text{OH})_6]_2(\text{SO}_4)_3 \cdot 26\text{H}_2\text{O}$ a shift of the peaks to smaller d -values (i.e. to bigger 2Θ values) from the mol ratio of $X_{\text{Al, total}} = 0.0$ to 1.0 ($X_{\text{Al, total}} = \text{mol}(\text{Al})/(\text{mol}(\text{Al}) + \text{mol}(\text{Fe}))$) added to the each sample) was visible, due to the fact that aluminum has a smaller ion radius than iron (0.51 Å compared to 0.64 Å (Holleman and Wiberg, 1985)). For four peaks ($2\Theta \approx 19, 23, 29$, and 35° (hkl data: 104,

114, 116 and 216, cf. Table 1), dashed lines in Fig. 3.1A) a peak broadening between $X_{\text{Al,total}} = 0.3$ and $X_{\text{Al,total}} = 0.6$ could be observed. The presence of two peaks would indicate that in the Al- and Fe-ettringite solid solution series a miscibility gap between $X_{\text{Al,total}} = 0.25 \pm 0.05$ and $X_{\text{Al,total}} = 0.65 \pm 0.05$ could exist.

The absence of a broadening of the main peak at $2\Theta \approx 9^\circ$; CuK α radiation (see Table 3.1) could indicate a continuous solid solution, but the main peaks of pure Al- and Fe-ettringite are very close to each other (cf. Fig. 3.1B and Table 3.1). Thus, it is difficult to decide if between $X_{\text{Al,total}} = 0.3$ and 0.6 a peak broadening occurred.

Table 3.1: Shortlist of X-ray diffraction powder patterns of Al- and Fe-ettringite.

| 2 Θ Cu K α | | | | |
|--------------------------|--|------------------------------|---|------------------------------|
| hkl | Al-ettringite Moore and Taylor, 1970 | Al-ettringite* this study | Fe-ettringite McMurdie et al., 1987 | Fe-ettringite* this study |
| 100 | 9.091 | 9.130 | 9.131 | 9.115 |
| 104 | 18.911 | 18.912 | 18.539 | 18.525 |
| 114 | 22.944 | 22.937 | 22.662 | 22.634 |
| 116 | 29.645 | 29.631 | 29.099 | 29.075 |
| 216 | 35.023 | 34.985 | 34.598 | 34.566 |

*Samples contained 10% SiO₂ as internal standard and were displacement corrected.

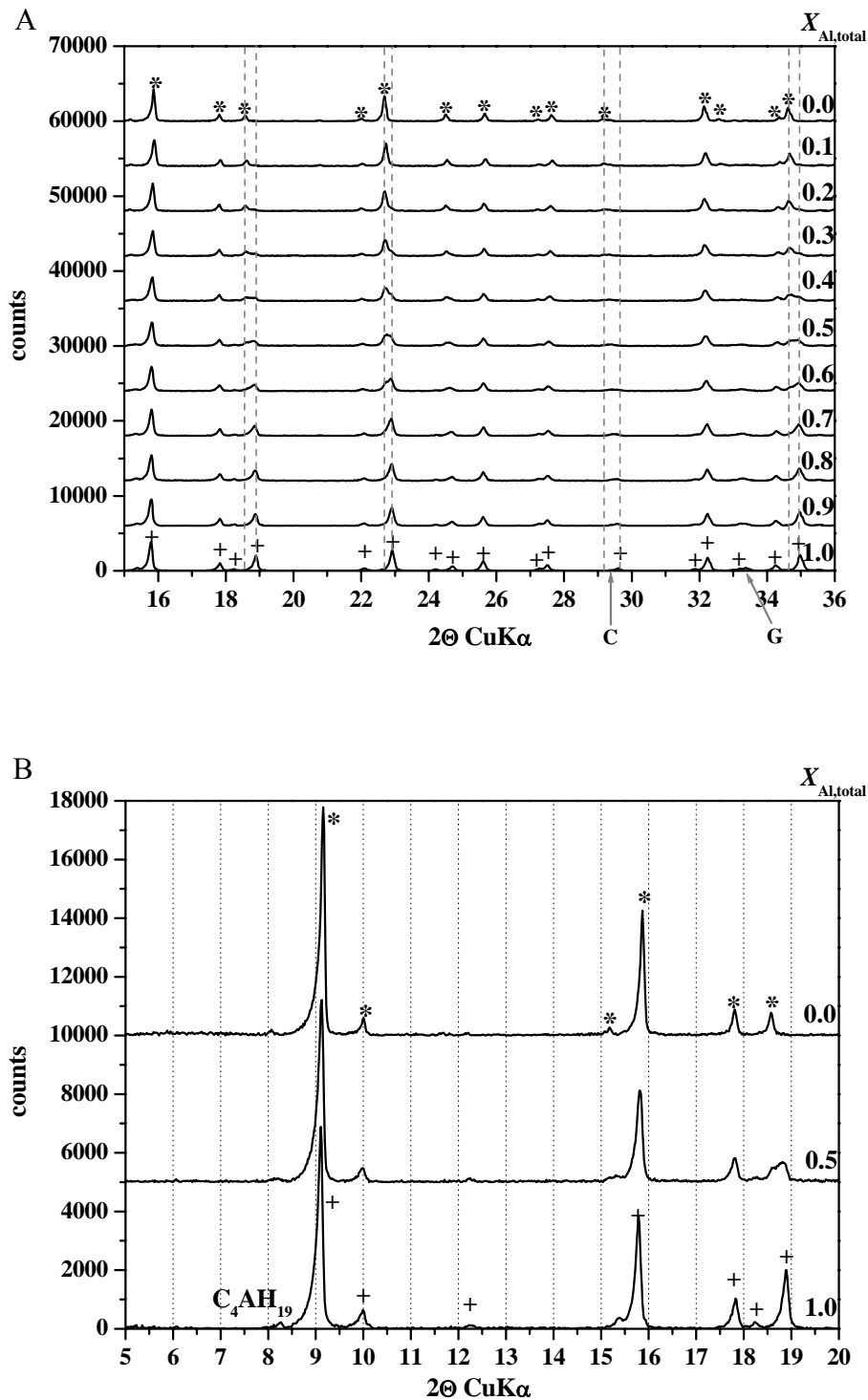


Fig. 3.1. X-ray diffraction spectra for ettringite synthesized with different $X_{Al, total}$ ratios. (A) *: Fe-ettringite (main peak at $2\theta = 9.13$ (McMurdie et al., 1987)); +: Al-ettringite (main peak at $2\theta = 9.09$); C: calcite (main peak at $2\theta = 29.62$); G: gypsum (main peak at $2\theta = 11.59$). The dashed lines mark the peak broadening between $X_{Al, total} = 0.3$ and $X_{Al, total} = 0.6$. (B) *: Fe-ettringite (main peak at $2\theta = 9.13$ (McMurdie et al., 1987)); +: Al-ettringite (main peak at $2\theta = 9.09$), C_4AH_{19} : $Ca_4[Al(OH)_6]_2(OH)_2 \cdot 12H_2O$ (main peak at $2\theta = 8.30$).

The c-parameter of pure Fe-ettringite equaled approximately 22.0 Å. With increasing amount of Al(III) incorporated in the solid phase the length of the c-parameter decreased (Fig. 3.2A). The c-parameter of the pure Al-ettringite lattice as determined by XRD was about 21.5 Å. This shift of 0.5 Å is again in accordance to the different ion radii of aluminum and iron. In contrast to that, the determined a-parameter in the ettringite lattice increased when more Al(III) entered the solid phase (Fig. 3.2B). For pure Al-ettringite the determined value was about 11.24 Å, while for pure Fe-ettringite a value of about 11.19 Å was found. This shift of 0.05 Å of the a-parameter was ten times smaller than the shift of the c-parameter. For comparison Fig. 3.2 also shows the determined values of the a- and c-parameters of previous studies (Moore and Taylor, 1970; Buhlert and Kuzel, 1971; McMurdie et al., 1987; Goetz-Neunhoeffler and Neubauer, 2006; Goetz-Neunhoeffler et al., 2006). Taking the observed peak broadening between $X_{\text{Al,total}} = 0.3$ and 0.6 into account, a miscibility gap between $X_{\text{Al,total}} = 0.25 \pm 0.05$ and 0.65 ± 0.05 is possible (contrary to the study of Buhlert and Kuzel (1971), who observed a miscibility gap between $X_{\text{Al,total}} = 0.2 - 0.3$).

Furthermore, traces of other phases were detected: from $X_{\text{Al,total}} = 0.5$ to 1.0 $\text{Ca}_4[\text{Al}(\text{OH})_6]_2(\text{OH})_2 \cdot 12\text{H}_2\text{O}$, from $X_{\text{Al,total}} = 0.6$ to 1.0 gypsum, and since TGA analysis revealed traces of CO_2 , traces of calcite seemed to be in the system from $X_{\text{Al,total}} = 0.0$ to 1.0, although it was paid special attention to exclude CO_2 intrusion during sample preparation.

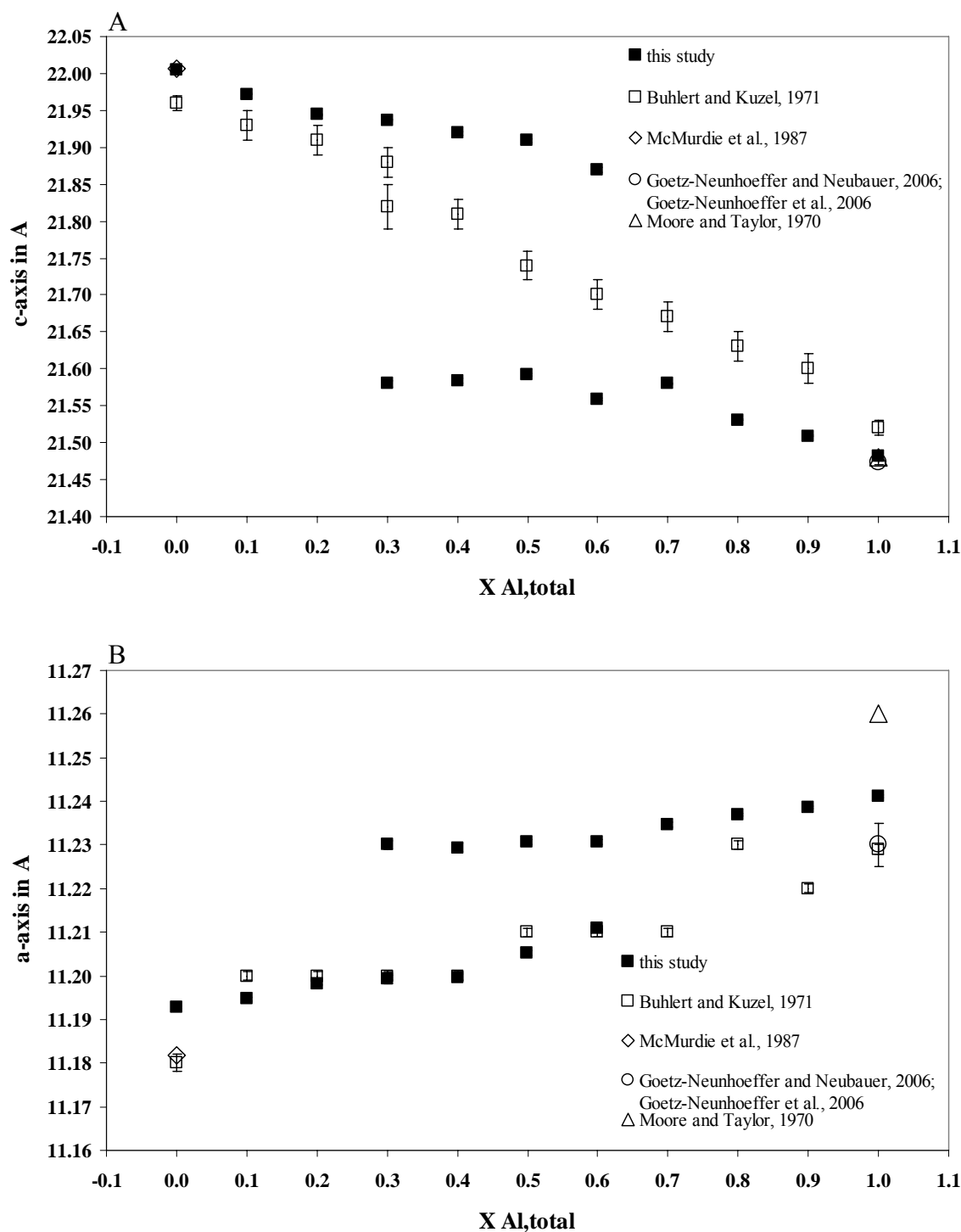


Fig. 3.2. Values of the c-parameter (A) and the a-parameter (B) determined by XRD for ettringite synthesized with different $X_{Al,total}$ ratios.

Thermogravimetric analysis showed that the ettringite phases lost their water molecules between 30 and 150 °C (cf. Fig. 3.3). Besides the loss of water the loss of traces of CO₂ between 625 and 700 °C, which is an evidence for calcite, was detected. In Fig. 3.3A the loss of weight during heating is presented for three selected samples: $X_{Al,total} = 1.0$,

$X_{\text{Al,total}} = 0.5$ and $X_{\text{Al,total}} = 0.0$. The sample $X_{\text{Al,total}} = 1.0$ showed a slightly higher loss of weight than the sample $X_{\text{Al,total}} = 0.5$ and $X_{\text{Al,total}} = 0.0$. The more iron is present in the solid phase the “heavier” is the solid phase and the smaller is the proportion of the water in the solid phase. The theoretical total weight loss of Al-ettringite is about 45.9 % and of Fe-ettringite 43.9 %. This difference of 2% is almost the same difference as measured in these experiments (43.7 % and 41.6 %, respectively). The pure Al-containing ettringite showed a small second peak at approximately 250 °C (Fig. 3.3B). This is in accordance to other findings (Schwiete and Ludwig, 1968; Buhlert and Kuzel, 1971; Perkins and Palmer, 1990). However, for pure Fe-containing ettringite this peak and thus the loss of water at this temperature, was not observed (Schwiete and Ludwig, 1968; Buhlert and Kuzel, 1971). Hence, this small peak can be taken as indicator of Al-containing ettringite. It can be assumed that this peak only occurs for ettringite phases where aluminum is the dominant element. And with a close look at the differentiated relative weight curves (Fig. 3.3B) the peak at ~ 250 °C decreased from $X_{\text{Al,total}} = 1.0$ to $X_{\text{Al,total}} = 0.5$ and was not observable anymore at smaller $X_{\text{Al,total}}$ ratios.

TGA analyses indicated for the ettringite phases in the presence of saturated CaCl_2 solutions a total water content of 29 to 30 H_2O molecules. From the loss of water of the solid phases the masses of the different phases were calculated. The results are presented in Table 3.2.

As discussed in Chapter 2, the formation of Fe-hydroxide at low molar ratio of $X_{\text{Al,total}}$ is likely and was indicated by the slight reddish color of the these samples. But freshly precipitated Fe-hydroxide is XRD amorphous and thus difficult to detect. TGA reference curves of $\text{Fe}(\text{OH})_3$, lepidocrocite and goethite (Fig. 3.4) showed that the loss of water of X-ray amorphous Fe-hydroxide overlapped with the loss of water of ettringite. Hence, the formation of Fe-hydroxides could not be excluded, and the molar ratios of $X_{\text{Fe,solid}}$, and $X_{\text{Al,solid}}$ respectively, could not be determined exactly. Therefore, always $X_{\text{Al,total}}$ is given in this article and refers to the total amount of aluminum added to the system.

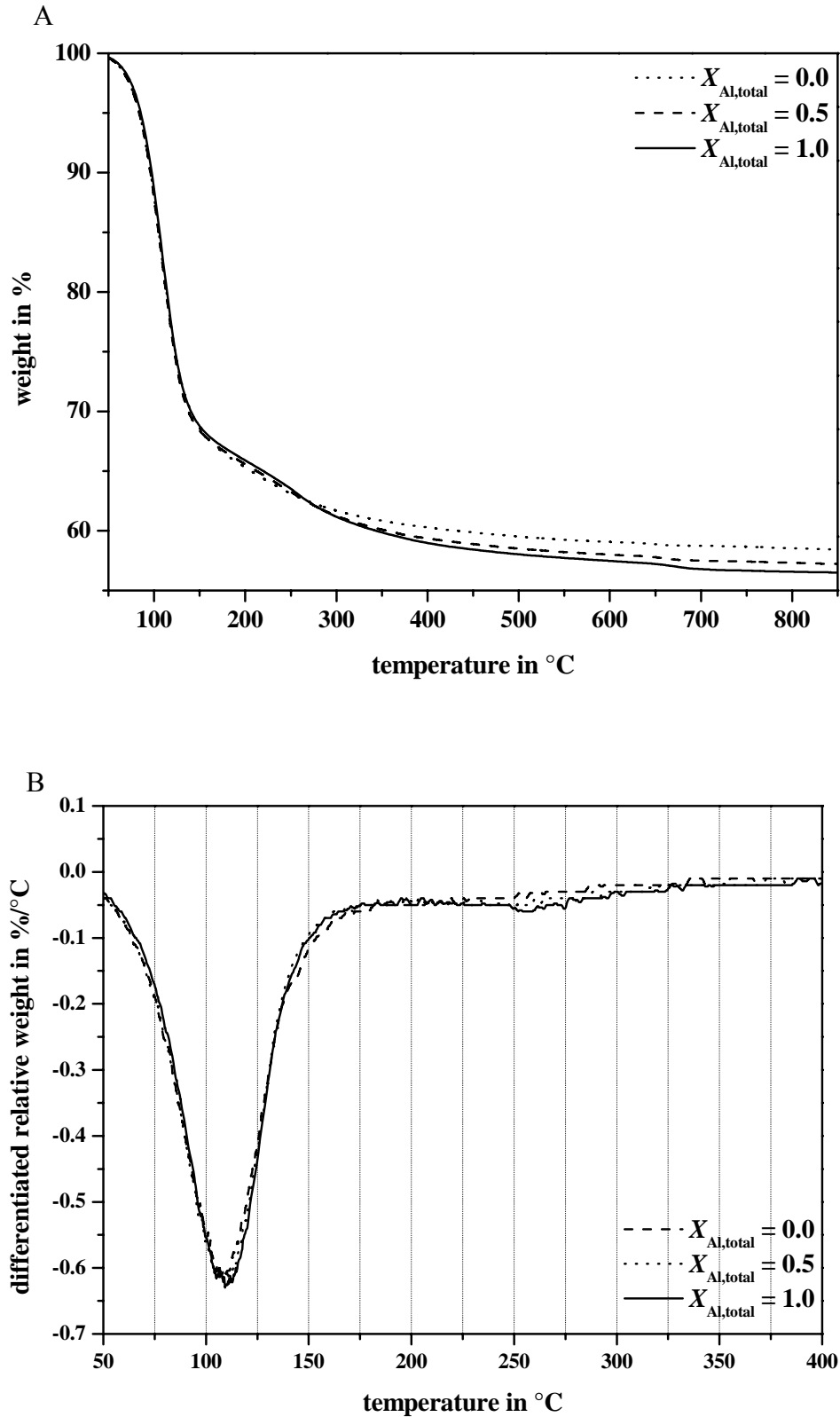


Fig. 3.3. (A) Weight loss of the solid phases at the $X_{Al,total}$ ratios of 0.0, 0.5 and 1.0 during TGA measurements. (B) Derivative curves of thermogravimetric analysis for ettringite synthesised at the $X_{Al,total}$ ratios of 0.0, 0.5 and 1.0.

Table 3.2: Weight of the solid phases after drying.
Masses of ettringite and calcite calculated from TGA measurements.

| $X_{\text{Al,total}}$ | ettringite [g] | calcite [g] | Sum of the solid phases [g] |
|-----------------------|-------------------|----------------|--------------------------------|
| 0.0 | 4.63 | 0.03 | 4.66 |
| 0.1 | 3.96 | 0.04 | 4.00 |
| 0.2 | 4.80 | 0.05 | 4.85 |
| 0.3 | 4.13 | 0.04 | 4.17 |
| 0.4 | 3.98 | 0.04 | 4.02 |
| 0.5 | 4.19 | 0.05 | 4.24 |
| 0.6 | 4.29 | 0.07 | 4.36 |
| 0.7 | 4.34 | 0.07 | 4.41 |
| 0.8 | 4.05 | 0.05 | 4.10 |
| 0.9 | 3.71 | 0.05 | 3.76 |
| 1.0 | 3.68 | 0.06 | 3.74 |

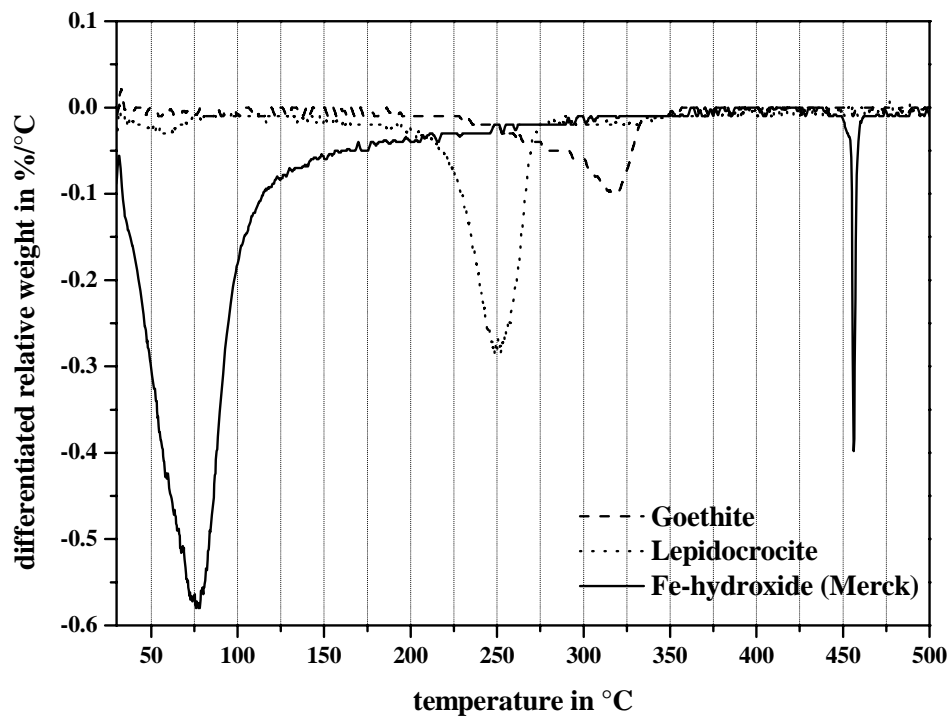


Fig. 3.4: Derivative curves of thermogravimetric analyses of $\text{Fe}(\text{OH})_3$ (Merck), lepidocrocite, and goethite.

ESEM studies showed that both, Al- and Fe-ettringite, precipitated in their typically needle-like shape. Fig. 3.5 shows one picture for $X_{\text{Al,total}} = 0.5$ as an example. The shape of the ettringite needles did not change significantly at different $X_{\text{Al,total}}$ ratios. ESEM studies also revealed the presence of some poorly or non-crystalline areas. EDX analyses did not confirm that these small areas consisted only of Fe-hydroxides, since also some Ca and Al were detected, suggesting the formation of a non-crystalline Ca-Fe-Al-gel. But it has to be pointed out that the observed Ca and Al could also be stem from ettringite phases lying underneath the observed poorly crystalline area.

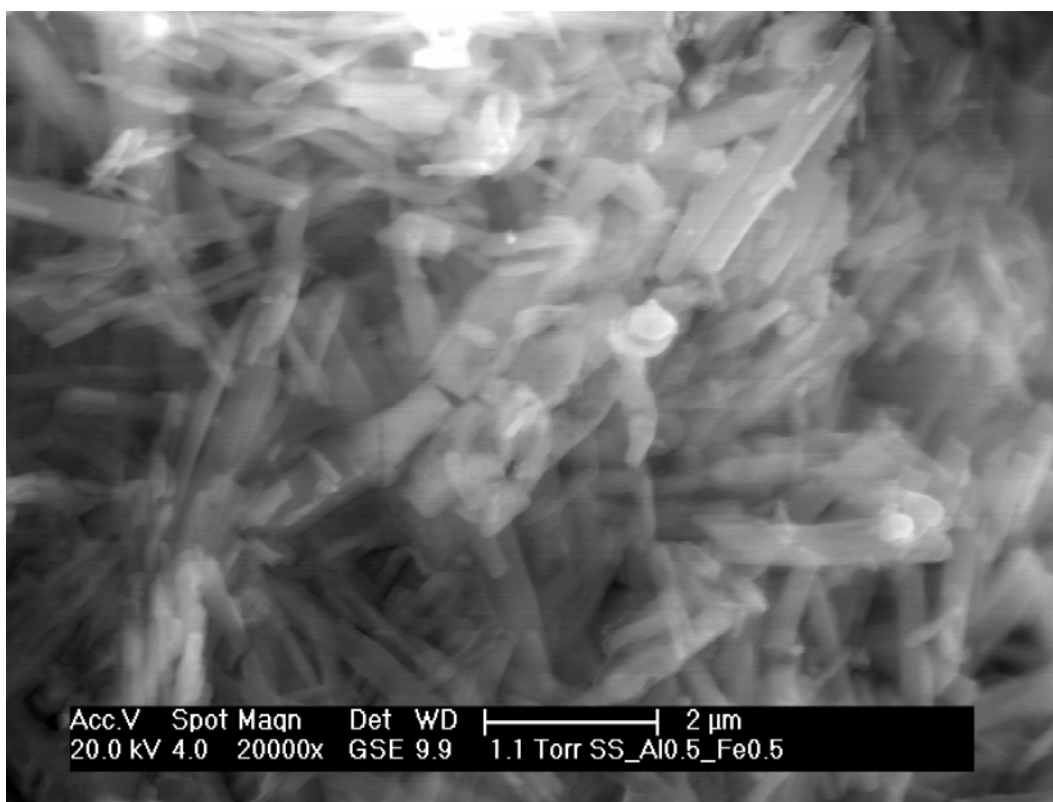


Fig. 3.5. Microstructure of ettringite at $X_{\text{Al,total}} = 0.5$ (ESEM).

3.4.2 Liquid phase of the solid solution series

Analyses of the liquid phases of the solid solution series gave information about the composition of the aqueous solution in equilibrium with the different solid phases. The results are presented in Table 3.3.

Table 3.3: Measured ion concentrations in the aqueous solution.

| $X_{\text{Al,total}}$ | Measured pH | OH ⁻ [mmol/L] | Al [μmol/L] | Ca [mmol/L] | Fe [μmol/L] | S [mmol/L] | K [mmol/L] |
|-----------------------|----------------|-----------------------------|----------------|-----------------|------------------|-----------------|-----------------|
| 0.0 | 12.3 | 17 | 10.6 ± 0.1 | 14.90 ± 0.03 | 0.04 ± 0.04 | 24.42 ± 0.12 | 35.58 ± 0.11 |
| 0.0 ^a | 12.2 | 17 | n.d. | 4.38 ± 0.01 | 0.094 ± 0.001 | 9.11 ± 0.07 | 26.45 ± 0.05 |
| 0.0 ^b | 12.4 | 23 | n.d. | 3.95 ± 0.01 | 0.148 ± 0.001 | 5.54 ± 0.04 | 26.52 ± 0.05 |
| 0.1 | 12.3 | 13 | 7.5 ± 0.0 | 4.35 ± 0.00 | 0.5 ± 0.04 | 14.11 ± 0.18 | 33.04 ± 0.46 |
| 0.2 | 12.3 | 13 | 10.7 ± 0.1 | 3.53 ± 0.01 | 0.24 ± 0.05 | 13.26 ± 0.07 | 32.94 ± 0.13 |
| 0.3 | 12.3 | 17 | 12.0 ± 0.2 | 2.81 ± 0.01 | 0.18 ± 0.02 | 11.97 ± 0.08 | 33.89 ± 0.14 |
| 0.4 | 12.3 | 19 | 10.2 ± 0.4 | 3.15 ± 0.01 | 0.28 ± 0.14 | 11.50 ± 0.09 | 34.22 ± 0.07 |
| 0.5 | 12.3 | 20 | 10.4 ± 0.3 | 3.90 ± 0.05 | 0.57 ± 0.01 | 10.53 ± 0.04 | 33.63 ± 0.03 |
| 0.6 | 12.3 | 21 | 12.6 ± 0.3 | 3.06 ± 0.01 | 0.79 ± 0.07 | 9.79 ± 0.05 | 34.53 ± 0.07 |
| 0.7 | 12.2 | 20 | 10.3 ± 0.3 | 2.32 ± 0.01 | 0.41 ± 0.02 | 8.47 ± 0.02 | 32.61 ± 0.07 |
| 0.8 | 12.1 | 20 | 17.6 ± 0.6 | 1.72 ± 0.01 | 0.61 ± 0.07 | 7.36 ± 0.07 | 31.92 ± 0.06 |
| 0.9 | 12.1 | 19 | 1300 ± 17 | 0.27 ± 0.00 | 1.25 ± 0.06 | 5.48 ± 0.08 | 32.51 ± 0.39 |
| 1.0 | 12.2 | 20 | 1945 ± 40 | 0.25 ± 0.00 | 0.52 ± 0.01 | 4.30 ± 0.03 | 31.84 ± 0.03 |
| KOH- solution | | | 12.6 ± 0.4 | < DL | < DL | < DL | 33.34 ± 0.14 |
| Detection limit | - | - | < 0.2 | < 0.2 | < 0.04 | < 2.0 | < 0.3 |

(a) Results from precipitation and

(b) from dissolution experiments given in Chapter 2.

n.d.: not determined.

Detection limits are given for the undiluted solutions.

The concentration of the dissolved iron in the aqueous solutions was in the range of 0.0 to 1.3 $\mu\text{mol/L}$. The lowest concentration was obtained when iron is the dominating element in the solid phase ($X_{\text{Al,total}} = 0.0$ and 0.1). At higher ratios of $X_{\text{Al,total}}$ the iron concentration was slightly higher. Nevertheless, at a ratio of $X_{\text{Al,total}} = 1.0$, where no Fe-sulfate has been added, iron could be detected (Table 3.3). This had to be traced back to contamination during sample preparation or to contamination of the Al-sulfate.

The concentration of aluminum in the aqueous solutions of the different solid phases showed its maximum at the ratios of $X_{\text{Al,total}} = 1.0$ and $X_{\text{Al,total}} = 0.9$. Then it decreased rapidly and remained constant at about 10 $\mu\text{mol/L}$ at lower $X_{\text{Al,total}}$ values. But it can not be excluded that the measured low concentration of aluminum in the samples at ratios between $X_{\text{Al,total}} = 0.8$ and 0.0 was due to contamination, since in the used KOH-solution, which was treated like the samples, also an Al concentration about 10 $\mu\text{mol/L}$ could be detected, even though special attention was paid to exclude contamination (see section 3.3.3).

The highest calcium and sulfur concentrations occurred at a ratio of $X_{\text{Al,total}} = 0.0$, i.e. in the absence of aluminum. Both, calcium and sulfur, decreased between $X_{\text{Al,total}} = 0.0$ and $X_{\text{Al,total}} = 0.8$. At $X_{\text{Al,total}} = 0.9$ to 1.0 significant lower concentrations were measured. Thus the low iron concentrations, which are limited by the presence of Fe-hydroxide, were reflected in higher calcium and sulfur concentrations, while the relatively high aluminum concentrations led to lower Ca and S concentrations in the aqueous solutions.

3.5 Thermodynamic modeling

The ion concentrations and the solubility of $\text{Ca}_6[\text{Al}_{1-x}\text{Fe}_x(\text{OH})_6]_2(\text{SO}_4)_3 \cdot 26\text{H}_2\text{O}$ ($x = 0.0, 0.1, 0.2, \dots, 1.0$) at 20 °C were calculated using the geochemical code GEMS (Kulik, 2006). The thermodynamic data used are compiled in Table 3.4. Lothenbach et al. (2007) give for Al-ettringite a solubility product of $\log K_{\text{SO, Al-ettringite}} = -44.9 \pm 0.7$ at 25 °C for the reaction

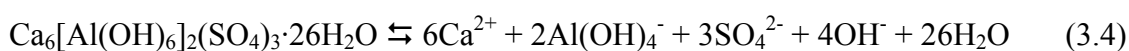


Table 3.4. Thermodynamic data given at 25 °C.

| Aqueous species | Reactions | log K or log β | Reference |
|--------------------------------|--|------------------------|-----------|
| | $\text{Ca}^{2+} + \text{H}_2\text{O} \rightleftharpoons \text{CaOH}^+ + \text{H}^+$ | -12.78 | a |
| | $\text{Ca}^{2+} + \text{SO}_4^{2-} \rightleftharpoons \text{CaSO}_4^0$ | 2.30 | a |
| | $\text{Ca}^{2+} + \text{HCO}_3^- \rightleftharpoons \text{CaHCO}_3^+$ | 1.106 | a |
| | $\text{Ca}^{2+} + \text{HCO}_3^- \rightleftharpoons \text{CaCO}_3^0 + \text{H}^+$ | -7.105 | a |
| | $\text{K}^+ + \text{H}_2\text{O} \rightleftharpoons \text{KOH}^0 + \text{H}^+$ | -14.46 | a |
| | $\text{K}^+ + \text{SO}_4^{2-} \rightleftharpoons \text{KSO}_4^-$ | 0.85 | a |
| | $\text{H}_2\text{O} \rightleftharpoons \text{OH}^- + \text{H}^+$ | -14.00 | a |
| | $\text{Fe}^{3+} + \text{H}_2\text{O} \rightleftharpoons \text{Fe(OH)}^{2+} + \text{H}^+$ | -2.19 | a |
| | $2\text{Fe}^{3+} + 2\text{H}_2\text{O} \rightleftharpoons \text{Fe}_2(\text{OH})_2^{4+} + 2\text{H}^+$ | -2.95 | a |
| | $3\text{Fe}^{3+} + 4\text{H}_2\text{O} \rightleftharpoons \text{Fe}_3(\text{OH})_4^{5+} + 4\text{H}^+$ | -6.30 | a |
| | $\text{Fe}^{3+} + 2\text{H}_2\text{O} \rightleftharpoons \text{Fe(OH)}_2^+ + 2\text{H}^+$ | -5.67 | a |
| | $\text{Fe}^{3+} + 3\text{H}_2\text{O} \rightleftharpoons \text{Fe(OH)}_3^0 + 3\text{H}^+$ | -12.56 | a |
| | $\text{Fe}^{3+} + 4\text{H}_2\text{O} \rightleftharpoons \text{Fe(OH)}_4^- + 4\text{H}^+$ | -21.60 | a |
| | $\text{Fe}^{3+} + \text{H}^+ + \text{SO}_4^{2-} \rightleftharpoons \text{FeHSO}_4^{2+}$ | 4.47 | a |
| | $\text{Fe}^{3+} + \text{SO}_4^{2-} \rightleftharpoons \text{FeSO}_4^+$ | 4.04 | a |
| | $\text{Fe}^{3+} + 2\text{SO}_4^{2-} \rightleftharpoons \text{Fe(SO}_4)_2^-$ | 5.38 | a |
| | $\text{Al}^{3+} + \text{H}_2\text{O} \rightleftharpoons \text{Al(OH)}^{2+} + \text{H}^+$ | -4.96 | a |
| | $\text{Al}^{3+} + 2\text{H}_2\text{O} \rightleftharpoons \text{Al(OH)}_2^+ + 2\text{H}^+$ | -10.59 | a |
| | $\text{Al}^{3+} + 3\text{H}_2\text{O} \rightleftharpoons \text{Al(OH)}_3^0 + 3\text{H}^+$ | -16.43 | a |
| | $\text{Al}^{3+} + 4\text{H}_2\text{O} \rightleftharpoons \text{Al(OH)}_4^- + 4\text{H}^+$ | -22.88 | a |
| | $\text{Al}^{3+} + \text{SO}_4^{2-} \rightleftharpoons \text{AlSO}_4^+$ | 3.90 | a |
| | $\text{Al}^{3+} + 2\text{SO}_4^{2-} \rightleftharpoons \text{Al(SO}_4)_2^-$ | 5.90 | a |
| Minerals | | log K_{S0} | Reference |
| Gypsum | $\text{CaSO}_4 \cdot 2\text{H}_2\text{O(s)} \rightleftharpoons \text{Ca}^{2+} + \text{SO}_4^{2-} + 2\text{H}_2\text{O}$ | -4.58 | a |
| Portlandite | $\text{Ca(OH)}_2(\text{s}) + 2\text{H}^+ \rightleftharpoons \text{Ca}^{2+} + 2\text{H}_2\text{O}$ | 22.80 | a |
| Calcite | $\text{CaCO}_3(\text{s}) + \text{H}^+ \rightleftharpoons \text{CaHCO}_3^+$ | 1.849 | a |
| Fe-ettringite | $\text{Ca}_6[\text{Fe(OH)}_6]_2(\text{SO}_4)_3 \cdot 26\text{H}_2\text{O} \rightleftharpoons 6\text{Ca}^{2+} + 2\text{Fe(OH)}_4^- + 3\text{SO}_4^{2-} + 4\text{OH}^- + 26\text{H}_2\text{O}$ | -44.0 | b |
| Al-ettringite | $\text{Ca}_6[\text{Al(OH)}_6]_2(\text{SO}_4)_3 \cdot 26\text{H}_2\text{O} \rightleftharpoons 6\text{Ca}^{2+} + 2\text{Al(OH)}_4^- + 3\text{SO}_4^{2-} + 4\text{OH}^- + 26\text{H}_2\text{O}$ | -44.9 | c |
| Fe(OH) ₃ (am.) | $\text{Fe(OH)}_3(\text{am}) + 3\text{H}^+ \rightleftharpoons \text{Fe}^{3+} + 3\text{H}_2\text{O}$ | 5.00 | a |
| Fe(OH) ₃ (microcr.) | $\text{Fe(OH)}_3(\text{mic}) + 3\text{H}^+ \rightleftharpoons \text{Fe}^{3+} + 3\text{H}_2\text{O}$ | 3.30 | d |

(a) Hummel et al., 2002

(b) Chapter 2

(c) Lothenbach et al., 2007

(d) this work

Using the data given in Table 3.5 and using Eq. 3.1 this refers to a solubility product of $\log K_{SO, Al\text{-ettringite}} = -45.5 \pm 0.7$ at 20 °C. The thermodynamic data of the ion species used for calculating the Gibbs free energy of reaction at 20 °C as well as at 25 °C are presented in Table 3.6. For Fe-ettringite a solubility product of $\log K_{SO, Fe\text{-ettringite}} = -44.7 \pm 0.7$ has been measured at 20 °C (cf. Chapter 2). For modeling the solid solution series between Fe- and Al-ettringite, the total solubility product were normalized so that the number of exchangeable sites was reduced to 1: $Ca_3[Al_{1-x}Fe_x(OH)_6](SO_4)_{1.5} \cdot 13H_2O$.

Table 3.5. Thermodynamic data of Al-ettringite and Fe-ettringite at 25 °C.

| | Al-ettringite (Lothenbach et al., 2007) | Fe-ettringite (cf. Chapter 2) |
|--------------------------|---|----------------------------------|
| $\Delta_f G^0$ in kJ/mol | -15206 | -14282 |
| $\Delta_f H^0$ in kJ/mol | -17535 | -16600 |
| S^0 in J/(mol·K) | 1900 | 1937 |
| C_p^0 in J/(mol·K) | 2174 | 2200 |
| a_0 | 1939 | 1922.384 |
| a_1 | 0.789 | 0.855 |
| a_2 | | 2020870 |

Table 3.6. Thermodynamic data at 20 and 25 °C used to calculate the apparent Gibbs free energy of formation of Al-ettringite and Fe-ettringite.

| Species | $\Delta_a G^0$ [kJ/mol] at 20 °C | $\Delta_f G^0$ [kJ/mol] at 25 °C | Reference |
|------------------------------------|-------------------------------------|-------------------------------------|-----------|
| H ₂ O _{liquid} | -236.835 | -237.183 | a |
| OH ⁻ | -157.318 | -157.270 | a |
| Ca ²⁺ | -553.071 | -552.790 | a |
| CO ₃ ²⁻ | -528.220 | 527.982 | a |
| Al(OH) ₄ ⁻ | -1301.298 | -1301.845 | a |
| Fe(OH) ₄ ⁻ | -841.696 | -842.624 | a |
| SO ₄ ²⁻ | -744.353 | -744.459 | a |
| Al-ettringite | -15196.53 | -15205.94 | b,c |
| Fe-ettringite | -14272.73 | -14282.36 | d |

(a) In GEMS, the log K data of the PSI Database (Hummel et al., 2002), which are applicable at standard pressure and temperature only, are merged with a subset of the supcrt database, as is documented in detail in (Thoenen and Kulik, 2003).

(b) this study

(c) Lothenbach et al., 2007

(d) Chapter 2

Assuming a continuous solid solution between Al- and Fe-ettringite the calculated ion concentrations agreed well with the measured concentrations, except for the ratio of $X_{\text{Al,total}} = 0.0$, where the measured concentrations were scattered (Fig. 3.6A). Although the standard deviation of the single measurements was small, the reproducibility seemed not to be that good. Fig. 3.6B shows the composition of the modeled solid phases.

Since calcite was detected by TGA (see Fig. 3.3A and Table 3.2), CO_2 was additionally fed into the initial bulk composition of the modeled experiments corresponding to the observed amount of calcite in the solid phases.

Taking the results of XRD analysis into account, the ion concentration were modeled taking the miscibility gap between $X_{\text{Al,total}} = 0.25$ and 0.65 into account. For modeling the binary Redlich-Kister model was used (Eq. 3.5), which is based on Guggenheim's expansion series for the excess Gibbs energy (G_{EX}) of mixing.

$$G_{\text{EX}} = RT \cdot X_{\text{Al-ettringite}} \cdot X_{\text{Fe-ettringite}} [a_0 + a_1 (X_{\text{Al-ettringite}} - X_{\text{Fe-ettringite}})] \quad (3.5)$$

where X stands for the mole fraction and a_0 and a_1 are the Guggenheim parameters. For further details see (Glynn, 1991; Anderson and Crerar, 1993; Glynn, 2000).

The dimensionless Guggenheim parameters (see Table 3.7) were calculated using the computer program MBSSAS (Glynn, 1991); these parameters were then fed into the model established by GEMS.

Table 3.7. Guggenheim parameters for a non-ideal solid solution between Al- and Fe-ettringite with a miscibility gap. (The parameters used in the model are in **bold**).

| | | | | | |
|----------------------------|-----------|-----------|------------------|-----------|-----------|
| Miscibility gap | 0.20-0.60 | 0.20-0.70 | 0.25-0.65 | 0.30-0.60 | 0.30-0.70 |
| Guggenheim parameter a_0 | 2.02 | 2.18 | 2.10 | 2.04 | 2.12 |
| Guggenheim parameter a_1 | -0.368 | -0.194 | -0.169 | -0.153 | 0 |

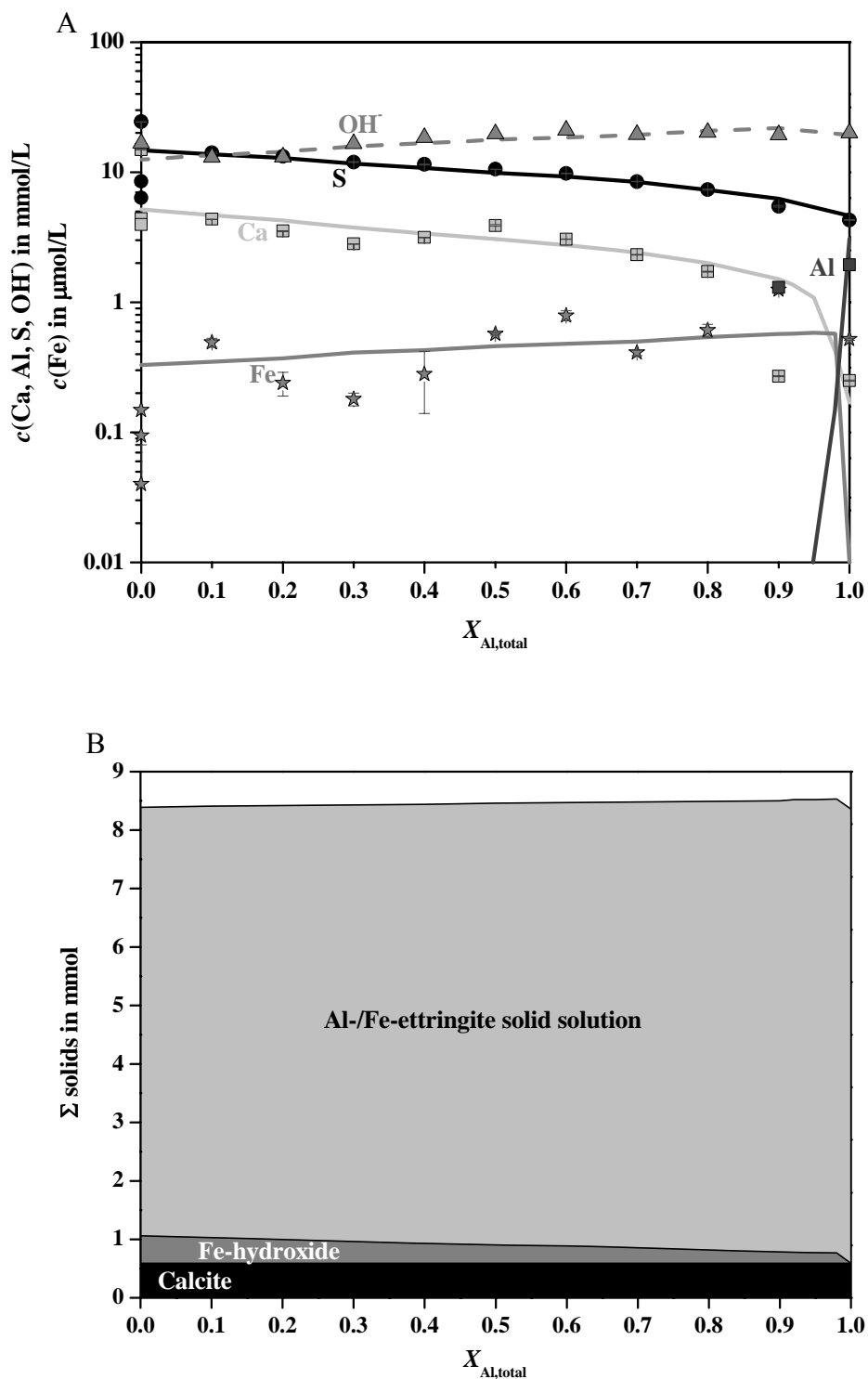
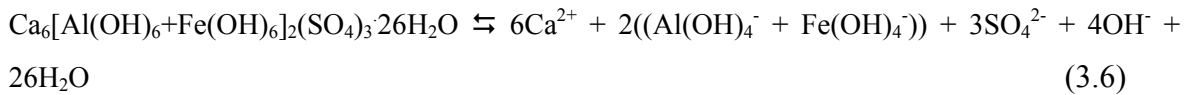


Fig. 3.6. (A) Measured and calculated concentrations of calcium (Ca), sulfur (S), iron (Fe), aluminum (Al), and OH⁻ concentration in the aqueous solution for ettringite synthesized with different $X_{\text{Al,total}}$ ratios assuming a continuous solid solution and the formation of calcite and Fe-hydroxide. Symbols present the measured and lines present the calculated concentrations. (B) Calculated solids assuming a continuous solid solution and the formation of calcite and Fe-hydroxide.

The calculated ion concentrations and the composition of the solid phases of the solid solution series with a miscibility gap between $X_{\text{Al,total}} = 0.25$ and 0.65 are presented (together with the experimental data) in Fig. 3.7. The modeled concentrations did not differ much from the calculated data of a continuous solid solution, but between $X_{\text{Al,total}} = 0.6$ and 0.9 for sulfur and hydroxide ions the concentrations were somewhat higher and for calcium even clearly higher concentrations were calculated (see Fig. 3.7A). The model without a miscibility gap fitted somewhat better to the experimental data of the aqueous phase (cf. Fig. 3.6A and 3.7A), which was contrary to XRD results.

Since the results obtained from experiments and modeling were ambiguous the solubility products of Fe-ettringite and Al-ettringite as well as the total solubility products of the solid solution series were determined. The dissolution reaction of $\text{Ca}_6[\text{Al}_{1-x}\text{Fe}_x(\text{OH})_6]_2(\text{SO}_4)_3 \cdot 26\text{H}_2\text{O}$ is given by



According to this dissolution reaction the total solubility product (ΣII) can be calculated (cf. Glynn et al., 1990; Glynn, 1991).

$$\Sigma II = \{\text{Ca}^{2+}\}^6 \cdot \{(\text{Al}(\text{OH})_4^- + \text{Fe}(\text{OH})_4^-)\}^2 \cdot \{\text{SO}_4^{2-}\}^3 \cdot \{\text{OH}^-\}^4 \cdot \{\text{H}_2\text{O}\}^{26} \quad (3.7)$$

where $\{\}$ denotes the activity.

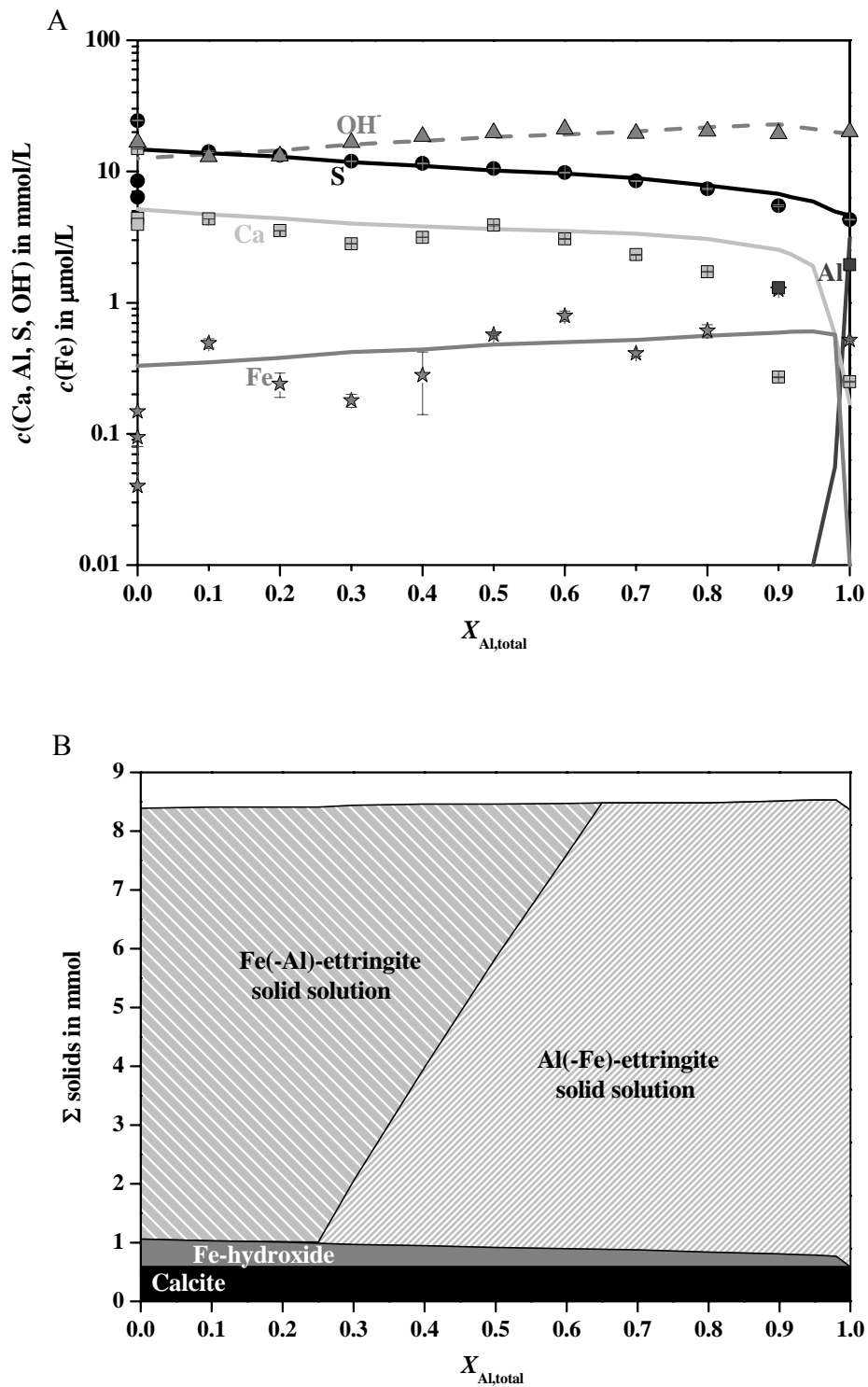


Fig. 3.7. (A) Measured and calculated concentrations of calcium (Ca), sulfur (S), iron (Fe), aluminum (Al), and OH⁻ concentration in the aqueous solution for ettringite synthesized with different $X_{\text{Al,total}}$ ratios assuming a miscibility gap between $X_{\text{Al,total}} = 0.25-0.65$ and the formation of calcite and Fe-hydroxide. Symbols present the measured and lines present the calculated concentrations. (B) Calculated solids assuming a miscibility gap between $X_{\text{Al,total}} = 0.25-0.65$ and the formation of calcite and Fe-hydroxide.

On the basis of the measured ion concentrations and the analyzed composition of the solid phases ΣII could be calculated with GEMS using the activities of the species for every sample. The calculated total solubility products at 20 °C are presented in Fig. 3.8. The obtained solubility products varied between $\log \Sigma II = -46.4$ ($X_{Al,total} = 0.3$) and $\log \Sigma II = -43.6$ ($X_{Al,total} = 0.0$) and did not show a clear trend. If the formation of an ideal solid solution was assumed, the modeled total solubility product between the two endmembers showed an almost linear trend (dashed line in Fig. 3.8 presents ΣII of an ideal solid solution), while, assuming a miscibility gap between $X_{Al,total} = 0.25$ and 0.65 , ΣII (dashed-dotted line) stayed constant in the range of the miscibility gap, and then decreased abruptly from $X_{Al,total} = 0.85 - 1.0$. In the case of a miscibility gap the total solubility products are higher than for an ideal solid solution. Some of the experimentally determined solubilities were much lower and visually it seemed that the observed solubilities were better represented by an ideal solid solution. The measurements of the dissolved concentration of a single solubility experiment showed a good reproducibility and thus a low standard deviation (see Table 3.3 and Fig. 3.6-3.8). The reproducibility of such a solubility experiment, however, is much smaller as illustrated in Fig. 3.6-3.8. Small differences in the concentration of the different ion species result in relatively large difference in the total solubility product of the solid solution series of ettringite (cf. Eq. 3.7.). As the solubility products of pure Al- and Fe-ettringite differ only in 0.8 log units and as the standard deviation of the two endmembers is ± 0.7 log units, the observed scatter of the total solubility products represented rather the scatter of the experimental data than any real trend. Hence, neither an ideal solid solution, nor a miscibility gap could be excluded by calculating the total solubility products.

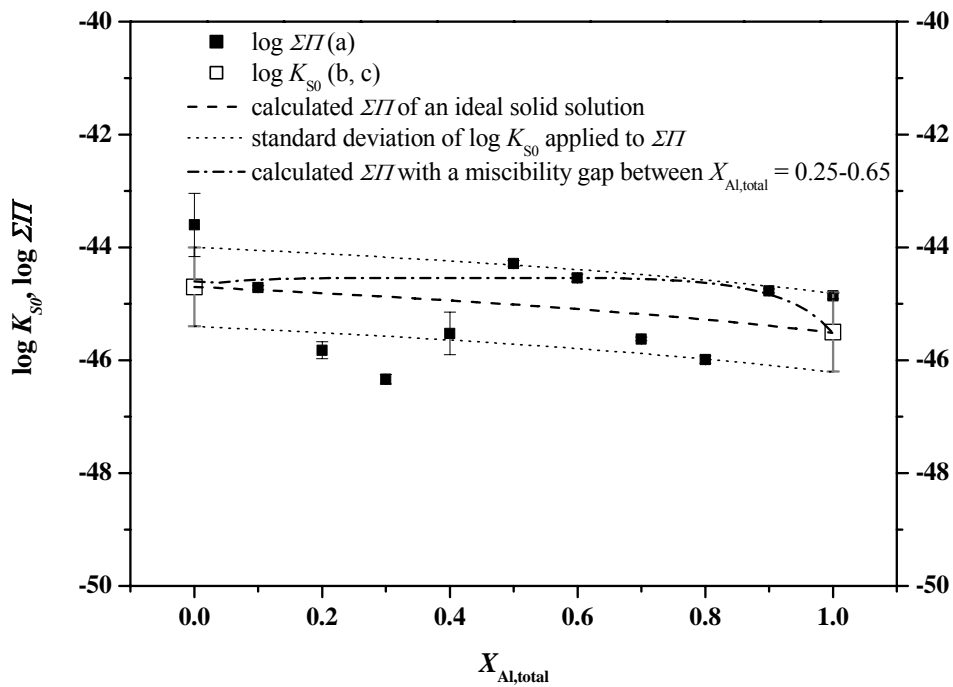


Fig. 3.8. Calculated and published solubility products of ettringite phases at different $X_{Al,total}$ ratios. (a) this study, (b) Chapter 2, (c) Lothenbach et al., 2007.

3.6 Conclusion

Both, pure aluminum and pure iron ettringite are well investigated minerals. But the miscibility of these two phases is sparsely investigated. Buhlert and Kuzel (1971) assumed the presence of a miscibility gap between the molar ratios of $X_{Al,total} = 0.2$ to 0.3 , since they found by XRD analysis a broadening of the main peak in this range. In this study XRD analysis indicated the presence of a miscibility gap between the molar ratios of $X_{Al,total} = 0.25 \pm 0.05$ and 0.65 ± 0.05 in the solid solution series of Al- and Fe-ettringite. Though the main peak (100) of the synthesized ettringite phases did not show a broadening, other peaks (104, 114, 116 and 216) clearly showed a broadening for the samples from $X_{Al,total} = 0.3$ to $X_{Al,total} = 0.6$.

Thermodynamic modeling was carried out to confirm the assumption of a miscibility gap in the solid solution series of Al- and Fe-ettringite. Therefore, the conditions of the

experiments were simulated, considering both cases: miscibility gap and an ideal solid solution. The calculated ion concentrations agreed slightly better when an ideal solid solution between Al- and Fe-ettringite was assumed.

Although the analyses of the aqueous phases were somewhat ambiguous, analyses of the solid phases indicated the existence of a miscibility gap for the solid solution series $\text{Ca}_6[\text{Al}_{1-x}\text{Fe}_x(\text{OH})_6]_2(\text{SO}_4)_3 \cdot 26\text{H}_2\text{O}$ between $X_{\text{Al, total}} = 0.25 \pm 0.05$ and 0.65 ± 0.05 .

Finally it has to be pointed out that within other systems, with different conditions as used in these experiments, the formation of a solid solution series between Al- and Fe-ettringite can be preferred or inhibited. For example, the formation of Fe-ettringite is much slower than the formation of Al-ettringite (cf. Chapter 2), therefore for the formation of Al-/Fe-ettringite phases enough time is required. Higher temperature will lead to a diminution of the miscibility gap.

Acknowledgments

The authors would like to thank Luigi Brunetti for his support during laboratory work. The financial support (Grant 20021-103546) of the Swiss National Foundation is gratefully acknowledged.

3.7 References

- Albino, V., Cioffi, R., Marroccoli, M., and Santoro, L., 1996. Potential application of ettringite generating systems for hazardous waste stabilization. *Journal of Hazardous Materials* **51**, 241-252.
- Anderson, G. M. and Crerar, D. A., 1993. *Thermodynamics in Geochemistry. The Equilibrium Model*. Oxford University Press, New York, Oxford.

- Antao, S. M., Duane, M. J., and Murdoch, J., 2002. DTA, TG and XRD studies of sturmanite and ettringite. *The Canadian Mineralogist* **40**, 1403-1409.
- Bannister, F. A., 1936. Ettringite from Scawt Hill, Co. Antrim.. *Mineralogical Magazine* **6**, 324-329.
- Baur, I. and Johnson, C. A., 2003. The solubility of selenate-Aft ($3\text{CaO}\cdot\text{Al}_2\text{O}_3\cdot 3\text{CaSeO}_4\cdot 37.5\text{H}_2\text{O}$) and selenate-AFm ($3\text{CaO}\cdot\text{Al}_2\text{O}_3\cdot\text{CaSeO}_4\cdot x\text{H}_2\text{O}$). *Cement and Concrete Research* **33**, 1741-1748.
- Berry, L. G., 1963. The unit cell of ettringite. *The American Mineralogist* **48**, 939-940.
- Black, L., Breen, C., Yarwood, J., Phipps, J., and Maitland, G., 2006. In situ Raman analysis of hydrating C₃A and C₄AF pastes in presence and absence of sulphate. *Advances in Applied Ceramics* **105**, 209-216.
- Brown, P. W., 1993. Kinetics of tricalcium aluminate and tetracalcium aluminoferrite hydration in the presence of calcium sulfate. *Journal of the American Ceramic Society* **76**, 2971-2976.
- Buhlert, R. and Kuzel, H.-J., 1971. Ueber den Einbau von Cr³⁺ und Fe³⁺ in Ettringit. *Zement-Kalk-Gips* **2**, 83-85.
- Chrysochoou, M. and Dermatas, D., 2006. Evaluation of ettringite and hydrocalumite formation for heavy metal immobilization: Literature review and experimental study. *Journal of Hazardous Materials* **136**, 20-33.
- Collepari, M., Monosi, S., and Moriconi, G., 1979. Tetracalcium aluminoferrite hydration in the presence of lime and gypsum. *Cement and Concrete Research* **9**, 431-437.
- Csizmadia, J., Balazs, G., and Tamas, F. D., 2001. Chloride ion binding capacity of aluminoferrites. *Cement and Concrete Research* **31**, 577-588.
- Dunn, P. J., Peacor, D. R., Leavens, P. B., and Baum, J. L., 1983. Charlesite, a new mineral of the ettringite group, from Franklin, New Jersey. *The American Mineralogist* **68**, 1033-1037.

- Emanuelson, A. and Hansen, S., 1997. Distribution of iron among ferrite hydrates. *Cement and Concrete Research* **27**, 1167-1177.
- Fukuhara, M., Goto, S., Asage, K., Daimon, M., and Kondo, R., 1981. Mechanisms and kinetics of C₄AF hydration with gypsum. *Cement and Concrete Research* **11**, 407-414.
- Galimova, L. A., Danilov, V. P., Lepeshkov, I. N., Yudovich, B. E., and Shebanov, N. A., 1988. A study of the formation and decomposition of the calcium iron(III) double hydroxide sulphate Ca₆Fe₂(OH)₁₂(SO₄)₃ · 26H₂O in the 3Ca(OH)₂ + Fe₂(SO₄)₃ --> 3CaSO₄ + 2Fe(OH)₃-H₂O system at 20 °C. *Russian Journal of Inorganic Chemistry* **33**, 445-448.
- Glynn, P. D., Reardon, E. J., Plummer, L. N., and Busenberg, E., 1990. Reaction paths and equilibrium end-points in solid-solution aqueous-solution systems. *Geochimica et Cosmochimica Acta* **54**, 267-282.
- Glynn, P. D., 1991. MBSSAS: A code for the computation of Margules parameters and equilibrium relations in binary solid-solution aqueous-solution systems. *Computers & Geosciences* **17**, 907-966.
- Glynn, P., 2000. Solid-solution solubilities and thermodynamics: Sulfates, carbonates and halides, Sulfate minerals - Crystallography, Geochemistry and Environmental Significance. *Reviews in Mineralogy & Geochemistry* **40**, 481-511.
- Goetz-Neunhoeffler, F., Neubauer, J., and Schwesig, P., 2006. Mineralogical characteristics of ettringites synthesized from solutions and suspensions. *Cement and Concrete Research* **36**, 65-70.
- Goetz-Neunhoeffler, F. and Neubauer, J., 2006. Refined ettringite (Ca₆Al₂(SO₄)₃(OH)₁₂·26H₂O) structure for quantitative X-ray diffraction analysis. *Powder Diffraction* **21**, 4-11.
- Holleman, A. F. and Wiberg, E., 1985. *Lehrbuch der anorganischen Chemie*. de Gruyter, Berlin.

- Hummel, W., Berner, U., Curti, E., Pearson, F. J., and Thoenen, T., 2002. *Nagra/PSI Chemical Thermodynamic Data Base 01/01*. Universal Publishers/uPublish.com, Parkland, Florida.
- Hurlbut, C. S., and Baum, J. L., 1960. Ettringite from Franklin, New Jersey. *The American Mineralogist* **45**, 1137-1143.
- Kulik, D. A., 2002. Minimising uncertainty induced by temperature extrapolations of thermodynamic data: A pragmatic view on the integration of thermodynamic databases into geochemical computer codes. *The use of thermodynamic databases in performance assessment*. OECD, Paris, Barcelona, Spain.
- Kulik, D. A., 2006. GEMS-PSI 2.12, PSI Villigen, Switzerland; available at <http://les.web.psi.ch/Software/GEMS-PSI/index.html>
- Liang, T. and Nanru, Y., 1994. Hydration products of calcium aluminoferrite in the presence of gypsum. *Cement and Concrete Research* **24**, 150-158.
- Lothenbach, B., Matschei, T., Möschner, G., and Glasser, F. P., 2007. Thermodynamic modelling of the effect of temperature on the hydration and porosity of Portland cement. *Cement and Concrete Research* **submitted**.
- Meller, N., Hall, C., Jupe, A. C., Colston, S. L., Jacques, S. D. M., Barnes, P., and Phipps, J., 2004. The paste hydration of brownmillerite with and without gypsum: a time resolved synchrotron diffraction study at 30, 70, 100 and 150 °C. *Journal of Materials Chemistry* **14**, 428-435.
- McConnell, D. and Murdoch, J., 1962. Crystal chemistry of ettringite. *Mineralogical Magazine* **15**, 59-64.
- McMurdie, H. F., Morris, M. C., Evans, E. H., Paretzkin, B., Wong-Ng, W., and Zhang, Y., 1987. Standard X-ray diffraction powder patterns from the JCPDS research associateship. *Powder Diffraction* **2**, 41-52.
- Moore, A. and Taylor, H. F. W., 1968. Crystal structure of ettringite. *Nature* **218**, 1048.

- Moore, A. and Taylor, H. F. W., 1970. Crystal structure of ettringite. *Acta Crystallographica Section B* **26**, 386-393.
- Peacor, D. R., Dunn, P. J., and Duggan, M., 1983. Sturmanite, a ferric iron, boron analogue of ettringite. *The Canadian Mineralogist* **21**, 705-709.
- Pearson, F. J. and Berner, U., 1991. Nagra thermochemical data base. I. Core data. *Nagra – Technical Report 91-17*. Nagra, Wettingen (Switzerland).
- Perkins, R. B. and Palmer, C. D., 1999. Solubility of ettringite ($\text{Ca}_6[\text{Al}(\text{OH})_6]_2(\text{SO}_4)_3 \cdot 26\text{H}_2\text{O}$) at 5-75°C. *Geochimica et Cosmochimica Acta* **63**, 1969-1980.
- Perkins, R. B. and Palmer, C. D., 2000. Solubility of $\text{Ca}_6[\text{Al}(\text{OH})_6]_2(\text{CrO}_4)_3 \cdot 26\text{H}_2\text{O}$, the chromate analogue of ettringite; 5-75°C. *Applied Geochemistry* **15**, 1203-1218.
- Pushcharovsky, D. Y., Lebedeva, Y. S., Zubkova, N. V., Pasero, M., Bellezza, M., Merlino, S., and Chukanov, N. V., 2004. The crystal structure of sturmanite. *The Canadian Mineralogist* **42**, 723-729.
- Rodgers, K. A. and Courtney, S. F., 1988. New mineral records from Funafuti, Tuvalu: gypsum, brucite, ettringite. *Mineralogical Magazine* **52**, 411-414.
- Schwiete, H.-E. and Ludwig, U., 1968. Crystal structures and properties of cement hydration products (hydrated calcium aluminates and ferrites). *Proceedings of the Fifth International Symposium on the Chemistry of Cement*, Tokyo.
- Taylor, H. F. W., 1997. *Cement Chemistry*. Thomas Telford Publishing, London.
- Thoenen, T. and Kulik, D.A., 2003. Nagra/PSI Chemical Thermodynamic Data Base 01/01 for the GEM-Selektor (V.2-PSI) Geochemical Modeling Code: Release 28-02-03. Internal report TM-44-03-04, available at <http://les.web.psi.ch/software/GEMS-PSI/thermodata/index.html>.

Ulrich, A. and Wichser, A., 2003. Analysis of additive metals in fuel and emission aerosols of diesel vehicles with and without particle traps. *Analytical and Bioanalytical Chemistry* **377**, 71-81.

Wieczorek-Ciurowa, K., Fela, K., and Kozak, A.J., 2001. Chromium(III)-ettringite formation and its thermal stability. *Journal of Thermal Analysis and Calorimetry* **65**, 655-660.

4 **Thermodynamic modeling of the influence of citric acid on the hydration of Portland cement**

G. Möschner, B. Lothenbach, R. Figi, R. Kretzschmar

Submitted for publication in Cement and Concrete Research

4.1 Abstract

Citric acid can be used to retard the hydration of cement. Experiments were carried out to investigate the influence of citric acid on the composition of solid and liquid phases during cement hydration. Analyses of the solid phases showed that dissolution of alite and aluminate slowed down while analyses of the pore solution showed that citric acid was removed almost completely from the pore solution within the first hours of hydration. The complexation of the ions by citrate was weak, which could also be confirmed by thermodynamic calculations. Only 9 % of the citrate formed complexes (mainly with calcium) during the first hours. Thus, citric acid retards cement hydration not by complex formation, but by slowing down the dissolution of the clinker grains by adsorbing and/or precipitating on the surface and forming a protective layer (K-citrate).

4.2 Introduction

Citric acid retards the hydration of Portland cements or its constituents. Tinnea and Young (1977) and Singh et al. (1990) showed that citric acid has a retarding effect on the hydration in the system C₃A-gypsum-portlandite-water, while Stadelmann (1987) showed that citric acid has the same effect on the hydration of C₃S. Wilding et al. (1984) and Ramachandran and Lowery (1992) investigated the effect of citric acid, and citrate

respectively, on Portland cement and showed by conduction calorimetry that the hydration of Portland cement is retarded. Other investigations aimed to understand the mechanisms of the retardation. Pore solutions (collected after different times of hydration) have been analyzed for ion concentrations and organic carbon. The zeta potential as well as the composition of the hydrated solid phases have been studied (Singh et al., 1986; Schwarz, 1995; Smillie and Glasser, 1999). Singh et al. (1986) found that the zeta potential of cement decreases with increasing amounts of citric acid added, which was explained by the adsorption of citrate ions onto the positively charged surfaces of the Portland cement grains. Schwarz (1995) concluded that citrate increases the dissolution rate of the ferrite phase. Smillie and Glasser (1999) found that citric acid (15.6 mmol/l) is removed almost quantitatively from the cement pore water within the first hour of cement hydration. Schwarz et al. (1994) postulated that citrate forms stable complexes with polyvalent metal cations, which were claimed to affect both, the solution and the (ferro-)aluminate-surface chemistry.

Thermodynamic modeling has been used to calculate the composition of pore solution and solid phases after different hydration times, which gives an insight into the chemical processes during cement hydration (Lothenbach and Winnefeld, 2006). Lothenbach et al. (2007) have also studied the influence of temperature on the hydration products of cement by thermodynamic modeling and have shown that thermodynamic modeling can be a powerful tool to predict the phase assemblage during cement hydration.

In the title study the influence of citric acid on the hydration of Portland cement was studied. The changes in the composition of the liquid and solid phase as a function of time and amount of citric acid added were investigated. Thermodynamic modeling was used to calculate the extent of complex formation of the dissolved ions and the results were compared with the experimentally determined concentration.

4.3 Materials and methods

4.3.1 Experiments

All experiments were carried out using an ordinary Portland cement (OPC), CEM I 42.5 N, at 20 °C. The composition of the unhydrated cement and the calculated amount of the clinker phases are shown in Table 4.1. The chemical composition of the unhydrated cement was determined by X-ray fluorescence (XRF).

Cement pastes were prepared with a w/c of 0.4 by adding 1 kg cement to 400 g distilled water. To study the retardation of citric acid ($C_6H_8O_7$) on the hydration, three different concentration of citric acid were added to the mixing water, equivalent to 0.1, 0.4 and 0.5 weight-% of cement resulting in concentrations of citric acid of 13, 52 and 65 mmol/l. The solutions were mixed for 3 minutes with the cement in an EN 196-1 type mixer. The pastes were stored in 0.5 l PE bottles (0.1 l for fresh cement pastes) under controlled conditions at 20 °C. For experiments with fresh pastes (up to 8 hours) the pore solution was collected by vacuum filtration using a 0.45 μm nylon filter. For longer hydration times the pore solution was extracted using the steel die method with pressure up to 250 N/mm². The solutions were also filtered through a 0.45 μm nylon filter. One part of the pore solution was then immediately used to measure the pH value. Another part was acidified with HNO₃ supra pure for ICP-OES (and ICP-MS) analysis and diluted 1:10 (1:100 respectively) to prevent the precipitation of solids. A third part was diluted 1:10 using 0.1 M HCl solution to determine the dissolved organic carbon (DOC). The pH-electrode used had been calibrated against KOH solutions with known concentrations ($c(\text{KOH}) = 0.1 - 1.0 \text{ mol/L}$) before measurements. The concentrations of Al, Ba, Ca, K, Li, Mo, Na, S, Si and Sr were determined with ICP-OES. Fe and Cr concentrations were determined with ICP-MS.

Table 4.1. Composition of the OPC used (CEM I 42.5 N) ^a.

| Chemical analysis | | Normative phase composition ^b | |
|---|--------|--|--------|
| | g/100g | | g/100g |
| SiO ₂ | 19.6 | alite | 50.0 |
| Al ₂ O ₃ | 4.60 | belite | 18.5 |
| Fe ₂ O ₃ | 2.90 | aluminate | 7.3 |
| CaO | 62.4 | ferrite | 8.8 |
| MgO | 1.60 | CaO | 0.46 |
| SrO | 0.06 | CaCO ₃ | 4.8 |
| K ₂ O | 0.97 | CaSO ₄ ^c | 4.3 |
| Na ₂ O | 0.12 | K ₂ SO ₄ ^e | 1.4 |
| CaO (free) | 0.46 | Na ₂ SO ₄ ^e | 0.08 |
| CO ₂ | 2.11 | SrO | 0.06 |
| SO ₃ | 3.25 | K ₂ O ^d | 0.24 |
| <i>Readily soluble alkalis</i> ^e | | Na ₂ O ^d | 0.09 |
| K ₂ O | 0.30 | MgO ^d | 1.6 |
| Na ₂ O | 0.012 | SO ₃ ^d | 0.05 |

Blaine surface area: 316 m²/kg. Ignition loss: 2.7g/100g.

^a The OPC used contained 0.2 % FeSO₄·7H₂O as chromate reducing agent.

^b Calculated from the chemical analysis.

^c Present as anhydrite (1.8g/100g), hemihydrate (1.3g/100g), and gypsum (1.6g/100g).

^d Present as solid solution in the major clinker phases (distributed according to Table 1.3 in Taylor (1997)).

^e Readily soluble alkalis were calculated from the concentrations of alkalis measured in the solution after 5 minutes agitation at a w/c of 10.

After the different hydration times, hydration was stopped by immersion of the crushed samples in isopropanol for about 15 minutes. The samples were then dried at 40 °C, ground by hand to < 63 μm and used for XRD and thermogravimetric analyses. XRD analyses were performed on a PANalytical X'Pert Pro using CuKα radiation. For TGA (Mettler Toledo TGA/SDTA851^e) about 8 – 12 mg per sample were heated under N₂ over a temperature range of 30 to 980 °C at a rate of 20 °C/min.

Calorimetric measurements were carried out with a Thermometric TAM Air on 6 g of the fresh paste at w/c = 0.4.

4.3.2 Thermodynamic calculations

Thermodynamic calculations were carried out using the geochemical code GEMS-PSI (Kulik, 2006). GEMS-PSI is a broad-purpose geochemical modeling code, which computes equilibrium phase assemblage and speciation in a complex chemical system from its total bulk elemental composition. Chemical interactions involving solids, solid solutions, gas mixture and aqueous electrolyte are considered simultaneously. The default database of GEMS code was used, which is based on the PSI chemical thermodynamic database (Hummel et al., 2002) expanded with additional data for solids that are expected to form under cementitious conditions (Lothenbach and Winnefeld, 2006) as well as with constants for citric acid and some citrate complexes (thermodynamic constants used for citrate are summarized in Table 4.2).

Table 4.2. Thermodynamic data used to consider citrate-complexes ($H_3cit = citric\ acid$).

| Species | Reaction | $\log K_{S0}$ | Reference |
|-------------------------|---|--------------------|----------------------------|
| <i>Aqueous</i> | | | |
| $Hcit^{2-}$ | $Hcit^{2-} \rightleftharpoons cit^{3-} + H^+$ | 6.36 | NEA, 2006 |
| H_2cit^{1-} | $H_2cit^{1-} \rightleftharpoons Hcit^{2-} + H^+$ | 4.78 | NEA, 2006 |
| H_3cit^0 | $H_3cit^0 \rightleftharpoons H_2cit^-$ | 3.13 | NEA, 2006 |
| $Mgcit-1$ | $Mgcit^- \rightleftharpoons Mg^{2+} + cit^{3-}$ | 4.81 | NEA, 2006 |
| $MgHcit^0$ | $MgHcit^0 \rightleftharpoons Mg^{2+} + Hcit^{2-}$ | 2.60 | NEA, 2006 |
| MgH_2cit^+ | $MgH_2cit^+ \rightleftharpoons Mg^{2+} + H_2cit^-$ | 1.31 | NEA, 2006 |
| $Cacit^-$ | $Cacit^- \rightleftharpoons Ca^{2+} + cit^{3-}$ | 4.80 | NEA, 2006 |
| $CaHcit^0$ | $CaHcit^0 \rightleftharpoons Ca^{2+} + Hcit^{2-}$ | 2.92 | NEA, 2006 |
| CaH_2cit^+ | $CaH_2cit^+ \rightleftharpoons Ca^{2+} + H_2cit^-$ | 1.53 | NEA, 2006 |
| $Kcit^{2-}$ | $K^+ + cit^{3-} \rightleftharpoons Kcit^{2-}$ | 1.03 | Zelenina and Zelenin, 2005 |
| K_2cit^- | $2K^+ + cit^{3-} \rightleftharpoons K_2cit^-$ | 1.39 | Zelenina and Zelenin, 2005 |
| $Nacit^{2-}$ | $Na^+ + cit^{3-} \rightleftharpoons Nacit^{2-}$ | 1.00 | Zelenina and Zelenin, 2005 |
| Na_2cit^- | $2Na^+ + cit^{3-} \rightleftharpoons Na_2cit^-$ | 1.81 | Zelenina and Zelenin, 2005 |
| $AlHcit^+$ | $Al^{3+} + Hcit^{2-} \rightleftharpoons AlHcit^+$ | 4.70 | Martin, 1986 |
| $Alcit^0$ | $AlHcit^+ \rightleftharpoons Alcit^0 + H^+$ | -2.50 | Martin, 1986 |
| $AlcitOH^-$ | $Alcit^0 \rightleftharpoons AlcitOH^- + H^+$ | -3.40 | Martin, 1986 |
| $Fe(III)cit^0$ | $Fe^{3+} + cit^{3-} \rightleftharpoons Fe(III)cit^0$ | 7.67 ^a | Königsberger et al., 2000 |
| $Fe(III)citOH^-$ | $Fe^{3+} + cit^{3-} + H_2O \rightleftharpoons Fe(III)citOH^- + H^+$ | 5.48 ^a | Königsberger et al., 2000 |
| $Fe(III)(cit)_2^{3-}$ | $Fe^{3+} + 2cit^{3-} \rightleftharpoons Fe(III)(cit)_2^{3-}$ | 11.64 ^a | Königsberger et al., 2000 |
| $Fe(III)(cit)_2H^{2-}$ | $Fe^{3+} + 2cit^{3-} + H^+ \rightleftharpoons Fe(III)(cit)_2H^{2-}$ | 14.84 ^a | Königsberger et al., 2000 |
| $Fe(III)(cit)_2OH^{4-}$ | $Fe^{3+} + 2cit^{3-} + H_2O \rightleftharpoons Fe(III)(cit)_2OH^{4-} + H^+$ | 7.51 ^a | Königsberger et al., 2000 |
| <i>Solids</i> | | | |
| $H_3cit(cr)$ | $H_3cit(H_2O)(cr) \rightleftharpoons H_3cit^0 + H_2O$ | -1.33 | NEA, 2006 |
| $Ca_3cit_2(H_2O)_4(cr)$ | $Ca_3cit_2(H_2O)_4(cr) \rightleftharpoons 3Ca^{2+} + 4H_2O + 2cit^{3-}$ | 1.79 | NEA, 2006 |
| $K_3cit(H_2O)(cr)$ | $K_3cit(H_2O)(cr) \rightleftharpoons 3K^+ + cit^{3-} + H_2O$ | -1.24 | Apelblat, 1994 |
| KH_2citer | $KH_2cit(cr) \rightleftharpoons K^+ + H_2cit^-$ | -6.21 | Apelblat, 1994 |
| $Na_3cit(H_2O)_2(cr)$ | $Na_3cit(H_2O)_2(cr) \rightleftharpoons 3Na^+ + cit^{3-} + 2H_2O$ | -1.19 | Apelblat, 1994 |
| $Na_2Hcit(cr)$ | $Na_2Hcit(cr) \rightleftharpoons 2Na^+ + Hcit^{2-}$ | -3.94 | Apelblat, 1994 |
| $NaH_2cit(cr)$ | $NaH_2cit(cr) \rightleftharpoons Na^+ + H_2cit^-$ | -4.87 | Apelblat, 1994 |

(a) Solubility product was corrected with the Davis equation from $I = 1$ to $I = 0$ (Königsberger et al., 2000).

4.4 Results and discussion

4.4.1 Calorimetry

Isothermal heat conduction calorimetry allows following the progress of hydration. In the absence of citric acid the main peak of heat release, related mainly to C_3S hydration, was found after approx. 12 hours (see Fig. 4.1). This maximum of heat release was shifted to ~17 hours, if 0.1 wt.-% citric acid had been added. With 0.4 wt.-% citric acid the main peak of heat release occurred only after ~84 hours and with 0.5 wt.-% citric acid the main peak did not occur before 180 hours. With increasing amounts of citric acid the maximum heat release decreased continuously, and the peak broadened, indicating that the addition of citrate strongly retarded the hydration of the used Portland cement. Similarly the total heat release after 180 hours decreased from 20.5 kJ/(g*h) to 7.6 kJ/(g*h) in the presence of 0.5 wt.-% citric acid. In the presence of 0.1 wt.-% citric acid the total heat release amounted 20.5 kJ/(g*h) like in the plain paste while in the presence of 0.4 wt.-% citric acid the amount was 16.8 kJ/(g*h).

Ramachandran and Lowery (1992) observed similar to our observations that the addition of 0.2 wt.-% Na-citrate (at a w/c of 0.5) shifted the main peak of heat release from 9 to approximately 20 hours. With increasing addition of Na-citrate (up to 0.4 wt.-%) the maximum of heat release decreased and the peak broadened. In contrast to these findings Singh et al. (1986) stated that 0.1 wt.-% citric acid accelerated the hydration of Portland cement.

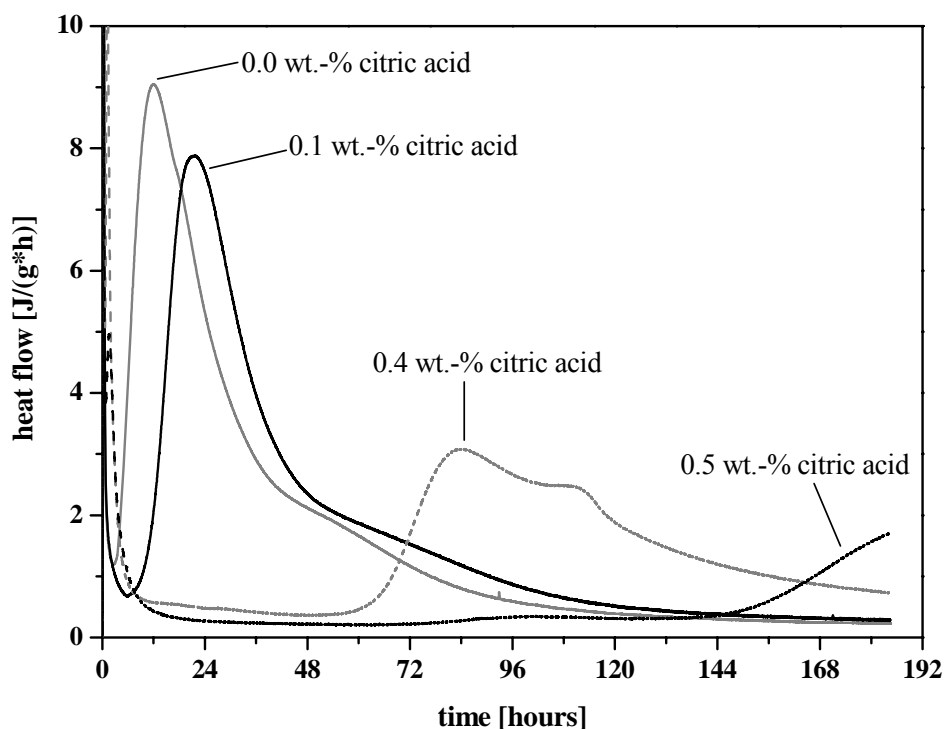


Fig. 4.1. Calorimetry curves of the OPC used (CEM I 42.5 N) with different amounts of added citric acid.

4.4.2 Solid phases

The changes of the composition of the solid phases during hydration were followed by XRD and TGA/DTA. The unhydrated cement contained small quantities of calcite, portlandite and gypsum as observed by TGA measurements. During hydration the quantities of alite, belite, aluminate, and ferrite decreased (cf. Fig. 4.2). The semi-quantitative XRD analysis showed that in the absence of citric acid, the amount of alite and aluminate decreased relatively fast, while the amount of belite and ferrite diminished only very slowly (Fig. 4.2). The addition of citric acid to the mixing water showed clearly a retarding effect on the dissolution of the clinker phases. This is in agreement with the observations by calorimetry (Fig. 4.1). The XRD analysis showed that upon the addition of citric acid the dissolution of alite slowed down considerably (Fig. 4.3). For aluminate a

much less pronounced retardation in the presence of citric acid was observed (Fig. 4.4). For belite and ferrite no clear trends could be observed.

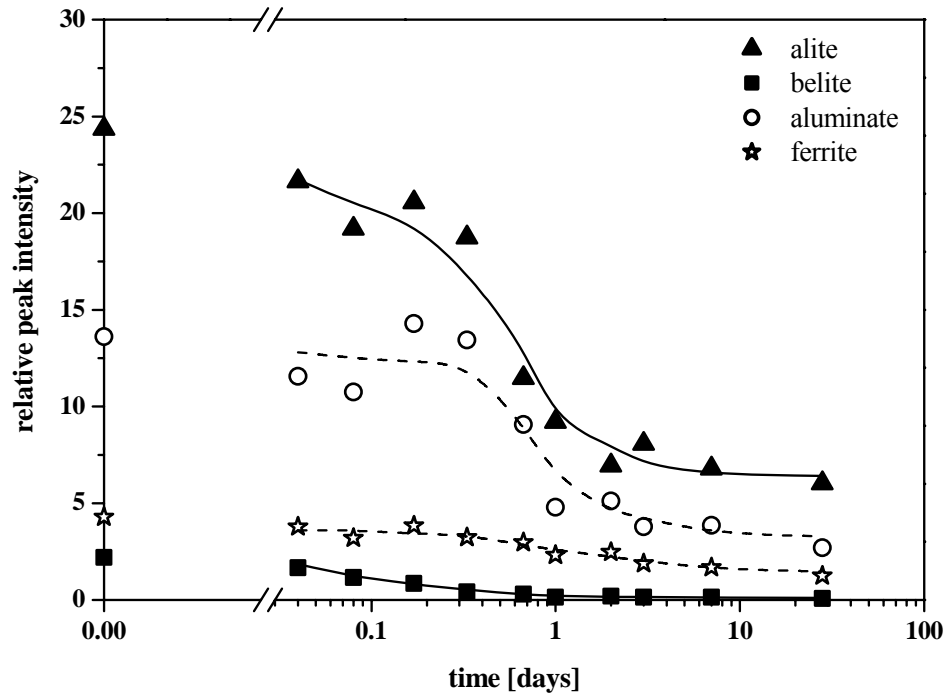


Fig. 4.2. Changes in the relative peak intensities of XRD pattern of alite, belite, aluminate, and ferrite for the samples prepared without citric acid at different hydration times. Lines are intended as eye guides only.

In addition, the consumption of gypsum was found to be clearly affected by the presence of citric acid. Thermogravimetric analysis indicated for the samples with 0.0 and 0.1 wt.-% citric acid that gypsum is consumed within 16 hours. For the samples containing 0.4 and 0.5 wt.-% citric acid gypsum still was present after one day (Fig. 4.5). Also the formation of ettringite was slowed down significantly in the presence of citric acid as illustrated in Fig. 4.6. The retardation of ettringite formation and the retardation in the dissolution of gypsum indicate indirectly a hindrance in the dissolution of aluminate (and/or ferrite). The XRD showed that after 3 and 7 days, the amount of ettringite was higher for the samples prepared with 0.4 and 0.5 wt.-% citric acid than for the samples with 0.0 and 0.1 wt.-% citric acid (Fig. 4.6). In TGA, however, no such effect was evident. Similar to our findings, Rottstegge et al. (2006) observed by solid state NMR also the formation of more ettringite in the presence of citric acid.

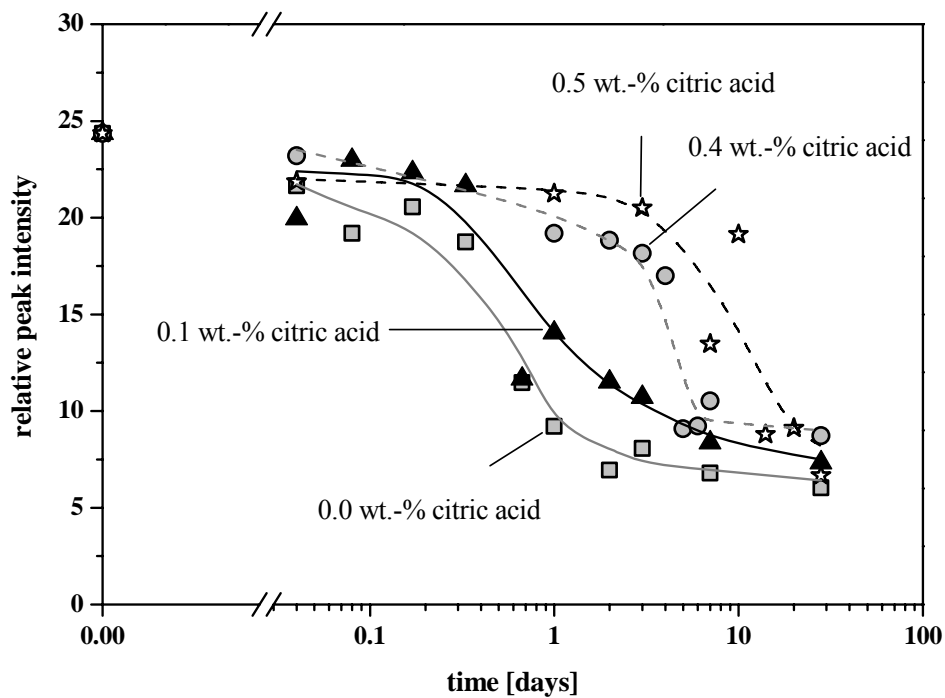


Fig. 4.3. Changes in the relative peak intensities of the XRD pattern of alite for the samples with and without citric acid at different hydration times. Lines are intended as eye guides only.

The amount of calcite declined slightly in all samples during hydration. No significant differences in the presence of the various concentrations of citric acid could be observed. The amount of portlandite increased strongly during hydration in samples with and without citric acid. The formation of portlandite was retarded significantly by the addition of citric acid (Fig. 4.7). In the presence of 0.5 wt% of citric acid, only after more than 20 days a similar amount of portlandite was formed as in the absence of citric acid. Also the formation of C-S-H was retarded in the presence of citric acid as illustrated in Fig. 4.8. The observed slow down of portlandite and C-S-H formation is consistent with the retardation in the dissolution of C_3S and possibly also of C_2S (Fig. 4.8B). After 28 days the amount of C_3S and C_2S was similar in all samples indicating that also a similar amount of C-S-H-phases was present in all samples (Fig. 4.8B).

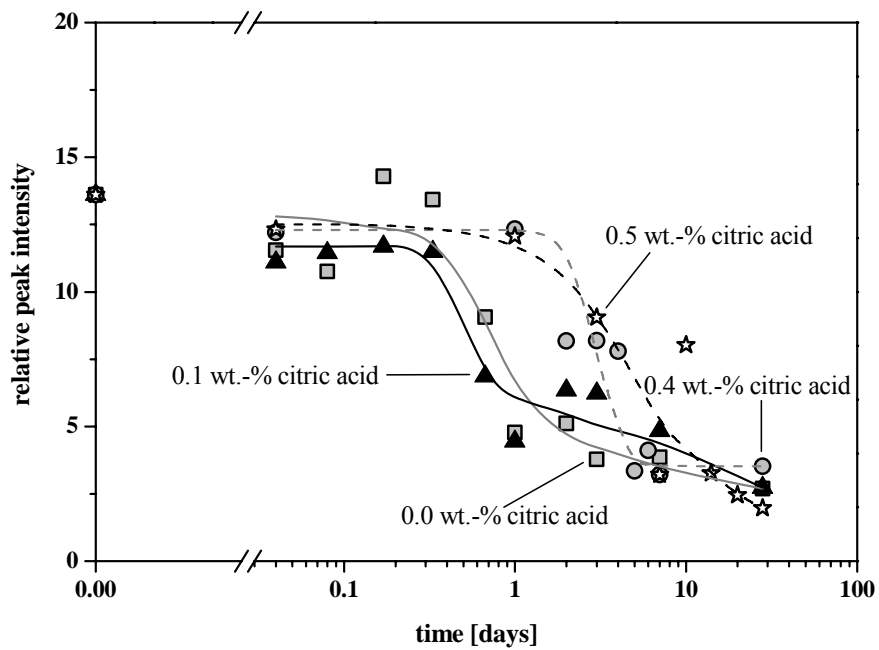


Fig. 4.4. Changes in the relative peak intensities of the XRD pattern of aluminate for the samples with and without citric acid at different hydration times. Lines are intended as eye guides only.

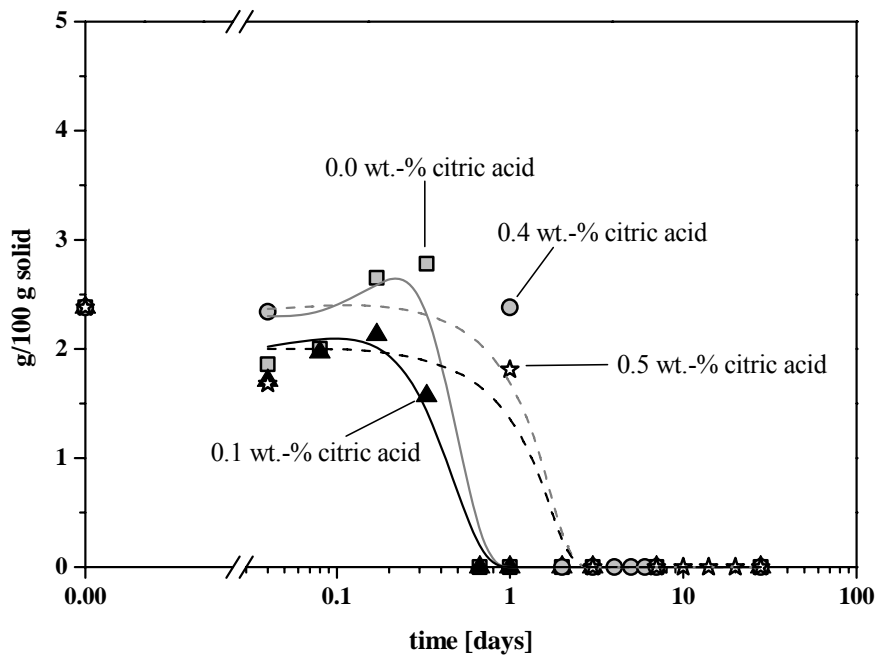


Fig. 4.5. Gypsum consumption of samples with and without citric acid as a function of times (from TGA measurements). Lines are intended as eye guides only.

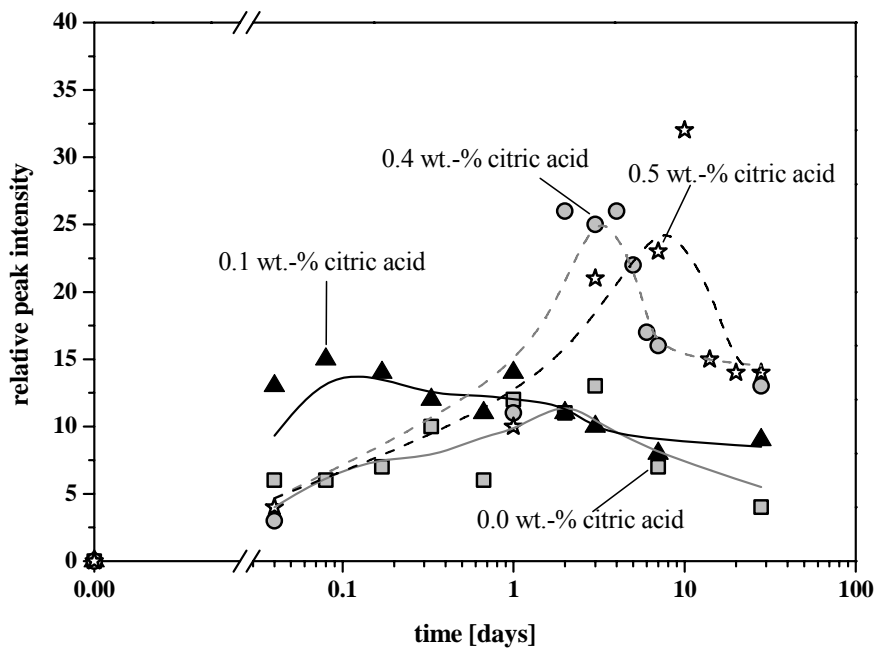


Fig. 4.6. Changes in ettringite content of samples with and without citric acid as a function of hydration time based on the semi-quantitative evaluation of the XRD pattern. Lines are intended as eye guides only.

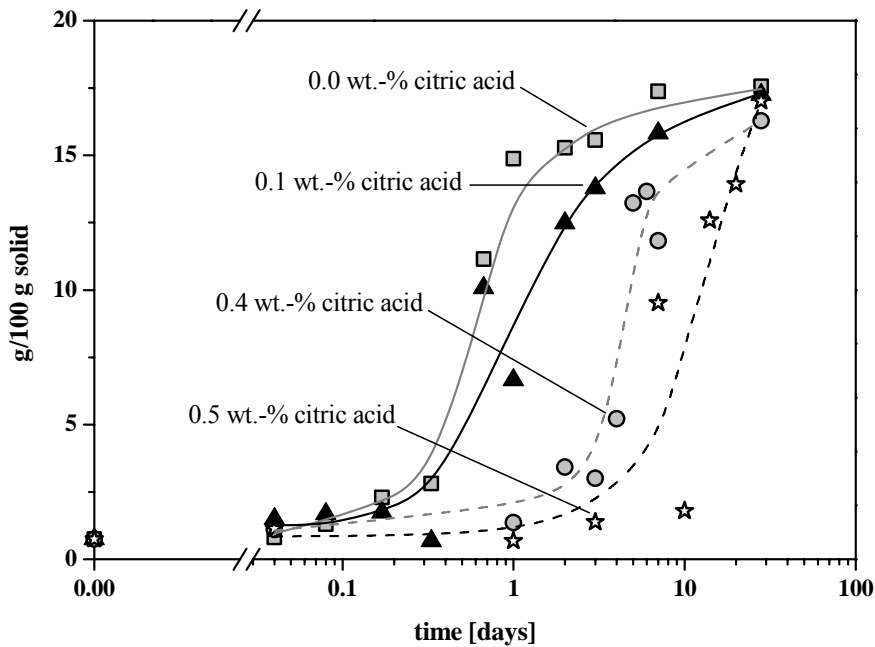


Fig. 4.7. Portlandite content of samples with and without citric acid as a function of hydration time (from TGA measurements). Lines are intended as eye guides only.

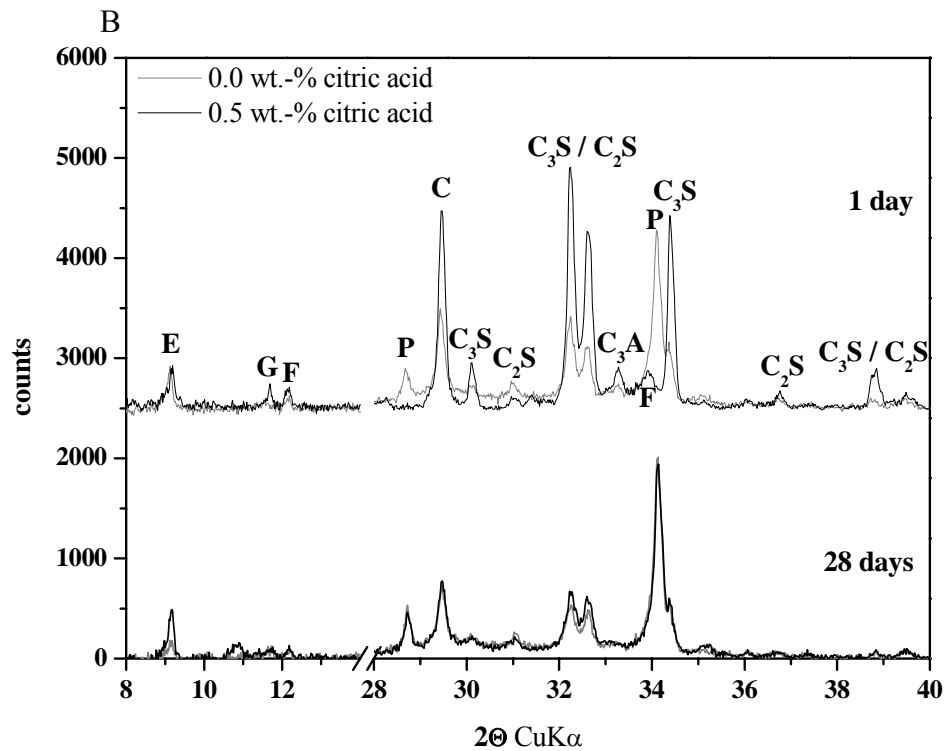
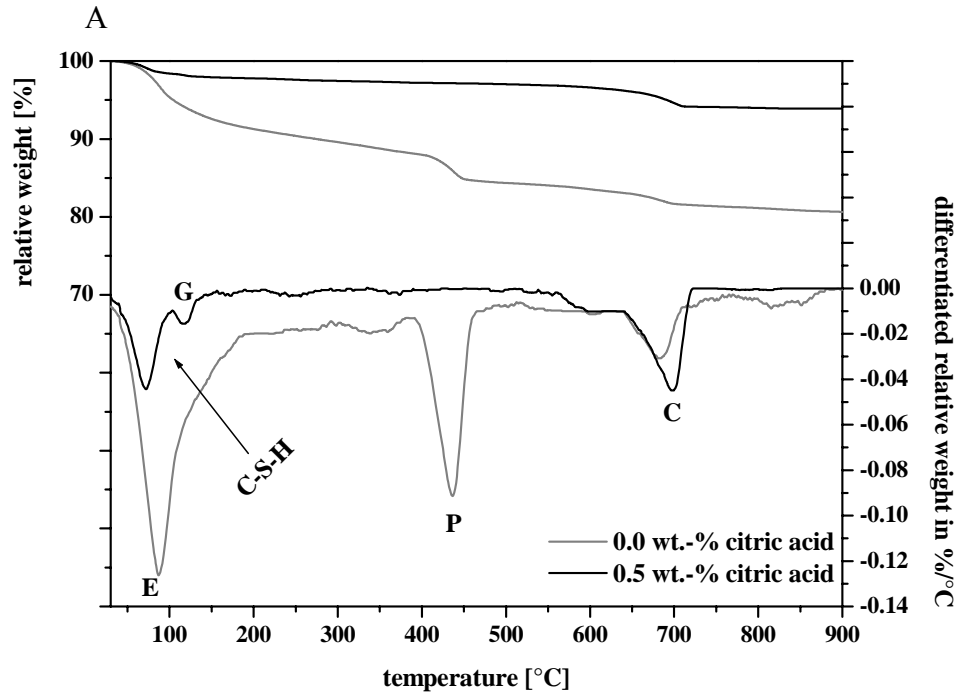


Fig. 4.8. Thermogravimetric (A) and XRD (B) analyses for the samples without and 0.5 wt.-% citric acid after one day (28 days respectively) of hydration. E: ettringite; G: gypsum; F: ferrite; P: portlandite; C: calcite.

Our investigations of the changes of the solid phases during hydration showed that citric acid retarded the dissolution of C_3S and C_3A significantly, resulting in corresponding retardation of the formation of the hydrates. Whether also the dissolution of C_2S and C_4AF was affected by the presence of citric acid could not be verified as the semi-quantitative XRD analysis showed no significant differences for these two phases.

Our observations agree with Rottstegge et al. (2006) who reported a retardation of the dissolution of C_3S . In addition, these authors found, by solid state NMR that the C_3A dissolution altered. In contrast to our finding, Schwarz (1995) postulated an accelerated hydration of ferrite in the presence of citrate, which could not be confirmed in the title study.

4.4.3 Pore solution

Citrate forms complexes with a number of cations, such as Ca^{2+} , Al^{3+} or Fe^{3+} . Complexes of citrate with three-valent cations such as Al^{3+} or Fe^{3+} are generally more stable than complexes with bivalent or monovalent cations (Königsberger et al., 2000; NEA, 2006). Such a complexation of the cations present in the pore solution could lead to a retardation of the formation of hydrates. Thus, the composition of the liquid phase was investigated in the presence and absence of citric acid.

In the absence of citric acid, the composition of the pore solution was dominated by K, sulfate, hydroxide, Na and Ca (Table 4.3) during the first day. The high concentrations of K, Na and sulfate were due to the fast dissolution of alkali-sulfate phases. K and Na increased constantly during hydration time as i) the amount of pore solution present decreases with time as the water is consumed by the different hydration products and ii) the alkalis present in the clinker phases (cf. Table 4.1) were released slowly. In the absence of citric acid the concentrations of Ca, sulfate, and hydroxide stayed relatively constant during the first day as their concentrations in the pore solution were limited by the presence of gypsum and portlandite (cf. Fig. 4.5 and Fig. 4.7). The disappearance of gypsum after approximately one day led to an abrupt decrease of the concentrations of Ca and S and to a strong increase in pH (Table 4.3). The concentrations of Al, Fe, and Si were

very low during the first day of hydration and showed a slight decrease during the first 16 hours. After one day, however, as pH increased also the concentrations of Al, Fe, and Si increased (cf. Table 4.3).

In the presence of 0.1 wt.-% citric acid the composition of the pore solution did not differ much from the composition of the pore solution in the absence of citric acid. Only the concentrations of potassium were considerably lower in the presence of 0.1 wt.-% citric acid than in the absence of citric acid. In average, 40 mmol less K were present in the absence of citrate than in the present of 0.1 wt% of citric acid (corresponding to 13 mmol/l citrate). A possible explanation for this decrease of K concentration could be that the potassium can act as a counterion for citrate $C_6H_5O_7^{3-}$ which has been sorbed or precipitated as K-citrate. The K concentrations of the samples containing 0.4 and 0.5% of citric acid (corresponding to 52 and 65 mmol/l) were after 1 hour approx. 110 mmol/l lower than in the absence of citrate (cf. Table 3). These observations are again consistent with the idea that a significant part of the negative charge of citrate which either precipitated or sorbed on the solids present, is compensated by K. In contrast to K, the concentrations of Na were not significantly affected by the presence of citrate.

For the samples with 0.4 and 0.5 wt.-% citric acid the strong retardation effect of citric acid could be seen in the composition of the pore solution even more clearly than in the results of XRD and TGA. The sharp decrease of Ca and sulfate in the pore solution happened for the samples containing 0.4 wt.-% citric acid not until four days of hydration, and after 10 days in the samples containing 0.5 wt.-% citric acid. Also the corresponding increase of hydroxide, Al and Si concentrations could be observed at these hydration times (cf. Table 4.3). This strong retardation agreed with the later consumption of gypsum in the presence of citric acid as observed by TGA and XRD analyses (Fig. 4.5) and the retardation of the dissolution of alite and aluminate (Fig. 4.3 and 4.4).

Table. 4.3. Composition of the pore solution after different hydration times.

| Time in days | K | Na | Li | Ca | Sr | Ba | Cr | Mo | Fe | Al | Si | S | OH ⁻ | DOC |
|--------------------------|-----|----|-----|-----|------|-------|---------|---------|---------|---------|------|-------|-----------------|-----|
| mmol/l | | | | | | | | | | | | | | |
| <i>no citric acid</i> | | | | | | | | | | | | | | |
| 0.04 | 392 | 25 | 0.5 | 16 | 0.13 | 0.004 | 0.002 | 0.022 | 0.249 | 0.011 | 0.12 | 151 | 123 | 22 |
| 0.08 | 361 | 23 | 0.5 | 21 | 0.15 | 0.004 | 0.0003 | 0.019 | 0.142 | 0.007 | 0.13 | 131 | 144 | 11 |
| 0.2 | 365 | 23 | 0.5 | 23 | 0.16 | 0.003 | 0.00001 | 0.019 | 0.036 | < 0.004 | 0.10 | 123 | 156 | 10 |
| 0.3 | 488 | 33 | 0.7 | 10 | 0.19 | 0.003 | 0.0007 | 0.018 | 0.027 | 0.005 | 0.08 | 177 | 176 | 10 |
| 0.7 | 385 | 30 | 0.8 | 19 | 0.25 | 0.004 | 0.0002 | 0.004 | 0.003 | < 0.004 | 0.08 | 147 | 142 | 18 |
| 1 | 410 | 34 | 0.8 | 9.5 | 0.15 | 0.003 | 0.0004 | < 0.003 | 0.004 | 0.006 | 0.10 | 122 | 190 | 4.1 |
| 2 | 437 | 37 | 0.8 | 3.0 | 0.06 | 0.002 | 0.0005 | < 0.003 | 0.009 | 0.028 | 0.17 | 36 | 394 | 4.2 |
| 3 | 474 | 42 | 0.7 | 2.3 | 0.05 | 0.003 | 0.0008 | < 0.003 | 0.018 | 0.074 | 0.21 | 10 | 432 | 4.6 |
| 7 | 531 | 49 | 0.9 | 1.8 | 0.04 | 0.002 | 0.001 | < 0.003 | 0.02 | 0.130 | 0.21 | 8.0 | 537 | 5.3 |
| 28 | 626 | 62 | 1.1 | 1.6 | 0.04 | 0.002 | 0.007 | < 0.003 | 0.064 | 0.137 | 0.25 | 15 | 603 | 7.2 |
| <i>0.1 % citric acid</i> | | | | | | | | | | | | | | |
| 0.04 | 341 | 23 | 0.5 | 18 | 0.15 | 0.005 | n.d. | 0.019 | 0.086 | 0.010 | 0.16 | 138 | 113 | 15 |
| 0.08 | 350 | 23 | 0.6 | 19 | 0.16 | 0.004 | n.d. | 0.019 | 0.063 | 0.012 | 0.13 | 135 | 133 | 13 |
| 0.2 | 362 | 24 | 0.6 | 22 | 0.18 | 0.004 | n.d. | 0.019 | 0.050 | 0.004 | 0.10 | 129 | 150 | 13 |
| 0.3 | 349 | 23 | 0.6 | 23 | 0.18 | 0.003 | n.d. | 0.017 | 0.024 | 0.009 | 0.09 | 118 | 162 | 13 |
| 0.7 | 355 | 24 | 0.6 | 20 | 0.22 | 0.003 | n.d. | 0.013 | 0.006 | 0.005 | 0.06 | 125 | 142 | 8.2 |
| 1 | 372 | 29 | 0.8 | 17 | 0.23 | 0.004 | n.d. | 0.005 | < 0.003 | 0.005 | 0.08 | 136 | 156 | 3.0 |
| 2 | 417 | 35 | 0.7 | 3.4 | 0.06 | 0.003 | n.d. | < 0.003 | < 0.003 | 0.018 | 0.16 | 36 | 379 | 4.3 |
| 3 | 449 | 39 | 0.7 | 2.3 | 0.05 | 0.003 | n.d. | < 0.003 | < 0.003 | 0.063 | 0.20 | 8.2 | 399 | 3.8 |
| 7 | 494 | 45 | 0.9 | 1.8 | 0.05 | 0.002 | n.d. | < 0.003 | < 0.003 | 0.122 | 0.20 | 6.8 | 516 | 3.7 |
| 28 | 574 | 56 | 1.0 | 1.7 | 0.05 | 0.002 | n.d. | < 0.003 | < 0.003 | 0.133 | 0.23 | 12 | 557 | 7.2 |
| <i>0.4 % citric acid</i> | | | | | | | | | | | | | | |
| 0.04 | 281 | 28 | 0.3 | 47 | 0.09 | 0.029 | n.d. | 0.021 | 0.394 | < 0.004 | 0.04 | 147 | 64 | 61 |
| 1 | 332 | 36 | 0.4 | 25 | 0.16 | 0.004 | n.d. | 0.021 | 0.018 | < 0.004 | 0.04 | 115 | 188 | 21 |
| 2 | 377 | 26 | 0.7 | 19 | 0.21 | 0.003 | n.d. | 0.016 | 0.006 | 0.006 | 0.07 | 109 | 203 | 14 |
| 3 | 384 | 27 | 0.8 | 20 | 0.23 | 0.003 | n.d. | 0.015 | 0.005 | < 0.004 | 0.08 | 122 | 194 | 13 |
| 4 | 357 | 25 | 0.7 | 17 | 0.21 | 0.002 | n.d. | 0.013 | < 0.003 | 0.005 | 0.07 | 113 | 187 | 9.2 |
| 5 | 411 | 34 | 0.6 | 2.9 | 0.06 | 0.004 | n.d. | < 0.003 | < 0.003 | 0.103 | 0.19 | 1.6 | 407 | 2.5 |
| 6 | 430 | 35 | 0.7 | 2.8 | 0.06 | 0.004 | n.d. | < 0.003 | < 0.003 | 0.097 | 0.22 | 1.8 | 407 | 3.2 |
| 7 | 424 | 37 | 0.6 | 2.3 | 0.05 | 0.003 | n.d. | < 0.003 | < 0.003 | 0.158 | 0.20 | 1.5 | 453 | 8.3 |
| 28 | 534 | 53 | 0.9 | 1.6 | 0.05 | 0.003 | n.d. | < 0.003 | < 0.003 | 0.221 | 0.27 | 5.0 | 525 | 10 |
| <i>0.5 % citric acid</i> | | | | | | | | | | | | | | |
| 0.04 | 281 | 29 | 0.3 | 50 | 0.09 | 0.029 | 0.02 | 0.021 | 1.1 | < 0.004 | 0.07 | 147 | 66 | 63 |
| 1 | 289 | 19 | 0.4 | 40 | 0.13 | 0.009 | 0.004 | 0.019 | 0.168 | 0.007 | 0.09 | 142 | 77 | 45 |
| 3 | 327 | 21 | 0.5 | 25 | 0.16 | 0.004 | 0.0002 | 0.017 | 0.046 | 0.005 | 0.04 | 101 | 180 | 27 |
| 7 | 363 | 24 | 0.6 | 25 | 0.22 | 0.003 | 0.0006 | 0.018 | 0.014 | 0.004 | 0.06 | 110 | 204 | 18 |
| 10 | 402 | 29 | 0.9 | 16 | 0.19 | 0.003 | 0.0001 | 0.017 | 0.028 | < 0.004 | 0.08 | 101 | 231 | 16 |
| 14 | 427 | 38 | 0.6 | 2.8 | 0.05 | 0.004 | 0.016 | 0.004 | 0.008 | 0.129 | 0.22 | < 1.6 | 406 | 3.9 |
| 20 | 448 | 42 | 0.6 | 2.6 | 0.05 | 0.003 | 0.012 | 0.004 | 0.012 | 0.127 | 0.21 | 1.9 | 383 | 5.1 |
| 28 | 574 | 57 | 0.9 | 1.7 | 0.05 | 0.003 | 0.026 | < 0.003 | 0.014 | 0.250 | 0.26 | 4.9 | 526 | 7.6 |

During the first day the pore solutions were oversaturated in all samples with respect to gypsum, portlandite and ettringite (Fig. 4.9). The saturation indices SI, given by $\log IAP/K_{S0}$ (IAP: ion activity product; K_{S0} : solubility product), of gypsum, portlandite and ettringite were > 0 , indicating that thermodynamic equilibrium had not yet been reached. In absence of citric acid, after one day the calculated SI of gypsum dropped to < 0 , indicating the complete dissolution of gypsum. This observation agreed well with TGA measurements, where no gypsum was detected for the sample without citric acid after one day of hydration (Fig. 4.5). The retarded consumption of gypsum in the presence of citric acid (cf. section 4.4.2.) is also mirrored in the saturation factors: for 0.1 wt.-% citric acid SI was < 0 after 2 days, for 0.4 wt.-% citric acid after 5 days, and for 0.5 wt.-% citric acid SI was < 0 only after 10 days (Fig. 4.9A). Even though the degree of oversaturation of ettringite dropped strongly upon the consumption of gypsum, the solution remained oversaturated with respect to ettringite as well as with respect to portlandite.

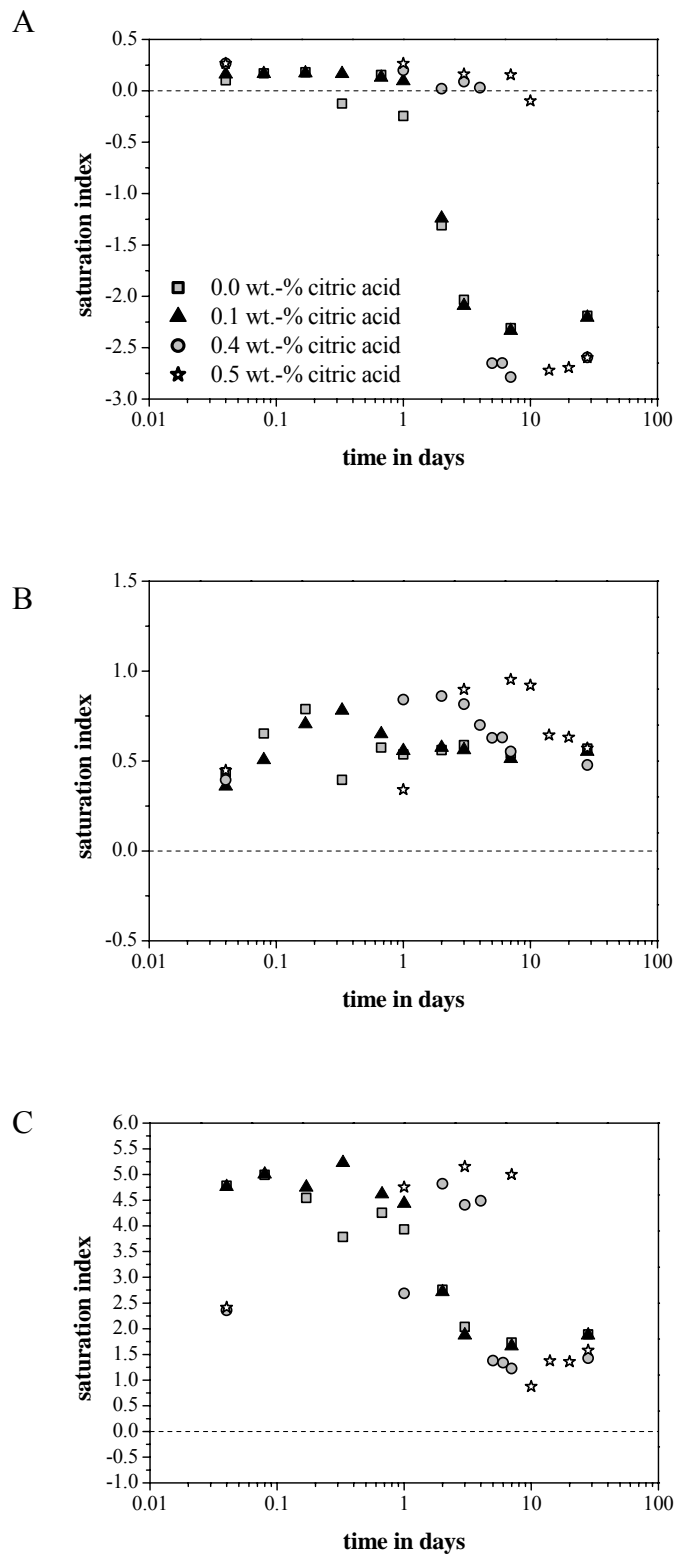


Fig. 4.9. Saturation indices of gypsum (A), portlandite (B), and ettringite (C) calculated as a function of hydration time. A saturation index of 0 indicates equilibrium between liquid and solid phase.

4.4.4 Citrate

The amount of dissolved citrate, $C_6H_5O_7^{3-}$, was measured as dissolved organic carbon (DOC). The measured DOC concentrations (6 mmol of DOC correspond to 1 mmol of citrate) are reproduced in Fig. 4.10A and Table 4.3. The measured concentrations showed that citric acid was quickly removed from pore solution. After one hour already up to 90 % of the citric acid added has been removed from the pore solution and with increasing hydration times the removal increased up to nearly 100 % independent from the initial concentration of citric acid. A similar fast and high removal of citric acid from the pore solution was also found by Smillie and Glasser (1999). They observed the complete removal of citric acid within the first two hours when 2.6 mmol/l citric acid have been added. At higher concentrations (15.6 mmol/l) citric acid has been removed from the pore solution after 14 hours (Smillie and Glasser, 1999).

Since the citric acid added is basically removed from the solution within the first hours, it can be expected that only a small fraction of the cations (K, Ca, Na,...) present in the solution is complexed by citrate. This agrees with the experimental data as presented in Table 4.3 where no significant increase of Na, K, Al or Fe concentration was observed. Only Ca concentrations were increased in the presence of higher concentrations of citrate in solution (Fig. 4.10B).

Thermodynamic calculations showed that in the presence of e.g. 10.5 mmol/l citrate (as measured after 1 hour of hydration for the sample containing 65 mmol/l citric acid) 9 % of the total citrate in solution was expected to be present as $CaCit^-$ ($CaC_6H_5O_7^-$) complexes (Table 4.4). This means that less than 1 mmol/l of measured Ca ($c(Ca) = 50$ mmol/l, Table 4.3) was complexed by citrate after 1 hour. With proceeding hydration the percentage of complexed Ca even decreased (Table 4.4). The fraction of K and Na complexed by citrate was even smaller. Considerably less than 1 % of the total dissolved citrate was calculated to form complexes with K and Na. The calculated complexation of Al and Fe by citrate was < 0.001 % due to the very low concentrations of both elements present in the pore solution (Table 4.3). Fig. 4.10B shows the correlation between Ca, Na, Fe and dissolved organic carbon (C). Ca and C show a linear correlation for the sample in the presence with 0.5 wt.-% citric acid.

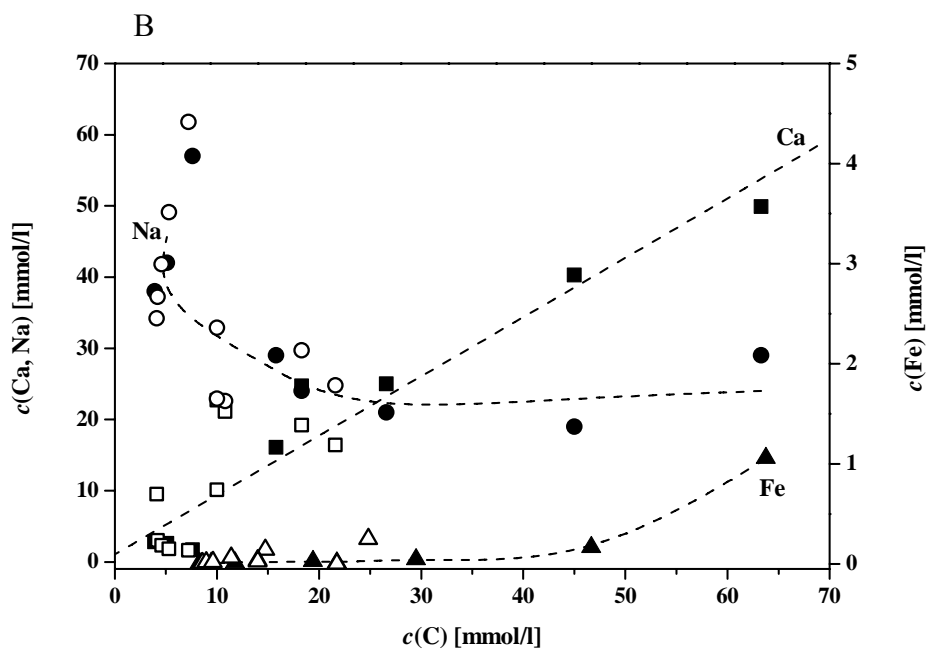
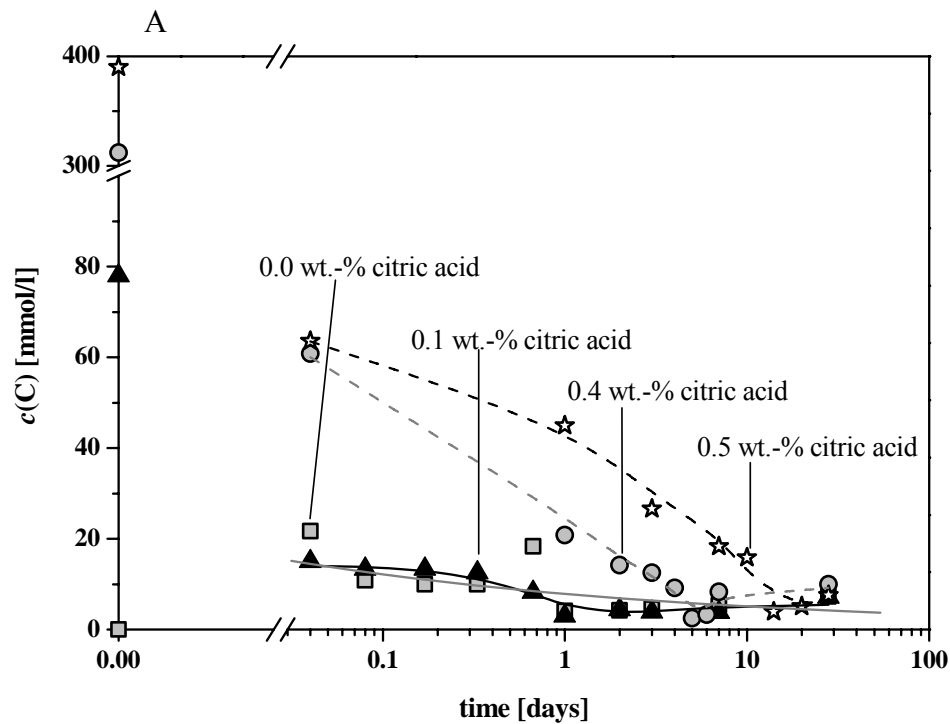


Fig. 4.10. A) Concentration of the dissolved organic carbon (DOC) of samples with and without citric acid as a function of hydration time and B) measured concentrations of Ca, Na, Fe, and C in presence of 0.5 wt.-% citric acid (filled symbols) and in the absence of citric acid (empty symbols). Lines are intended as eye guides only.

Table 4.4. Calculated concentrations of complexes of the different cations with citrate for the samples with 0.5 wt.-% citric acid. Retardation of cement hydration was not considered.

| | days | | | | |
|--|---------|---------|---------|---------|---------|
| | 0.04 | 1 | 3 | 7 | 28 |
| Measured citrate in mmol/l | 10.5 | 7.5 | 4.4 | 3.1 | 1.3 |
| Calculated percentage of citrate complexes | | | | | |
| | % | | | | |
| Cacit ⁻ | 9.0 | 1.0 | 0.2 | 0.2 | 0.1 |
| Kcit ²⁻ | 0.03 | 0.03 | 0.04 | 0.03 | 0.03 |
| Nacit ²⁻ | 0.002 | 0.004 | 0.006 | 0.006 | 0.006 |
| AlcitOH ⁻ | < 0.001 | < 0.001 | < 0.001 | < 0.001 | < 0.001 |
| Fe(III)citOH ⁻ | < 0.001 | < 0.001 | < 0.001 | < 0.001 | < 0.001 |
| cit ³⁻ | 90.9 | 99.0 | 99.7 | 99.8 | 99.8 |
| Total citrate | 100 | 100 | 100 | 100 | 100 |
| Calculated total citrate in mmol/l | 10.5 | 7.5 | 4.5 | 3.0 | 1.2 |

Citrate can form mononuclear tridentate surface complexes with metal oxides (e.g. Pokrovsky et al., 2005; Golubev and Pokrovsky, 2006; Golubev et al., 2006). The formation of bi- or multidentate mononuclear surface complexes increases the dissolution rate of solids, especially at low and neutral pH. Pokrovsky et al. (2005) and Gobulev and Pokrovsky (2006) observed at pH 7.6 and 6 an acceleration of brucite (Mg(OH)₂) and diopside (CaMgSi₂O₆) dissolution in the presence of citrate. At pH 10.5, however, no increase of diopside dissolution was observed in the presence of citrate. Ahmed and Youssof (1997) observed that the dissolution rate of soda-lime-silica glass decreased upon the addition of citrate ($c(\text{citrate}) = 33.0 \text{ mM}$ corresponding to a pH-value of 2.2). They attributed it to the formation of citrate-containing solids on the surface of the glass then acting as an effective barrier against the further dissolution of the glass. Teng and Grandstaff (1996) also observed that in the presence of citric acid the dissolution of basaltic glass decreases at $\text{pH} \geq 7$ and they also observed that secondary phases are formed, but contrary to Ahmed and Youssof (1997), Teng and Grandstaff (1996) did not state that citrate is incorporated into these secondary phases. Even though the mechanisms of the

decrease of the glass dissolution are not fully understood, the formation of such complexes on the surface of the hydrating clinkers could be a possible explanation for the observed decrease of the dissolution rate at high pH-values.

Based on the experimental observation and on the modeling results the addition of citric acid lead after one hour or longer to a very limited complexation of aqueous ions by citrate due to the quick removal of citric acid from pore solution. This makes retardation of the precipitation of the hydrates by complex formation improbable. The observed strong retardation seemed rather caused by a blocking of the surface of the clinker grain by the strong adsorption or precipitation of K-citrate.

4.5 Conclusion

Observations of the solid phases showed that the dissolution of alite and aluminate slowed down considerably in the presence of citric acid and therefore, also the formation of the different hydration products. Analyses of the dissolved organic carbon showed that citric acid was removed almost quantitatively from the pore solution after the first hours of cement hydration.

The compositions of the pore solutions did not differ much. Only for calcium a moderate correlation between measured concentrations of citrate and Ca could be found. The addition of citric acid decreased the potassium concentrations in pore solution, indicating that K acts as a counter ion for precipitation of the negatively charged citrate ($C_6H_5O_7^{3-}$) on the surface of the Portland cement clinker grains.

Thermodynamic calculations could confirm that the complexation of ions by citrate is very limited in cementitious systems and thus, could not be the retarding mechanism.

The observed retarded dissolution of alite and aluminate and the mainly unchanged composition of the pore solution as well as the fast removal of citrate from the pore solution argue for the precipitation or adsorption of citrate onto the surface of the clinker

grains. The precipitated or adsorbed citrate formed a protective layer around the clinker grains and retarded the dissolution of the clinker phases.

Acknowledgments

The authors would like to thank Luigi Brunetti and Marcel Käppeli for their support during laboratory work and Dmitrii Kulik for his assistance with thermodynamical questions. The financial support (Grant 20021-103546) of the Swiss National Foundation is gratefully acknowledged.

4.6 References

- Ahmed, A. A. and Youssof, I. M., 1997. Attack on soda-lime-silica glass bottles by acetic, citric and oxalic acids. *Glass Science and Technology* **70**, 76-85.
- Apelblat, A., 1994. Enthalpies of solution of citrates and hydrogen citrates of lithium, sodium, and potassium. *Journal of Chemical Thermodynamics* **26**, 49-51.
- Golubev, S. V. and Pokrovsky, O. S., 2006. Experimental study of the effect of organic ligands on diopside dissolution kinetics. *Chemical Geology* **235**, 377-389.
- Golubev, S. V., Bauer, A., and Pokrovsky, O. S., 2006. Effect of pH and organic ligands on the kinetics of smectite dissolution at 25 °C. *Geochimica et Cosmochimica Acta* **70**, 4436-4451.
- Hummel, W., Berner, U., Curti, E., Pearson, F. J., and Thoenen, T., 2002. *Nagra/PSI Chemical Thermodynamic Data Base 01/01*. Universal Publishers/uPublish.com, Parkland, Florida.

- Königsberger, L.-C., Königsberger, E., May, P. M., and Hefter, G. T., 2000. Complexation of iron (III) and iron (II) by citrate. Implications for iron speciation in blood plasma. *Journal of Inorganic Biochemistry* **78**, 175-184.
- Kulik, D. A., 2006. GEMS-PSI 2.12, PSI Villigen, Switzerland; available at <http://les.web.psi.ch/Software/GEMS-PSI/index.html>
- Lothenbach, B. and Winnefeld, F., 2006. Thermodynamic modelling of the hydration of Portland cement. *Cement and Concrete Research* **36**, 209-226.
- Lothenbach, B., Matschei, T., Möschner, G., and Glasser, F. P., 2007. Thermodynamic modelling of the effect of temperature on the hydration and porosity of Portland cement. *Cement and Concrete Research* **submitted**.
- Martin, R. B., 1986. Citrate binding of Al^{3+} and Fe^{3+} . *Journal of Inorganic Biochemistry* **28**, 181-187.
- NEA – Nuclear Energy Agency, 2006. Thermochemical Database Project (TDB), <http://www.nea.fr/html/dbtdb/>
- Pokrovsky, O. S., Schott, J., and Castillo, A., 2005. Kinetics of brucite dissolution at 25 °C in the presence of organic and inorganic ligands and divalent metals. *Geochimica et Cosmochimica Acta* **69**, 905-918.
- Rachmachandran, V. S. and Lowery, M. S., 1992. Conduction calorimetric investigation of the effect of retarders on the hydration of Portland cement. *Thermochimica Acta* **195**, 373-387.
- Rottstegge, J., Wilhelm, M., and Spiess H. W., 2006. Solid state NMR investigations on the role of organic admixtures on the hydration of cement pastes. *Cement & Concrete Composites* **28**, 417-246.
- Schwarz, W., 1995. Novel cement matrices by accelerated hydration of the ferrite phase in Portland cement via chemical activation: kinetics and cementitious properties. *Advanced cement based materials* **2**, 189-200.

- Schwarz, W., Sujata, K., Jennings, H. M., Gerdes, A., Sadouki, H., and Wittmann, F. H., 1994. *Chemically modified hydration of Portland cement*. AEDIFICATIO Publishers, Freiburg i. Br. (D) and Unterengstringen (CH).
- Singh, N. B., Singh, A. K., and Prabha Singh, S., 1986. Effect of citric acid on the hydration of Portland cement. *Cement and Concrete Research* **16**, 911-920.
- Singh, N. B., Singh, A. K., and Prabha Singh, S., 1990. Hydration study of the system $\text{Ca}_3\text{Al}_2\text{O}_6\text{-CaSO}_4\cdot 2\text{H}_2\text{O-Ca(OH)}_2\text{-H}_2\text{O}$ with and without citric acid. *Journal of the American Ceramic Society* **73**, 3063-3068.
- Smillie, S. and Glasser, F. P., 1999. Reaction of EDTA, oxalic acid and citric acid with Portland cement. *Advances in Cement Research* **11**, 97-101.
- Stadelmann, C., 1987. Zur Wirkung von Citronensäure auf die Hydratation von Tricalciumsilicat (Ca_3SiO_5). *Zeitschrift für anorganischen und allgemeine Chemie* **547**, 127-132.
- Taylor, H. F. W., 1997. *Cement Chemistry*. Thomas Telford Publishing, London.
- Teng, H. and Grandstaff, D. E., 1996. Dissolution of basaltic glass effects of pH and organic ligands. *European Materials Research Society* **412**, 249-256.
- Tinnea, J. and Young, J. F., 1977. Influence of citric acid on reactions in the system $3\text{CaO}\cdot\text{Al}_2\text{O}_3\text{-CaSO}_4\cdot 2\text{H}_2\text{O-CaO-H}_2\text{O}$. *Journal of the American Ceramic Society* **60**, 387-389.
- Wilding, C. R., Walter, A., and Double D. D., 1984. A classification of inorganic and organic admixtures by conduction calorimetry. *Cement and Concrete Research* **14**, 185-194.
- Zelenina, T. E. and Zelenin, O. Y., 2005. Complexation of citric acid and tartaric acids with Na and K ions in aqueous solution. *Russian Journal of Coordination Chemistry* **31**, 235-242.

5 Conclusions

The purpose of this study was i) to enlighten the fate of iron during the process of cement hydration by the means of thermodynamical properties of Fe-containing hydrates as well as ii) to explain the retardation of cement hydration caused by citric acid by applying thermodynamic calculations.

The synthesis of Fe-ettringite ($\text{Ca}_6[\text{Fe}(\text{OH})_6]_2(\text{SO}_4)_3 \cdot 26\text{H}_2\text{O}$) showed that in aqueous solutions Fe-ettringite is stable up to a pH of approximately 13. At higher pH-values Fe-monosulfate ($\text{Ca}_4[\text{Fe}(\text{OH})_6]_2(\text{SO}_4) \cdot 6\text{H}_2\text{O}$), Fe-monocarbonate ($\text{Ca}_4[\text{Fe}(\text{OH})_6]_2(\text{CO}_3) \cdot 6\text{H}_2\text{O}$) as well as portlandite ($\text{Ca}(\text{OH})_2$) are formed. Since during cement hydration the pH-values ranges between ~13 and ~14 the formation of Fe-ettringite, Fe-monosulfate, and Fe-monocarbonate is generally possible. The determination of the solubility product of Fe-ettringite

($\log K_{\text{S0}} = -44.0 \pm 0.7$) revealed that Fe-ettringite is somewhat less stable than its Al-containing analogue ($\text{Ca}_6[\text{Al}(\text{OH})_6]_2(\text{SO}_4)_3 \cdot 26\text{H}_2\text{O}$, $\log K_{\text{S0}} = -44.9 \pm 0.7$ (Lothenbach et al., 2007)), if equal amounts of Fe and Al are available. In the case of Fe-monosulfate ($\log K_{\text{S0}} = -33.2 \pm 0.5$) and Fe-monocarbonate ($\log K_{\text{S0}} = -35.5 \pm 0.3$) the calculated solubility products are approximately 4 log units lower than the solubility products of their Al-containing analogues (Al-monosulfate: $\log K_{\text{S0}} = -29.3$ (Matschei et al., 2007); Al-monocarbonate $\log K_{\text{S0}} = -31.5$ (Lothenbach et al., 2007)) and thus, the Fe-containing solids are more stable than the Al-containing solids assuming equal amounts of Al and Fe available. As in cementitious systems the aluminum concentrations are usually up to 1000 times higher than the iron concentrations it is more likely that Fe precipitates as Fe-monosulfate and/or Fe-monocarbonate or, since during cement hydration the pore solution is near equilibrium with respect to Fe-hydroxide, as an amorphous Fe-containing gel. But there is also the possibility that Fe substitutes partially for Al in the respective hydrates and solid solutions are formed.

Experimental investigations of the solid solution series between Al- and Fe-ettringite ($\text{Ca}_6[\text{Al}_{1-x}\text{Fe}_x(\text{OH})_6]_2(\text{SO}_4)_3 \cdot 26\text{H}_2\text{O}$) revealed that Fe can substitute partially for Al in the

ettringite structure. But not a continuous solid solution is formed: there is a miscibility gap between $x = 0.35$ and $x = 0.75$. In this range a peak broadening was observed by XRD analyses as well as a sudden decline of the c-parameter. However, thermodynamic calculations could not confirm this miscibility gap. The calculated ion concentrations agree slightly better with the calculated solution composition when an ideal solid solution between Al- and Fe-ettringite is assumed. But it has to be mentioned that differences of the calculated ion concentrations in both cases (ideal solid solution and miscibility gap) are small.

Experiments with an ordinary Portland cement and citric acid showed that citric acid retards the cement hydration. Analyses of the solid phases revealed that citric acid affects mainly the dissolution of alite and aluminate. As citric acid is removed quickly from the pore solution the complexation of ions (mainly Ca) by citrate seems not to be the mechanism which causes retardation. Thus, the retarding mechanism must be the adsorption or precipitation of citrate on the positively charged surface of the clinker phases and the formation of a protective layer. In order to confirm these experimental results thermodynamic calculations were carried out using a thermodynamic database which enfolds data for solids that are expected to form under cementitious conditions as well as data for citric acid and citrate complexes. By calculating phase assemblage at different hydration times it could be shown that the complexation of ions by citrate is very limited. After one hour of hydration only 9 % of the present citrate forms a complex with Ca ($\text{CaC}_6\text{H}_5\text{O}_7^{-1}$). With proceeding hydration this percentage decreases to 0.1 %. This and the observed retarded dissolution of alite and aluminate argue for the precipitation or adsorption of citrate on the surface of the clinker grains. The precipitated or adsorbed citrate forms a protective layer around the clinker grains and retards the dissolution of the clinker phases. As for many admixtures, which are used to change the behavior of concrete and cements, the influence of the chemistry (e.g. complex formation, co-precipitation) besides the known working mechanisms is still unclear, thermodynamic modeling can be an effective tool for explaining chemical mechanisms of admixtures on cement hydration.

Overall, the results of thesis enabled to refine thermodynamic modeling of cement hydration by inserting thermodynamic data of Fe-ettringite, Fe-monosulfate, and Fe-monocarbonate. With respect to Fe-ettringite it is now also possible to consider the

miscibility gap in the solid solution between Al- and Fe-ettringite in the thermodynamic model. Furthermore, it could be shown that a thermodynamic model can be used to explain chemical mechanisms between cement, water, and admixture.

5.1 References

Lothenbach, B., Matschei, T., Möschner, G., and Glasser, F. P., 2007. Thermodynamic modelling of the effect of temperature on the hydration and porosity of Portland cement. *Cement and Concrete Research* **submitted**.

Matschei, T., Lothenbach, B., and Glasser, F. P., 2007. The AFm-phase in Portland cement. *Cement and Concrete Research* **37**, 118-130.

6 Outlook

With regard to the refinement of thermodynamic modeling of cement hydration it was a first fundamental step to insert thermodynamic data of Fe-ettringite, Fe-monosulfate, and Fe-monocarbonate. However, there are still data missing (e.g. Fe-hemicarbonate, Fe-hydrogarnet, Fe-hydrotalcite). For completion of the thermodynamic database it is thus necessary to determine the thermodynamic data of the missing hydrates.

Synthesis of different Fe-containing hydrates showed that either equilibration of these mixtures takes a long time (> 1 year, Fe-ettringit ~ 6 months) or that synthesis was not possible because Fe-hydroxide precipitates. Thus, the determination of thermodynamic data of Fe-hydrates is very difficult since steady state conditions are required. Those Fe-containing hydrates only formed at relatively high pH-values ($\text{pH} > 11$) and the mixtures are always near equilibrium with respect to Fe-hydroxide. Analyses of the formation of Fe-ettringite after different equilibration times showed that amorphous Fe-hydroxide precipitates in the beginning (together with gypsum) but is consumed after longer equilibration times. Experiments of synthesis of $\text{Ca}_3[\text{Fe}(\text{OH})_6]_2$ (Fe-hydrogarnet) and $\text{Ca}_4[\text{Fe}(\text{OH})_6]_2(\text{OH})_2 \cdot 6\text{H}_2\text{O}$ (C_4FH_{13}) showed that the solids evolve during drying. During equilibration and directly after filtering the solids had a dark yellowish color but turned red during drying. XRD analyses showed that the dried solids contained only portlandite ($\text{Ca}(\text{OH})_2$) as crystalline phase. Since freshly precipitated Fe-hydroxide is XRD amorphous it is likely that the red color stemmed from Fe-hydroxide. A possible answer could be gained by XRD, ESEM, and XAFS analyses of non-dried solids.

Besides the determination of thermodynamic data of the Fe-containing hydrates the existence of these phases must be experimentally proved in the phase assemblage during cement hydration. As the incorporation of Fe into the Al-containing hydrates is difficult to detect it would be reasonable to investigate phase assemblage during hydration of oilwell cements. In oilwell cements aluminates are usually absent or present only in very small quantities, i.e. the quantities of ferrite are relatively high and the Fe/Al-ratio is higher than in ordinary Portland cements.

Thermodynamic modeling of cement hydration in presence of citric acid showed that complexation of ions by citrate could be calculated. But the removal of citrate from the pore solution, i.e. the adsorption of citrate onto the clinker surface, could not be considered. The decrease of citrate during cement hydration was set in accordance to measured concentrations at the different hydration times. Thus, it would be a good improvement of the model if adsorption of admixtures could be considered by implementing adsorption constants. The rate of cement hydration during modeling is taken into account by a set of experimentally obtained equations which describe the dissolution of the clinker phases (Parrot and Killoh, 1984). These equations were acquired in the absence of any admixtures. Hence, retardation and also acceleration caused by admixtures cannot be considered using this set of equations without manual changing the different constants which still requires experimental data. In order to avoid manual setting of the constants again detailed information about the used admixture is required for implementing adsorption or other thermodynamic constants.

6.1 References

Parrot, L. J. and Killoh, D. C., 1984. Prediction of cement hydration. *British Ceramic Proceedings* **35**, 41-53.

Appendix 1: Solubility of Fe-ettringite

(referring to work presented in chapter 2)

Table A1.1. Water loss and calculated amount of water molecules of Fe-ettringite measured by TGA.

| | Loss of water [%] | Water molecules |
|----------------------------------|-------------------|-----------------|
| Precipitation experiments | | |
| 11.8 | 42.1 | 29.7 |
| 11.6 | 42.0 | 29.6 |
| 11.7 | 42.3 | 30.0 |
| 11.8 | 41.7 | 29.3 |
| 11.9 | 42.3 | 30.0 |
| 12.1 | 42.5 | 30.2 |
| 12.2 | 42.7 | 30.4 |
| 12.5 | 43.2 | 31.1 |
| 12.7 | 43.5 | 31.4 |
| 12.9 | 44.8 | 33.2 |
| Dissolution experiments | | |
| 11.7 | 38.5 | 25.6 |
| 11.8 | 38.4 | 25.5 |
| 11.8 | 40.6 | 27.9 |
| 11.8 | 40.7 | 28.1 |
| 11.9 | 39.9 | 27.1 |
| 12.0 | 41.0 | 28.4 |
| 12.2 | 41.4 | 28.9 |
| 12.4 | 40.5 | 27.9 |
| 12.5 | 41.8 | 29.3 |

Table A1.2. Composition of the solid phases estimated by TGA presented in Fig. 2.8.

| OH | Fe-ettringite | Sum of Fe-monosulfate and Fe-monocarbonate | Portlandite | CO ₂ |
|----------------------------------|---------------|---|-------------|-----------------|
| [mmol/L] | [g] | [g] | [g] | [g] |
| Precipitation experiments | | | | |
| 5.9 | 1.82 | - | - | - |
| 3.7 | 2.03 | - | - | - |
| 4.9 | 2.08 | - | - | - |
| 5.5 | 1.98 | - | - | - |
| 6.3 | 2.04 | - | - | - |
| 7.1 | 2.14 | - | - | - |
| 12 | 2.14 | - | - | - |
| 17 | 2.18 | - | - | - |
| 34 | 2.31 | - | - | - |
| 55 | 3.31 | - | - | - |
| 96 | 3.68 | - | - | 0.11 |
| 134 | 3.03 | 0.65 | - | 0.12 |
| 178 | 1.61 | 1.07 | 0.19 | 0.14 |
| 253 | 0.39 | 0.93 | 0.32 | 0.13 |
| 476 | - | 1.44 | 0.39 | 0.06 |
| 808 | - | 1.43 | 0.40 | 0.11 |
| Dissolution experiments | | | | |
| 5.1 | 0.83 | - | - | - |
| 6.0 | 0.86 | - | - | - |
| 6.4 | 0.93 | - | - | - |
| 6.2 | 0.95 | - | - | - |
| 7.8 | 0.90 | - | - | - |
| 10 | 0.99 | - | - | - |
| 15 | 1.02 | - | - | - |
| 23 | 0.97 | - | - | - |
| 34 | 1.00 | - | - | - |
| 55 | 0.90 | 0.18 | - | - |
| 89 | 0.84 | 0.19 | - | - |
| 133 | 0.75 | 0.18 | 0.04 | - |
| 192 | 0.25 | 0.31 | 0.09 | 0.02 |
| 292 | 0.07 | 0.29 | 0.11 | 0.01 |
| 473 | - | 0.65 | 0.16 | 0.04 |
| 770 | - | 0.65 | 0.15 | 0.07 |

Table A1.3. Thermodynamically calculated composition of the solid phases presented in Fig. 2.8.

| OH | Fe- ettringite | Sum of Fe- monosulfate and Fe- monocarbonate | Fe- monosulfate | Fe- monocarbonate | Portlandite | CO ₂ | Fe(OH) ₃ |
|----------------------------------|-------------------|---|--------------------|----------------------|-------------|-----------------|---------------------|
| [mmol/L] | [g] | [g] | [g] | [g] | [g] | [g] | [g] |
| Precipitation experiments | | | | | | | |
| 7.1 | 2.37 | - | - | - | - | - | 0.03 |
| 7.3 | 2.38 | - | - | - | - | - | 0.03 |
| 7.7 | 2.38 | - | - | - | - | - | 0.03 |
| 8.4 | 2.39 | - | - | - | - | - | 0.03 |
| 9.6 | 2.40 | - | - | - | - | - | 0.03 |
| 12 | 2.42 | - | - | - | - | - | 0.02 |
| 16 | 2.44 | - | - | - | - | - | 0.02 |
| 24 | 2.45 | - | - | - | - | - | 0.02 |
| 38 | 2.44 | 0.02 | 0.02 | - | - | - | 0.01 |
| 54 | 2.28 | 0.15 | 0.15 | - | - | - | - |
| 94 | 2.25 | 0.16 | 0.16 | - | - | 0.04 | - |
| 144 | 2.05 | 0.27 | 0.27 | - | 0.02 | 0.04 | - |
| 200 | 1.05 | 0.79 | 0.79 | - | 0.14 | 0.04 | - |
| 265 | - | 1.33 | 1.33 | - | 0.26 | 0.04 | - |
| 432 | - | 1.26 | 0.10 | 0.16 | 0.40 | 0.00 | - |
| 797 | - | 1.26 | - | 1.26 | 0.41 | 0.00 | - |
| Dissolution experiments | | | | | | | |
| 8.4 | 1.13 | - | - | - | - | - | 0.02 |
| 8.7 | 1.14 | - | - | - | - | - | 0.02 |
| 9.1 | 1.14 | - | - | - | - | - | 0.02 |
| 10 | 1.15 | - | - | - | - | - | 0.02 |
| 11 | 1.16 | - | - | - | - | - | 0.02 |
| 14 | 1.17 | - | - | - | - | - | 0.02 |
| 19 | 1.19 | - | - | - | - | - | 0.02 |
| 27 | 1.20 | - | - | - | - | - | 0.01 |
| 37 | 1.13 | 0.06 | 0.06 | - | - | - | 0.01 |
| 59 | 1.06 | 0.11 | 0.11 | - | - | - | - |
| 98 | 1.02 | 0.13 | 0.13 | - | - | - | - |
| 143 | 0.77 | 0.26 | 0.26 | - | 0.03 | - | - |
| 234 | - | 0.66 | 0.66 | - | 0.13 | 0.04 | - |
| 323 | - | 0.64 | 0.26 | 0.38 | 0.17 | 0.02 | - |
| 553 | - | 0.63 | - | 0.63 | 0.21 | 0.00 | - |
| 922 | - | 0.63 | - | 0.63 | 0.21 | 0.04 | - |

Table A1.4. Thermodynamically calculated composition of the aqueous solutions of the precipitation experiments presented in Fig. 2.9A.

| OH ⁻ [mmol/L] | Ca [mmol/L] | S [mmol/L] | Fe [mmol/L] |
|--|-------------|------------|---------------------|
| Mean average of the calculated solubility products at 25 °C. | | | |
| log $K_{S0, \text{Fe-ettringite}} = -44.0$; log $K_{S0, \text{Fe-monosulfate}} = -33.2$; log $K_{S0, \text{Fe-monocarbonate}} = -35.5$ | | | |
| 7.1 | 12.05 | 8.93 | $8.7 \cdot 10^{-5}$ |
| 7.3 | 11.70 | 8.76 | $9.0 \cdot 10^{-5}$ |
| 7.7 | 11.16 | 8.49 | $9.5 \cdot 10^{-4}$ |
| 8.4 | 10.36 | 8.09 | $1.0 \cdot 10^{-4}$ |
| 9.6 | 9.21 | 7.52 | $1.2 \cdot 10^{-4}$ |
| 12 | 7.71 | 6.77 | $1.5 \cdot 10^{-4}$ |
| 16 | 6.04 | 5.93 | $2.0 \cdot 10^{-4}$ |
| 24 | 4.58 | 5.20 | $3.0 \cdot 10^{-4}$ |
| 38 | 3.45 | 5.17 | $4.6 \cdot 10^{-4}$ |
| 54 | 2.83 | 8.64 | $4.4 \cdot 10^{-4}$ |
| 94 | 3.77 | 9.57 | $1.4 \cdot 10^{-4}$ |
| 144 | 3.56 | 15.81 | $1.0 \cdot 10^{-4}$ |
| 200 | 2.59 | 35.74 | $1.4 \cdot 10^{-4}$ |
| 265 | 2.02 | 78.02 | $1.9 \cdot 10^{-4}$ |
| 432 | 1.00 | 113.80 | $4.8 \cdot 10^{-4}$ |
| 797 | 0.40 | 116.52 | $9.5 \cdot 10^{-4}$ |
| Positive standard deviation of the solubility products | | | |
| log $K_{S0, \text{Fe-ettringite}} = -43.3$; log $K_{S0, \text{Fe-monosulfate}} = -32.7$; log $K_{S0, \text{Fe-monocarbonate}} = -35.2$ | | | |
| 8.5 | 13.51 | 9.66 | $1.0 \cdot 10^{-4}$ |
| 8.7 | 13.17 | 9.49 | $1.1 \cdot 10^{-4}$ |
| 9.1 | 12.63 | 9.22 | $1.1 \cdot 10^{-4}$ |
| 8.2 | 11.87 | 8.84 | $1.2 \cdot 10^{-4}$ |
| 11 | 10.73 | 8.27 | $1.4 \cdot 10^{-4}$ |
| 13 | 9.20 | 7.51 | $1.6 \cdot 10^{-4}$ |
| 18 | 7.42 | 6.62 | $2.1 \cdot 10^{-4}$ |
| 24 | 5.82 | 6.45 | $2.9 \cdot 10^{-4}$ |
| 30 | 4.60 | 10.00 | $3.6 \cdot 10^{-4}$ |
| 54 | 5.49 | 11.30 | $1.2 \cdot 10^{-4}$ |
| 92 | 6.79 | 13.20 | $4.3 \cdot 10^{-5}$ |
| 124 | 5.08 | 26.61 | $5.8 \cdot 10^{-5}$ |
| 162 | 4.03 | 53.65 | $7.6 \cdot 10^{-5}$ |
| 265 | 2.02 | 78.02 | $1.9 \cdot 10^{-4}$ |
| 510 | 0.74 | 78.58 | $8.1 \cdot 10^{-4}$ |
| 797 | 0.40 | 116.53 | $1.4 \cdot 10^{-3}$ |
| Negative standard deviation of the solubility products | | | |
| log $K_{S0, \text{Fe-ettringite}} = -44.7$; log $K_{S0, \text{Fe-monosulfate}} = -33.7$; log $K_{S0, \text{Fe-monocarbonate}} = -35.8$ | | | |
| 5.9 | 10.81 | 8.31 | $7.3 \cdot 10^{-5}$ |
| 6.1 | 10.45 | 8.13 | $7.5 \cdot 10^{-5}$ |
| 6.5 | 9.90 | 7.86 | $8.0 \cdot 10^{-5}$ |
| 7.1 | 9.08 | 7.45 | $8.8 \cdot 10^{-5}$ |
| 8.3 | 7.92 | 6.87 | $1.0 \cdot 10^{-4}$ |
| 11 | 6.44 | 6.13 | $1.3 \cdot 10^{-4}$ |
| 15 | 4.89 | 5.35 | $1.9 \cdot 10^{-4}$ |
| 23 | 3.62 | 4.72 | $2.8 \cdot 10^{-4}$ |
| 38 | 2.74 | 4.28 | $4.6 \cdot 10^{-4}$ |
| 61 | 2.10 | 4.75 | $7.6 \cdot 10^{-4}$ |
| 94 | 2.41 | 8.21 | $2.7 \cdot 10^{-4}$ |
| 159 | 3.01 | 10.36 | $1.1 \cdot 10^{-4}$ |
| 232 | 2.05 | 25.09 | $1.6 \cdot 10^{-4}$ |
| 324 | 1.49 | 59.31 | $2.3 \cdot 10^{-4}$ |
| 425 | 1.04 | 116.78 | $3.3 \cdot 10^{-4}$ |
| 797 | 0.40 | 116.52 | $6.7 \cdot 10^{-4}$ |

Table A1.5. Thermodynamically calculated composition of the aqueous solutions of the dissolution experiments presented in Fig. 2.9B.

| OH ⁻ [mmol/L] | Ca [mmol/L] | S [mmol/L] | Fe [mmol/L] |
|--|-------------|------------|----------------------|
| Mean average of the calculated solubility products at 25 °C. | | | |
| log $K_{S0, \text{Fe-ettringite}}$ = -44.0; log $K_{S0, \text{Fe-monosulfate}}$ = -33.2; log $K_{S0, \text{Fe-monocarbonate}}$ = -35.5 | | | |
| 8.4 | 10.63 | 6.85 | 1.0·10 ⁻⁴ |
| 8.7 | 10.34 | 6.70 | 1.1·10 ⁻⁴ |
| 9.1 | 9.89 | 6.48 | 1.1·10 ⁻⁴ |
| 10 | 9.23 | 6.15 | 1.2·10 ⁻⁴ |
| 11 | 8.30 | 5.68 | 1.4·10 ⁻⁴ |
| 14 | 7.12 | 5.09 | 1.7·10 ⁻⁴ |
| 19 | 5.81 | 4.44 | 2.3·10 ⁻⁴ |
| 27 | 4.66 | 3.86 | 3.3·10 ⁻⁴ |
| 37 | 3.48 | 5.11 | 4.6·10 ⁻⁴ |
| 59 | 3.64 | 6.70 | 2.4·10 ⁻⁴ |
| 98 | 4.67 | 7.73 | 9.0·10 ⁻⁵ |
| 143 | 3.59 | 15.56 | 1.0·10 ⁻⁴ |
| 234 | 2.61 | 35.16 | 1.4·10 ⁻⁴ |
| 323 | 1.35 | 50.83 | 3.5·10 ⁻⁴ |
| 553 | 0.63 | 58.35 | 6.2·10 ⁻⁴ |
| 922 | 0.31 | 58.22 | 1.1·10 ⁻³ |
| Positive standard deviation of the solubility products | | | |
| log $K_{S0, \text{Fe-ettringite}}$ = -43.3; log $K_{S0, \text{Fe-monosulfate}}$ = -32.7; log $K_{S0, \text{Fe-monocarbonate}}$ = -35.2 | | | |
| 9.8 | 12.15 | 7.61 | 1.2·10 ⁻⁴ |
| 10 | 11.85 | 7.46 | 1.2·10 ⁻⁴ |
| 11 | 11.41 | 7.24 | 1.3·10 ⁻⁴ |
| 11 | 10.76 | 6.91 | 1.4·10 ⁻⁴ |
| 13 | 9.81 | 6.44 | 1.6·10 ⁻⁴ |
| 15 | 8.58 | 5.82 | 1.9·10 ⁻⁴ |
| 20 | 7.15 | 5.11 | 2.4·10 ⁻⁴ |
| 24 | 5.85 | 6.40 | 2.9·10 ⁻⁴ |
| 34 | 5.44 | 8.50 | 2.1·10 ⁻⁴ |
| 58 | 6.53 | 9.59 | 7.6·10 ⁻⁵ |
| 91 | 6.83 | 13.03 | 4.3·10 ⁻⁵ |
| 123 | 5.10 | 26.24 | 5.8·10 ⁻⁵ |
| 191 | 2.85 | 38.99 | 1.2·10 ⁻⁴ |
| 349 | 1.16 | 38.96 | 4.6·10 ⁻⁴ |
| 553 | 0.63 | 58.35 | 8.8·10 ⁻⁴ |
| 922 | 0.31 | 58.22 | 1.6·10 ⁻³ |
| Negative standard deviation of the solubility products | | | |
| log $K_{S0, \text{Fe-ettringite}}$ = -44.7; log $K_{S0, \text{Fe-monosulfate}}$ = -33.7; log $K_{S0, \text{Fe-monocarbonate}}$ = -35.8 | | | |
| 7.1 | 9.33 | 6.20 | 8.8·10 ⁻⁵ |
| 7.4 | 9.01 | 6.03 | 9.5·10 ⁻⁵ |
| 7.9 | 8.58 | 5.82 | 9.7·10 ⁻⁵ |
| 8.7 | 7.92 | 5.49 | 1.1·10 ⁻⁴ |
| 8.1 | 7.01 | 5.04 | 1.2·10 ⁻⁴ |
| 13 | 5.88 | 4.47 | 1.6·10 ⁻⁴ |
| 18 | 4.69 | 3.88 | 2.2·10 ⁻⁴ |
| 26 | 3.72 | 3.40 | 3.2·10 ⁻⁴ |
| 41 | 2.99 | 3.02 | 5.0·10 ⁻⁴ |
| 60 | 2.12 | 4.67 | 7.3·10 ⁻⁴ |
| 99 | 2.62 | 5.68 | 3.0·10 ⁻⁴ |
| 158 | 2.87 | 8.28 | 1.7·10 ⁻⁴ |
| 222 | 2.07 | 24.65 | 1.6·10 ⁻⁴ |
| 306 | 1.50 | 58.42 | 2.3·10 ⁻⁴ |
| 553 | 0.63 | 58.35 | 4.4·10 ⁻⁴ |
| 922 | 0.31 | 58.22 | 7.8·10 ⁻⁴ |

Appendix 2: Solid solution Al-/Fe-ettringite

(referring to work presented in chapter 3)

Table A2.1. Values of the c-parameter determined by XRD for ettringite synthesized with different $X_{\text{Al,total}}$ ratios presented in Fig. 3.2A.

| $X_{\text{Al,total}}$ | This study | Buhlert and Kuzel, 1971 | McMurdie et al., 1987 | Goetz-Neunhoeffer and Neubauer, 2006; Goetz-Neunhoeffer et al., 2006 | Moore and Taylor, 1970 |
|-----------------------|---------------------|-------------------------|-----------------------|--|------------------------|
| 0.0 | 22.0052 ± 0.0007 | 21.96 ± 0.01 | 22.007 | | |
| 0.1 | 21.9720 ± 0.0009 | 21.93 ± 0.02 | | | |
| 0.2 | 21.9440 ± 0.001 | 21.91 ± 0.02 | | | |
| 0.3 | 21.9370 ± 0.001 | 21.88 ± 0.02 | | | |
| | 21.5800 ± 0.004 | 21.82 ± 0.03 | | | |
| | 21.9190 ± 0.002 | 21.81 ± 0.02 | | | |
| 0.4 | 21.5840 ± 0.003 | | | | |
| | 21.9090 ± 0.002 | 21.74 ± 0.02 | | | |
| 0.5 | 21.5920 ± 0.002 | | | | |
| | 21.8700 ± 0.003 | 21.70 ± 0.02 | | | |
| 0.6 | 21.5590 ± 0.002 | | | | |
| | 21.5800 ± 0.001 | 21.67 ± 0.02 | | | |
| 0.7 | 21.5309 ± 0.0008 | 21.63 ± 0.02 | | | |
| | 21.5091 ± 0.0007 | 21.60 ± 0.02 | | | |
| 0.8 | 21.4819 ± 0.0006 | 21.52 ± 0.01 | | | |
| | | | | 21.473 ± 0.003 | 21.48 |

Table A2.2. Values of the a-parameter determined by XRD for ettringite synthesized with different $X_{Al,total}$ ratios presented in Fig. 3.2B.

| $X_{Al,total}$ | This study | Buhlert and Kuzel, 1971 | McMurdie et al., 1987 | Goetz-Neunhoeffer and Neubauer, 2006; Goetz-Neunhoeffer et al., 2006 | Moore and Taylor, 1970 |
|----------------|---|-------------------------|-----------------------|--|------------------------|
| 0.0 | 11.1929 ± 0.0003 | 11.180 ± 0.002 | 11.1817 | | |
| 0.1 | 11.1947 ± 0.0004 | 11.200 ± 0.001 | | | |
| 0.2 | 11.1983 ± 0.0005 | 11.200 ± 0.001 | | | |
| 0.3 | 11.1992 ± 0.0005 11.2330 ± 0.001 | 11.200 ± 0.001 | | | |
| 0.4 | 11.1997 ± 0.0006 11.2294 ± 0.0009 11.2053 | 11.200 ± 0.001 | | | |
| 0.5 | ± 0.0008 11.2307 ± 0.0007 11.2110 | 11.210 ± 0.001 | | | |
| 0.6 | ± 0.001 11.2307 ± 0.0005 | 11.210 ± 0.001 | | | |
| 0.7 | 11.2346 ± 0.0005 | 11.210 ± 0.001 | | | |
| 0.8 | 11.2369 ± 0.0007 | 11.230 ± 0.001 | | | |
| 0.9 | 11.2385 ± 0.0003 | 11.220 ± 0.001 | | | |
| 1.0 | 11.2411 ± 0.0003 | 11.229 ± 0.002 | | 11.230 ± 0.005 | 11.26 |

Table A2.3. Water loss and calculated amount of water molecules of the different ettringite phases.

| $X_{Al,total}$ | Loss of water [%] | Water molecules |
|----------------|-------------------|-----------------|
| 0.0 | 41.6 | 29.1 |
| 0.1 | 42.2 | 29.6 |
| 0.2 | 42.5 | 29.7 |
| 0.3 | 42.1 | 29.0 |
| 0.4 | 42.1 | 28.8 |
| 0.5 | 42.9 | 29.5 |
| 0.6 | 42.2 | 28.5 |
| 0.7 | 44.1 | 30.4 |
| 0.8 | 42.8 | 28.7 |
| 0.9 | 43.1 | 28.8 |
| 1.0 | 43.7 | 29.2 |

Table A2.4. Calculated concentrations in the aqueous solution for the different ettringite phases assuming a continuous solid solution and the formation of calcite and Fe-hydroxide. Presented in Fig. 3.6A.

| $X_{Al, total}$ | Ca [mmol/L] | S [mmol/L] | Al [mmol/L] | Fe [μ mol/L] | OH ⁻ [mmol] |
|-----------------|-------------|------------|-------------|-------------------|------------------------|
| 0.00 | 5.17 | 14.74 | - | 0.01 | 13 |
| 0.10 | 4.67 | 13.75 | - | 0.57 | 13 |
| 0.20 | 4.26 | 12.9 | - | 0.58 | 14 |
| 0.30 | 3.74 | 11.61 | - | 0.58 | 16 |
| 0.40 | 3.41 | 10.81 | - | 0.57 | 17 |
| 0.50 | 3.05 | 9.88 | - | 0.54 | 18 |
| 0.60 | 2.76 | 9.26 | - | 0.50 | 18 |
| 0.70 | 2.41 | 8.43 | - | 0.48 | 19 |
| 0.80 | 2.01 | 7.30 | - | 0.46 | 21 |
| 0.90 | 1.51 | 6.24 | - | 0.43 | 22 |
| 0.92 | 1.36 | | - | 0.41 | |
| 0.95 | 1.09 | | 3.09 | 0.37 | |
| 0.98 | 0.42 | | 0.15 | 0.35 | |
| 1.00 | 0.17 | 4.63 | 0.01 | 0.33 | 19 |

Table A2.5. Calculated solids assuming a continuous solid solution and the formation of calcite and Fe-hydroxide. Presented in Fig. 3.6B.

| | Fe-ettringite [mmol] | Calcite [mmol] | Fe-hydroxide [mmol] |
|------|----------------------|----------------|---------------------|
| 0.00 | 7.33 | 0.59 | 0.47 |
| 0.10 | 7.38 | 0.59 | 0.44 |
| 0.20 | 7.42 | 0.59 | 0.41 |
| 0.30 | 7.47 | 0.59 | 0.37 |
| 0.40 | 7.51 | 0.59 | 0.34 |
| 0.50 | 7.55 | 0.59 | 0.32 |
| 0.60 | 7.58 | 0.59 | 0.30 |
| 0.70 | 7.62 | 0.59 | 0.27 |
| 0.80 | 7.67 | 0.59 | 0.23 |
| 0.90 | 7.71 | 0.59 | 0.20 |
| 0.92 | 7.74 | 0.59 | 0.19 |
| 0.95 | 7.75 | 0.59 | 0.18 |
| 0.98 | 7.76 | 0.59 | 0.18 |
| 1.00 | 7.77 | 0.59 | - |

Table A2.6. Calculated concentrations in the aqueous solution for the different ettringite phases assuming a miscibility gap between $X_{\text{Al,total}} = 0.25-0.65$ and the formation of calcite and Fe-hydroxide. Presented in Fig. 3.7A.

| $X_{\text{Al,total}}$ | Ca [mmol/L] | S [mmol/L] | Al [mmol/L] | Fe [$\mu\text{mol/L}$] | OH ⁻ [mmol] |
|-----------------------|-------------|------------|-------------|--------------------------|------------------------|
| 0.00 | 5.17 | 14.74 | - | 0.33 | 13 |
| 0.10 | 4.71 | 13.77 | - | 0.35 | 14 |
| 0.20 | 4.38 | 12.96 | - | 0.38 | 14 |
| 0.30 | 4.00 | 11.74 | - | 0.42 | 16 |
| 0.40 | 3.82 | 11.02 | - | 0.44 | 17 |
| 0.50 | 3.63 | 10.17 | - | 0.48 | 18 |
| 0.60 | 3.52 | 9.64 | - | 0.50 | 19 |
| 0.70 | 3.36 | 8.90 | - | 0.52 | 20 |
| 0.80 | 3.06 | 7.83 | - | 0.56 | 22 |
| 0.90 | 2.53 | 6.75 | - | 0.59 | 23 |
| 0.92 | 2.34 | 6.37 | - | 0.60 | |
| 0.95 | 1.91 | 5.89 | 0.01 | 0.60 | |
| 0.98 | 0.57 | 4.95 | 0.06 | 0.57 | |
| 1.00 | 0.17 | 4.63 | 3.09 | 0.01 | 19 |

Table A2.7. Calculated solids assuming a miscibility gap between $X_{\text{Al,total}} = 0.25-0.65$ and the formation of calcite and Fe-hydroxide. Presented in Fig. 3.7B.

| $X_{\text{Al,total}}$ | Fe(-Al)-ettringite [mmol] | Al(-Fe)-ettringite [mmol] | Calcite [mmol] | Fe-hydroxide [mmol] |
|-----------------------|---------------------------|---------------------------|----------------|---------------------|
| 0.00 | 7.33 | - | 0.59 | 0.47 |
| 0.10 | 7.38 | - | 0.59 | 0.44 |
| 0.25 | 7.40 | - | 0.59 | 0.42 |
| 0.30 | 6.39 | 1.08 | 0.59 | 0.38 |
| 0.40 | 4.48 | 3.03 | 0.59 | 0.36 |
| 0.50 | 2.61 | 4.93 | 0.59 | 0.33 |
| 0.60 | 0.87 | 6.70 | 0.59 | 0.31 |
| 0.65 | - | 7.60 | 0.59 | 0.29 |
| 0.80 | - | 7.64 | 0.59 | 0.25 |
| 0.90 | - | 7.70 | 0.59 | 0.22 |
| 0.92 | - | 7.72 | 0.59 | 0.21 |
| 0.95 | - | 7.74 | 0.59 | 0.20 |
| 0.98 | - | 7.76 | 0.59 | 0.18 |
| 1.00 | - | 7.77 | 0.59 | - |

Table A2.8. From experiments calculated total solubility products (ΣII) of the different ettringite phases at 20 °C. Presented in Fig. 3.8.

| $X_{Al, total}$ | $\log \Sigma II$ |
|-----------------|-------------------|
| 0.0 | -43.60 ± 0.56 |
| 0.1 | -44.71 ± 0.03 |
| 0.2 | -45.82 ± 0.15 |
| 0.3 | -46.34 ± 0.08 |
| 0.4 | -45.52 ± 0.38 |
| 0.5 | -44.29 ± 0.05 |
| 0.6 | -44.54 ± 0.07 |
| 0.7 | -45.63 ± 0.03 |
| 0.8 | -45.99 ± 0.07 |
| 0.9 | -44.77 ± 0.03 |
| 1.0 | -44.86 ± 0.05 |

Table A2.9. Calculation of the theoretical developing of the total solubility products (ΣII) assuming i) an ideal solid solution and ii) a miscibility gap between $X_{Al,total} = 0.25$ and 0.65. Presented in Fig. 3.8.

| $X_{Al,total}$ | $\log \Sigma II$ (i) | $\log \Sigma II$ (ii) |
|----------------|----------------------|-----------------------|
| 0.00 | -44.70 | -44.60 |
| 0.04 | -44.72 | -44.63 |
| 0.06 | -44.73 | -44.60 |
| 0.08 | -44.74 | -44.59 |
| 0.10 | -44.75 | -44.57 |
| 0.12 | -44.76 | -44.57 |
| 0.13 | -44.77 | -44.56 |
| 0.15 | -44.78 | -44.56 |
| 0.17 | -44.80 | -44.55 |
| 0.19 | -44.81 | -44.55 |
| 0.21 | -44.82 | -44.55 |
| 0.23 | -44.83 | -44.55 |
| 0.25 | -44.84 | -44.55 |
| 0.27 | -44.85 | -44.55 |
| 0.29 | -44.87 | -44.55 |
| 0.31 | -44.88 | -44.55 |
| 0.33 | -44.89 | -44.55 |
| 0.35 | -44.90 | -44.55 |
| 0.37 | -44.92 | -44.55 |
| 0.38 | -44.93 | -44.55 |
| 0.40 | -44.94 | -44.55 |
| 0.42 | -44.96 | -44.55 |
| 0.44 | -44.97 | -44.55 |
| 0.46 | -44.99 | -44.55 |
| 0.48 | -45.00 | -44.55 |
| 0.50 | -45.01 | -44.55 |
| 0.52 | -45.03 | -44.55 |
| 0.54 | -45.04 | -44.55 |
| 0.56 | -45.06 | -44.55 |
| 0.58 | -45.07 | -44.55 |
| 0.60 | -45.09 | -44.55 |
| 0.62 | -45.11 | -44.55 |
| 0.63 | -45.12 | -44.55 |
| 0.65 | -45.14 | -44.55 |
| 0.67 | -45.16 | -44.55 |
| 0.69 | -45.17 | -44.56 |
| 0.71 | -45.19 | -44.56 |
| 0.73 | -45.21 | -44.57 |
| 0.75 | -45.23 | -44.58 |
| 0.77 | -45.25 | -44.60 |
| 0.79 | -45.27 | -44.62 |
| 0.81 | -45.29 | -44.64 |
| 0.83 | -45.31 | -44.66 |
| 0.85 | -45.33 | -44.70 |
| 0.87 | -45.35 | -44.73 |
| 0.88 | -45.37 | -44.78 |
| 0.90 | -45.39 | -44.84 |
| 0.92 | -45.42 | -44.92 |
| 0.94 | -45.44 | -45.01 |
| 0.96 | -45.46 | -45.13 |
| 0.98 | -45.49 | -45.30 |
| 1.00 | -45.51 | -45.50 |

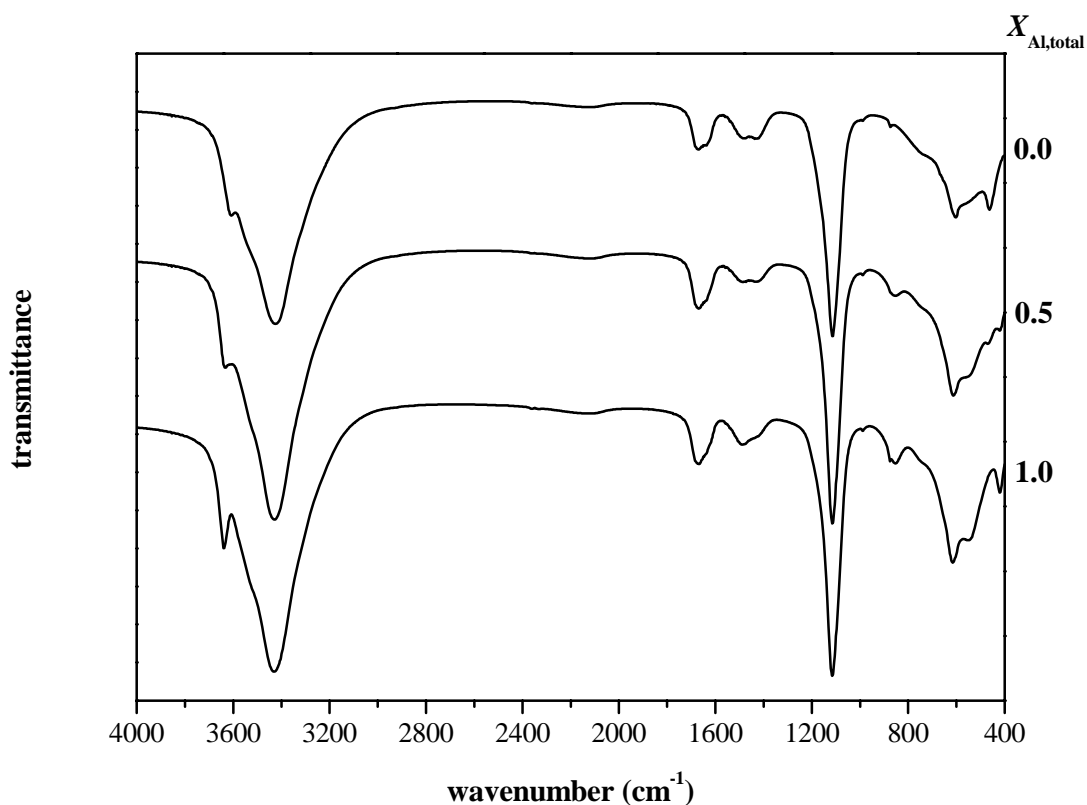


Fig. A2.1. IR spectra of the ettringite solid solutions.

Table A2.10. Wavenumbers of adsorption bands (in: Barnett, S. J., Macphee, D. E., and Crammond, N. J., 2003. Extent of immiscibility in the ettringite-thaumasite system. *Cement & Concrete Composites* **25**, 851-855). Refers to Fig. A2.1.

| Wavenumber (cm ⁻¹) | Assignment |
|--------------------------------|--|
| 3600 – 3200 | O – H stretch |
| 1680 | O – H bend |
| 1400 | C – O stretch (CO ₃ ²⁻) |
| 1100 | S – O stretch (SO ₄ ²⁻) |
| 875 | C – O bend (CO ₃ ²⁻) |
| 850 | AlO ₆ |

Appendix 3: Influence of citric acid on the hydration of OPC

(referring to work presented in chapter 4)

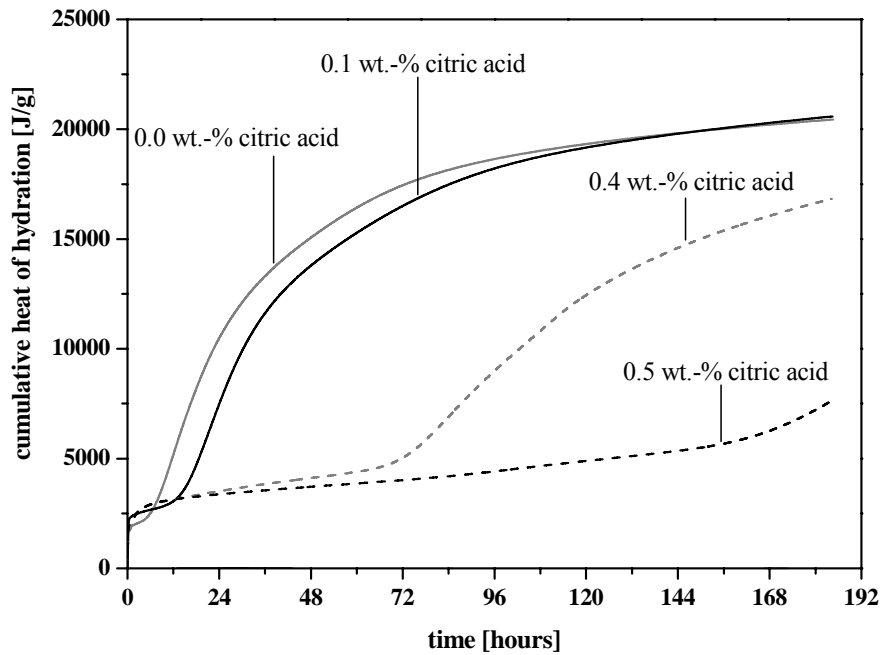


Fig. A3.1. Cumulative heat of hydration for the samples with and without citric acid.

Table A3.1. XRD pattern used for semi-quantitative analysis. Referring to Fig 4.2 – 4.8.

| Phase | 2 θ CuK α (rounded) |
|--------------------|-----------------------------------|
| Alite | 30.0, 52.0, 62.5 |
| Belite | 37.5, 31.1, 19.0 |
| Aluminate | 33.2 |
| Ferrite | 12.1, 24.3 |
| Gypsum | 11.7, 20.7 |
| Bassanite | 15.0 |
| Anhydrite | 25.5 |
| Portlandite | 18.0, 28.6, 51.0, 54.5 |
| Etringite | 9.0, 15.8 |
| Monocarboaluminate | 11.7 |
| Calcite | 29.5, 36.0, 43.0 |
| Quartz | 26.8 |

Table A3.2. Calculated relative peak intensities of the XRD pattern of the sample prepared without citric acid. Presented in Fig. 4.2.

| Time in days | Alite | Belite | Aluminate | Ferrite |
|--------------|-------|--------|-----------|---------|
| 0 | 24.4 | 2.2 | 13.6 | 4.3 |
| 0.04 | 21.6 | 1.7 | 11.6 | 3.8 |
| 0.08 | 19.2 | 1.2 | 10.8 | 3.2 |
| 0.17 | 20.6 | 0.8 | 14.3 | 3.8 |
| 0.33 | 18.7 | 0.4 | 13.4 | 3.2 |
| 0.67 | 11.5 | 0.3 | 9.1 | 3.0 |
| 1 | 9.2 | 0.1 | 4.8 | 2.3 |
| 2 | 6.9 | 0.2 | 5.1 | 2.5 |
| 3 | 8.1 | 0.1 | 3.8 | 1.9 |
| 7 | 6.8 | 0.1 | 3.9 | 1.7 |
| 28 | 6.0 | 0.1 | 2.7 | 1.2 |

Table A3.3. Calculated relative peak intensities of the XRD pattern of alite. Presented in Fig. 4.3.

| Time in days | 0.0 wt.-% citric acid | 0.1 wt.-% citric acid | 0.4 wt.-% citric acid | 0.5 wt.-% citric acid |
|--------------|--------------------------|--------------------------|--------------------------|--------------------------|
| 0 | 24.4 | 24.4 | 24.4 | 24.4 |
| 0.04 | 21.6 | 19.9 | 23.2 | 21.9 |
| 0.08 | 19.2 | 23.0 | - | - |
| 0.17 | 20.6 | 22.3 | - | - |
| 0.33 | 18.7 | 21.7 | - | - |
| 0.67 | 11.5 | 11.7 | - | - |
| 1 | 9.2 | 14.0 | 19.2 | 21.2 |
| 2 | 6.9 | 11.5 | 18.8 | - |
| 3 | 8.1 | 10.7 | 18.2 | 20.5 |
| 4 | - | - | 17.0 | - |
| 5 | - | - | 9.1 | - |
| 6 | - | - | 9.2 | - |
| 7 | 6.8 | 8.4 | 10.5 | 13.5 |
| 10 | - | - | - | 19.1 |
| 14 | - | - | - | 8.8 |
| 20 | - | - | - | 9.1 |
| 28 | 6.0 | 7.3 | 8.7 | 6.7 |

Table A3.4. Calculated relative peak intensities of the XRD pattern of aluminate. Presented in Fig. 4.4.

| Time in days | 0.0 wt.-% citric acid | 0.1 wt.-% citric acid | 0.4 wt.-% citric acid | 0.5 wt.-% citric acid |
|--------------|--------------------------|--------------------------|--------------------------|--------------------------|
| 0 | 13.6 | 13.6 | 13.6 | 13.6 |
| 0.04 | 11.6 | 11.1 | 12.2 | 12.3 |
| 0.08 | 10.8 | 11.4 | - | - |
| 0.17 | 14.3 | 11.7 | - | - |
| 0.33 | 13.47 | 11.5 | - | - |
| 0.67 | 9.1 | 6.9 | - | - |
| 1 | 4.8 | 4.5 | 12.3 | 12.1 |
| 2 | 5.1 | 6.3 | 8.2 | - |
| 3 | 3.8 | 6.2 | 8.2 | 9.1 |
| 4 | - | - | 7.8 | - |
| 5 | - | - | 3.4 | - |
| 6 | - | - | 4.1 | - |
| 7 | 3.9 | 4.8 | 3.2 | 3.2 |
| 10 | - | - | - | 8.0 |
| 14 | - | - | - | 3.3 |
| 20 | - | - | - | 2.5 |
| 28 | 2.7 | 2.7 | 3.5 | 2.0 |

Table A3.5. From TGA measurements calculated amount of gypsum. Presented in Fig. 4.5.

| Time in days | 0.0 wt.-% citric acid | 0.1 wt.-% citric acid | 0.4 wt.-% citric acid | 0.5 wt.-% citric acid |
|--------------|--------------------------|--------------------------|--------------------------|--------------------------|
| | [g/100g] | | | |
| 0 | 2.4 | 2.4 | 2.4 | 2.4 |
| 0.04 | 1.9 | 1.7 | 2.3 | 1.7 |
| 0.08 | 2.0 | 2.0 | - | - |
| 0.17 | 2.7 | 2.1 | - | - |
| 0.33 | 2.8 | 1.6 | - | - |
| 0.67 | 0 | 0 | - | - |
| 1 | 0 | 0 | 2.4 | 1.8 |
| 2 | 0 | 0 | 0 | - |
| 3 | 0 | 0 | 0 | 0 |
| 4 | - | - | 0 | - |
| 5 | - | - | 0 | - |
| 6 | - | - | 0 | - |
| 7 | 0 | 0 | 0 | 0 |
| 10 | - | - | - | 0 |
| 14 | - | - | - | 0 |
| 20 | - | - | - | 0 |
| 28 | 0 | 0 | 0 | 0 |

Table A3.6. Calculated relative peak intensities of the XRD pattern of aluminate. Presented in Fig. 4.6.

| Time in days | 0.0 wt.-% citric acid | 0.1 wt.-% citric acid | 0.4 wt.-% citric acid | 0.5 wt.-% citric acid |
|--------------|--------------------------|--------------------------|--------------------------|--------------------------|
| 0 | 0 | 0 | 0 | 0 |
| 0.04 | 5.9 | 12.7 | 2.8 | 3.9 |
| 0.08 | 5.8 | 15.6 | - | - |
| 0.17 | 6.7 | 14.4 | - | - |
| 0.33 | 9.9 | 12.3 | - | - |
| 0.67 | 6.4 | 11.4 | - | - |
| 1 | 11.7 | 14.1 | 11.2 | 10.2 |
| 2 | 11.4 | 11.4 | 25.7 | - |
| 3 | 13.3 | 9.5 | 24.6 | 21.4 |
| 4 | - | - | 26.0 | - |
| 5 | - | - | 21.7 | - |
| 6 | - | - | 16.9 | - |
| 7 | 7.2 | 7.9 | 15.6 | 23.4 |
| 10 | - | - | - | 31.6 |
| 14 | - | - | - | 14.8 |
| 20 | - | - | - | 13.9 |
| 28 | 4.4 | 8.8 | 12.8 | 14.4 |

Table A3.7. From TGA measurements calculated amount of portlandite. Presented in Fig. 4.7.

| Time in days | 0.0 wt.-% citric acid | 0.1 wt.-% citric acid | 0.4 wt.-% citric acid | 0.5 wt.-% citric acid |
|--------------|--------------------------|--------------------------|--------------------------|--------------------------|
| | [g/100g] | | | |
| 0 | 0.8 | 0.8 | 0.8 | 0.8 |
| 0.04 | 0.8 | 1.5 | 1.1 | 1.1 |
| 0.08 | 1.3 | 1.7 | - | - |
| 0.17 | 2.3 | 1.7 | - | - |
| 0.33 | 2.8 | 0.7 | - | - |
| 0.67 | 11.1 | 10.1 | - | - |
| 1 | 14.9 | 6.7 | 1.4 | 0.7 |
| 2 | 15.3 | 12.5 | 3.4 | - |
| 3 | 15.6 | 13.8 | 3.0 | 1.4 |
| 4 | - | - | 5.2 | - |
| 5 | - | - | 13.2 | - |
| 6 | - | - | 13.7 | - |
| 7 | 17.4 | 15.8 | 11.8 | 9.5 |
| 10 | - | - | - | 1.8 |
| 14 | - | - | - | 12.6 |
| 20 | - | - | - | 13.9 |
| 28 | 17.6 | 17.3 | 16.3 | 17.0 |

Table A3.8. Calculated saturation indices of gypsum. Presented in Fig. 4.9A.

| Time in days | 0.0 wt.-% citric acid | 0.1 wt.-% citric acid | 0.4 wt.-% citric acid | 0.5 wt.-% citric acid |
|--------------|--------------------------|--------------------------|--------------------------|--------------------------|
| 0.04 | 0.10 | 0.16 | 0.27 | 0.27 |
| 0.08 | 0.17 | 0.16 | - | - |
| 0.17 | 0.18 | 0.17 | - | - |
| 0.33 | -0.13 | 0.17 | - | - |
| 0.67 | 0.15 | 0.13 | - | - |
| 1 | -0.25 | 0.09 | 0.20 | 0.27 |
| 2 | -1.31 | -1.24 | 0.02 | - |
| 3 | -2.04 | -2.09 | 0.09 | 0.16 |
| 4 | - | - | 0.03 | - |
| 5 | - | - | -2.65 | - |
| 6 | - | - | -2.65 | - |
| 7 | -2.31 | -2.34 | -2.79 | 0.15 |
| 10 | - | - | - | -0.10 |
| 14 | - | - | - | -2.72 |
| 20 | - | - | - | -2.69 |
| 28 | -2.19 | -2.21 | -2.59 | -2.60 |

Table A3.9. Calculated saturation indices of portlandite. Presented in Fig. 4.9B.

| Time in days | 0.0 wt.-% citric acid | 0.1 wt.-% citric acid | 0.4 wt.-% citric acid | 0.5 wt.-% citric acid |
|--------------|--------------------------|--------------------------|--------------------------|--------------------------|
| 0.04 | 0.44 | 0.35 | 0.39 | 0.45 |
| 0.08 | 0.65 | 0.50 | - | - |
| 0.17 | 0.79 | 0.71 | - | - |
| 0.33 | 0.39 | 0.78 | - | - |
| 0.67 | 0.57 | 0.65 | - | - |
| 1 | 0.54 | 0.56 | 0.84 | 0.34 |
| 2 | 0.56 | 0.57 | 0.86 | - |
| 3 | 0.59 | 0.56 | 0.82 | 0.90 |
| 4 | - | - | 0.70 | - |
| 5 | - | - | 0.63 | - |
| 6 | - | - | 0.63 | - |
| 7 | 0.54 | 0.51 | 0.55 | 0.95 |
| 10 | - | - | - | 0.92 |
| 14 | - | - | - | 0.64 |
| 20 | - | - | - | 0.63 |
| 28 | 0.57 | 0.55 | 0.48 | 0.57 |

Table A3.10. Calculated saturation indices of ettringite. Presented in Fig. 4.9C.

| Time in days | 0.0 wt.-% citric acid | 0.1 wt.-% citric acid | 0.4 wt.-% citric acid | 0.5 wt.-% citric acid |
|--------------|--------------------------|--------------------------|--------------------------|--------------------------|
| 0.04 | 4.78 | 4.76 | 2.36 | 2.41 |
| 0.08 | 4.99 | 5.00 | - | - |
| 0.17 | 4.55 | 4.75 | - | - |
| 0.33 | 3.78 | 5.23 | - | - |
| 0.67 | 4.26 | 4.62 | - | - |
| 1 | 3.93 | 4.44 | 2.69 | 4.75 |
| 2 | 2.76 | 2.72 | 4.82 | - |
| 3 | 2.03 | 1.87 | 4.41 | 5.15 |
| 4 | - | - | 4.49 | - |
| 5 | - | - | 1.38 | - |
| 6 | - | - | 1.34 | - |
| 7 | 1.73 | 1.66 | 1.23 | 5.00 |
| 10 | - | - | - | 0.86 |
| 14 | - | - | - | 1.37 |
| 20 | - | - | - | 1.36 |
| 28 | 1.89 | 1.87 | 1.43 | 1.58 |

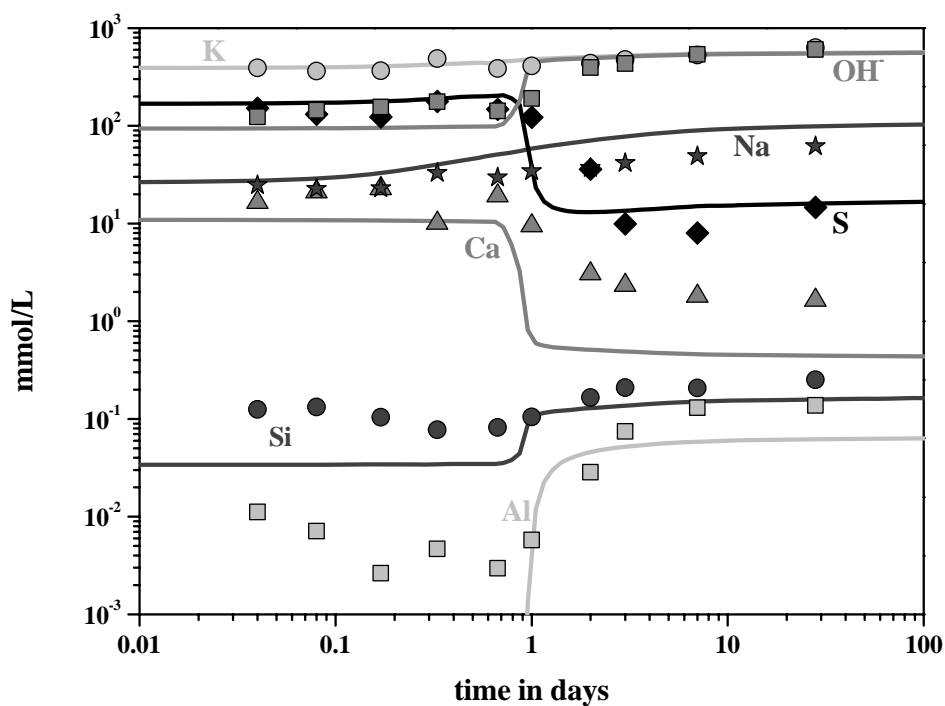


Fig. A3.2. Measured (symbols) and calculated (lines) concentrations of the pore solution of the samples without citric acid at different hydration times.

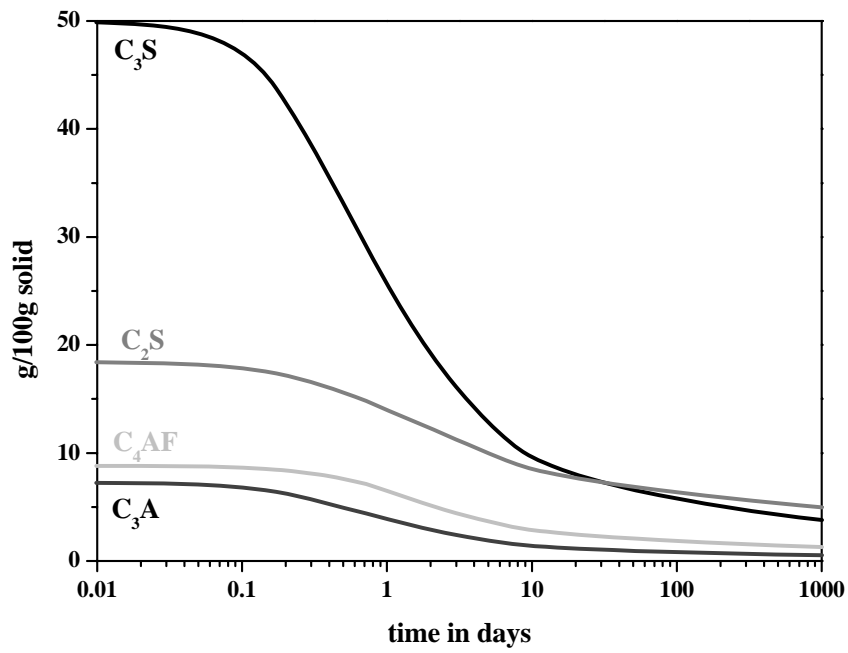


Fig. A3.3. Calculated amounts of the clinker phases of the samples without citric acid at different hydration times.

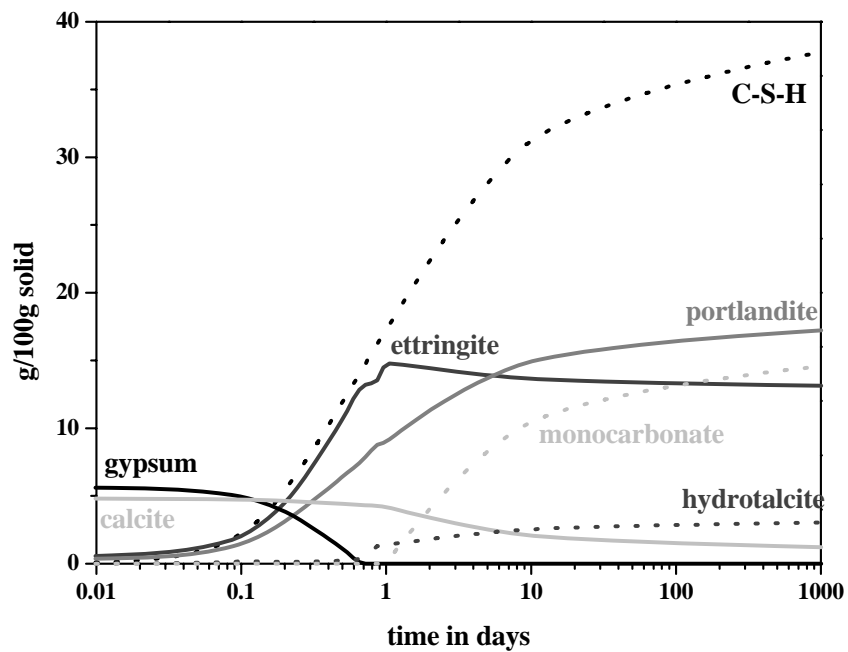


Fig. A3.4. Calculated amounts of the different solid phases of the samples without citric acid at different hydration times.

Appendix 4: Chromate reducing agent in OPC

(results of the investigation of the differences between the cement described in chapter 4 and a cement without 0.2 % Fe(II)SO₄·7H₂O as chromate reducing agent)

Table A4.1. Chemical analysis of the two OPCs used (CEM I 42.5 N).

| | <i>Without Fe(II)-sulfate as chromate reducing agent</i> | <i>With Fe(II)-sulfate as chromate reducing agent</i> |
|---|--|---|
| | g/100g | |
| SiO ₂ | 19.9 | 19.6 |
| Al ₂ O ₃ | 4.80 | 4.60 |
| Fe ₂ O ₃ | 2.90 | 2.90 |
| CaO | 62.7 | 62.4 |
| MgO | 2.00 | 1.60 |
| SrO | 0.14 | 0.06 |
| K ₂ O | 0.96 | 0.97 |
| Na ₂ O | 0.13 | 0.12 |
| CaO (free) | 0.68 | 0.46 |
| CO ₂ | 1.71 | 2.11 |
| SO ₃ | 3.16 | 3.25 |
| <i>Readily soluble alkalis</i> ^a | | |
| K ₂ O | 0.36 | 0.30 |
| Na ₂ O | 0.025 | 0.012 |

(a) Readily soluble alkalis were calculated from the concentrations of alkalis measured in the solution after 5 minutes agitation at a w/c of 10.

Table A4.2. Normative phase composition of the two OPCs used (CEM I 42.5 N).

| | <i>Without Fe(II)-sulfate as chromate reducing agent</i> | <i>With Fe(II)-sulfate as chromate reducing agent</i> |
|--|--|---|
| | g/100g | |
| Alite | 49.9 | 50.0 |
| Belite | 20.1 | 18.5 |
| Aluminate | 7.8 | 7.3 |
| Ferrite | 8.8 | 8.8 |
| CaO | 0.68 | 0.46 |
| CaCO ₃ | 3.9 | 4.8 |
| CaSO ₄ | 4.2 | 4.3 |
| K ₂ SO ₄ ^a | 1.6 | 1.4 |
| Na ₂ SO ₄ ^a | 0.16 | 0.08 |
| SrO | 0.14 | 0.06 |
| K ₂ O ^b | 0.09 | 0.24 |
| Na ₂ O ^b | 0.06 | 0.09 |
| MgO ^b | 2.0 | 1.6 |
| SO ₃ ^b | 0.0 | 0.05 |

(a) Readily soluble alkalis were calculated from the concentrations of alkalis measured in the solution after 5 minutes agitation at a w/c of 10.

(b) Present as solid solution in the major clinker phases.

Table A4.3. Composition of the pore solution after different hydration times.

| Time in days | K | Na | Li | Ca | Sr | Ba | Cr | Mo | Fe | Al | Si | S | OH ⁻ |
|--|-----|----|-----|-----|------|-------|---------|------------|-------|---------|------|-----|-----------------|
| mmol/l | | | | | | | | | | | | | |
| <i>Without Fe(II)-sulfate as chromate reducing agent</i> | | | | | | | | | | | | | |
| 0.04 | 424 | 52 | 2.3 | 22 | 0.24 | 0.005 | 1.36 | 0.071 | 0.019 | < 0.004 | 0.03 | 165 | 169 |
| 0.08 | 426 | 53 | 2.4 | 23 | 0.25 | 0.004 | 1.40 | 0.070 | 0.014 | < 0.004 | 0.03 | 158 | 182 |
| 0.2 | 444 | 54 | 2.5 | 22 | 0.31 | 0.004 | 1.23 | 0.063 | 0.014 | < 0.004 | 0.03 | 170 | 169 |
| 0.3 | 444 | 55 | 2.5 | 20 | 0.43 | 0.005 | 0.91 | 0.033 | 0.003 | < 0.004 | 0.04 | 176 | 149 |
| 0.7 | 487 | 64 | 2.5 | 11 | 0.31 | 0.005 | 0.61 | 0.014 | 0.001 | < 0.004 | 0.06 | 170 | 204 |
| 1 | 495 | 65 | 2.0 | 4.1 | 0.14 | 0.005 | 0.45 | 0.011 | 0.003 | 0.009 | 0.08 | 98 | 338 |
| 2 | 573 | 74 | 1.7 | 2.1 | 0.09 | 0.005 | 0.16 | 0.006 | 0.015 | 0.070 | 0.11 | 13 | 517 |
| 3 | 592 | 78 | 1.7 | 1.6 | 0.08 | 0.005 | 0.15 | 0.005 | 0.014 | 0.107 | 0.14 | 10 | 580 |
| 7 | 628 | 86 | 1.9 | 1.7 | 0.09 | 0.005 | 0.22 | 0.005 | 0.017 | 0.104 | 0.16 | 14 | 619 |
| 28 | 690 | 96 | 2.0 | 1.7 | 0.09 | 0.005 | 0.22 | 0.004 | 0.011 | 0.117 | 0.20 | 18 | 666 |
| <i>With Fe(II)-sulfate as chromate reducing agent</i> | | | | | | | | | | | | | |
| 0.04 | 392 | 25 | 0.5 | 16 | 0.13 | 0.004 | 0.002 | 0.022 | 0.249 | 0.011 | 0.12 | 151 | 123 |
| 0.08 | 361 | 23 | 0.5 | 21 | 0.15 | 0.004 | 0.0003 | 0.019 | 0.142 | 0.007 | 0.13 | 131 | 144 |
| 0.2 | 365 | 23 | 0.5 | 23 | 0.16 | 0.003 | 0.00001 | 0.019 | 0.036 | < 0.004 | 0.10 | 123 | 156 |
| 0.3 | 488 | 33 | 0.7 | 10 | 0.19 | 0.003 | 0.0007 | 0.018 | 0.027 | 0.005 | 0.08 | 177 | 176 |
| 0.7 | 385 | 30 | 0.8 | 19 | 0.25 | 0.004 | 0.0002 | 0.004 | 0.003 | < 0.004 | 0.08 | 147 | 142 |
| 1 | 410 | 34 | 0.8 | 9.5 | 0.15 | 0.003 | 0.0004 | < 0.003 | 0.004 | 0.006 | 0.10 | 122 | 190 |
| 2 | 437 | 37 | 0.8 | 3.0 | 0.06 | 0.002 | 0.0005 | < 0.003 | 0.009 | 0.028 | 0.17 | 36 | 394 |
| 3 | 474 | 42 | 0.7 | 2.3 | 0.05 | 0.003 | 0.0008 | < 0.003 | 0.018 | 0.074 | 0.21 | 10 | 432 |
| 7 | 531 | 49 | 0.9 | 1.8 | 0.04 | 0.002 | 0.001 | < 0.003 | 0.02 | 0.130 | 0.21 | 8.0 | 537 |
| 28 | 626 | 62 | 1.1 | 1.6 | 0.04 | 0.002 | 0.007 | < 0.003 | 0.064 | 0.137 | 0.25 | 15 | 603 |

Table A4.4. Measured concentrations after digestion of cement with HCl.

| K | Na | Li | Mg | Ca | Sr | Ba | Cr | Mo |
|--|------|-------|------|----|-------|-------|-------|-------|
| mmol/l | | | | | | | | |
| <i>Without Fe(II)-sulfate as chromate reducing agent</i> | | | | | | | | |
| 0.55 | 0.13 | 0.032 | 0.67 | 18 | 0.021 | 0.002 | 0.003 | 0.003 |
| <i>With Fe(II)-sulfate as chromate reducing agent</i> | | | | | | | | |
| 0.56 | 0.14 | 0.027 | 0.50 | 20 | 0.009 | 0.001 | 0.001 | 0.001 |

Table A4.5. Measured concentrations after extraction with demineralized water.

| K | Na | Li | Ca | Sr | Ba | Cr | Mo | Fe | Al | Si | S |
|--|-----|------|----|------|-------|--------|---------|-------|-------|------|----|
| mmol/l | | | | | | | | | | | |
| <i>Without Fe(II)-sulfate as chromate reducing agent</i> | | | | | | | | | | | |
| 18 | 2.2 | 0.10 | 20 | 0.05 | 0.007 | 0.023 | 0.003 | 0.007 | 0.006 | 0.07 | 17 |
| <i>With Fe(II)-sulfate as chromate reducing agent</i> | | | | | | | | | | | |
| 16 | 1.1 | 0.03 | 19 | 0.03 | 0.006 | 0.0008 | < 0.003 | 0.005 | 0.007 | 0.28 | 19 |

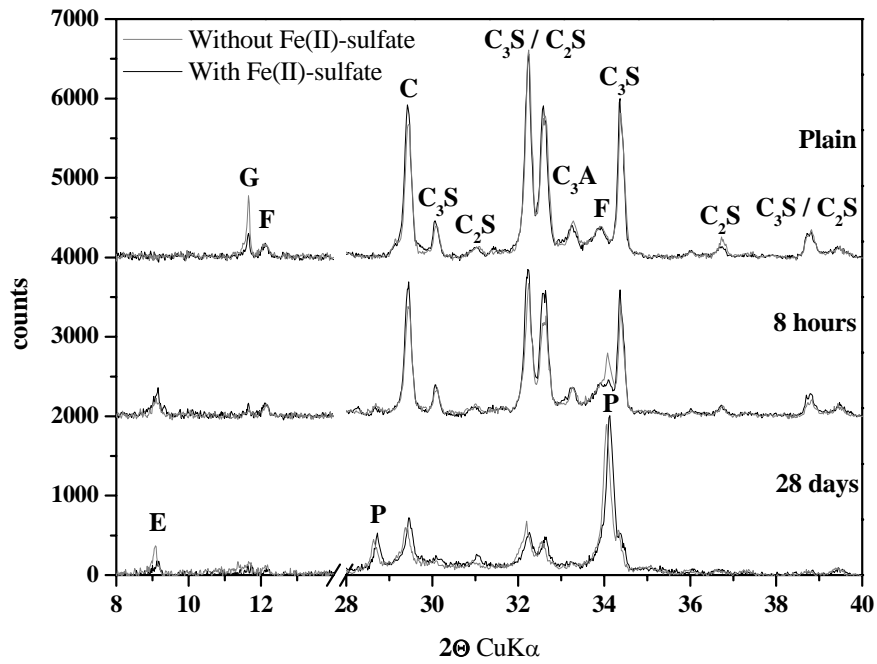


Fig. A4.1. X-ray diffraction spectra of the used cements.

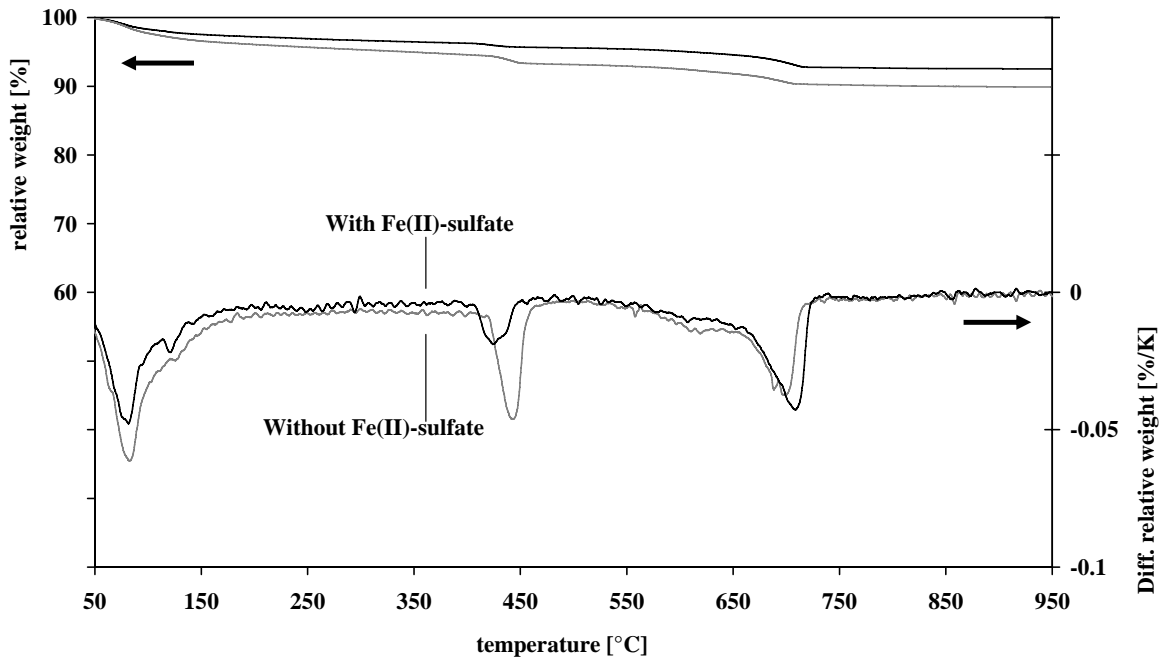


Fig. A4.2. TGA/DTA measurements after 8 hours of hydration.

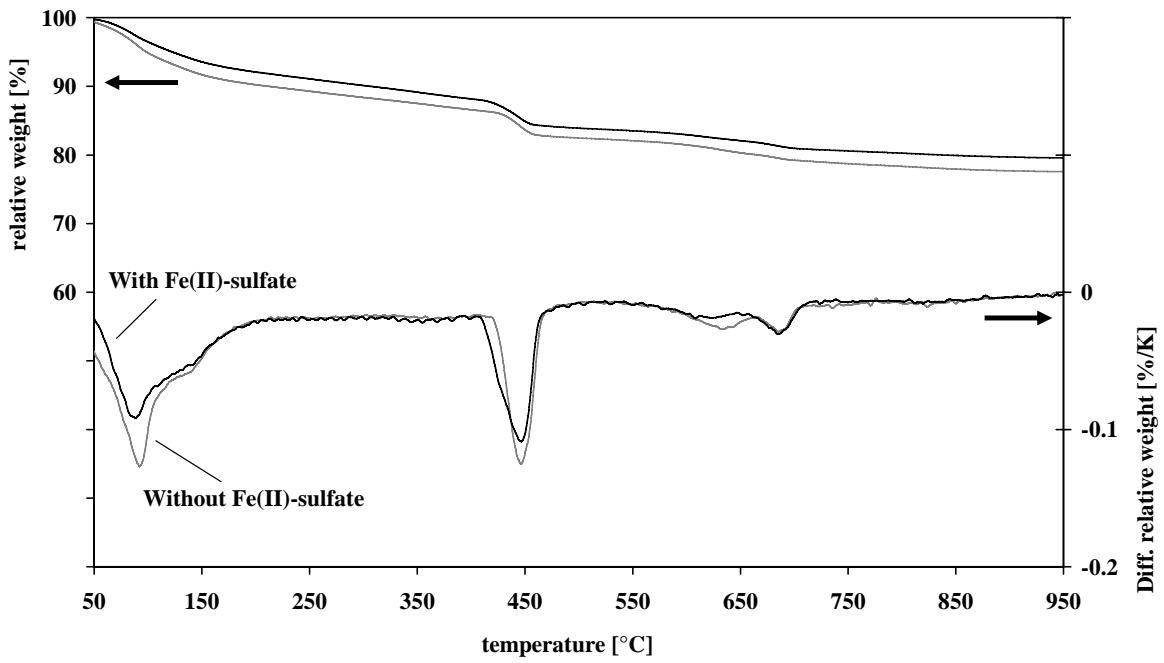


Fig. A4.3. TGA/DTA measurements after 28 days of hydration.

Acknowledgements

I would like to thank the following people for their help during my PhD studies:

Dr. Barbara Lothenbach, Prof. Dr. Ruben Kretzschmar, Prof. Dr. Neubauer, Dr. Jérôme Rose, Dr. Frank Winnefeld, Luigi Brunetti, Dr. Andrea Ulrich, Renato Figi, Dr. Dmitrii Kulik, Oliver Nagel, Adrian Wichser, Dr. Christoph Zwicky, Marcel Käppeli, Arnd Eberhardt, Walter Trindler, Hansjürgen Schindler, Hermann Mönch, Dr. Astrid Gruskovnjak, PD Dr. Friedline Götz-Neunhoeffler, Boris Ingold, Urs Gfeller, Daniel Fliegel, Anatol Zingg, and Axel Metzger for being there.

CURRICULUM VITAE

Göril Möschner

Born on January, 26th, 1979 in Erbach im Odenwald, Germany

Citizen of Germany

- | | |
|-----------|---|
| 1985-1989 | Primary school in Erbach im Odenwald, Germany |
| 1989-1998 | Gymnasium in Michelstadt, Germany |
| 1998-2003 | Studies in geoecology, University of Karlsruhe (TH), Germany |
| 2003 | Diploma in geoecology |
| 2004-2007 | PhD studies at the Federal Institute for Material Testing and Research (Empa), Laboratory for Concrete & Construction Chemistry, Dübendorf, Switzerland and at the Institute of Biogeochemistry and Pollutant Dynamics, Soil Chemistry Group of Prof. Ruben Kretzschmar, ETH Zurich, Zürich, Switzerland. |

This PhD thesis is part of the ETH E-Collection and available online
in electronic format:

<http://e-collection.ethbib.ethz.ch/diss>